



HAL
open science

Fundamental aspects and preparation of silicone foams by CO₂ foaming processes

Thibaud Métivier

► **To cite this version:**

Thibaud Métivier. Fundamental aspects and preparation of silicone foams by CO₂ foaming processes. Material chemistry. Université de Lyon, 2018. English. NNT : 2018LYSE1048 . tel-01891072

HAL Id: tel-01891072

<https://theses.hal.science/tel-01891072>

Submitted on 9 Oct 2018

HAL is a multi-disciplinary open access archive for the deposit and dissemination of scientific research documents, whether they are published or not. The documents may come from teaching and research institutions in France or abroad, or from public or private research centers.

L'archive ouverte pluridisciplinaire **HAL**, est destinée au dépôt et à la diffusion de documents scientifiques de niveau recherche, publiés ou non, émanant des établissements d'enseignement et de recherche français ou étrangers, des laboratoires publics ou privés.



N°d'ordre NNT : 2018LYSE1048

THESE de DOCTORAT DE L'UNIVERSITE DE LYON

opérée au sein de
l'Université Claude Bernard Lyon 1

Ecole Doctorale : Matériaux ED34

Spécialité de doctorat : Matériaux polymères et composites

Discipline : Physique-Chimie

Soutenue publiquement le 21/03/2018, par :

Thibaud Métivier

Fundamental aspects and preparation of silicone foams by CO₂ foaming processes

Devant le jury composé de :

Dr. PEUVREL-DISDIER Edith	Mines ParisTech-CEMEF	Rapporteure
Pr. SOULESTIN Jérémie	Mines de Douai	Rapporteur
Dr. BOUNOR-LEGARÉ Véronique	Université de Lyon 1	Examinatrice
Dr. GANACHAUD François	Université de Lyon 1	Examineur
M. GAROIS Nicolas	Hutchinson	Examineur
Pr. CASSAGNAU Philippe	Université de Lyon 1	Directeur de thèse
Dr. MARCHAL Frédéric	Elkem	Invité

UNIVERSITE CLAUDE BERNARD - LYON 1

Président de l'Université

Président du Conseil Académique

Vice-président du Conseil d'Administration

Vice-président du Conseil Formation et Vie Universitaire

Vice-président de la Commission Recherche

Directrice Générale des Services

M. le Professeur Frédéric FLEURY

M. le Professeur Hamda BEN HADID

M. le Professeur Didier REVEL

M. le Professeur Philippe CHEVALIER

M. Fabrice VALLÉE

Mme Dominique MARCHAND

COMPOSANTES SANTE

Faculté de Médecine Lyon Est – Claude Bernard

Directeur : M. le Professeur G.RODE

Faculté de Médecine et de Maïeutique Lyon Sud – Charles Mérieux

Directeur : Mme la Professeure C. BURILLON

Faculté d'Odontologie

Directeur : M. le Professeur D. BOURGEOIS

Institut des Sciences Pharmaceutiques et Biologiques

Directeur : Mme la Professeure C. VINCIGUERRA

Institut des Sciences et Techniques de la Réadaptation

Directeur : M. X. PERROT

Département de formation et Centre de Recherche en Biologie Humaine

Directeur : Mme la Professeure A-M. SCHOTT

COMPOSANTES ET DEPARTEMENTS DE SCIENCES ET TECHNOLOGIE

Faculté des Sciences et Technologies

Directeur : M. F. DE MARCHI

Département Biologie

Directeur : M. le Professeur F. THEVENARD

Département Chimie Biochimie

Directeur : Mme C. FELIX

Département GEP

Directeur : M. Hassan HAMMOURI

Département Informatique

Directeur : M. le Professeur S. AKKOUCHE

Département Mathématiques

Directeur : M. le Professeur G. TOMANOV

Département Mécanique

Directeur : M. le Professeur H. BEN HADID

Département Physique

Directeur : M. le Professeur J-C PLENET

UFR Sciences et Techniques des Activités Physiques et Sportives

Directeur : M. Y.VANPOULLE

Observatoire des Sciences de l'Univers de Lyon

Directeur : M. B. GUIDERDONI

Polytech Lyon

Directeur : M. le Professeur E.PERRIN

Ecole Supérieure de Chimie Physique Electronique

Directeur : M. G. PIGNAULT

Institut Universitaire de Technologie de Lyon 1

Directeur : M. le Professeur C. VITON

Ecole Supérieure du Professorat et de l'Education

Directeur : M. le Professeur A. MOUGNIOTTE

Institut de Science Financière et d'Assurances

Directeur : M. N. LEBOISNE

A ma famille et mes amis...

« La science consiste à passer d'un étonnement à un autre. »

Aristote

« Ambition : une bulle de savon qui voudrait être un peu plus grosse au moment qu'elle crèvera. »

Jean Rostand

Remerciements

Je suis reconnaissant envers la docteure Édith Peuvrel-Disdier et le Professeur Jérémie Soulestin pour leur rôle de rapporteur, et membres du jury de thèse. Je tiens à les remercier pour leurs temps et leurs compétences mises à ma disposition pour juger de ce travail. Je tiens également à remercier la docteure Véronique Bounor-Legaré d'avoir acceptée d'être la présidente du jury. Je remercie également le docteur François Ganachaud d'avoir accepté d'examiner ces travaux de thèse.

Ce travail de thèse a été réalisé au sein du laboratoire d'Ingénierie des Matériaux Polymères (IMP), UMR 5223 à l'Université de Lyon 1. Je tiens donc à remercier en premier lieu le Professeur Philippe Cassagnau de m'avoir accueilli. Étant également mon directeur de thèse, je tiens à le remercier pour la confiance et la liberté d'action qu'il m'a accordées tout au long de ce projet. Ses intuitions scientifiques, ses blagues souvent bien placées, son exigence et ses encouragements donnés avec parcimonie m'ont permis de m'enrichir et de me préparer au futur travail de chercheur (et peut être trouveur). Je le remercie d'avoir partagé une partie de son savoir et de m'avoir permis d'assister à plusieurs congrès élargissant ma culture scientifique. Je souhaite également le remercier pour sa grande réactivité en particulier pendant la période de rédaction.

Les travaux présentés dans ce mémoire sont le fruit de la collaboration entre le laboratoire universitaire IMP, les entreprises Hutchinson, Serge Ferrari, BlueStar et RSISOLSEC et les financeurs du projet FUI SMOUSSIF. Je tiens donc à remercier les gens avec qui j'ai pu travailler durant ces trois années. Et plus particulièrement, Aurélie Vanhille de l'entreprise Hutchinson pour son suivie et son implication tout au long de mes travaux de thèse, ainsi que Gregory Martin, Nicolas Garois et Charlène Forest, mes responsables au sein d'Hutchinson. Je tiens à remercier également Clément Paul, qui était chef de projet au sein d'Hutchinson, pour nos nombreuses discussions. Je souhaite aussi remercier les techniciens qui m'ont permis de faire les essais à savoir Bruno, Fabien, Sylvain et Cécile.

Je dédicace de spécial remerciements à Sylvie Novat et Nadia Yacoub pour leur gentillesse et sans qui on ne pourrait pas résoudre les problèmes administratifs, de commandes ni aller au congrès internationaux.

Je souhaiterais remercier le personnel du laboratoire qui offre un soutien tant technique que moral à savoir Adrien, Olivier, Thierry, Laurent, Agnès, Noëllie, Florian, Ali et Sabine. Un remerciement spécial à Flavien pour son aide, sa bonne humeur et sa capacité à pouvoir résoudre tous les problèmes. Je souhaite remercier Pierre pour son expertise dans le domaine de la microscopie, sa disponibilité et son sourire.

Je voudrais remercier également les chercheurs de l'IMP avec qui j'ai pu échanger sur les différents problèmes scientifiques rencontrés durant cette thèse à savoir Véronique, Emmanuel, René, Guillaume et Matthieu F. Et puis comment oublier l'intarissable Gisèle ainsi que sa gentillesse.

Je voudrais remercier chaleureusement les gens de mon bureau 327, les plus vieux comme les plus récents: Edwin, Manue, MC, Marjo, Oleksi, Antoine et Clément (TEAM NERF), Claire, Noémie et Renaud (son bureau de cœur s'il se l'avoue un jour). Une dédicace particulière à MC et Marjo avec lesquelles j'ai passé 3 super années de thèse dans la bonne ambiance tout en mangeant du chocolat... Je tiens à remercier tous les doctorants que j'ai pu croiser au cours de ces 3 années mémorables. Spécialement ceux qui sont maintenant plus que des collègues avec qui j'ai pu partagé d'inoubliables moments (apéros, sorties,...): Imed, Yann, Marjo, Bastien, Pierre, MC, Michaël, Mel, Christoche, Guillaume, Anaïs, Fab, Clément, Antoine... Grâce à vous, j'ai appris et partagé de nombreuses choses et les moments difficiles de cette thèse ont été bien plus agréables!

Je voudrais remercier mes vieux amis du Périgord, Gaylord, Thomas, Arnaud, Guillaume, Romain, Delphine, fanny... qui m'ont permis de me ressourcer lors des retours au « pays ».

Je voudrais également saluer mes acolytes de prépa, spécialement Thomas et Antoine. Bon courage à eux pour leur fin de thèse!

Je n'aurai jamais terminé cette thèse sans le soutien de la DREAM TEAM : Adrien, Boboc, Fanf, Elssa, Erf, Chaille, Nono, Joss, Sisi, Perrine, Max, Anne Laure, Raquel, Nico, Mel, Vincent, Marie, Soiz', Bebe, Jeanneski et Remy. Merci à tous pour ces week-ends passés ensemble et à votre bonne humeur. Je tiens à faire une dédicace spéciale à Fanf, mon coloc! On a passé ces 3 ans de thèse ensemble, à souffrir et à s'entraider. On a commencé nos thèses ensemble, on finit ensemble que demander de mieux!

Finalement, j'aimerais particulièrement remercier mes parents et ma famille qui m'ont toujours soutenu et sans qui je ne serai pas là! Je vous avais toujours dit que je ne ferais pas d'études longues, la preuve aujourd'hui j'ai fait les plus longues possible... J'espère qu'aujourd'hui, vous êtes fiers et comblés.

Et à vous lecteur, puissiez-vous trouver votre bonheur dans cette thèse et bon courage pour la lecture!

Abstract

Fundamental aspects and preparation of silicone foams by CO₂ foaming processes

This work is devoted to the study of the foaming behavior of a silicone elastomer and thermoplastic vulcanizates (TPV) based silicone. The foaming step was carried out by batch and extrusion foaming processes with CO₂ as blowing agent. The foamability of silicone elastomer was improved by a microstructuration of fluorosilicone which is a highly CO₂-philic elastomer through heterogeneous nucleation. The foam and blend morphologies as well as the rheology in shear and bi-elongation modes were further fitted by branching silicone chains under shearing conditions in a roll mill with a small amount of peroxide. Indeed, this dynamic chemical modification reduces the size of fluorosilicone droplets which leads to increase the volume density of nucleating sites and consequently lowers the mean bubble size. Furthermore, it allows also the formation of multi-scale branched structures inducing a strain hardening behavior in bi-elongational flow which restrict the cell growth and coalescence during foam expansion.

The second part deals with the foaming behavior of TPV silicone in which partially crosslinked silicone nodules are dispersed. Surprisingly, formulations exhibit close rheological behavior in elongation modes that the neat polyethylene (LDPE) matrix and reach prerequisites for foaming applications in terms of elongation at break. However, their foaming behavior are far different and are correlated to the extrusion foaming parameters which are known to control the nucleation i.e. the pressure before the die and the depressurization rate at the die exit. A proper choice of the gel content allows a TPV foamability close to that of LDPE.

Keywords: Foaming processes, Thermoplastics Vulcanizates (TPV), silicone, fluorosilicone, rheology

Résumé

Aspects fondamentaux et élaboration de mousses silicone via des procédés de moussage au CO₂

Cette thèse porte sur l'étude du comportement au moussage d'un élastomère silicone et de thermoplastiques vulcanisés (TPV) à base de silicone. Le moussage a été réalisé à l'aide des procédés batch et d'extrusion moussage en utilisant le CO₂ comme agent moussant. La microstructuration de fluorosilicone, ayant une grande affinité avec le CO₂, dans la silicone favorise grandement le moussage par nucléation hétérogène. La morphologie du mélange et des mousses résultantes ainsi que la rhéologie en cisaillement et en écoulement bi-élongationnel ont été améliorés en élaborant sous cisaillement des structures branchées de chaînes silicones en présence d'un faible taux de peroxyde. En effet, la modification chimique sous écoulement permet de réduire la taille des nodules de fluorosilicone augmentant ainsi la densité volumique de sites de nucléation potentiels. Elle permet également de créer des structures hyperbranchées générant des propriétés de durcissement des contraintes en écoulement bi-élongationnel ce qui a pour effet de réduire la croissance cellulaire et la coalescence lors de l'expansion de la mousse.

La deuxième partie est dédiée à l'étude du moussage de TPV silicone pour lesquels la phase silicone est partiellement réticulée. Ces TPV ont étonnement le même comportement en rhéologie élongationnelle que la matrice polyéthylène basse densité (PEBD). Bien que les TPVs atteignent des bonnes propriétés en termes d'élongation à rupture à l'état fondu, leur comportement au moussage est très différent. En effet il est principalement lié à leur viscosité sous fort taux de cisaillement ainsi qu'aux conditions d'extrusion i.e. la pression avant filière et la détente en sortie de filière. Avec un taux de réticulation approprié de la phase élastomère, le TPV mousse de manière similaire que le PEBD.

Mots clés: Procédés de moussage, Thermoplastiques vulcanisés (TPV), silicone, fluorosilicone, rhéologie

Intitulé et adresse du laboratoire :

Laboratoire Ingénierie des Matériaux Polymères (IMP@Lyon1), UMR CNRS 5223
Bâtiment Polytech'Lyon
15 boulevard Latarjet
69622 VILLEURBANNE
Discipline : **Physique-Chimie**

Résumé substantiel de la thèse

Fondamentalement, les mousses sont produites par la création de bulles de gaz dans un milieu solide ou liquide tel que l'eau, les polymères, les métaux... La formulation, la morphologie de mousse (porosité ouverte/fermée) ainsi que leur densité ont un impact direct sur les propriétés qui en découlent. En effet, les mousses à porosité fermée possèdent des propriétés supérieures en compression, en absorption de chocs ou en isolation thermique. À l'opposé, les mousses à cellules ouvertes montrent d'excellentes propriétés pour des applications d'isolation phonique ou d'ingénierie tissulaire.

L'utilisation de produits moussés devrait fortement augmenter dans le secteur automobile car depuis le dernier décret européen, les constructeurs automobiles doivent produire des voitures émettant moins de 95 g/km de gaz à effet de serre d'ici à 2020. Ainsi, pour remplir ce challenge, l'allègement des véhicules est obligatoire et passe par l'élaboration de mousses innovantes pour remplacer les matériaux usuellement utilisés.

Dans cette optique, le projet FUI SMOUSSIF (2014-2018) a pour but de développer de nouvelles mousses silicone utilisables dans des conditions plus sévères que les mousses conventionnelles. En effet, les mousses silicone associent les propriétés des mousses décrites précédemment avec les excellentes propriétés de l'élastomère silicone à savoir de bonnes propriétés mécaniques tant à basse qu'à haute température ainsi qu'une excellente résistance aux dégradations thermiques.

Le moussage du silicone est habituellement conduit par l'expansion d'une phase gazeuse qui est initialement générée in situ dans l'élastomère. La formation de la mousse silicone fait appel à deux réactions parallèles : la réticulation et le moussage. Deux méthodes conventionnelles de réticulation peuvent être utilisées : à haute température (peroxyde) ou à température ambiante (polycondensation or polyaddition). Les produits gonflants sont produits soit par les réactions de réticulation soit par la dégradation thermique d'un agent porogène. Un des principaux challenges dans le moussage du silicone est la synchronisation de ces deux réactions pour générer des mousses ayant de bonnes propriétés. De par le comportement de type liquide viscoélastique à température ambiante de la silicone et la linéarité de ses chaînes, un autre point important est d'assurer une expansion suffisante et en même temps d'être capable de limiter la post-relaxation et l'effondrement de la mousse pour produire une mousse stabilisée de faible densité. Enfin, la grande perméabilité aux gaz des silicones induit que la majorité du gaz dissous diffuse vers l'environnement plutôt que de participer à la nucléation et à l'expansion. Par conséquent et par rapport à d'autres polymères, il est très difficile d'obtenir une mousse silicone ayant une faible densité et une densité élevée de cellules.

En plus, des propriétés intrinsèques particulières du silicone, le procédé de moussage fait intervenir de nombreux autres paramètres qui ont des impacts majeurs sur les

propriétés finales de la mousse. En effet, la morphologie cellulaire est affectée par les paramètres procédé (température, pression, concentration de gaz...), la rhéologie élongationnelle, la présence d'agents nucléant, de surfactants, de charges...

Dans ce contexte, l'objectif principal de cette thèse est de comprendre les mécanismes fondamentaux mis en jeu lors de la nucléation, la croissance cellulaire et la coalescence des bulles tout en tenant compte de la diffusion de gaz, de la rhéologie et des réactions de réticulation dans un élastomère silicone. La production de mousse est réalisée à l'aide d'un procédé « batch » utilisant le CO₂ comme agent moussant. Cette étude sera étendue à l'élaboration de mousses Thermoplastiques Vulcanisés (TPV) à base de silicone.

Ce travail de thèse s'articule en deux grandes parties subdivisées en cinq chapitres. Le premier chapitre est dédié à l'étude bibliographique sous la forme d'une revue en cours de soumission. La deuxième partie regroupe les principaux résultats expérimentaux obtenus durant ces trois années de thèse. Elle est composée de quatre publications (chapitres) également en cours de soumission.

L'étude bibliographique (chapitre 1) a montré que la nucléation et l'expansion des cellules étaient les deux paramètres à contrôler et à maîtriser. Ceci est d'autant plus difficile pour les silicones que la diffusivité des gaz dans ces milieux est 100 à 1000 fois plus élevée que dans les autres polymères thermoplastiques. La stratégie adoptée a été de tenter d'augmenter la nucléation par l'ajout et la micro-structuration d'une phase fluorosilicone CO₂-phile dispersée dans le silicone. De plus, les propriétés viscoélastiques qui gouvernent l'expansion des cellules ont été adaptées à l'aide d'un procédé original (réticulation dynamique) de façon à conférer au milieu silicone des propriétés de durcissement de contraintes sous écoulement bi-élongationnel.

Dans le chapitre 2, la modification chimique radicalaire des chaînes silicones vinyliques a été menée sous écoulement (réticulation dynamique) à l'aide d'un mélangeur à rouleaux et en présence d'une faible concentration en peroxyde (0,2% massique). Les caractérisations rhéologiques et SEC révèlent que les réactions radicalaires donnent naissance à des structures hyperbranchées de masses molaires atteignant 10⁷ g/mol. De plus, les échantillons ainsi modifiés dynamiquement ont un comportement de durcissement de contraintes sous écoulement bi-élongationnel.

Nous avons toutefois voulu comprendre la formation de ces structures hyperbranchées. Des réticulations dynamiques sous azote et sous air ont permis de comprendre que l'oxygène réduit fortement la consommation de groupes vinyliques en inhibant la réaction de réticulation créant ainsi ces structures hyperbranchées.

Finalement, le comportement rhéologique peut être expliqué par une microstructure originale constituée de chaînes polymères non réticulées jouant le rôle de matrice tandis que des structures branchées et miscibles jouent le rôle de renforçant.

Le troisième chapitre est dédié à l'étude et l'amélioration des morphologies de mélange d'un mélange fluorosilicone/silicone en utilisant deux voies de compatibilisation afin d'augmenter la densité de nucléation.

Tout d'abord, la tension interfaciale entre ces deux polymères a été déterminée par la méthode de la relaxation de forme d'une goutte ($\approx 3.5\text{mN/m}$). Ensuite, le modèle de Serpe a été utilisé pour prédire la morphologie de mélange tout en tenant compte des phénomènes de coalescence.

Ce mélange de polymères silicones de natures différentes a été compatibilisé suivant deux voies. Premièrement, la réticulation du mélange dans un mélangeur à rouleaux (conditions dynamiques) a permis de réduire la taille des nodules de fluorosilicone de $7\ \mu\text{m} \pm 6.0$ à $3.5\ \mu\text{m} \pm 2.0$. De plus, les morphologies des échantillons dynamiquement réticulés sont stables dans des conditions de recuits (mélanges laissés 1 an au repos ou re-mélangés à température ambiante). Cette compatibilisation par « réticulation dynamique » est essentiellement attribuée au changement du rapport de viscosités entre les deux phases silicones et la réduction de tension interfaciale dont l'origine est la création de copolymères à l'interface. Mais la formation de ce type de copolymère n'a pas pu être formellement démontrée.

Dans un deuxième temps, l'influence de l'ajout de silices pyrogénées, ayant une surface spécifique de $200\text{m}^2/\text{g}$ et deux chimies de surface différentes (hydrophile et hydrophobe), sur la morphologie de mélange a été également étudiée. La silice hydrophile permet de réduire efficacement la taille des nodules de fluorosilicone jusqu'à $500\ \text{nm}$ tandis que la silice hydrophobe ne montre aucune influence. Cette compatibilisation est due à la présence de silice hydrophile à l'interface entre les deux élastomères réduisant la tension interfaciale et la coalescence par effet Pickering. La compatibilisation peut être également attribuée aux interactions hydrogènes et dipolaires entre les chaînes de silicone, les groupes CF_3 et les silanols présents à la surface de la silice hydrophile modifiant le rapport des viscosités.

Dans le quatrième chapitre, la microstructuration de fluorosilicone a été utilisée afin d'augmenter la densité de nucléation. En effet, les nodules de fluorosilicone jouent le rôle d'agent nucléant et permettent la formation d'une densité plus importante de nucléi qui a pour effet de réduire la taille des bulles par la croissance compétitive de ces nucléi. Ainsi avec le mélange de 10% en masse de fluorosilicone, le diamètre des bulles diminue de $670\ \mu\text{m} \pm 550$ à $120\ \mu\text{m} \pm 70$ et la densité de cellule augmente de 600 à $5 \times 10^6\ \text{cells}/\text{cm}^{-3}$.

Enfin, la réticulation dynamique a été utilisée sur le mélange silicone/fluorosilicone pour compatibiliser le mélange et allier l'amélioration des propriétés élongationnelles apportées par la réticulation dynamique avec la nucléation hétérogène apportée par les nodules de fluorosilicone. Grâce à cette stratégie, la taille des bulles est réduite à $65\ \mu\text{m} \pm 40$ et la densité de cellule augmente jusqu'à $3 \times 10^8\ \text{cells}/\text{cm}^{-3}$. D'après la littérature, ces résultats

n'ont jamais été obtenues avec du CO₂ gazeux mais le sont avec des silicones fortement chargés en silice dans des conditions supercritiques.

Le dernier chapitre se concentre sur le moussage de TPVsilicone dans lesquels des nodules de silicones partiellement réticulés sont dispersés dans du polyéthylène basse densité (PEBD). Dans ces TPV, les nodules de silicone ont une taille moyenne voisines de 1 µm et la viscoélasticité de ces nodules de silicone a été choisie en fonction de leur taux de gel (0, 40 et 60%). La rhéologie linéaire et non linéaire en cisaillement s'est révélée étonnement plus sensible vis-à-vis de la formulation que la rhéologie élongationnelle. En effet, l'ajout de 40wt% de silicone ne modifie en rien le comportement des TPV montrant ainsi un comportement élongationnelle équivalent à celui du PEBD seul. Bien que les TPVs atteignent de bonnes propriétés en termes d'élongation à la rupture, leur comportement au moussage est très différent. En effet, l'élaboration de la mousse est principalement liée à leur viscosité sous fort taux de cisaillement et à leur condition d'extrusion i.e. la pression avant filière et la détente en sortie de filière. Avec un taux de gel de 60% de la phase élastomère, le TPV mousse de manière similaire que le PEBD. Ce TPV moussé atteint une densité de mousse de 0.54 avec une taille moyenne de bulle de 140±50 µm et une densité de cellule de 3x10⁵ cells/cm³.

En conclusion, au cours de cette thèse, nous avons développé une approche basée sur la microstructuration et la réticulation sous cisaillement d'un mélange silicone/fluorosilicone. La réticulation dynamique permet d'améliorer les propriétés élongationnelles de l'élastomère ce qui a pour effet d'améliorer l'expansion de la mousse, de limiter la coalescence et de retarder la post-relaxation. La microstructuration de fluorosilicone, quant à elle, permet d'augmenter significativement la nucléation et ainsi de réduire la taille des bulles et d'augmenter la densité volumique de bulles. La réticulation dynamique effectuée sur le mélange silicone/fluorosilicone a permis d'allier les avantages des deux stratégies précédentes. Malheureusement le procédé de réticulation dynamique est difficilement transposable à l'industrie, car il nécessite de longs temps de réaction et que la structure branchée n'est pas forcément contrôlée.

Bien que les résultats soient prometteurs, les mousses obtenues lors de l'extrusion moussage de TPV silicone sont le fruit de premiers essais et ne sont donc pas optimisées. Il est nécessaire d'étudier et d'optimiser le procédé d'extrusion moussage afin d'obtenir une réduction de densité plus importante.

Nomenclature

Abbreviations or chemical formulae

A200	Hydrophilic fumed silica
ABS	Acrylonitrile butadiene styrene
AC	Azodicarbonamide or <i>azobisformamide</i>
AIBN	2,2-Azobisisobutyronitrile
Ar	Argon
ATH	Alumina trihydrate
$B(C_6F_5)_3$	Tris(pentafluorophenyl)borane
BSED	Back-Scattered Electron detector
CBA	Chemical Blowing Agent
$CDCl_3$	Deuterated Chloroform
CFC	Chlorofluorocarbon
CH_4	Methane
C_3H_8	Propane
C_4H_{10}	Butane
CH_3COOH	Acetic acid
$(CH_3)_2SiO_x$	Poly(dimethylsiloxane)
$(CH_3C_3H_7SiO)_x$	Poly(methyl propyl siloxane)
$(CH_3C_8H_{17}SiO)_x$	Poly(methyl octyl siloxane)
$[(CF_3C_2H_4)CH_3SiO]_x$	Poly(trifluoropropyl methyl siloxane)
$(C_6H_5CH_3SiO)_x$	Poly(phenyl methyl siloxane)
$[(CH_3)_2Si(CH_2)_6Si(CH_3)_2O]_x$	Poly(silhexylene siloxane)
$[(CH_3)_2SiCH_2]_x$	Poly(dimethyl silmethylene)
$[(CH_3)_2Si-p-C_6H_4Si(CH_3)_2O]_x$	Poly(para-silphenylene siloxane)
CNT	Classical Nucleation Theory
CNT	Carbon Nanotube
CO_2	Carbon dioxide
D_3	Hexamethylcyclotrisiloxane
DBPH	2,5-Dimethyl-2,5-di(tert-butylperoxy)hexane
DCBP	2,4-Dichlorobenzoyl peroxide
DCP	Dicumyl peroxide
DSC	Differential Scanning Calorimetry
DTBP	Di-tert-butyl peroxide
d-THF	Deuterated THF
DVB	Divinyl benzene
EDX	Energy dispersive X-ray spectroscopy
EHA	2-ethylhexyl acrylate
EPDM	Ethylene propylene diene monomer
EVA	Ethylene-Vinyl Acetate Block Copolymer
FFV	Fractional free volume
FGS	Functionalized graphene sheets
FS	Fluorosilicone elastomer
FTIR	Fourier transform infrared
H_2	DiHydrogen
HCFC	Hydrochlorofluorocarbon
HDPE	High Density Polyethylene

He	Helium
HGB	hollow glass bead
HMSPP	High melt strength polypropylene
H ₂ O	Water
LDPE	Low Density PolyEthylene
LLDPE	Linear Low Density PolyEthylene
LSF	Lubricated Squeezing Flow
LSR	Liquid Silicone Rubber
MAM	Methyl methacrylate
MD	Molecular dynamic
MMD	Molar mass distribution
MVQ	Methyl Vinyl Silicone
N ₂	Dinitrogen
NaHCO ₃	Sodium Carbonate
(NH ₄) ₂ CO ₃	Ammonium Carbonate
(NH ₄)HCO ₃	Ammonium hydrogen Carbonate
NMR	Nuclear Magnetic Resonance
O ₂	Di-oxygen
OIT	Oxidation induction time
PC	Polycarbonate
PDMS	Polydimethylsiloxane
PEG	Polyethylene glycol
PE-g-AM	Copolymer PE grafted anhydride maleic
PMMA	Poly(methyl methacrylate)
PMMA-g-PDMS	Graft copolymer poly(methyl methacrylate)- Polydimethylsiloxane
PMMA-b-PFOMA	Block copolymer poly(methyl methacrylate)-1,1-dihydroperfluorooctyl methacrylate
PP	Polypropylene
PS	Polystyrene
PS-PFMA	Poly[styrene-block-perfluorooctylethyl methacrylate]
PS-PFS	Poly[styrene-block-4-(perfluorooctylpropyloxy)styrene]
PVA	Polyvinylalcohol
PVC	Polyvinylchloride
PolyHIPE	Polymerization of a High Internal Phase Emulsion
R974, R972	Hydrophobic fumed silica
REACH	Registration, Evaluation, Authorization and Restriction of Chemicals
RTV	Room Temperature Vulcanize
S	Silicone elastomer
SCFT	Self-consistent field theory
SEBS	Polystyrene-b-poly(ethylene-butylene)-b-polystyrene
SEC	Size exclusion chromatography
SEM	Scanning Electron Microscopy
SR	Silicone rubber
TGA	ThermoGravimetric Analysis
TGA/GC	TGA coupled to Gas Chromatography
THF	Tetrahydrofuran
TPE	thermoplastic elastomers
TPU	thermoplastic urethane
TPV	thermoplastic vulcanizates
TPVSi	thermoplastic vulcanizates silicone
TTS	Time Temperature Superposition
UHF	Ultra High Frequency

WLF	Williams-Landel-Ferry model
ZnO	Zinc Oxide

Symbols in arabic letters

A	Pre-exponential factor [s^{-1}]
A	Area of the micrograph [m^2]
A_n	Average diameter of the dispersed phase (Serpe Model) [m]
$a_{T/T0}$	Rheological shift factor [-]
b	Screw channel depth [m]
B	Minor axis of the ellipsoid [m]
B_f	Width of flat die exit [m]
C	Dissolved gas concentration [cm^3 (STP)/ cm^3 (pol)]
C_0	Initial gas concentration of the blowing agent (homogeneous nucleation) [$mol.m^{-3}$]
C_1	Initial gas concentration of the blowing agent (heterogeneous nucleation) [$mol.m^{-3}$]
C_1	WLF parameters [-]
C_2	WLF parameters [K]
Ca	Capillary Number [-]
d_0	Initial cell density [$cell.cm^{-3}$]
d_{cell}	Cell density [$cell.cm^{-3}$]
$d_{spacing}$	Chain-packing density [Å]
D	Diffusivity [cm^2/s]
D	Droplet deformability [-]
D	Extruder diameter [m]
D_0	Initial droplet deformability [-]
D_1	Solvent self-diffusion coefficient [cm^2/s]
D_{12}	Mutual binary diffusion coefficient [cm^2/s]
d_b	Desintegrated bubble size [m]
dP	Depressurization rate [MPa/s]
$\frac{dt}{dr}$	Cell growth rate [$m.s^{-1}$]
E	Elastic diffusion coefficient [$mol.Pa^{-1}.m^{-1}.s^{-1}$]
E_a	Activation Energy [kJ/mol]
f	Cross-link functionality [-]
f_0	Molecular jump frequency homogeneous nucleation [s^{-1}]
f_1	Molecular jump frequency heterogeneous nucleation [s^{-1}]
$f(m, n)$	Heterogeneous nucleation reduction factor [-]
$F(t)$	Compression force [N]
G'	Storage modulus [Pa]
G''	Loss modulus [Pa]
G_e	Shear equilibrium modulus [Pa]
G_N^0	Rubbery plateau modulus [Pa]
$h(t)$	Exponential profile gap in compression [m]
h_0	Sample height [m]
H_f	Width of flat die exit [m]
J_{hom}	Rate of homogeneous nucleation [$mol.m^{-3}.s^{-1}$]
J_{het}	Rate of heterogeneous nucleation [$mol.m^{-3}.s^{-1}$]
k	Boltzmann constant [$m^2.kg.s^{-2}.K^{-1}$]

$1/K_i$	Henry's constants [$\text{cm}^3/\text{kg}\cdot\text{pol}\cdot\text{atm}$]
k_p	Consistency [$\text{Pa}\cdot\text{s}^n$]
L	Roll mill gap [m]
L	Major axis of the ellipsoid [m]
L	Length of the die [m]
L/D	Length over diameter of the extruder [-]
L/D	Length over diameter of the capillary die [-]
M	Molar mass [kg/mol]
M	Magnification factor [-]
M_0	Molar mass between two consecutive vinyl groups [kg/mol]
M_e	Molar mass between entanglements [kg/mol]
m_g	Mass of a gas molecule [kg]
M_n	Number average molar mass [kg/mol]
M_w	Mass average molar mass [kg/mol]
M_z	Z-average molar mass [kg/mol]
n	Number of cells observed in a micrograph [-]
n	Pseudoplasticity index [-]
N	Number of gas molecules per unit of volume [cm^{-3}]
N_p	Density of CBA particles [particles/ cm^3]
p	Extent of the reaction [-]
p	Shear viscosity ratio [-]
P	Pressure [Pa]
P_C	Pressure of the surrounding pressure [Pa]
P_D	Pressure inside the bubble [Pa]
Pe	Permeability [cm^3 (STP) $\text{cm}/\text{scm}^2\text{cmHg}$]
P_{sol}	Solubility pressure [Pa]
Q	Melt flow rate [kg/h]
r	Bubble radius [m]
R	Gas constant [J/(mol.K)]
R	Radius of parallel plate geometry [m]
R_0	Initial spherical radius [m]
r_c	Critical nucleus radius [m]
r_s	Screw radius [m]
s	Striation thickness [m]
S	Solubility [cm^3 (STP)/ $\text{cm}^3(\text{pol})/\text{atm}$]
S_0	Solubility pre-exponential factor [cm^3 (STP)/ $\text{cm}^3(\text{pol})/\text{atm}$]
S_g	Geometric factor for nucleation calculation [-]
t	Time [s]
T	Temperature [$^{\circ}\text{C}$] or [K]
T_0	Reference temperature (TTS) [K]
$t_{1/2}$	DCP half life time [s]
t_b	DCP dispersion time [s]
T_b	Boiling temperature [$^{\circ}\text{C}$] or [K]
T_c	Critical temperature [$^{\circ}\text{C}$] or [K]
T_c	Crystallization temperature [$^{\circ}\text{C}$]
t_d	Gas dissolution time [s]
T_e	Ratio of entanglements contributing to shear modulus [-]
T_f	Fusion temperature [$^{\circ}\text{C}$]
T_g	Glass transition temperature [$^{\circ}\text{C}$]
U_1, U_2	Roll speeds [rpm]
\bar{V}	Partial molar volume [$\text{cm}^3\cdot\text{mol}^{-1}$]

v_f	free volume element between chains [nm^3]
V_f	Void fraction [-]
V_S	Volume of a mole of ideal gas at 0°C and 1 atm [m^3]

Greek symbols

α	Ratio of lubricant to sample viscosities [-]
γ	Interfacial energy per unit area between the phases [N/m]
γ_{12}	Interfacial tension between 1 and 2 components [N/m]
γ_i	Sum of dispersive and polar part of surface tension of component i [N/m]
γ_i^d	Dispersive part of surface tension of component i [N/m]
γ_i^p	Polar part of surface tension of component i [N/m]
$\dot{\gamma}$	Shear rate [s^{-1}]
δ	Lubricant thickness [m]
δ_i	Solubility parameter [$\text{MPa}^{1/2}$]
$\tan\delta$	Loss tangent [-]
Δ	Characteristic frequency separating a many-chain regime from a single-chain regime [s^{-1}]
ΔG	Free energy [J]
ΔG_{hom}	Free energy barrier for homogeneous nucleation [J]
ΔG_{het}	Free energy barrier for heterogeneous nucleation [J]
ΔH_c	Enthalpy of crosslinking [J/g]
ΔH_{oxy}	Enthalpy of oxidation [J/g]
ΔH_s	Enthalpy of solution [cal/(g.mol)]
ΔH_t	Total enthalpy of reaction [J/g]
ΔP	Pressure difference [Pa]
ε	Shear strain [-]
ε	Elongational strain [-]
ε_b	Bi-elongational Hencky strain [-]
$\dot{\varepsilon}$	Elongational rate [s^{-1}]
$\dot{\varepsilon}_b$	Bi-elongational Hencky strain rate [s^{-1}]
η_0	Zero shear viscosity [Pa.s]
η^*	Complex shear viscosity [Pa.s]
$ \eta^* $	Absolute value of the complex viscosity [Pa.s]
η^+	Transient shear viscosity [Pa.s]
η_B^+	Transient bi-elongational viscosity [Pa.s]
η_E^+	Transient elongational viscosity [Pa.s]
η_g	Viscosity of CO ₂ [Pa.s]
η_i	Shear viscosity (Maxwell Model) [Pa.s]
η_m	Viscosity of polymer matrix [Pa.s]
λ_i	Relaxation time (Maxwell Model) [s]
λ_g	Stretching ratio of the bubble [-]
λ_{PDMS}	Thermal conductivity [$\text{W.m}^{-1}.\text{K}^{-1}$]
$H(\lambda)$	Continuous relaxation spectrum [Pa]
μ	Density of cross-link bonds [mol.m^{-3}]
μ_L	Lubricant viscosity [Pa.s]
ν	Density of active elastic strands [mol.m^{-3}]
ρ	Density [g.cm^{-3}]
σ	concentration dependence of solubility [$\text{cm}^3(\text{pol})/\text{cm}^3(\text{STP})$]
σ	Surface tension [N/m]

$\sigma_B(t)$	Bi-elongational stress [Pa]
σ_S	Stress [Pa]
τ_c	Characteristic relaxation time [s]
τ_d	Droplet relaxation time [s]
ϕ_{cell}	mean cell size [m]
ϕ_i	Volume fraction of component i [-]
χ	Flory-Huggins interaction parameter [-]
χ_c	Cristallinity [-]
ω	Angular frequency [rad.s ⁻¹]
ω	Wetting parameter [-]
ω_1	Volume fraction of the solvent [-]
ω_c	Characteristic angular frequency (G', G'' crossover) [rad.s ⁻¹]
ω_s	Soluble fraction [-]
Ω	Screw rotation speed [rpm]

Mathematical symbols

[DCP]	Concentration of DCP [mol.m ⁻³]
$\frac{\partial}{\partial t}$	Differential operator of time
∇	Differential operator of space (Nabla)
∇^2	Differential operator of space (Laplacian)

Contents

Remerciements	i
Abstract.....	iii
Résumé	iv
Présentation synthétique des travaux	v
Nomenclature.....	ix
Contents	xv
Introduction	1
Part I.....	5
Chapter 1: State of Art	7
Introduction.....	11
I. General trends in polymer foaming	13
I.1. Gas sorption and diffusion	13
I.2. Cell nucleation theory	20
I.3. Cell growth and Coalescence	22
II. Chemical Foaming	26
II.1. CBA degradation	26
II.2. H ₂ and other gas.....	28
III. Physical Foaming of silicone.....	33
III.1. CO ₂ foaming	34
III.2. Physical foaming with silicone polymer/copolymer as additive	37
III.3. Solvent evaporation-induced phase separation	38
IV. Templated Silicone Foams.....	40
IV.1. PolyHIPE	40
IV.2. Supercritical drying	41
IV.3. Sacrificial template.....	41
IV.4. Syntactic foam.....	42
V. Porous silicone fabrications summary	44
Conclusions.....	49
References.....	52

Chapter 2: Materials and methods	59
I. Materials.....	59
I.1. Silicone polymers	59
I.2. Peroxide	61
I.3. Fumed silicas	62
I.4. Thermoplastic vulcanizates (TPV) silicone components.....	62
I.5. Chemical blowing agent	63
II. Materials processing.....	64
II.1. Premix procedures	64
II.2. Static crosslinking.....	65
II.3. Dynamic crosslinking.....	65
II.4. Twin screw extrusion of TPV Silicone	66
III. Foaming processes.....	67
III.1. CO ₂ batch foaming	67
III.2. Extrusion foaming	68
IV. Characterization techniques.....	70
I.1. Characterizations before foaming	78
I.2. Foam characterization	75
Part II	79
Chapter 3: Mechanisms of dynamic cross-linking of a silicone elastomer	81
Introduction.....	83
I. Experimental part.....	85
II. Results and discussions.....	91
Conclusions.....	104
References.....	105
Chapter 4: Compatibilization of Fluorosilicone/Silicone blends by dynamic crosslinking and fumed silica addition.....	109
Introduction.....	111
I. Experimental part.....	113
II. Results and discussions.....	119
Conclusions.....	129
References.....	130

Chapter 5: Fluorosilicone/Silicone blends. Part.II : Foaming behavior.....	133
Introduction.....	135
I. Experimental part.....	137
II. Results and discussions.....	141
Conclusions.....	154
References.....	155
Chapter 6: Rheology and Extrusion foaming of partially crosslinked Thermoplastic vulcanizates Silicone.....	157
Introduction.....	159
I. Experimental part.....	161
II. Results and discussions.....	170
Conclusions.....	181
References.....	182
Conclusions and outlooks.....	187

Introduction

Since the dawn of time, Nature is used to creating foam structures with for example sea sponge, cork oak or sepiolite,... According to cosmology, even our Universe might have a foam structure with the galaxies located within giant cell walls. In daily life, most people meet, without noticing, a foam when they drink a beer, they shave or they simply drive their car. But intriguingly, it is only in 1994 that the optimum structure of foam was theorized by Weaire and Phelan [1] and experimentally reproduced by Gabbrielli et al.[2] in 2012.

Fundamentally, foams are produced by incorporating gas bubbles into a solid or liquid medium such as water, metals, ceramics or polymers. On the one hand, in closed-cell foams (Figure 1-a), the gas is dispersed as discrete bubbles within the matrix which forms the continuous phase. On the other hand, if cell wall rupture occurs, the foam may have an open-cell structure as illustrated in Figure 1-b). The foam morphology and its foam density have direct impact on the foam properties. Indeed, closed-cell foams show superior mechanical, thermal insulation, shock-absorbing or fatigue properties. Alternatively, the open-cell foams are more relevant for acoustic insulation, membranes and tissue engineering applications [3].

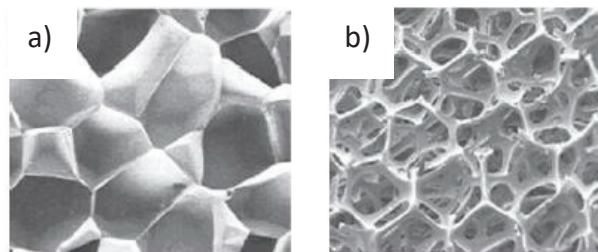


Figure 1 : Typical foam morphologies : a) Closed-cell foam ; b) Open-cell foam. Copyright © 2016. Reproduced with permission from Elsevier Ltd. [4]

Since the 40s, polymer foams are widely used in all kinds of industries for their lightness, compressibility, sealing, insulation and/or shock-absorbing properties [3]. The consumption of foam products should greatly increase in the automotive sector since the new European instructions decrees to reduce greenhouse gas emission of a car to 95 g/km for 2020 [5]. Moreover, to fulfill these new requirements, innovative foam products must be developed to replace materials usually used.

In this context, the SMOUSSIF project in 2014, aspires to develop new silicone foam products which will be used in harsher conditions than traditional foam products. Indeed, silicone foams associate the low density and good mechanical properties in compression of foams with the excellent properties of silicone elastomer such as biocompatibility, fireproof, good low and high temperature mechanical properties and weathering, chemical, thermal and electrical resistances. Therefore, silicone foams will certainly know a strong development in challenging sectors such as automotive, aeronautic or biomedical

applications. Silicone foams are perfectly suited for high-performance gaskets, heat shields, vibration dampers, prosthesis,... [6-11]. Other applications are also illustrated in Figure 2.

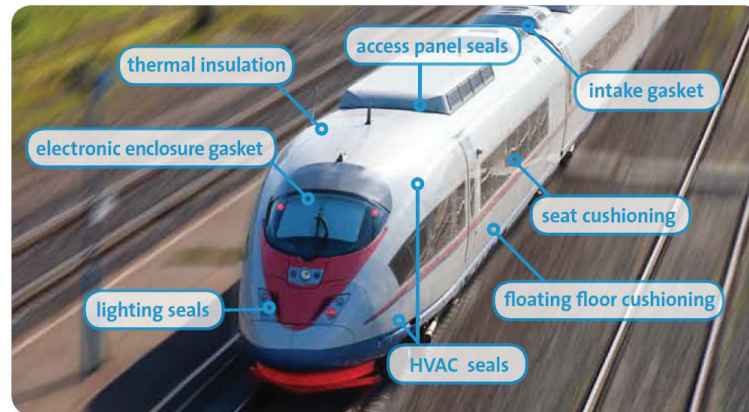


Figure 2: Silicone foam for mass transport applications [12]

Silicone foaming is usually carried out through the expansion of a gaseous phase which is dispersed in the rubber melt. Foaming silicone development involves two parallel processes: crosslinking and foaming reactions. Two conventional methods of silicone elastomer crosslinking may be used: high-temperature (peroxide) and room-temperature (polycondensation or polyaddition) vulcanizations [13]. Volatile gaseous products formed in the crosslinking reactions or by the thermal decomposition of porogens play the role of blowing agents. The main challenge in the foaming of silicone elastomer is the synchronization of these two parallel reactions to ensure the formation of a foam with excellent properties [14, 15]. From its viscoelasticity, another hard task with silicone foaming is to achieve high expansion and at the same time to be able to hinder the post-relaxation and shrinkage to generate stable foams with very low foam bulk densities. Furthermore due to its high gas permeability, most of the dissolved gas escapes to the surroundings resulting in a low nucleation and expansion [16]. Therefore, it is very difficult to achieve low density silicone foam with high cell density and low cell size.

Apart from the restrictive intrinsic properties of silicone, several parameters may also have a major effect on the foam properties. Different combinations of processing parameters, rheological and morphological properties of the formulation can impair cell structure. The foam morphology (cell size and density, porosity, bubble shapes) is mainly affected by parameters like productions' conditions (gas concentration, saturation pressure, foaming temperature,...) as well as the fillers and the elongational viscosity.

This thesis takes part of FUI SMOUSSIF project which gathers companies such as Bluestar Silicones, Serge Ferrari, RS Isolsec and Hutchinson. These firms think that silicone foams may allow the development of new products by adding new functionalities, by developing new foaming strategies or by improving the existing foams. Innovations in silicone foam formulations which can be coated, injected or extruded may also open up the scope of possibilities.

From this standpoint, the main objective of this thesis, which has started in November 2014, is to understand the fundamental mechanisms of nucleation, cell growth and coalescence while taking into account gas diffusion, crosslinking reactions and rheology in silicone elastomer. The production of silicone foam is carried out with a batch-foaming process under carbon dioxide because of the high CO₂ solubility in polydimethylsiloxane (PDMS) copolymers and its innocuousness. This theoretical study will only be conducted within the IMP laboratory. We will develop an approach based on the microstructuration and the crosslinking under shearing of a blend made of silicone and fluorosilicone elastomers. As in ThermoPlastic Vulcanizates (TPV) Silicone, at least 40wt% of the blend is composed of silicone rubber, we will also study the extrusion foaming behavior of this engineering alloy. To achieve this study, a blend of low density polyethylene (LDPE) and partially crosslinked Liquid Silicone Rubber (LSR) will be processed and foamed within the Hutchinson company Research Center.

This thesis work is organized into two main parts which are made of five chapters. The first part corresponds to the state of the art, a review in submission process. The second part gathers the main experimental works performed during these three years of thesis. It is constituted of four papers (chapters) also in submission process.

The first chapter is a complete state of art of the silicone foaming. This chapter gathers the commonly used processes to manufacture porous silicone structure and their applications. In addition, theory of sorption, diffusion, nucleation and cell growth will be detailed to explain gas foaming. The second chapter deals with the mechanisms of dynamic crosslinking (under shearing) and their impact on the rheology of dynamically crosslinked silicone elastomer. The third chapter concerns the study of a blend between a silicone and a fluorosilicone. The compatibilization of this blend will be explored using two approaches: the dynamic crosslinking and the addition of fillers. The fourth chapter is about the foaming behavior of the previous blends. In the fifth and last chapter, the extrusion foaming of TPV silicone is studied.

[1] D. Weaire, R. Phelan, A counter-example to Kelvin's conjecture on minimal surfaces, *Philosophical Magazine Letters* **69** (2) (1994) 107-110.

[2] R. Gabbriellini, A.J. Meagher, D. Weaire, K.A. Brakke, S. Hutzler, An experimental realization of the Weaire–Phelan structure in monodisperse liquid foam, *Philosophical Magazine Letters* **92** (1) (2012) 1-6.

[3] D.P.K.S. S. T. Lee, Polymeric foams: Technology and development in regulation, process and products, (2008).

[4] D. Tammaro, G. D'Avino, E. Di Maio, R. Pasquino, M.M. Villone, D. Gonzales, M. Groombridge, N. Grizzuti, P.L. Maffettone, Validated modeling of bubble growth, impingement and retraction to predict cell-opening in thermoplastic foaming, *Chemical Engineering Journal* **287** (Supplement C) (2016) 492-502.

[5] https://ec.europa.eu/clima/policies/transport/vehicles/cars_en#tab-0-0

[6] P. Liu, D. Liu, H. Zou, P. Fan, W. Xu, Structure and properties of closed-cell foam prepared from irradiation crosslinked silicone rubber, *Journal of Applied Polymer Science* **113** (6) (2009) 3590-3595.

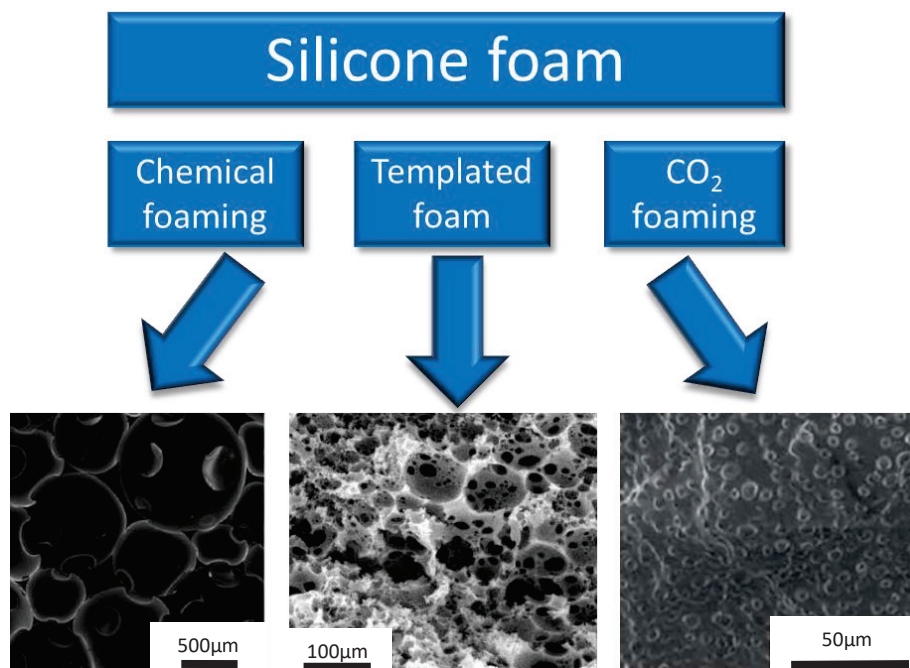
- [7] K. Zimny, A. Merlin, A. Ba, C. Aristégui, T. Brunet, O. Mondain-Monval, Soft Porous Silicone Rubbers as Key Elements for the Realization of Acoustic Metamaterials, *Langmuir* **31** (10) (2015) 3215-3221.
- [8] P. Fahr, M.Y.a. , A. Shukla, Shock response of filled corrugated sandwich structures under extreme temperatures, *Journal of Sandwich Structures and Materials* (2016).
- [9] J.P. Fuller, D. Pegg, R.M.L. Bird, T.B. Clifford, T. Clayson, Preparation of porous silicone rubber for growing cells or living tissue, 2005, US6900055 B1
- [10] M. Kessler, A. Troeger, B. Heil, A. Schnettler, Investigation of the Electrical Properties of Elastic Syntactic Foam, Electrical Insulation, 2008. ISEI 2008. Conference Record of the 2008 IEEE International Symposium on, 2008, pp. 261-264.
- [11] R. Verdejo, F. Barroso-Bujans, M.A. Rodriguez-Perez, J. Antonio de Saja, M. Arroyo, M.A. Lopez-Manchado, Carbon nanotubes provide self-extinguishing grade to silicone-based foams, *Journal of Materials Chemistry* **18** (33) (2008) 3933-3939.
- [12] <http://www.foams.saint-gobain.eu/News/SiliconeFoamsForMassTransit.aspx>
- [13] P. Lucas, J.-J. Robin, *Silicone-Based Polymer Blends: An Overview of the Materials and Processes*, Functional Materials and Biomaterials, Springer Berlin Heidelberg, Berlin, Heidelberg, 2007, pp. 111-147.
- [14] M.-C.D. Jawhar, D. Blanc, P. Chaumont, P. Cassagnau, Study of the Coalescence Mechanisms During Silicone Foaming, *Macromolecular Materials and Engineering* **299** (3) (2014) 336-343.
- [15] M.N. Shimbo, T, On foaming process of vulcanized rubber using physical blowing agent, *Proceedings of ICAD2004* (2004).
- [16] S.A. Stern, V.M. Shah, B.J. Hardy, Structure-permeability relationships in silicone polymers, *Journal of Polymer Science Part B: Polymer Physics* **25** (6) (1987) 1263-1298.

Part I

Chapter 1: State of Art

ABSTRACT

The purpose of this article is to provide an overview of manufacturing processes used in the development of cellular silicone for a wide variety of applications. The combination of intrinsic properties of silicone and foam is considered as an attractive solution in many applications. With regard to the long-standing interest of the industry in silicone chemistry, foaming is very common from hydrosilylation / condensation reactions. This well-known technology leads to homogeneous, elastic, low density and biocompatible foams. However, the size of the cells remains large, the reactions are sensitive to humidity and the dangerousness of the hydrogen could be an industrial concern. Many researches are moving towards alternatives to the manufacture of silicone cellular materials such as gas foaming, phase separation, emulsion and sacrificial models, and syntactic charges. In addition in this review, the theory of sorption, diffusion, nucleation and cell growth is detailed to explain the formation of gaseous foam. CO₂ is commonly used to physically foam silicone because of its good solubility. However, the diffusive behavior of CO₂ is high in silicone as explained by the free volume theory. Silicone-CO₂ foaming is essentially triggered by rapid depressurization leading to a cell density around 1×10^9 cells/ cm³ in the best case. In addition, templated foams are divided into emulsion polymerization (polyHIPE), sacrificial foams and syntactic foams. These methods are simple because they do not need specific devices of foaming. Pore sizes are also tunable as function of template sizes.



**Reformatted version of paper originally published in Journal of cellular
Plastics:**

New Trends in Porous Silicone: Innovations and Applications

Authors:

T. Métivier^a, P. Cassagnau^{a,*}

^a *Univ Lyon, Université Lyon1, Ingénierie des Matériaux Polymères, CNRS UMR 5223, 15 Bd Latarjet, 69622
Villeurbanne, France*

Contents

Part I	5
Chapter 1: State of Art	7
Introduction	11
I. General trends in polymer foaming	13
I.1. Gas sorption and diffusion	13
I.2. Cell nucleation theory	20
I.3. Cell growth and Coalescence	22
II. Chemical Foaming	26
II.1. CBA degradation	26
II.2. H ₂ and other gas.....	28
III. Physical Foaming of silicone	33
III.1. CO ₂ foaming	34
III.2. Physical foaming with silicone polymer/copolymer as additive	37
III.3. Solvent evaporation-induced phase separation	38
IV. Templated Silicone Foams	40
IV.1. PolyHIPE	40
IV.2. Supercritical drying	41
IV.3. Sacrificial template.....	41
IV.4. Syntactic foam.....	42
V. Porous silicone fabrications summary	44
Conclusions	49
Reference	52

Introduction

Silicones offer interesting properties from their structure. Indeed, silicone molecules are helical and their intermolecular force is very low, resulting in high elasticity, flexibility at low and high temperature and very low glass transition temperatures (T_g), around -120°C , high gas permeability, excellent dielectric properties and physiological inertness or biocompatibility [1]. Another very interesting property of the (Si-O) bond is its very high bond dissociation energy of 460 kJ/mol, when compared with the (C-O) (335 kJ/mol), (C-C) (347 kJ/mol) or even with (Si-C) (318 kJ/mol) bonds. Unusual thermal, particle radiation and oxidative stability of silicone polymers are a direct result of such a high (Si-O) bond dissociation energy [2]. Moreover, silicones have low surface tension around 24 mN/m, which is lower at 16.3 mN/m for nonafluorohexyl substituted silicones [3]. Radiation resistant and hydrophobic behaviors of silicones make them a first order choice for weathering applications [4]. Silicone chemistry is also very flexible which allows the preparation of telechelic reactive silicone oligomers with controlled molar mass, wide variety of reactive organo-functional end-groups or side-groups, and tailor-designed backbone compositions displaying a wide range of physicochemical properties [3]. The silicone's main drawbacks remain its expensive cost compared with others usual polymers when used in industry.

Foam materials are composed of a polymer matrix, a gaseous phase and optional additives such as fillers, surfactants, etc. Fillers may be under a wide variety of forms (fibrous, platelet like or spherical) and materials (metallic, ceramic, polymeric). The bubble geometry is characterized through its size and shape. Bubbles may be interconnected; foams are then classified as open-cell foams or closed-cell foams. Open-cell foams are basically used in acoustical insulation whereas closed-cell foams are more suitable for thermal insulation. Bubble size, shape and foam density affect the resulting foam properties. For example, mechanical properties are also dependent on the foam density. Indeed, micro-cellular foam has better compression properties in comparison with macro-cellular foam. Foams are classified as rigid or flexible foam depending on the glass temperature (T_g) of the polymer. For instance, structural foams would be made from a rigid polymer matrix with relatively high density and also additional reinforcing fillers while low density and closed-cell foams would be used in wall insulation applications [5].

Before the Montreal Protocol in 1987 [6], which banned some products in order to protect the ozone atmospheric layer, chlorofluorocarbons (CFCs) and hydrochlorofluorocarbons (HCFCs) were widely used in foam processing [7]. As a consequence new blowing agents, more environmentally friendly, were investigated such as CO_2 , N_2 , water,... or chemical blowing agents (CBAs). CBAs are usually added into a polymer in solid form and later activated through addition of heat. CBA release gas such as nitrogen (N_2), carbon dioxide (CO_2) or water [8]. In general, physical foaming implies a low boiling volatile liquids such as ethers, alcohols (ethanol, methanol,...) or hydrocarbons (n-heptane,

isobutane, methane...), gas like N₂, CO₂, H₂O, air, Ar... or supercritical gases [9, 10]. Physical foaming agents undergo a generally reversible physical change of state, e.g. vaporization. There are two ways to foam a material by physical foaming, batch [11] and continuous foaming [12].

Accordingly, porous materials can be created through various methods, which will be detailed in this review, such as gas foaming (physical or chemical), phase separation, emulsion templating, hollow filler templating and sacrificial templating. Gas foaming theory will be thoroughly examined through theory of sorption, diffusion, nucleation and cell growth. From these theories, nanostructured polymers with copolymers or fillers may achieve nano-foams because of their enhanced rheological behavior and their improved heterogeneous nucleation. Silicone foams are widely used in medical, shock absorbing, aerospace and many other applications, because of their combined excellent intrinsic characteristics of silicone and foam. The studies reported in this review are focused on the recent developments in the production of silicone foam. In addition, the objective of this article is to give an overview of foam silicones properties and how they can be processed.

I. General trends in polymer foaming

At the onset of chemical and physical foaming process, gas is injected or generated in a polymer medium. Gas and polymer will produce a homogeneous solution by dissolution and diffusion of the gas, if the saturation time is long enough. Foaming is triggered when a thermodynamic instability occurs, gas becomes supersaturated and bubbles are generated. These bubbles will grow and coalesce until it remains no gas dissolved into the polymer. These basic steps are applicable for physical, chemical foaming as well as for batch and continuous foaming processes. The present part describes the main factors involved in polymer foaming with a specific attention to silicone and CO₂. During the solution formation, pressure and concentration gradients are applied in the polymer medium by gas incorporation which induces two phenomena: the sorption and the diffusion of the gas within the polymer sheet.

I.1. Gas sorption and diffusion

From a thermodynamic point of view, the solubility, S , refers to the maximum absorbed gas content within a material in contact with a gaseous phase during a saturation step, at a given temperature. In our case, S represents the solubility coefficient in the Henry's Law. At a given temperature and for rubbery polymers, the dissolved gas concentration C depends on the pressure P defined by a simplified equation of the Flory-Huggins dissolution [13].

$$C = (Se^{\sigma C})P \quad (1)$$

Where $\sigma = 2\left(\frac{1+\chi}{\bar{V}/V_S}\right)$ which represents concentration dependence, χ is the Flory-Huggins interaction parameter, \bar{V} is the partial molar volume and V_S is the volume of a mole of ideal gas at 0°C and 1 atm.

Gas solubility is only dependent on the process temperature by:

$$S = S_0 e^{-\Delta H_s/RT} \quad (2)$$

Where S_0 : pre-exponential factor; ΔH_s : enthalpy of solution (negative) as shown in Table 1

Table 1: Enthalpy of solution of CO₂, CH₄ and C₃H₈ in silicone [14]

Polymer	Enthalpy of solution ΔH_s (cal/g/mol)		
	CH ₄	CO ₂	C ₃ H ₈
(Me ₂ SiO) _x	-1840	-2890	-4970
(MePrSiO) _x	-2510	-3510	-5080
(MeOcSiO) _x	-1490	-2310	-4400
(F ₃ PrMeSiO) _x	-1530	-2670	-3630
(PhMeSiO) _x	-1630	-2980	-4870

Garg et al. [15] reported the equilibrium weight fraction (gas concentration) in PDMS (Molar mass = 308 000 g/mol) versus temperature and pressure (Fig.1). As expected, gas

concentration at equilibrium increase when pressure increases. The data are correlated by two lattice-theory-based equations of state, the Sanchez-Lacombe [16-18] and Panayiotou-Vera [19] equations of state. Both models show good agreements with experimental data. According to these models, it is possible to predict swollen volume, isothermal compressibility and thermal expansion coefficient for PDMS-CO₂ mixtures.

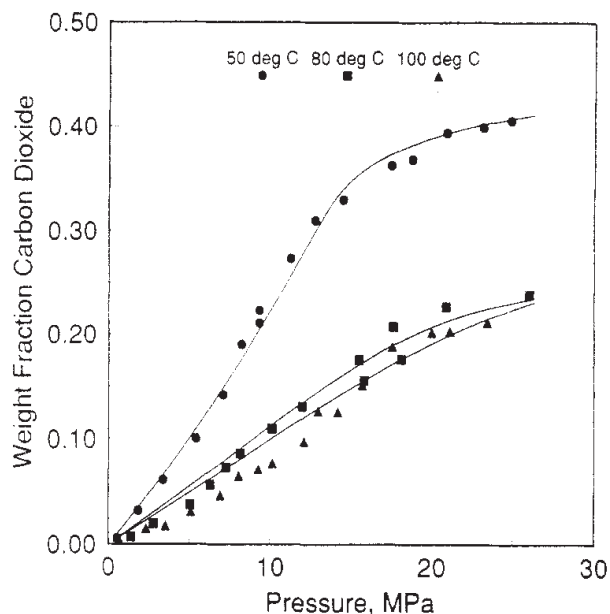


Fig. 1: Weight fraction of carbon dioxide in PDMS at equilibrium. The solid curves represent the predictions of the Panayiotou-Vera equation of state [15]. Copyright © 1994, Reproduced with permission from American Chemical Society.

When a solvent (gas) and a solute (polymer) are in contact, the Flory-Huggins parameter, χ , is calculated in order to characterize the solvent/solute affinity [20]. This interaction parameter is proportional to $(\delta_1 - \delta_2)^2$ where δ_i is the solubility parameter of the specie i . As solubility parameters are getting closer, solubility will increase. Basically, the solubility parameters can be estimated by the model developed by Hildebrand and Scott based on cohesive energy density of the solvent-solute system [21]. It was shown that gaseous CO₂ has a lower solubility parameter than supercritical CO₂ [22]. This model and those developed by Hansen [23], which takes into account hydrogen bonding, polar and dispersion interaction, are limited. Indeed, neither model includes the contribution of quadrupole moments of CO₂, which may contribute as much as 20% of the solubility parameter [24], and specific chemical interactions which increase gas solubility [25]. Flory-Huggins parameters for silicone-gas system, calculated from Henry law's coefficient [26], are given in Table 2.

As shown in Fig.1, carbon dioxide concentration increases when temperature is decreased because ΔH_s is negative for CO₂ (exothermic), an increase in the temperature causes a decrease in gas solubility [27].

The solubilities increase exponentially with the Lennard-Jones constant for the gases [28]. Gas critical temperatures, T_c , normal boiling point, T_b , are measures of condensability which correlate well with the Lennard-Jones constant [28]. For instance, in most polymers, more iso-C₄H₁₀ ($T_c=134.7^\circ\text{C}$) or CO₂ ($T_c=31^\circ\text{C}$) may be dissolved than CH₄ ($T_c=-82.1^\circ\text{C}$), O₂ ($T_c=-118.4^\circ\text{C}$), as reported in Table 2 [26-28].

As reported in Table 2, fluorinated gases are less soluble than their hydrocarbon analogues or than other gases with similar critical temperatures [29] due to unfavorable interaction between fluorinated gases and the silicone matrix. This behavior is correlated to a higher polymer–penetrant interaction parameters for fluorinated gases than those of their hydrocarbon analogues [29].

Table 2: Critical temperatures, Henry Law's coefficients, concentration dependence and interaction parameters for PDMS at 25°C [26]

Gas	T_c [30]	S	σ	χ
He	-267.96	0.028	-	5.8
Ar	-122.4	0.225	-	0.18
H ₂	-239.95	0.071	-	2.4
O ₂	-118.4	0.205	-	0.2
CO ₂	31.1	1.35	0.0043	0.65
CF ₄	-45.75	0.166	-	1.3
C ₂ F ₆	1.95	0.382	-	1.6
C ₃ F ₈	71.9	0.803	0.033	2.1
CH ₄	-82.1	0.436	-	0.09
C ₂ H ₆	32.05	2.34	0.0046	0.21
C ₃ H ₈	96.6	7.52	0.0064	0.33
Iso- C ₄ H ₁₀	134.7	64.4	0.014	0.48

Note: T_c , [$^\circ\text{C}$]; S, [cm^3 (STP)/ $\text{cm}^3(\text{pol})/\text{atm}$]; σ , [$\text{cm}^3(\text{pol})/\text{cm}^3$ (STP)]; χ , dimensionless

Permeability, Pe , of silicone rubber is controlled more by the solubility of a given gas than by its diffusivity [28] and is defined as the product of solubility, S, and diffusivity, D [31]. Diffusivity and solubility can be measured by time-lag [28], swelling technique [32] or gravimetric sorption methods [26, 33, 34].

$$Pe = D.S \quad (3)$$

Note: $P = (D \times S) / 75 \text{ cm Hg/atm}$, Units: Pe [cm^3 (STP) $\text{cm}/\text{s cm}^2 \text{cmHg}$]; D [cm^2/s]; S [cm^3 (STP)/ cm^3 (polymer) cmHg]

Gas solubility is also sensitive to specific interactions between gas and polymer molecules. CO₂, which has a quadrupole moment, has more affinity in polar polymers than nonpolar gases such as N₂, O₂. As a consequence the solubility of CO₂ increases with the increase of polar group in a polymer. Accordingly, Stern et al. [14] studied the influence of backbone and side-chain groups on the solubility of CO₂ in silicone rubber (Table 3).

Table 3: Topological silicone modifications effect on permeation for CO₂, CH₄ at 35°C [30, 34]

Polymer	d _{spacing}	T _g	$\overline{Pe}(\Delta Pe = 0) \times 10^8$		$\overline{D}(\Delta c = 0) \times 10^6$		$\overline{S}(P = 0) \times 10^2$		
			CO ₂	CH ₄	CO ₂	CH ₄	CO ₂	CH ₄	
Side chain modifications									
[(CH ₃) ₂ SiO] _x	7.99	-123	45.7	14.5	26.4	24.5	1.72	0.589	
(CH ₃ C ₃ H ₇ SiO) _x	9.1	-120	15.2	5.31	10.6	7.59	1.46	0.695	
(CH ₃ C ₈ H ₁₇ SiO) _x	-	-92	9.17	3.14	8.19	6.54	1.12	0.480	
[(CF ₃ C ₂ H ₄) CH ₃ SiO] _x	9.92	-70	12.1	2.01	5.26	5.58	2.31	0.361	
(C ₆ H ₅ CH ₃ SiO) _x	9.93	-28	2.26	0.363	2.03	1.22	1.12	0.296	
Backbone modifications									
[(CH ₃) ₂ Si(CH ₂) ₆ Si(CH ₃) ₂ O] _x	-	-90	13.1	3.95	11.5	8.85	1.14	0.446	
[(CH ₃) ₂ SiCH ₂] _x	7.23	-92	5.42	1.30	4.59	3.22	1.18	0.405	
[(CH ₃) ₂ Si-p-C ₆ H ₄ Si(CH ₃) ₂ O] _x	-	-18	0.523	0.104	0.753	0.444	0.695	0.234	

Units: \overline{Pe} [cm³ (STP) cm/scm²cmHg]; \overline{D} [cm²/s]; \overline{S} [cm³ (STP)/cm³ (polymer)cmHg], T_g [°C], d_{spacing} [Å]

They found the best CO₂ solubility in the silicone rubber with fluorine groups, poly(trifluoropropylmethylsiloxane) because this side group produces specific interaction with the penetrant gas [35]. It is assumed that fluorine atoms play the role of a Lewis base with the electron-deficient carbon of CO₂, acting as Lewis acid which is confirmed through high pressure ¹⁹F nuclear magnetic resonance (NMR) studies [36]. At the same time, fluorine atoms induce positive charges in nearby hydrogen atoms which may interact with the gas oxygen atoms as Lewis acids [37]. Another hypothesis could be that there is a weak complex between fluoropolymers and CO₂ [38]. Acrylate and acetate polymers also have strong interactions between carbonyl oxygen and carbon atom of CO₂ through Lewis acid/base interactions. Lewis acid/base interactions were detected by Fourier transform infrared (FTIR) spectroscopy between carbonyl group of PMMA and CO₂ [36]. Thus, the addition of carbonyl groups lowers the miscibility pressures of silicones in CO₂ for surfactant application by improving enthalpy of mixing [39]. Mertdogan et al. [40] concluded that a polymer should exhibit polarity upon fluorination, to create favorable dipole-quadrupole interactions, thus shielding quadrupole-quadrupole interactions between two CO₂ molecules thus lowering energy of mixing. The position of the polar groups in the chain is an important factor for solubility data. Indeed, poly(vinyl acetate) and poly(methyl acrylate) are isomers but their phase behavior in cloud point experiments are different [39]. According to Kirby and McHugh [41], CO₂ solubility in polydimethylsiloxane is high because its high free volume available. With this point of view, as the amount of carbon dioxide dissolved increases, solubility would increase because free volume will increase. That was observed by Stern et al. [35] under 10°C but not for temperature above 35°C under the pressure range explored. Concentration dependence of solubility in Henry's Law is useful for highly soluble gases like CO₂ but it is possible to see that σ_{CO_2} (Table 2) is low indicating little dependence of gas solubility on gas concentration. Concentration dependence will increase as solubility increase or, in other words, when condensability increases and temperature decreases (Table 2). Data reported in Table 3 are extrapolated to P=0 in order to remove plasticization

effect (solubility coefficients are dependent to pressure). With backbone and side-chain modifications, T_g is increased, reducing segmental motion, reducing permeability of these silicones (Table 3). $[(CH_3)_2Si-p-C_6H_4Si(CH_3)_2O]_x$ is also semi-crystalline which is not the case for its isomer meta. Its crystallinity could explain, in some part, its very low permeability because crystalline domains are known to increase tortuosity and decrease chain mobility [31]. Stern et al.[35] concluded that the substitution of methyl chains by bulkier groups decreases the solubility of the gases in PDMS. They also concluded that the substitution of bulkier group in the side chains seems to have greater effect than the substitutions of the same groups in the polymer backbone. Silicone backbone is extremely flexible ($T_g = -120^\circ C$), this may also allow easier access to the Lewis base groups by CO_2 or simply a higher entropy of mixing [42]. Silicones have a low solubility parameter pointing to weak solute-solute interactions [39]. According to O'Neil et al. [43], solubility is governed primarily by polymer-polymer interactions, while polymer- CO_2 interactions play a secondary role. So, CO_2 will be soluble in a polymer with weak interactions between polymer chains like silicone [44].

Since foaming process requires fully saturated polymers, the gas uptake is essential. The sorption time must be sufficient to polymer/gas equilibrium and is dependent on gas diffusion within the polymer. The Fick's second law describes the transient regime of diffusion which appears in a polymer material under high gas pressure. The diffusion coefficient in polymeric and non-homogeneous systems varies from point to point and largely depends on the concentration. During the transports of the penetrants through and in polymer swelling occurs, especially for PDMS at room temperature under high pressure [32, 45]. The polymer is deformed because of osmotic stress leading to non-Fickian diffusion. The modified transport equation becomes [46, 47].

$$\frac{\partial C}{\partial t} = \nabla \cdot (D_{12} \nabla C) + E \cdot \nabla^2 \sigma \quad (4)$$

Where C is the gas concentration within the polymer material and D_{12} is the mutual binary diffusion coefficient. E is the elastic diffusion coefficient associated with the stress, σ .

In the case of a polymer/solvent system, the polymer/solvent binary mutual diffusion coefficient, D_{12} , varies during the saturation stage, especially because of the polymer plasticisation by the solvent [48, 49].

$$D_{12} = D_1 f(\chi, \omega_1) \quad (5)$$

Where D_1 is the solvent self-diffusion coefficient, ω_1 is the volume fraction of the solvent, χ is the Flory-Huggins interaction parameter.

The solvent self-diffusivity may be explained and predicted by the free volume theory developed by Vrentas and Duda (48-50). From this theory, the free volume is directly linked to $T - T_g$. Silicone backbone is very flexible due to the mobility of the Si-O bond as compared to the C-C or C=C bond in other polymers [28]. As a result in silicones, T_g is very low ($T_g = -$

120°C) so there is a large free volume element between chains, v_f (Table 4) and, in turn, naturally increases diffusivity or permeability [50, 51], as shown in Table 3.

Table 4 : Free volume element as estimated by hydrogen and deuterium transport through elastomeric films [52]

Elastomer	$v_f(\text{nm}^3)$
Polydimethylsiloxane	0.15
Polyurethane	0.022
Poly-cis-isoprene	0.038
Poly (ethyl methacrylate)	0.026

Robb et al. [28] found that the CO_2 coefficient of diffusion is nearly equal to self-diffusion coefficient of a dimethylsiloxane with three Si atoms. This suggests that the volume needed for a carbon dioxide molecule to jump from one hole to another one is available when the motion of a silicone chain segment of about three monomer units in length is possible [28]. Samples of vinyl-silicone rubber were irradiated under several doses. It is estimated that 10^8 roentgens will form one crosslink every 50 monomer units, neither swelling experiments nor crosslinking data were reported. While this is sufficient to considerably change the viscoelastic properties of the rubber, it appears to have had little effect on permeation [28] which is consistent to Vrentas et al. formalism [52]. As crosslinking does not influence the solubility, the change in the permeability becomes therefore from the modification of the diffusivity [53].

In Table 3, the substitution of functional groups in the polymer side chains or backbones decreases the diffusivity of all penetrants, in a greater extent than solubility, because it increases significantly their T_g by lowering chain flexibility even though the chain-packing density (as reflected by the d-spacings) increases. The substitution of functional groups in the side chains appears to have a greater influence in decreasing the penetrant diffusivity than the substitution of such groups in the polymer backbone [35].

The dependence of diffusion coefficient on penetrant size is characterized by the Van der Waals volume of the penetrant. In general, diffusion coefficients decrease with increasing penetrant size (Table 5). The transport of small, asymmetric molecules is assumed to proceed with diffusion jumps of the penetrant through a polymer occurring principally parallel to the long axis of the penetrant [27, 54]. H_2 and He, which have low solubility in PDMS from their low T_c , have higher permeability than N_2 (higher T_c) because of their high diffusivity or small molecular size [31].

Table 5 : Solubilities and diffusion rates of gases in silicone rubber [28]

Gas	T [°C]	D x10 ⁶
He	28	60
H ₂	27.5	43
CH ₄	27.5	12.7
N ₂	28	15
O ₂	27.4	16
Ar	27.5	14
CO ₂	27.6	11
C ₄ H ₁₀	26	~5

The results in terms of carbon dioxide permeability, diffusivity and solubility are summed up and homogenized in order to compare poly(dimethylsiloxane) to common polymers (Table 6). We tried to keep polymers which obey to Henry's law, at least in the interval of measurement. Some are semi-crystalline so their permeability is obviously smaller because of their crystal domains. To sum-up, PDMS is one of the most permeable polymer because of its extraordinary chain flexibility, large free volume elements and specific interactions with carbon dioxide.

A very effective way to determine if CO₂ will have a good solubility in a polymer is to consider the surface tension of that polymer. Indeed, the surface tension is related to the work of cohesion, which is in turn related to the cohesion energy. Silicone-based polymers have very low surface tension in general so it is not surprising that CO₂ is highly soluble in silicone as compared to other common polymers (Table 6).

Table 6: Carbon dioxide transport properties in polymers

Polymer	T [°C]	Pe x10 ⁹	D x10 ⁶	S x10 ²	T _g (°C)	Ref.
Polyvinylchloride	25	0.149	0.00125	0.195	80	[55]
Polyurethane	28	1.6	1.9	0.1133	31	[56]
Polyisoprene	28	17	15	0.0842	-68	[56]
Polyoctenamer	28	10	6	0.1667	-23	[56]
Poly(dimethylsiloxane)	28	323	11	2.9	-125	[28]
Acrylonitrile-Butadiene-Styrene	25	0.522	0.0022	2.35	109	[57]
Polysulfone	35	0.56	0.02	2.7	185	[58]
Polytetrafluoroethylene (χ _c =60%)	25	1.17	0.095	1.23	-100	[59], [60]
Poly(vinylidene fluoride) (χ _c =50%)	70	0.647	0.098	0.66	-36	[61], [62]
Low Density Polyethylene (χ _c =35%)	40	2.93	0.67	0.44	-118	[62], [63]
High Density Polyethylene (χ _c =66%)	40	0.733	0.4	0.19	-102	[62], [63]
Polyamide 11 (χ _c =24%)	71	0.308	0.1	0.31	50	[62], [64]

Units: Pe [cm³ (STP) cm/scm²cmHg]; D [cm²/s]; S [cm³ (STP)/cm³ (polymer)cmHg]

I.2. Cell nucleation theory

After sorption/diffusion stages, foaming begins by cell nucleation triggered by thermodynamic destabilization and followed by cell growth. Basically, classical nucleation theory (CNT) is often used to explain the mechanisms of cell formation from a thermodynamic point of view only.

Classical Nucleation Theory (CNT) originated in 1930s and defined the concept of critical radius. In the classical approach, the energy of a system, which is about to bubble nucleate, can be expressed by Eq. (6) where ΔP is the pressure difference between P_D (pressure inside the bubble) and P_C (pressure of the surrounding pressure), r is the nucleus radius and γ is the interfacial energy per unit area between the phases.

$$\Delta G = -\frac{4\pi r^3}{3}\Delta P + 4\pi\gamma r^2 \quad (6)$$

Using Eq. (6), it's possible to define the critical radius as an unstable extremum of the function, Eq. (7). When the gas cluster has a radius lower than r_c , it will collapse; but if it has a radius higher than r_c , it will grow to become a bubble [65].

$$r_c = \frac{2\gamma}{\Delta P} \quad (7)$$

Combining equations above, the free energy barrier for homogeneous nucleation, ΔG_{hom} , is:

$$\Delta G_{hom} = \frac{16\pi\gamma^3}{3\Delta P^2} \quad (8)$$

The rate of homogeneous nucleation J_{hom} can be defined by:

$$J_{hom} = f_0 C_0 e^{-\frac{\Delta G_{hom}}{kT}} \quad (9)$$

Where C_0 is the initial gas concentration of the blowing agent in the polymer before depressurization and f_0 is the frequency in which the addition of one more gas molecule to a critical nucleus will convert it to a stable nucleus. f_0 is equivalent in the steady state nucleation model to the product of the Zeldovich non-equilibrium factor and the molecular jump frequency [66-68]. As regards latter equations, an increase in saturation pressure will increase the amount of carbon dioxide dissolved, reduce the energy level needed to enable nucleation and improve nucleation rate. That was found to be true in most studies [69].

Furthermore, a polymer in carbon dioxide has a lower surface tension than that of the pure polymer. The Gibbs free energy will be reduced by the cubic power of the surface tension, and the nucleation rate will increase exponentially. Therefore, the surface tension has crucial impact on polymer foaming processes. For example, Li et al. [70] and Park et al. [71] found, that the surface tension of polystyrene (PS) and polypropylene (PP) decreases

with increasing the pressure and the temperature. The interfacial tensions in polymer/CO₂ and polymer/polymer systems decrease significantly with increasing CO₂ pressure especially for PS. The interfacial tension was depressed dramatically in the pressure range up to 7 MPa from around 24 to 14 mN/m and then decreased at a much lower rate as the pressure further increased. For PP samples, the interfacial tension decreases rapidly in the pressure range up to 500 MPa, and then levels off. The interfacial tension decreases by more than 20%.

Furthermore, the heterogeneous nucleation is of importance in polymer foaming. Actually in terms of polymer formulations, fillers, impurities, residual catalyst, etc. are imbedded in polymers. Then, they will bring forth heterogeneous nucleation, in addition to homogeneous nucleation [72]. Indeed, the presence of these centers of nucleation decreases the free energy needed by a reduction factor, $f(m, n)$ [73]. Therefore nucleation will be much promoted as $\Delta G_{het}(r_{c,het})$ is lowered and can be expressed as [74]:

$$\Delta G_{het} = \Delta G_{hom} \frac{f(m, n)}{2} \quad (10)$$

The rate of heterogeneous nucleation J_{het} can be defined by:

$$J_{het} = N^{2/3} S_g \sqrt{\frac{2\gamma}{\pi m_g f(m, n)}} e^{-\frac{\Delta G_{het}}{kT}} = f_1 C_1 e^{-\frac{\Delta G_{het}}{kT}} \quad (11)$$

Where m is the mass of a gas molecule, N is the amount of gas molecules per unit of volume, S_g is a geometric factor [68]. C_1 is the initial gas concentration of the blowing agent in the polymer before depressurization and f_1 is similar to f_0 as expressed in Eq. (9) [66].

$f(m, n)$ varies as a function of the surface characteristics, more specifically the contact angle and surface curvature [66, 73-75]. Typical inorganic and organic fillers used in polymers are: alumina, calcium carbonate, clays, ferromagnetic particles, gypsum, mica flakes, quartz, talc, diatomaceous earth, silica, titanium dioxide, carbon black, glass fibers, kaolin, graphene, nanotubes... Another strategy to take advantage of heterogeneous nucleation is to use block copolymers for the melt nano-structuration. Indeed, nano-structuration may prevent the formation of microcells by limiting the foaming in a dispersed phase more-CO₂philic embedded in the surrounding polymer matrix. This strategy of the control of the heterogeneous nucleation by nano-structuration has been recently reviewed by Costeux ([76, 77]).

Classical nucleation theory enables to highlight and to gauge main parameters governing the foaming process namely critical radius, system-free energy, nucleation rate but most of the time this theory fails to predict experimental results. For example, it was observed that level of supersaturation was much lower in the case of the extrusion foaming [78]78. It is well known that in the die, polymer flow undergoes a combination of extensional and shear stresses [78]. Chen et al. [79] designed a set-up that apply a shear rate until 400s⁻¹

during the foaming step of filled or unfilled PS. When shear stress is applied, cell density may step up to one decade more. When shear stress contribution is added into free energy calculation (by using capillary number), experimental and theoretical results are well fitted. They also concluded [80] that shear stress becomes a significant parameter when supersaturation level is insufficient for cell nucleation. With lower supersaturation level, it is possible to keep the same cell density by applying shear stress. As elongational flow is predominant at the entrance of extruder die, Wong et al. [81] built an experimental set-up which enables in-visualization of the effects of extensional stress on the foaming behavior of PS. Extensional flows also have positive effects on the foaming. To explain shear and extensional strain induced nucleation, local pressure variation in the nearby volume of the bubble or filler particle needs to be taken into account [82]. Indeed, bubble expansion may induce tensile stresses that cause a decrease in local pressure. In this case, local pressure is not anymore equal to the system pressure leading to a higher supersaturation and a secondary nucleation of microbubbles in the surroundings of the pre-existing bubble [83]. Some researchers assume that nucleation may be enhanced by pre-existing gas cavities at the surface of fillers or of the equipments. These gas cavities may be the result of rough or porous surface of nucleating agents which is not perfectly wetted by polymer melt (high viscosity and high contact angle) [84-86]. As shown by Lee [84], shear stress may also speed up the extraction of gas from their cavities, thus enhancing nucleation rate.

More recent theories have been developed to replace classical nucleation theory. Kim et al. [87] compared self-consistent field theory (SCFT), a mechanical statistical approach, with CNT. Where CNT failed to predict cell density in nanocellular foam, because the curvature of the bubble is on the same order of size, SCFT enables to predict the upper limit for cell density for whatever foaming conditions, nano or conventional foams. The latest and most accurate theory is density-functional theory. It has been developed to study nucleation in polymer-CO₂ mixtures in the presence of nanoparticles and polymer-polymer-CO₂ mixtures [88]. Thanks to this theory, the formation of CO₂ gas bubbles is found to be a two-step process: a CO₂-rich nucleus is first in a state where CO₂ is in the liquid state. With further nucleation or growth the nucleus becomes a CO₂-rich gas region [88].

I.3. Cell growth and Coalescence

Once a nucleus is generated, its growth occurs by diffusion of gas from the swollen polymer matrix. Cell growth is described by the laws of mass and momentum transfer applied to polymer-gas systems. Consequently, system properties such as viscoelasticity and diffusivity, will govern the growth and coalescence of the cellular structure by affecting the kinetics of mass and momentum transfers.

$$\frac{dr}{dt} = \frac{r}{4\eta_{matrix}} \left(\Delta P - \frac{2\gamma}{r} \right) \quad (12)$$

Where $\frac{dr}{dt}$ is the cell growth rate; η_{matrix} is the viscosity of polymer matrix and r , the distance from the center of the bubble.

Mass transfer of gas at the gas-polymer interface of the bubble is generally expressed as follows [89]:

$$\frac{d}{dt} \left(\frac{4\pi r^3 P_D}{3 RT} \right) = 4\pi r^2 D \frac{\partial C}{\partial r} \Big|_{r=R_i} \quad (13)$$

Where P_D is the bubble inner pressure, R is the gas constant, r is bubble radius, D is diffusion coefficient and C is the gas concentration. Other expressions can be found in [89-91].

At a polymer–bubble interface, the gas exerts a stress on the polymer in function of P_D , then the polymer flows and bubbles expand until a bubble reaches its equilibrium state when $P_D = P_c$. Hence, the gas expansion is only due to the difference between the gas pressure and the ambient pressure. During the foam expansion step, capillary number, Ca , is far greater than 1, and then the surface tension effects can be neglected (in molten polymers) [92].

Taki [89] made a simulation of simultaneous bubble nucleation and growth was performed for a batch physical foaming process of polypropylene (PP)/CO₂ system under finite pressure release rate. These results showed that equilibrium between the pressure release rate and the consumption rate of the foaming agent by the growing bubbles determines the maximum bubble nucleation rate. An increase in the pressure drop rate causes an increase in the bubble growth rate. As shown in Fig. 2, before coalescence, cell growth is first controlled by the matrix viscosity and then by gas diffusion. As reported by Tuladhar et al. [93], higher diffusivity decreases the time to complete growth.

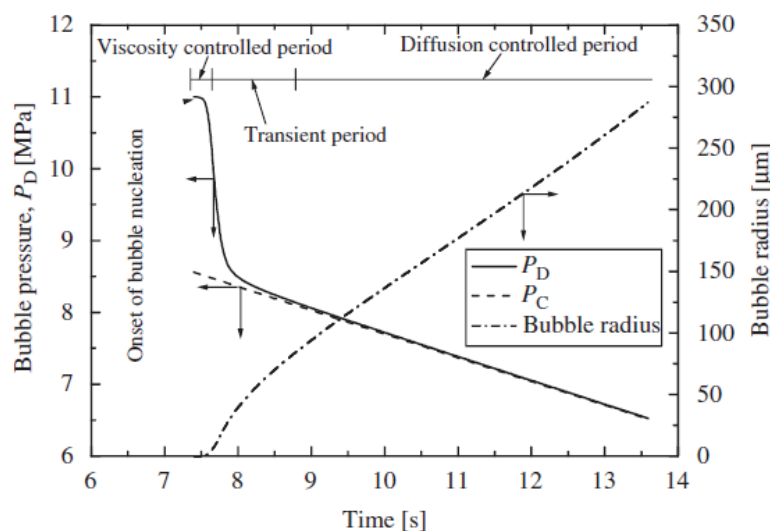


Fig. 2: Bubble pressure and radius evolution along foaming time [98]. Copyright © 2008. Reproduced with permission from Elsevier Ltd.

As previously discussed, PDMS is the most permeable polymer. This behavior has a fundamental impact on the CO₂ foaming of silicone. Indeed, Leung et al. [65] has demonstrated that an increase of diffusivity only by 1.5 times affects greatly bubble growth and collapsing. Bubble growth rates will be increased with a higher diffusivity which induced that more gas will be gathering in the gas-rich volume around the bubble. Higher bubble growth rate brings forth higher gas depletion rates. Bubble collapse will also happen earlier and faster. Due to this high permeation rate compared with other polymers; silicone foams have never achieved sub-micron bubble size.

The matrix viscosity depends on polymer molecular structure, temperature and content of dissolved CO₂ and is believed to be a main parameter to limit cell growth [69, 94]. However, the elongational viscosity is more relevant than the shear viscosity because cell growth induces biaxial elongational stress [95]. Dissolved gases may lower the viscosity of molten polymers through two mechanisms. The first mechanism is the dilution of chain entanglements when a solvent is added [15]. This is predicted by De Gennes [96], who defined a characteristic frequency $\Delta \sim c^{2.25}$, c polymer concentration, separating a many-chain regime from a single-chain regime. The second mechanism entails the addition of free volume; this mechanism depends directly on the mixture density [15]. The second mechanism seems to be the predominant mechanism for viscosity reduction in PDMS upon swelling [97]. Cell growth may also be stabilized by the Joule-Thomson effect resulting from the rapid expansion of CO₂ in the cells, during the fast depressurization, inducing a rapid decrease of the temperature in the foam [76]. However this mechanism was not fully demonstrated. In addition the viscoelastic behavior of polymer melts is not taken into account in equation (12). When a bubble rises in viscoelastic liquids, the bubble shape is ellipsoidal because of normal stress differences coming from nonlinear viscoelastic elongational flow around bubbles [98]. Some simulations tried to implement viscoelasticity by considering an unique cell surrounded by a shell of viscoelastic fluid with a finite volume [65, 89, 99, 100].

In a batch-foaming process, matrix viscosity can be drastically increased by setting nucleation temperature near or below T_g . This strategy is mainly used for nanofoaming. According to [101], cell density is optimum when foaming temperature is between the polymer/gas T_g and the neat polymer T_g .

High values of melt strength are desired in processes where the material is stretched in its molten state, such as in film blowing, thermoforming and foaming. High melt strength is associated to the strain hardening of the elongational viscosity. Some experimental results have clarified that a material that shows marked strain-hardening in uniaxial elongational viscosity also exhibits strain-hardening in biaxial viscosity [102]. The rheology of a polymer melt is strongly affected by its molecular architecture: chain branching, molar mass distribution (MMD) and addition of weakly crosslinked polymers. A broad or bimodal MMD can cause strain hardening in the melt elongational viscosity because it increases the

entanglement density and improves the network connectivity. This has been shown by Takahashi et al. [103] for blends of low and ultra-high molar mass PMMA and blends of polybutadienes. Forest et al. [104] blended two PMMAs with different molar masses in order to make a compromise between a viscoelastic liquid and a solid viscoelastic behavior of the matrix. Thanks to that, they kept low cell size, high cell density and succeeded in lowering foam density by almost 2.

If the nucleation stage is well controlled, a large number of nuclei are achieved. But the final cell density of foams may not be the same as the initial nuclei density because of cell coalescence. Cell coalescence is thermodynamically promoted because coalescence reduce the total surface area of cells [105]. When two bubbles approach each other, a thin liquid film of the continuous phase is formed. The coalescence rate depends upon the rate at which the liquid drains. At some critical film thickness, instability develops and the film ruptures [106]. Rodeheaver et al. [67] developed a bubble coalescence model in PS foaming with nitrogen. They took into account the three main forces acting on the free film between two bubbles when coalescence happens i.e. internal bubble pressure, calculated from Young Laplace equation, Van der Waals disjoining pressure, interaction between the molecules within the film, and electrostatic pressure, accumulation of particles within the film if particles are used. The film will break if thinning pressures are greater than thickening pressures. Film rupture occurs from the local effects of waves, developed from thermodynamic instabilities, which propagate on the surface of the film. These waves create locally thinner region and high curvature regions in their trough leading to locally larger internal pressure. According to their model, they were able to estimate the time required for the film to break. They also reported that as the film thins velocity thinning rates get faster. Coalescence will dominate at roughly $Ca \leq 10^{-1} - 10^{-2}$, which described the final stage of bubble growth [107]. Bubbles coalescence could be classified into four distinct patterns in terms of deformation dynamics of the interface and shape of the coalescing bubbles in polypropylene (PP) foam created by physical foaming with CO₂. The biaxial elongational viscosity is one of the key parameters in determining the coalescence patterns [98].

During a shaping process such as extrusion foaming, the shear field generated tends to stretch nucleated bubbles, and this will further accelerate cell coalescence [108]. Park et al. [108] proposed a means for suppressing cell coalescence by increasing the melt strength of polymer via temperature control in microcellular extrusion processing. The melt strength of polymer can be enhanced by branching, crosslinking, temperature reduction, control of molar mass and molar mass distribution, and blending of polymers and compatibilisation of blends [105].

To conclude and as shown in this part, polymer foaming is dependent of plenty of parameters such as process parameters, initial microstructure, polymers or additives used... According to theories, cell nucleation and cell growth have to be effectively controlled to produce homogeneous foam with low cell size. Compromises should be found between high

nucleation rate provided by a great thermodynamic instability (high temperature and pressure gradients), high content of blowing agent dissolved and a controlled cell growth to prevent macro-cells inside the foam. Besides, cell growth and coalescence have to be restricted by the surrounding polymer/gas matrix. This surrounding medium viscosity plays an important role but is not fully understood especially strain hardening effects and the modeling of cell growth and coalescence remain difficult.

CO₂ solubility in poly(dimethylsiloxane) is high due to its high free volume available and its low polymer-polymer interactions. Yet, silicones have gas diffusion coefficient of about 10⁻⁵ cm²/s which can be one to three decades more than common polymers, such as LDPE, PVC, ABS, PC. This special behavior brings forth important consequences on foaming. Foaming is extremely dependent on blowing agent solubility and diffusivity in the polymer used as described through nucleation rate, cell growth and mass transfer equations. Cell growth and coalescence rates are viscosity-controlled and diffusion-controlled. High gas concentration and diffusivity will lead to a matrix viscosity reduction and to faster mass transfers.

II. Chemical Foaming

Chemical foaming consists in blending a polymer with chemical blowing agents (CBAs) or by a side reaction between two chemical groups which produces a gas. CBAs are the most used in extrusion foaming process because their use needs limited modifications of the preexisting equipment. But silicone foaming is mainly carried out by two simultaneous side reactions. Silicone rubbers are mainly foamed and crosslinked at the same time. The synchronicity between both reactions is crucial to obtain foam with good properties.

II.1. CBA degradation

CBAs are usually added directly into the melt. By increasing temperature, CBA are activated and released gas. There are two kinds of blowing agent, exothermic and endothermic ones. Exothermic blowing agents, such as azobisisobutyronitrile, and azodicarbonamide [109], generally produce N₂ during their decomposition whereas endothermic ones, such as sodium bicarbonate, ammonium carbonate and ammonium hydrogenocarbonate, citric acid or citrates, generate CO₂. Endothermic blowing agents are now preferred because they released less toxic by-product during their decomposition, as referred to REACH regulations. On the contrary, existing acid/carbonate blowing agent may generate corrosive by-products [110]. Another disadvantage associated with existing acid/carbonate blowing agents is premature reaction with water or moisture of the blowing agents when they are associated with polymeric reaction mixtures[111]. For silicone rubber foam, chemical blowing agents have to be dispersible before foaming and do not interfere with the crosslinking reaction. The selected CBA also needs to decompose into a suitable gas near the optimum crosslinking temperature. Silicone rubber foam made from this technique

may be used for pads in plastic or metal forming equipment or localized scleral indentation treatment of retinal detachment of the eye [112].

Park [113] prepared silicone foams in the presence of several peroxide (DCBP, DTBP, DBPH) and AIBN (2,2-azobisisobutyronitrile), a blowing agent releasing nitrogen by thermal decomposition. When the peroxide concentration increased, the hardness, tensile strength of silicone foams are increased whereas the cell size and elongation at break are decreased. It was then observed that cell sizes decrease with an increasing crosslinking density due to less relaxation of chains and a matrix viscosity change. Foam density also increase when peroxide amount increases. This is linked to the decrease of expansion ratio limited by matrix viscosity. Foaming ratio and cell size also are directly linked to peroxide half-time. The shorter half-time is the lower cell size and foaming ratio.

Gao et al. [114] foamed and cured silicone rubber with (N,N'-dinitrosopentametylenetetramine) as blowing agent and carbamide as a promoter. They compared the foaming behavior of hollow glass bead (HGB) and nano-silica filled silicone rubber foams through thermal conductivity and mechanical properties. HGB filled silicone rubber foams achieved lower thermal conductivity as compared to silica filled silicone rubber foams due to their lower density, high cell size (500 μ m) and intrinsic thermal properties of HGB. Nanosilica filled and foamed samples obtained better mechanical results because of higher reinforcement of nanosilica, nucleation efficiency of nanosilica, homogeneous cell structure.

According to the invention detailed in [115], an extruded foamed silicone can be obtained at room temperature. Silicone is blended with acetic acid as promoter and ammonium bicarbonate as blowing agent, as described in Fig. 3. Silicone rubber is also crosslinked by condensation and water produced by ammonium salt degradation to complete reaction between silicone and crosslinker. The ammonium salt component can be adjusted to control the degree of foaming and the acetic acid amount can be adjusted to control the curing rate.

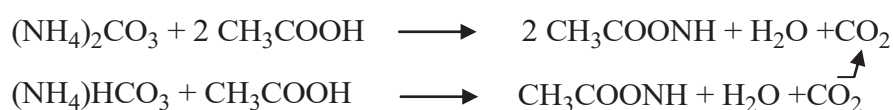


Fig. 3 : Ammonium salt and acetic acid foaming mechanism [115]

Silicone foams containing ammonium carbonate or ammonium hydrogen or alkali hydrogen carbonates and UHF-active substances can be generated by means of ultra-high frequency waves [116].

Silicone rubber foam was prepared through crosslinking with electron beam irradiation and foaming by the decomposing of blowing agent azobisformamide and its promoter, ZnO, in hot air [117]. The crosslinking and foaming of silicone rubber was carried out separately. With the increase of irradiation doses before foaming from 10 to 17.5 kGy,

the foam density increases. As the cell density is rather constant, the number of cells effectively nucleated is not sensitive to the irradiation level, but the resulting viscosity increase from crosslinking prevents full expansion of the cells (Table 7).

As discussed before, cell density only increase because of limitation of coalescence. As the content of azobisformamide increases, the gas yield increases leading to more bubbles and a lower density. High contents of silica are also added in order to increase viscosity, nucleation and maybe to lower the CO₂ diffusion. They also performed irradiation after foaming in order to improve foam density and mechanical properties mostly compression set.

Table 7 : Effect of irradiation dose before foaming MVQ/fumed silica/hydroxyl silicone oil/ AC=100/25/4.3/10, irradiation dose after foaming 30 kGy. Reproduced as it has been published. Copyright © 2009, Reproduced with permission from John Wiley and Sons. [117]

Irradiation dose before foaming (kGy)	d ₀ (cell/cm ³)	d (cell/cm ³)	Average cell size (μm)	Foam density
10	1.68x10 ⁸	4.86x10 ⁷	30	0.33
12.5	1.71x10 ⁸	7.88x10 ⁷	25	0.45
15	1.76x10 ⁸	9.56x10 ⁷	21	0.59
17.5	2.23x10 ⁸	1.29x10 ⁸	18	0.60

Liu et al. [118] presented the effect of neutron and gamma irradiation in the presence of air and nitrogen on silicone foam properties which are relevant for aerospace and nuclear plant applications where plural radiation coexist. In this paper, the foaming agent used is N,N'-Dinitrosopentamethylenetetramine which releases dihydrogen. The main results are that there is little effect of irradiation on foam morphology, with cell size of hundreds of microns; irradiation leads to higher crosslinking density and therefore lower elongation at break and lower crystallinity. The stiffening of the rubber foams was caused by cross-linking reactions in the Si-CH₃ [119].

II.2. H₂ and other gas

Silicone foams have been mainly produced by dihydrogen gas production since inventions have been patented by Dow Corning in 50's [120, 121]. Room Temperature Vulcanize (RTV) silicone foam can be produced in using a bi-component Liquid Silicone Rubber (A and B) (Fig.4)[121]. Silicone chains are crosslinked by addition catalyzed by platinum complexes or tin salts [120-122], in parallel it reacts with alcohol, silanol and so on in order to generate H₂ and bring forth foaming [123]. Reactions can be activated by heat or microwave (124). RTV foams keep good properties over a wide temperature range (-75-200°C), resist weathering and aging.

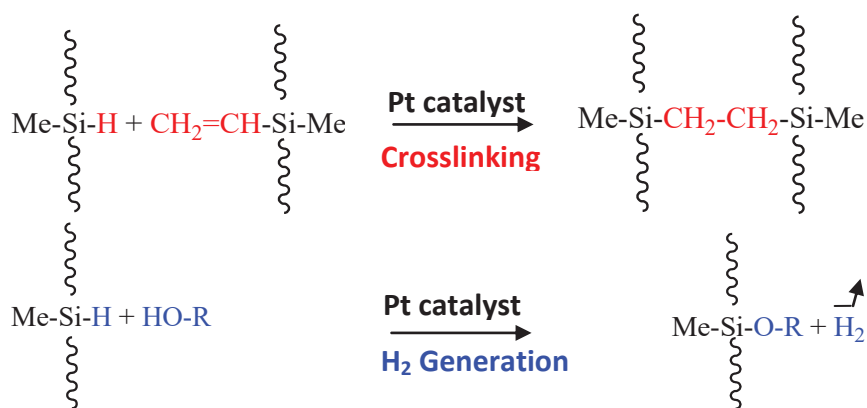


Fig.4: Bluestar silicones technology: Crosslinking and H₂ generation chemical reactions [123, 125]

Dib Jawhar et al. [124, 125] studied nucleation and cell growth of such silicone foam under optical microscopy. Basic foam morphology is shown in Fig. 5.

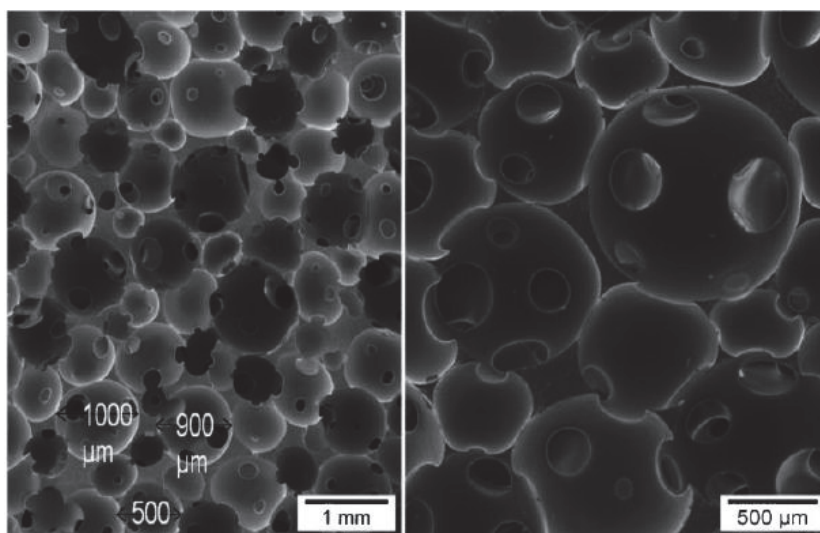


Fig. 5: Morphology of Silicone foam with H₂ foaming strategy [126]. Copyright © 2013, Reproduced with permission from John Wiley and Sons.

The bubble grows in time and reaches its final size at “gel point” and at the end of H₂ generation reaction (Fig.6). Crosslinking and gas generation reactions are synchronized through different ratios of inhibitor/catalyst in order to obtain excellent properties. Microscopic experiments showed that few bubbles grow by themselves due to the gas generation.

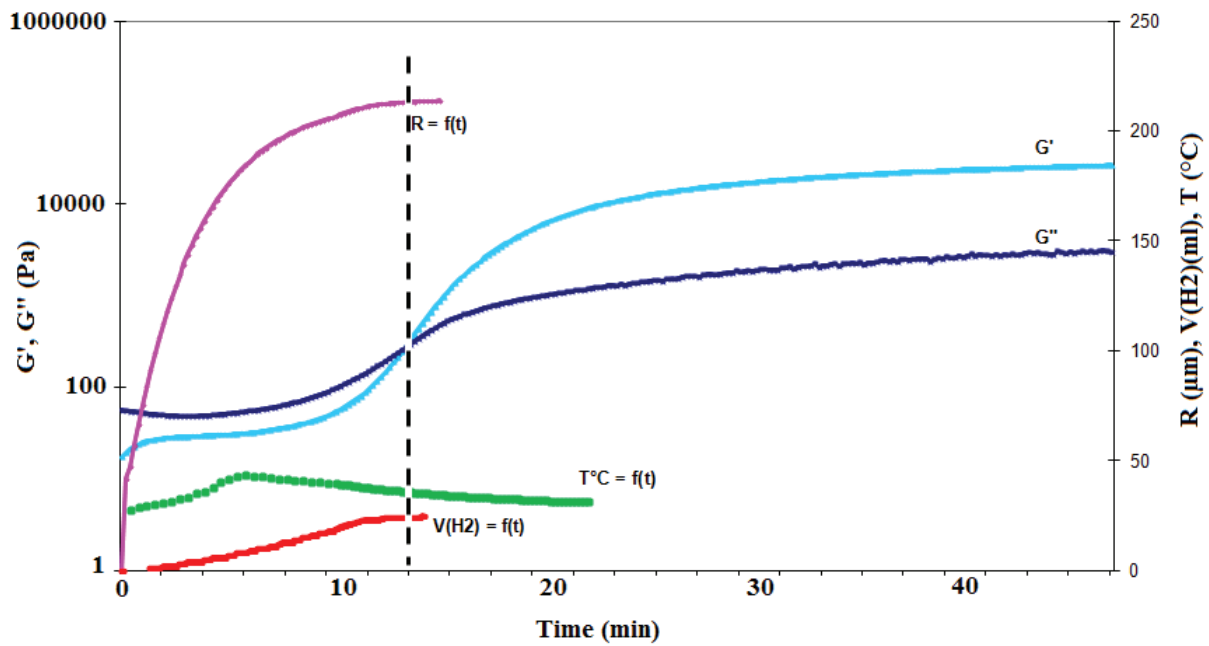


Fig.6: Variation of bubble radius, generated hydrogen volume and rheological parameters as a function of time [126]. Copyright © 2013, Reproduced with permission from John Wiley and Sons.

According to optical observations [125], cell growth is mainly controlled by cell coalescence. Cells come towards each other are deformed during the fusion until the new larger bubble reaches its final geometry by relaxing surface stress. Several cells may coalesce into one which also grows along time because of dihydrogen generation. The bubbles reach their final size ($R=210\ \mu\text{m}$) after undergoing five coalescences starting with bubble 1 (B1) until bubble 6 (B6). Since the crosslinking reaction is not completely finished during this period, the bubbles keep their high mobility which favors their coalescence.

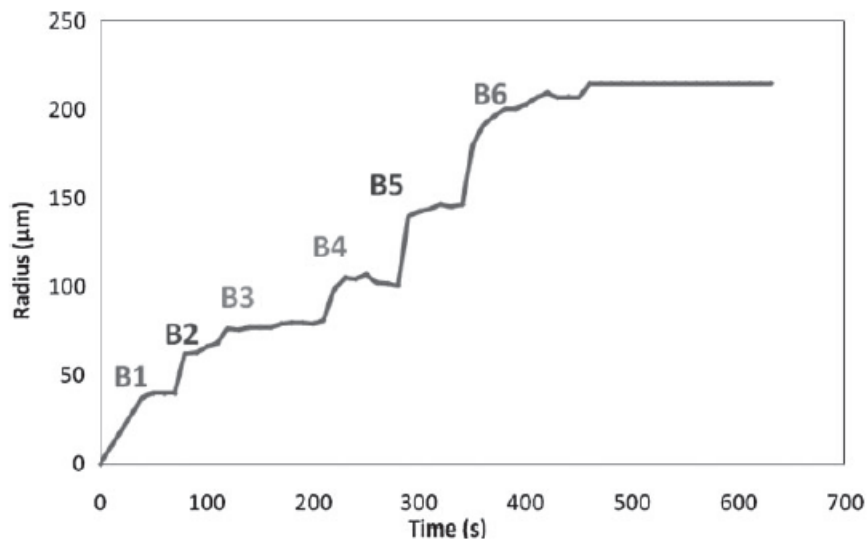


Fig. 7: Bubble radius evolution along time with 5 bubble coalescences [126]. Copyright © 2013, Reproduced with permission from John Wiley and Sons.

The authors also explained that bubbles can move more quickly because of air introduced during manual mixing. Air dissolved and incorporated during manual mixing is also essential because air bubbles act as nucleation sites and increase cell density. With the same amount of H₂ produced that leads to a homogeneous cell size distribution but without influencing cell size. They have studied the influence of fillers and hyperbranched polymers on foam structure. The presence of fillers limited the bubble radius but also generate a thicker skin, a heterogeneous size distribution with larger bubbles. It seems to be due to a good dispersion of silica which instead of forming a mechanical barrier preventing the film ruptures between the cells, silica particles induced faster film thinning and thus, bubble coalescence. Concerning hyperbranched polymers, the results proved that hyperbranched polymers increase the stability of the foam by thickening and adding yield to the continuous phase. Such polymers formed structured interfacial films, which effectively prevented or reduced the bubbles coalescence. The experiments showed that 1% of hyperbranched polymers is an optimum value.

Verdejo et al. [126-128] studied the influence of functionalized graphene sheets (FGS) and carbon nanotubes (CNT) fillers on the foaming of RTV silicone foam (Table 8) and their consequences on mechanical, acoustic absorption, flame retardants properties and morphology. Foam density (Table 8) and foam morphology are worsened (Fig. 8), as compared to pure silicone foam, by addition of nanofillers which might be due to a viscosity increase. Sound absorption is also less efficient along the whole frequency range because less acoustic energy is dissipated by vibration damping due to larger cell sizes and improved modulus of cell walls.

Table 8: Effect of functionalized graphene sheets (FGS) and carbon nanotubes (CNT) on silicone foam properties. Reproduced as it has been published. Copyright © 2008. Reproduced with permission from Elsevier Ltd.[129]

Samples wt.%	Mean cell size (μm)	Foam density (kg.m ⁻³)
0	486±6	197±17
0.10 FGS	488±9	278±11
0.2 FGS	608±13	282±8
0.25 FGS	578±13	291±9
0.10 CNT	489±8	258±18
0.50 CNT	677±15	272±10
1.00 CNT	816±22	291±19

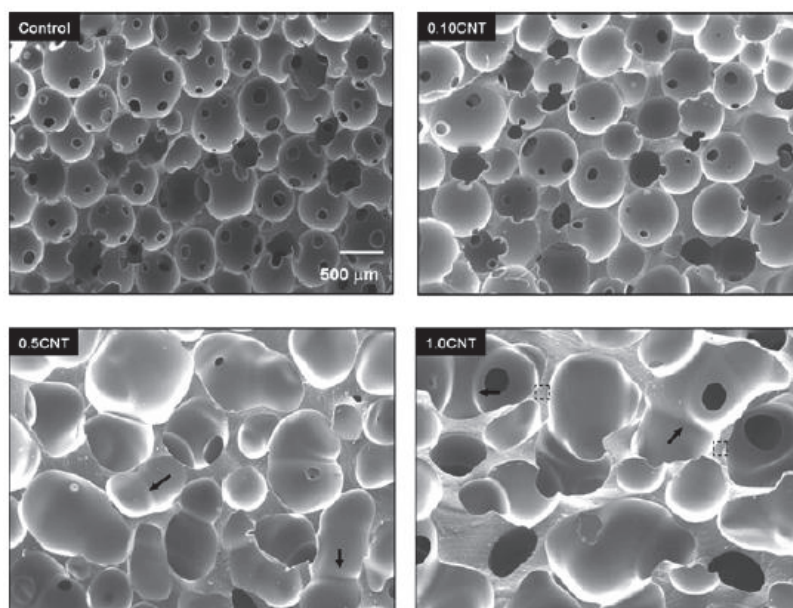
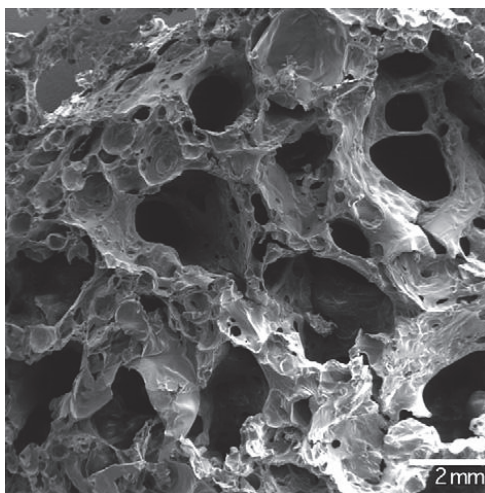


Fig. 8: Cell morphologies of nanocomposite foams at low and high CNT loading fractions [127].
 Copyright © 2008, Reproduced with permission from Royal Society of Chemistry.

Labouriau et al. [129] investigated ionizing radiation effects on silica filled poly (dimethyl siloxane) foam vulcanized at room temperature. The cellular structure of the irradiated foam remained unchanged. Radiation exposure causes a gas production, a reduction in crystallinity and in molar mass between crosslinks which harden the foam. NMR experiments show no chemical modifications. As conclusion, the main mechanism of radiolysis in their radiation conditions is the crosslinking stage. Labouriau et al. [130] also studied thermal aging under compressive strains of diatomaceous earth filled polysiloxane foams in the presence or not of humidity. Foam morphologies of these foams and compositions are described in [131]. Foams aged in presence of humidity showed higher compression set than foams aged in open-air environment. According to [130], some active catalysts left from the curing step may enable post-curing reactions such as hydrolysis and rearrangement of the network.

Kobayashi et al.[132] used this technology to perform porous silicone membrane with several foaming additives. They studied filtration of a diluted solution of PEG in water in function of cure temperature, additives used.

Silicone foams are mainly produced by hydrogen foaming through reaction with water, ethanol and catalyzed with tin or platinum catalysts but these foams are very sensitive to humidity. Grande et al. [133] conducted a study leading to a newly developed Piers-Rubinsztajn reaction by combining α - ω -hydride terminated polydimethylsiloxane with an alkoxy silane crosslinker catalyzed by $B(C_6F_5)_3$. Moisture is not detrimental to this latter reaction and it releases alkane gases (ethane, methane...) derived from alkoxy silane crosslinker. They obtained foams (Fig. 9) with densities between 0.08-0.46 with excellent reproducibility and fast induction time but too soft to measure mechanical properties in most cases.



*Fig. 9 : Silicone foam produced by a newly developed Piers-Rubinsztajn reaction [134] [133].
Copyright © 2012. Reproduced with permission from Elsevier Ltd.*

To conclude, chemical foaming consists in blending a polymer with chemical blowing agents which will be degraded later or by side-reactions between chemical groups which produce gas in situ. Chemical foaming with CBA has several drawbacks such as harmful or corrosive by-products formation during CBA degradation, premature or undesired reactions with polymers or moisture. With CBA foaming, foam with cell size between 18 and 800 μm and foam density between 0.25 and 0.85 can be achieved. When gas is produced by chemical reactions between chemicals group such as hydride and hydroxyl siloxane, water and so on, foam density can be as low as 0.07. But, with this method, cell size remains around 500 μm . It is necessary to introduce air by hand mixing to achieve homogeneous foams and the gas reaction is also sensitive to moisture. From the excellent intrinsic properties of silicone, these foams with appropriate fillers also represents an excellent candidate to fire retardant applications [127].

III. Physical Foaming of silicone

Physical foaming is an alternative way to produce foam without using chemical reaction or degradation. Physical foaming agents experience a reversible physical change of state. Physical foaming leads generally to more homogeneous foam structure with no residues and significantly lower blowing agent costs than when chemical foaming agents are used. Carbon dioxide is mainly used for the foaming of silicone because of its high solubility. Carbon dioxide is also environmentally friendly, nonflammable, nontoxic, and chemically inert. In spite of great concern on the industrial application of microcellular silicone rubber foams, such as in electric and medical devices, only a few works can be found about the physical foaming of silicone rubber. Silicone gum is a good candidate to study foaming because it possesses similar viscoelastic properties as entangled melt polymers at room temperature. In this section, carbon dioxide batch foaming of silicone will be detailed. Silicone turns out to be an effective additive to improve thermoplastic foaming. Solvent evaporation method will also be discussed.

III.1. CO₂ foaming

In a batch foaming experiment, polymer films are placed in a pressure vessel, pressurized with a gas until gas saturation is reached. During this stage, the injected gas could be in a gaseous or supercritical state, the latter being easily accessible with a critical point at 31.6°C for a pressure of 7.38 MPa for CO₂ [27]. In order to foam silicone, the rapid quenching method is usually used because of its molten state at room temperature and high permeability [31, 134].

As explained later most of the chemical foaming is carried out with a simultaneous crosslinking reaction. But, in physical foaming technology, the simultaneous control of foaming and crosslinking is not so obvious. Foaming and crosslinking are mainly carried out separately. Most of publications about CO₂ foaming of silicone [69, 134-136] use the strategy described in Fig. 10. Silicone rubber is partially crosslinked. Then, samples are placed in a batch-foaming process under high pressure of carbon dioxide for saturation. Foaming occurs via fast depressurization. Once foaming is over, samples are post-reticulate to stabilize cell morphology and enhance the foam mechanical properties.

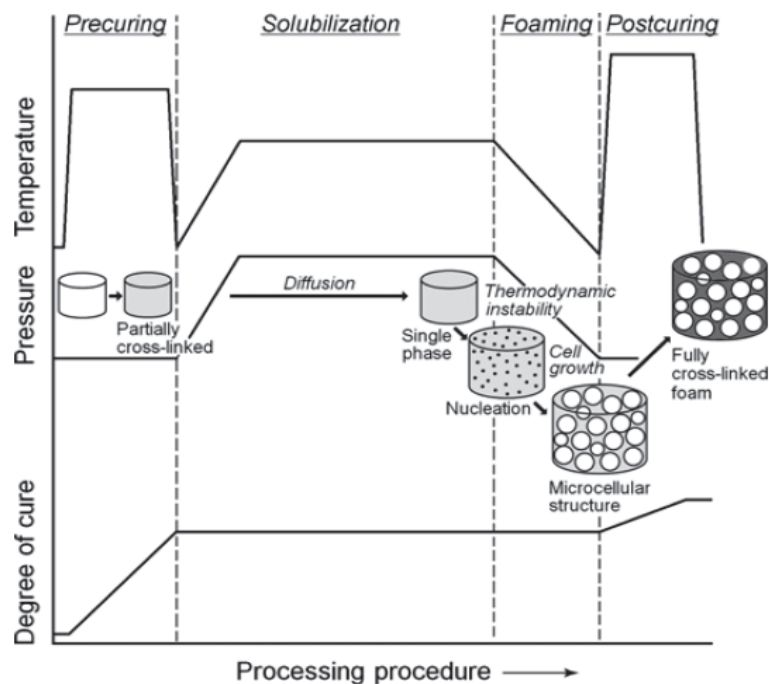


Fig. 10: Main path for foaming silicone rubber with carbon dioxide [136]. Copyright © 2013, Reproduced with permission from Korean Institute of Chemical Engineers, Seoul, Korea.

The crosslinking, which counterbalances CO₂ plasticization, greatly changed the viscoelastic behavior of the silicone rubber. Shimbo et al. [134] were the first to study the influence of the degree of vulcanization of silicone rubber before foaming (Fig. 11). Foaming conditions were investigated using samples with various degrees of vulcanization. When crosslinking density is too low, cell growth is unconstrained and coalescence occurs. If crosslinking density is too high, cell growth is hindered by network elasticity. By adjusting the degree of crosslinking, they achieved foamed rubber which has cell size of 100 μm whereas

the conventional chemistry foamed rubber has cell size around 250 μm . Hong et al. [135] give us a narrower range of viscoelasticity needed to ensure a well-developed foam, around $\tan\delta \sim 0.2$ so well above gel point. Gel point in PDMS is not necessary at $\tan\delta=1$ which is a rough approximation. Indeed, Chambon et al. [137] found higher value in the case of imbalanced crosslinker stoichiometry ($\tan\delta=1.29$ with $n=0.58$). The transition between viscoelastic liquid like and viscoelastic solid like behavior seems to be very sharp regarding the foaming process. Indeed, the sample foamed with a $\tan\delta \sim 0.3$ has large cells and a moderate cell density whereas the sample foamed with a $\tan\delta \sim 0.1$ has almost no cells.

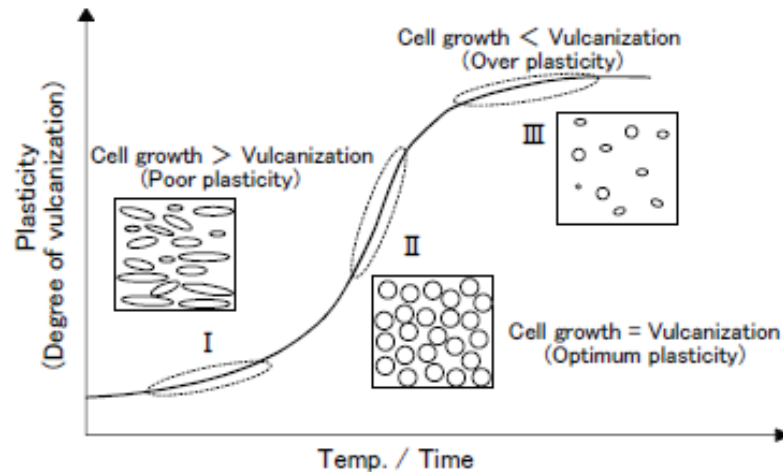


Fig. 11 : Influence of crosslinking degree on foaming[135]. Copyright © 2004 by ICAD2004.

Song et al. [136] and Liao et al. [69] used partially crosslinked (by addition cure and peroxide cure) and highly filled silicone rubber, respectively 27%wt and 30 phr (23%wt) up to 50 phr (33%wt). Liao et al. [69] characterized more thoroughly viscoelasticity provided by the addition of silica. Both elastic modulus and viscosity increase as silica content increases and counterbalances CO_2 plasticization. Viscosity stabilization under CO_2 is delayed as the amount silica introduced is large. As silicone and silica are compatible, diffusivity of carbon dioxide may be reduced by large amount of silica. Liao et al. [69] achieved best results for silicone rubber foam in terms of cell size and cell density with a mean cell size of 4.24 μm and a cell density of 1.4×10^9 cells/ cm^3 (Fig. 12). They did not mention foam density but as it can be seen in Fig. 12, cell walls are very thick and they introduced a large amount of silica. Yan et al. [138] also used high amount of silica up to 60phr but without pre-crosslinking. They achieved foam with cell size in the range between 8-120 μm , cell density between 10^5 - 10^8 cells/ cm^3 and density between 0.45-0.9. In almost the same conditions as [69], they obtained three orders of magnitude less cells. It is a good illustration of how pre-crosslinking is of importance. But they obtained very close results with 60phr of silica incorporated with higher saturation pressure (20 MPa), probably due to similar viscosity compared to the formulation pre-crosslinked with 50phr of silica under 14 MPa.

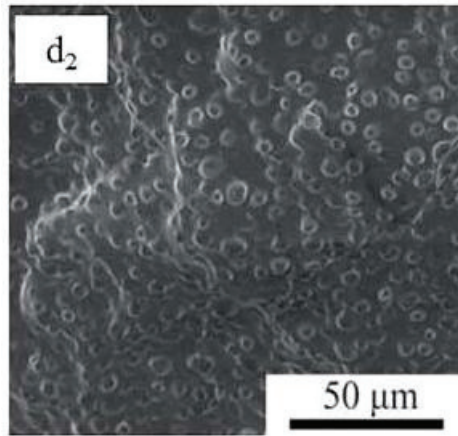


Fig. 12 : Silicone rubber foams (40 phr) with pre-curing time 18 min saturated at 50°C for 1 h under 14 MPa. Silicone foam morphology with the highest cell density and the lowest cell size ever reported [70]. Copyright © 2015, Reproduced with permission from Royal Society of Chemistry.

In agreement with classical nucleation theory, Liao et al. [69] found that an increase in pressure saturation or a decrease in temperature would lead to an enhanced foam (increase cell density and reduce cell size) because more carbon dioxide molecules would be dissolved inside the sample, also leading to a greater viscosity reduction. Pressure seems to prevail over all parameters tested. By increasing silica content, chains mobility is reduced and as a consequence cell coalescence is limited, foams have a higher cell density and a lower cell size (Fig. 13). But the contribution of silica on nucleation is unclear at these large amounts.

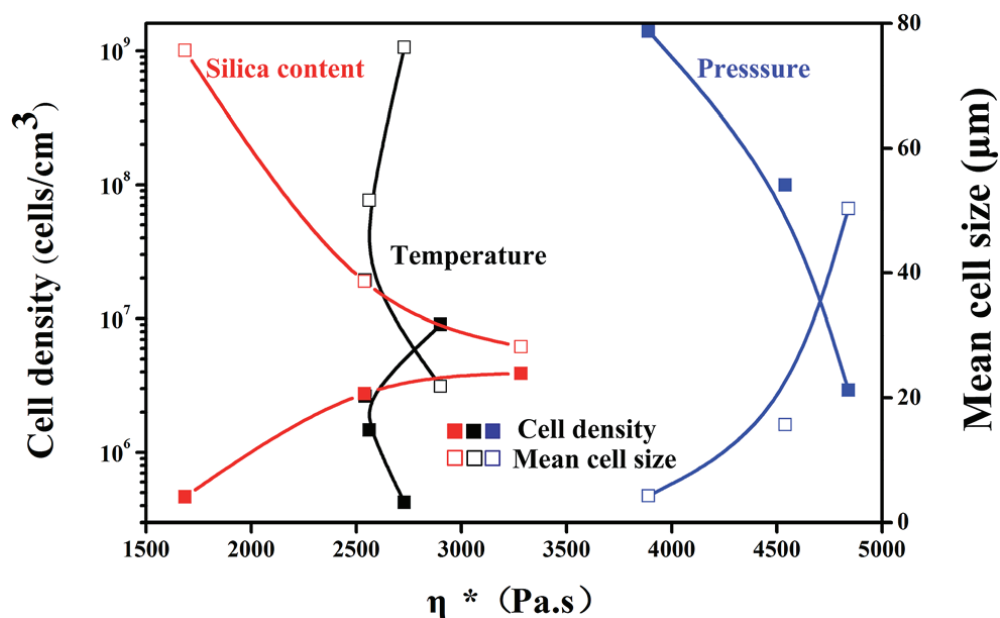


Fig. 13 : Relationship between cellular structure and complex viscosity of silicone rubber saturated with CO₂ [70]. Copyright © 2015, Reproduced with permission from Royal Society of Chemistry.

Batch foaming was also used for making microcellular ceramics [139]. They transformed the microcellular pre-ceramic made in silicone resins by pyrolysis and performed additional sintering if needed.

Studies discussed earlier are made in a lab-scale. Wolff et al. [140] successfully foamed silicone resin with carbon dioxide into a continuous foam extrusion process. Foamed silicone resins serve as pre-ceramic forms and were foamed with several die profiles (Fig.14). Moreover, foams show no morphological modification after a pyrolysis step. Foams have a density of 0.08, a mean cell size of about 90 μm with a cell density of 10^6 cells/ cm^3 . Their foams are independent of CO_2 amount injected. Carbon dioxide may escape from broken cell walls and by diffusion so it does not participate to foaming. With increasing temperature, the gas solubility is lower, the time to freeze is longer and more gas escape by diffusion from the surface leading to a pronounced increase of pore size as well as a thick compact skin layer.

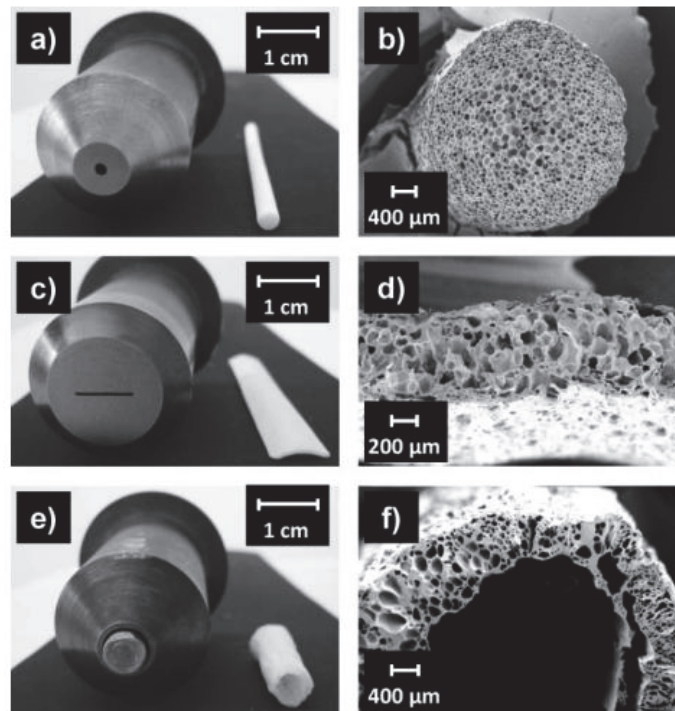


Fig.14 : SEM images of Si-O-C ceramic foam profiles after pyrolysis. Foams made at 87°C. (a-b) circular die, (c-d) slit die, (e-f) annular die. [141] Copyright © 2012, Reproduced with permission from John Wiley and Sons.

III.2. Physical foaming with silicone polymer/copolymer as additive

Poly(dimethylsiloxane) can be used as additive for the control of thermoplastic foaming. PDMS was blended with two different types of polypropylene (PP). In the case of the random copolymer PE-PP, it was found that the cell density of the blends containing PDMS increased significantly across a wide temperature range. PDMS induced high CO_2 concentration and low surface tension, which improve bubble nucleation [141]. Wang et al. [142] also added PDMS with different viscosity into high melt strength polypropylene (HSMPP). Though the CO_2 solubility of HSMPP decreases with the addition of PDMS; their foams exhibit narrow cell size distribution and high cell density. By observing the fracture morphology of HSMPP with PDMS, it is found that PDMS with low viscosity disperses more

easily and uniformly in HMSPP matrix and forms small domains during the extrusion process. These small domains act as bubble nucleation sites or CO₂ tank and thus should be responsible for the improved foaming performance of HMSPP.

Siripurapu et al. [143] modified PMMA film with either nanosilica particles, commercial short-chain fluorosurfactants, or designed CO₂-philic block/graft copolymers (PMMA-g-PDMS and PMMA-b-PFOMA). These copolymers greatly enhanced nucleation at low CO₂ pressure and at optimal content as compared to nanosilica and fluorosurfactants because they can self-organize into micelles. Spitael et al. [144] use a similar strategy for foaming polystyrene with diblock copolymers (Polystyrene-b-poly(ethylene propylene), polystyrene-b-poly(methyl methacrylate), Polystyrene-b-polydimethylsiloxane). Only PS-b-PDMS showed enhanced results because of an increase in CO₂ solubility and a decrease in surface tension, lowering the minimum work of bubble formation. But these results were not consistent with an effective heterogeneous nucleation because the increase in cell density is not sufficient as compared the micelle density in the blend. Micelles may be too small in size can still agglomerate into larger, non-equilibrium structures.

III.3. Solvent evaporation-induced phase separation

Strachota et al. [145] performed physical foaming of ethoxy-silicone resins by solvent method. This method consists in blending resins, surfactants, a blowing solvent and an acidic product for crosslinking reaction. Then crosslinking reaction and foaming occurred by heating the mold which bring forth ethanol volatilization as detailed in Fig. 15. Foam density is controlled by the amount of solvent added and nucleation is enhanced by stirring. They obtained polysiloxane foams with densities between 0.15-0.23 with cell size around 0.35mm in the best case. Then, a pyrolysis step was performed in order to produce SiOC ceramic foams with almost no morphological modifications.

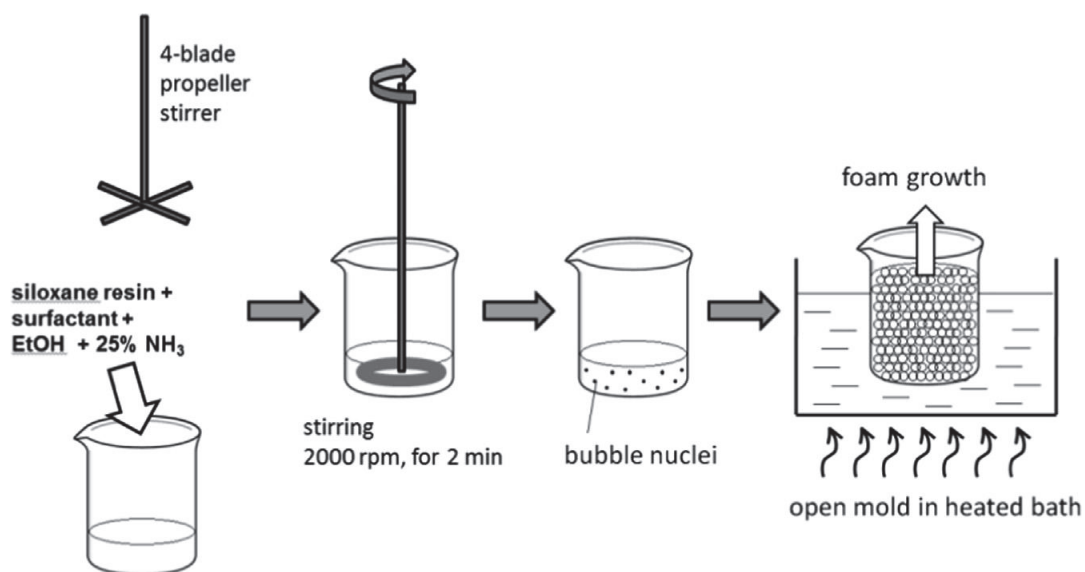


Fig. 15 : Physical foaming of ethoxy-silicone resins by solvent method [146] [145]. Copyright © 2015. Reproduced with permission from Elsevier Ltd.

Zhao et al. [146] made silicone rubber membrane with ordered micropores in the surface by means of the solvent evaporation-induced phase separation (Fig. 16). A solution containing liquid silicone rubber precursor, liquid paraffin, and hexane was cast to form a film with a two-phase structure after the hexane was evaporated [146]. By extracting liquid paraffin in the crosslinked silicone rubber, the pores are created. With increasing temperature, initial casting solution thickness and liquid paraffin concentration, the mean pore size increases. As expected, the addition of a surfactant effectively reduces mean pore size. This cellular structure in the surface of the membrane is developed by nucleation, growth and coalescence process. However, using this method there is a weak control over the degree of interconnectivity of pores and this technique is usually restricted to the fabrication of thin sheets.

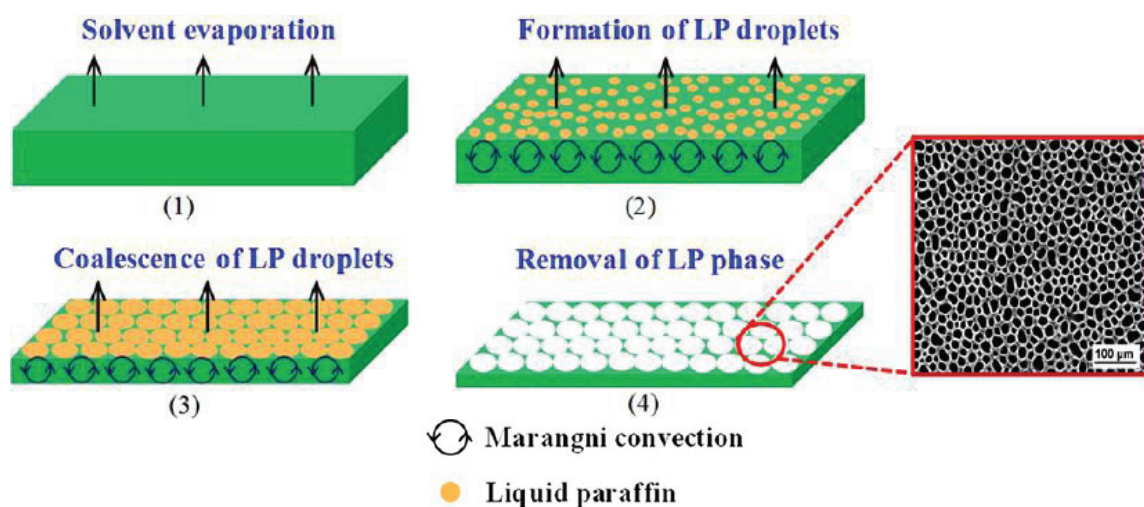


Fig. 16: Pore formation process in silicone rubber membrane [147] [146]. Copyright © 2013, Reproduced with permission from American Chemical Society.

To conclude this section, in most of studies, silicone foaming is triggered by a rapid quenching method because of its molten state. The control of the foaming is improved by pre-crosslinking and restricting chain motions by adding a large amount of compatible fillers. By using a combination of both previous methods, silicone foam with cell size less than $5\ \mu\text{m}$ and cell density higher than $10^9\ \text{cells}/\text{cm}^3$ was achieved. Only one publication was found in silicone extrusion foaming with physical agent while its high gas diffusivity is favorable for extrusion time scale.

Silicone is also blended with other polymers in low quantity. The silicone small domains act as bubble nucleation sites or CO_2 tank and thus should be responsible for the improved foaming performance of the thermoplastics used. Some studies reported the use of copolymer with grafted PDMS, as a nano-structuration strategy, but these results were not consistent with an effective heterogeneous nucleation because the increase in cell density is not sufficient as compared to the micelle concentration in the blend.

Other authors used a solvent evaporation method in competition with crosslinking reaction in order to create silicone foams with low density. But these methods are mainly used in film fabrications, time and solvent consuming.

IV. Templated Silicone Foams

In this section, the use of templates for the fabrication of porous materials is demonstrated. Template may be solid or liquid. If liquid, the materials around the liquid droplets need to be solidified. Then, solvent is removed by evaporation or supercritical drying which leads to the production of templated porous materials. If solid, templates may be hollow spheres, sacrificial fillers or architecture, made for instance by 3D printing. In the case of sacrificial templates, they are then removed by solvent extraction or heating degradation.

IV.1. PolyHIPE

Cellular polymers, known as polyHIPEs can also be generated through a polymerization of a High Internal Phase Emulsion (HIPE), that is, dispersion of a large volume of internal phase in a continuous phase. A HIPE is characterized by an internal phase volume ratio greater than 74% of the total volume, the compact stacking of rigid spheres. Then, the polymerization of the continuous phase holds the structure and the extraction of the dispersed phase creates voids. Holes may be created in the polymer film along polymerization leading to connections between adjacent droplets of dispersed phase. Because of the structural particularities of these materials (large interconnected cells), a lot of research has been conducted on the formation of these structures. Grosse et al. [147] succeeded in adapting this process to fabricate interconnected, microcellular polysiloxane monoliths. The monolith density is about 0.1-0.3 with an average cell size of 4-12 μm . The interconnection average size is about 0.2-1 μm . Their microstructure would enable to use polyHIPE in sound insulation applications, as shown in Fig. 17. Normatov et al. [148] made a highly cellular elastomeric nanocomposites through copolymerization of 2-ethylhexyl acrylate (EHA), divinyl benzene (DVB), and up to 9 mol % of a polyhedral oligomeric silsesquioxane bearing one propylmethacryl group and seven cyclohexyl groups (MACH-POSS). They achieved density between 0.13-0.18 with pore size between 2-15 μm . In spite of the significant mass loss and volume shrinkage during pyrolysis, their products form cellular inorganic monoliths with structural integrity. The cellular structures of these monoliths are similar to those of the original polyHIPE with density about 0.3. Zimny et al. [149, 150] controlled the porosity by adjusting volume fraction of the dispersed phase. Accordingly, they succeeded in slowing down the sound to 80m/s. There are several drawbacks of this technique. It is necessary to use an important amount of surfactant (min. 10%wt) for a limited pot life (24h). The emulsion will not stand high shear, once made. The emulsion contains a large amount of water requiring a long time of soft evaporation which could be limiting for industrial processes [151]. Zimny et al. [149, 150] developed then UV induced

polymerization which avoids hours of crosslinking in oven and evaporation of water before stabilization. Except insulation applications, PolyHIPE can also be used as inflatable materials for self-sealing fuel tanks [152]. Indeed, they modified a silicone polyHIPE by introducing NaHCO_3 inside the aqueous phase. This compound can be thermally decomposed to produce carbon dioxide inside polyHIPE pores. They suggest that under 10 mbar, this modified polyHIPE silicone film, between two plates, can fill and block a hole of 5 mm. Once the vacuum is over, the foam retracts and unblocks the hole. Expansion is repeatable but prolonged exposure to vacuum damages the materials through gas loss.

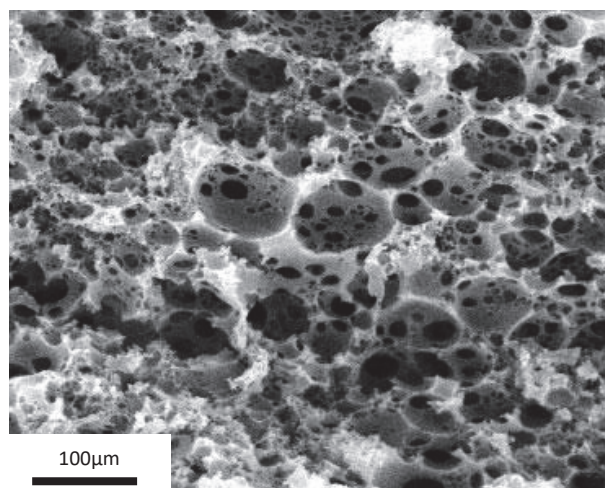


Fig. 17: PolyHIPE microstruktur[148]. Copyright © 2008, Reproduced with permission from John Wiley and Sons.

IV.2. Supercritical drying

Martina et al. [153] used another approach to produce injection moldable silicone foams with porosities at the micrometer scale. First, they prepared a reverse emulsion silicone-water-surfactant. Once, the emulsion is stable, they generated the porosity by evacuating water through supercritical drying. With supercritical drying, the surface tension effects are avoided and cell collapsing is prevented. They succeeded in producing foam with 300 nm pore sizes but a porosity of 15% for a system containing 10%wt water and 5%wt surfactant. The resulting samples had poor mechanical properties because of tacky internal pore surfaces due to the presence of water inside the domains during the curing of the siloxane. Then siloxane chains can interpenetrate, therefore the mechanical recovery at unload was inexistent.

IV.3. Sacrificial template

Sacrificial template can be used as scaffolds to produce silicone foams. Adam et al. used expanded beads of PS as templates to generate micro and macro-pores for catalytic applications [154]. Expanded beads were introduced in different volume fraction in silicone fluid. Then, the mix is crosslinked under different compression force and then pyrolyzed. The compression force influences cell connectivity, strut thickness and porosity. In this work, a

high compaction was adjusted to receive high cell interconnectivity and thin struts in order to obtain high specific surface area. Martina et al. [153] used a similar approach to create elastomeric foams by compounding a silicone rubber with polymethylmethacrylate (PMMA) micron-sized particles.

Fuller et al. [155] developed a cellular silicone rubber for growing cells or living tissue for breast implant applications. They blended food grade and water-soluble inorganic salt such as sodium bicarbonate or sodium chloride with a low viscosity RTV silicone rubber. They simply removed the sacrificial fillers by dissolution in water without any swelling and electrostatically charged the resulting surface to improve biocompatibility. Fabrication method and applications of three-dimensional (3D) interconnected microcellular PDMS for engineered tissue scaffolds by using sugar as template are reported by Lantada et al. [156] and Yuen et al. [157]. Lantada et al. achieved a rapid approach for development of cellular PDMS scaffolds adapted to the form of conventional implants or adapted to patient bio-structures. PDMS sponges are made by casting emulsions of PDMS, sugar crystals, and water. Then sugar was leached by water immersion. The resulting cellular PDMS scaffolds are excellent for chondrogenesis. Yuen et al. [157] also used this technique to create a microfluidic device for cell culture applications where gas perfusion can improve cell survival and functions. The main advantage of all of these methods is that pore size and overall porosity are tunable by changing the particle size and concentration within the pre-polymer [158]. Moreover, these techniques can be carried out on a small scale, rapidly and at low cost which is attractive for engineered tissue scaffolds applications.

Three-dimensional interconnected microcellular PDMS can also be done by water dissolvable sacrificial 3D printed scaffolds [159] (Fig. 18). Mohanty et al. 3D-printed a PVA mold network which defines channels of about 78 μm . PVA is then dissolved after curing the silicone cast around it. The fabricated scaffolds were tunable, scalable, compatible with cell culture, rapid, and inexpensive.

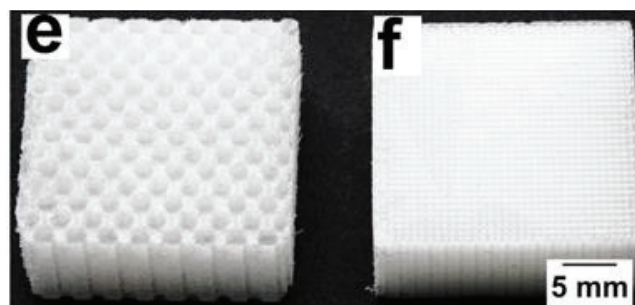


Fig. 18: PDMS scaffolds fabricated from 3D printed sacrificial molds [160]. Copyright © 2015. Reproduced with permission from Elsevier Ltd.

IV.4. Syntactic foam

Syntactic foams are a blend of hollow microspheres and a polymeric binder. The microspheres are gas filled, have very low density and high compressibility [160]. They have

a diameter in the range of 10-100 μm . They are used in applications for naval, aeronautical, aerospace, civil, industrial, and automotive engineering due to good acoustical attenuation [161, 162], excellent strength to weight ratio, shock absorption (Fig. 19) [163, 164], low density, electromagnetic and electrical properties [165]. Silicone syntactic foams are even more promising for electromagnetic applications like high performance radar or electric components, because silicone also has very good dielectric properties [166]. Syntactic foams filled with hollow glass beads possess better mechanical properties in compressive loading than polymer filled with solid glass microspheres [166]. The use of elastic syntactic foam may be a replacement solution for highly stressed systems compared to conventional insulation materials such as epoxy resins because elastic foams have better compressibility notably with big microspheres [167]. Elastic syntactic foams are insensitive against thermal load cycles but possess low thermal conductivity which is a problem for dissipating heat in conductor parts [160].

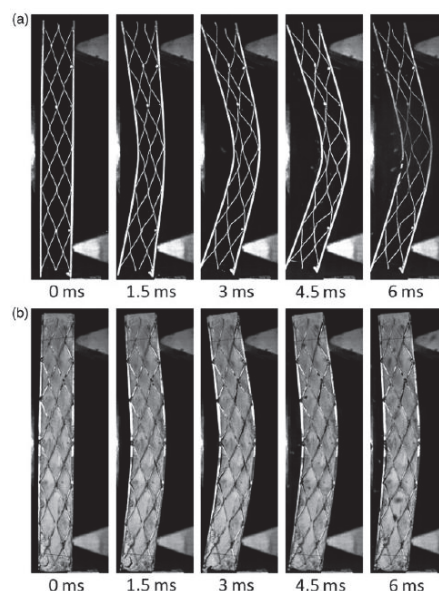


Fig. 19: Real-time of shock deformation of (a) empty and (b) silicone syntactic foam-filled sandwich structures at 25°C[165]. Copyright © 2016, Reproduced with permission from SAGE Publishing

In the patent by Nakanishi et al. [168], Expancel DE (5-300 μm) hollow microspheres are mixed with addition cure silicone in order to obtain an efficient shock absorbing material. Expanded microspheres have densities as low as 25 kg/m³. This is much lower than glass microspheres and makes them very lightweight filler [169]. The maximum impact force was divided by almost two with 3wt% of Expancel hollow microspheres in comparison to raw silicone and by three in comparison to a commercial foamed polyethylene-based shock absorbing. It was found, at the frequency of 1 Hz, that glass hollow sphere possess better shock absorbing properties than polymer hollow microspheres [163].

As conclusion, foaming is not the only way to produce cellular materials. First, polyHIPE is a recent way to produce a low density and cellular monolith of polymers or ceramic with plenty of interconnection (0.2-1 μm) between cells (2-15 μm). Their

microstructure is tunable and makes them very attractive for sound insulation applications. Their main drawbacks are the high quantity of water, surfactants and their very short pot life even in static conditions.

Sacrificial template can also be used as scaffolds to produce silicone foams. Sacrificial fillers are added and after a crosslinking step, fillers are degraded letting free their occupied volume. Cell size of the resulting foam is dependent on the size of the sacrificial template but also, in some cases, of the compaction of the templates. A high compaction can be applied to generate high cell interconnectivity and thin struts in order to obtain a high specific surface area. The sacrificial template can be something far different from fillers, it can be a 3D-printed network of water soluble polymer for example or directly 3D mold made of water dissolved material like sugar. These techniques enable to control effectively porosity, are cheap, biocompatible and relatively fast.

The last way available to form foams is to mix glass or polymer beads within a polymer, also called syntactic foams. Their filled porosities will vary only with fillers size. Syntactic foams are mainly used in sound isolation, shock absorbing, heat resistant, low weight and high compression strength exigencies. Silicone syntactic foams add benefits for electromagnetic applications like high performance radar electric components, because silicone has also relevant dielectric properties.

V. Porous silicone fabrications summary

The results in terms of density, cell size, cell density and the materials used are summed up and sorted by foaming strategy (Table 9). Cell density is not often given. The lowest cell sizes and density are obtained by polyHipe strategy. In case of gas foaming (chemical, chemical H₂, and CO₂ batch foaming), the best density is obtained for H₂ chemical foaming but cell size and cell density are largely better with CO₂ batch foaming.

Table 9: Porous silicone fabrication results summary

[ref]	Materials used	Mean Cell size (μm)	Cell density (cells/cm ³)	Foam density (g/cm ³)	Foaming strategy used
[117]	MVQ/ fumed silica/ hydroxyl silicone oil/ Azobisformamide	18-30	4.9x10 ⁷ - 1.3x10 ⁸	0.33-0.6	CBA degradation
[114]	MVQ/ N,N O- dinitrosopentametgyle ne Tetramine/ carbamide/ HGB/ silica	150-800	-	0.25-0.85	CBA degradation
[113]	MVQ/AIBN/ peroxides: DCBP, DTBP, DBPH	232-510	-	0.38-0.44	CBA degradation

[118]	silica-filled (~30% filler) methyl vinyl silicone rubber/ dibutyltin dilaurate/N,N- dinitrosopentamethyle netetramine/ DCP-BPO	~200	-	-	CBA degradation
[119]	methyl vinyl silicone rubber/precipitated silica/DCP/carbamide/3 , 7-dinitroso-1.3.5.7- tetraazobicyclo-nonane	-	-	-	CBA degradation
[115]	Silicone/ fillers/ Ammoniumcarbonate/ acetic acid	-	-	<1	CBA degradation
[116]	Vinyl-containing linear or branched organopolysiloxane/hy drogen siloxane/silica/ Pt- catalyst/inhibitor/amm onium carbonate/UHF- active fillers	-	-	-	CBA degradation
[126, 128]	RTFoam 3240/ Functionalized graphene sheets	490-610	-	0.19-0.29	Chemical H ₂ and other gas
[120]	Hydroxyl-phenyl- methyl Siloxane copolymer, hydroxylsiloxane resin, dibutyl-tin-dilaurate, trimethylsilyl end- blocked methylhy drogen polysiloxane and other additives/copolymers	-	-	0.07-0.14	Chemical H ₂ and other gas
[121]	Hydroxylated dimethylpoly siloxane/ methylhydrogen polysiloxane and other fillers/additives/copoly mers	-	-	0.2-0.5	Chemical H ₂ and other gas
[123]	RT FOAM 4241 A & B Bluestar Silicone	-	-	0.18-0.25	Chemical H ₂ and other gas
[170]	Hydroxyl- polydimethylsiloxane/p olymethylhydrogensilo xane/1- ethynylcyclohexan-1-ol/ chloroplatinic acid hexahydrate/ iron oxide	-	-	-	Chemical H ₂ and other gas

[124, 125]	RT foam from Bluestar Silicone	550	-	-	Chemical H ₂ and other gas
[127, 128]	RTFoam 3240/ Carbon nanotubes	480-820	-	0.19-0.29	Chemical H ₂ and other gas
[129-131]	dihydroxylterminated polydimethylsiloxane/ polymethylhydrosiloxane (PMHS)/ tetrapropyl orthosilicate (TPS)/ diphenylmethylsilanol (DPMS)/ diatomaceous earth	230	-	-	Chemical H ₂ and other gas
[132]	α,ω -bis(hydroxypropyl) polydimethylsiloxanes/ α,ω -bis(hydroxyl) polydimethylsiloxanes Carbofunctional polysiloxanes/Melanine / Graphite	-	-	0.25–0.45	Chemical H ₂ and other gas
[133]	poly(methyl hydrogen siloxane)/ poly (methyl vinyl siloxane)/ water/ ethylene glycol/ ethanol/ 2-methoxyethanol	200-400	-	-	Chemical H ₂ and other gas
[134]	α,ω -hydride-terminated/ tetraethyl orthosilicate/ B(C ₆ F ₅) ₃	-	-	0.08-0.46	Chemical H ₂ and other gas
[69]	silicone rubber MVQ	80-160	10 ⁵ - 10 ⁶	-	CO ₂ foaming
[135]	Silicone rubber MVQ/ precipitated silica/ hydroxyl silicone oil/ dicumyl peroxide (DCP)	4.2-77	4x10 ⁵ - 1.4x10 ⁹	-	CO ₂ foaming
[136]	LSR / silica	12-305	10 ³ - 10 ⁹	-	CO ₂ foaming
[138]	Silicone rubber MVQ/ Fumed silica/ DCP	-	-	0.24-1.1	CO ₂ foaming
[140]	Silicone rubber MVQ/ Fumed silica/ DCP	8-120	10 ⁵ - 10 ⁸	0.45-0.9	CO ₂ foaming
[145]	Silicone resin	~ 90	10 ⁶	0.08	CO ₂ foaming
[146]	Triethoxymethylsilane / diethoxydimethylsilane / industrial surfactants/ ethanol/aqueous ammonia	350-800	-	0.15-0.22	Phase separation
[141]	silicone rubber precursor/ liquid paraffin/ hexane	3-150	-	-	Phase separation
[142]	hPP/cPP-PE/cPP-g-MAH/PDMS	-	5x10 ⁶ - 8x10 ⁹	-	Physical / blend

[143]	PP-g-St/PDMS	40-140	$7 \times 10^6 - 4 \times 10^8$	-	Physical / blend
[144]	PMMA/PMMA-g-PDMS	-	$3 \times 10^{10} - 5 \times 10^{11}$	-	Physical / blend
[147]	PS/PS-g-PDMS	-	$2.4 \times 10^{10} - 6.1 \times 10^{10}$	-	Physical / blend
[148]	1,3-divinyltetramethyldisiloxane/ 1,3,5,7-tetramethyl-1,3,5,7-tetravinylcyclotetrasiloxane/ trimethylsilyl-terminated polymethylhydrosiloxane/ PGEO/ PGPR	4-12	-	0.1-0.3	PolyHIPE
[149]	2-ethylhexyl acrylate (EHA)/ divinyl benzene (DVB)/ polyhedral oligomeric silsesquioxane bearing one propylmethacryl group and seven cyclohexyl groups (MACH-POSS)	2-15	-	0.13-0.3	PolyHIPE
[152]	Silicone Silcolease UV-POLY200 / Isopropylthioxanthone/ Poly(ethylene oxide) (PEO)-block-poly(dimethylsiloxane)	11.2	-	-	PolyHIPE
[153]	Sylgard 184 silicone / Rhodorsil silicon oil 47 /sodium hydrogen carbonate/ surfactant Hypermer 2296 / Sunflower oil / Hydrophobic pyrogenic silica particles HDK, H2O	-	-	-	PolyHIPE
[154]	Siloxane rubber precursors/ Water/ Dimethyl siloxane ethylene oxide block copolymer	0.3-0.8	-	-	Super-critical drying / Sacrificial template
[155]	methylphenyl polysiloxane/ 3-aminopropyltriethoxysilane/ Expanded	1200-1600	-	-	Sacrificial template

	polystyrene beads				
[156]	RTV silicone rubber/ water soluble inorganic salt	1-500	-	-	Sacrificial template
[157]	Neukasil RTV-20 prepolymer/ Water/ Sugar	30-400	-	0.64-0.95	Sacrificial template
[159]	Sylgard 184 silicone/ Sugar	75-1000	-	-	Sacrificial template
[163]	PVA/ Sylgard 184 silicone	78-1400	-	-	Sacrificial template
[164]	Silastic MDX4-4210 / Expancel 461/ hollow SiO ₂ microspheres	40	-	0.9-1.5	Syntactic foam
[165]	Liquid silicone rubber resin/ A20/1000 Glass Bubbles	105	-	-	Syntactic foam
[166]	Siloxane rubber precursors/ Hollow plastic spheres	35,90,130	-	-	Syntactic foam
[167]	Phenylmethylsiloxane resin/Hollow silica microspheres	100	-	0.27-0.63	Syntactic foam
[168]	liquid silicone rubber resin/A16/ 500 and A20/1000 Glass bubbles	105-115	-	0.36-0.74	Syntactic foam
	Silicone rubber/ Expancel	5-300		0.51-0.98	Syntactic foam

As discussed throughout this review, the cell density is low and never higher than 10^9 cell/cm³ compared to other polymeric foams for which densities close to 10^{15} can be obtained in some cases. As a result, the density of silicone foams is generally not very low (0.3-0.6) or the bubble size is often more than 100 μ m. However, the originality of silicones in terms of microstructure and possible chemical crosslinking reactions makes it possible to use several methods of foaming. For structural foams, most of this table, the foaming is obtained from the thermal degradation of CBA or from the in situ release of H₂ which are promising and most industrially used routes. Silicone foams obtained from CO₂ injection are rather the result of academic research because, for the moment, the reported studies are done in the case of batch processes. All these foams have a close cellular morphology whereas the foams obtained by sacrificial template of PolyHIPE process have rather open morphologies.

Conclusions

This paper aimed to give an overview of the commonly used processes developments unicellular silicone fabrications such as gas foaming (physical or chemical), phase separation, emulsion and sacrificial templating and hollow microspheres (syntactic foam).

At first, gas foaming theory was reviewed through theory of sorption, diffusion, nucleation, cell growth and coalescence. Gas-silicone data are provided from open literature and discussed. A lot of studies have been interested in the correlations between silicone structure and their gas properties. It has been shown that silicone polymers have specific interactions with carbon dioxide. Silicone-gas properties are connected to its weak interactions between polymer chains and high chain flexibility. High gas concentration and diffusivity bring forth a matrix viscosity reduction and faster mass transfers leading to faster cell growth and coalescence rates. According to all the studies reported in this review, no silicone foam ever achieved nanocells and cell density higher than 1×10^9 cells/cm³, even if viscoelasticity and nucleation are optimized.

Another interesting approach, which can be applied to another system with highly CO₂-philic polymers, has been detailed. For these systems, silicone is dispersed at low amount in thermoplastics. The silicone domains act as bubble nucleation sites or CO₂ tank and thus should be responsible for the improved foaming performance of the thermoplastics used. But no study to date, has tried to use a blend procedure in silicone matrix with another highly CO₂-philic polymer or a nanostructuring approach with copolymers. However, we have recently demonstrated that the blending (and compatibilisation) of a fluorosilicone in silicone matrix could be a relevant strategy to improve the cell nucleation and then to control the cell morphology of silicone foams (171)

Chemical foaming with chemical blowing agents (CBA) is a cost-effective strategy and can be directly integrated to industry but CBAs can produce nasty gas and cause processing problems with relatively big cell and high foam density. In the case of hydrosilylation/condensation foaming reactions, intensively developed in the industrial applications, foams have far better density but still with big cells even with the addition of fillers or branched silicones. However, they have very good mechanical and fire retardant properties. This technology is also moisture sensitive, generates explosive gas so it is less subject to be directly integrated to mass production industry, such as extrusion foaming processes.

A third general method was presented to create cellular silicone materials, using a template strategy such as emulsion polymerization, sacrificial fillers or polymers and syntactic foams. In each case, cellular morphology is directly dependent and tunable in function of the template microstructure. These techniques are relatively straightforward to implement because they do not need any specific apparatus unlike physical foaming. Resulting foams are mainly used in biocompatible, sound or shock-absorbing applications.

We have presented in this section a solution using 3D-printing in order to create the mold that will receive the silicone matrix. Actually, no publications have tried to directly 3D-print silicone foams or silicone formulations that can foam a posteriori. However, 3D printing of silicone is well established for biomedical applications.

Silicone foams have far better properties than polymer foams already used (like PU foams...) in a number of applications, e.g. packaging, automotive; home construction, aerospace, medical prostheses, telecommunications, electromagnetic to name a few. However, their main drawback remains their cost so their use is limited to specific, cutting edge applications.

References

- [1] E. Yilgör, I. Yilgör, Silicone containing copolymers: Synthesis, properties and applications, *Progress in Polymer Science* **39** (6) (2014) 1165-1195.
- [2] R.G. Jones, W. Ando, J. Chojnowsk, Silicon Containing Polymers: The Science and Technology of Their Synthesis and Applications, *Silicon Chemistry* **1** (4) (2002) 185-212.
- [3] R.G. Jones, W. Ando, J. Chojnowsk, Silicon Containing Polymers: The Science and Technology of Their Synthesis and Applications, *Silicon Chemistry* **1** (4) (2002) 213-232.
- [4] A.R. Colas, Silicones: Preparation, Properties and Performance, Dow Corning, Life Sciences, 2005.
- [5] M.O. Okoroafor, K.C. Frisch, *1 - Introduction to foams and foam formation A2 Handbook of Plastic Foams*, William Andrew Publishing, Park Ridge, NJ, 1995, pp. 1-10.
- [6] <http://ozone.unep.org/en/handbook-montreal-protocol-substances-deplete-ozone-layer/27571>
- [7] P.H.T. Howard, J.L. ; Banerjee, S., Identification of CFC and HCFC substitutes for blowing polyurethane foam insulation products, Syracuse Univ. Research Corp., NY (United States), 1995.
- [8] D.P.K.S. S. T. Lee, Polymeric foams: Technology and development in regulation, process and products, (2008).
- [9] T. Chinniah, S. Ravi, D.C. Tansen, K. Muniratnam, K.S. Vikash, P. Asim, Nano-cellular polymer foam and methods for making them, Google Patents, 2008.
- [10] S.K. Wason, G. Mooney, M.E. Tarquini, R.A. Garcia, J.A. Kosin, C.R. Andrews, Endothermic blowing agents compositions and applications, Google Patents, 1992.
- [11] Y.-M. Corre, A. Maazouz, J. Duchet, J. Reignier, Batch foaming of chain extended PLA with supercritical CO₂: Influence of the rheological properties and the process parameters on the cellular structure, *The Journal of Supercritical Fluids* **58** (1) (2011) 177-188.
- [12] C.B. Park, N.P. Suh, D.F. Baldwin, Method for providing continuous processing of microcellular and supermicrocellular foamed materials, Google Patents, 1999.
- [13] M.S. Suwandi, S.A. Stern, Transport of heavy organic vapors through silicone rubber, *Journal of Polymer Science: Polymer Physics Edition* **11** (4) (1973) 663-681.
- [14] V.M. Shah, B.J. Hardy, S.A. Stern, Solubility of carbon dioxide, methane, and propane in silicone polymers: Effect of polymer side chains, *Journal of Polymer Science Part B: Polymer Physics* **24** (9) (1986) 2033-2047.
- [15] A. Garg, E. Gulari, C.W. Manke, Thermodynamics of Polymer Melts Swollen with Supercritical Gases, *Macromolecules* **27** (20) (1994) 5643-5653.
- [16] I.C. Sanchez, A.C. Balazs, Generalization of the lattice-fluid model for specific interactions, *Macromolecules* **22** (5) (1989) 2325-2331.
- [17] I.C. Sanchez, R.H. Lacombe, An elementary molecular theory of classical fluids. Pure fluids, *The Journal of Physical Chemistry* **80** (21) (1976) 2352-2362.
- [18] I.C. Sanchez, R.H. Lacombe, Statistical Thermodynamics of Polymer Solutions, *Macromolecules* **11** (6) (1978) 1145-1156.
- [19] C. Panayiotou, J.H. Vera, Statistical Thermodynamics of r-Mer Fluids and Their Mixtures, *Polym J* **14** (9) (1982) 681-694.
- [20] F. PJ, *Principles of polymer chemistry*, Ithaca NY, 1953.
- [21] S.R. Hildebrand JH, The solubility of nonelectrolytes, (1950) 488.
- [22] J.-J.S.R.B. Gupta, *Solubility in Supercritical Carbon Dioxide*, 2006.
- [23] C.M. Hansen, Aspects of solubility, surfaces and diffusion in polymers, *Progress in Organic Coatings* **51** (1) (2004) 55-66.
- [24] G.J. McFann, K.P. Johnston, S.M. Howdle, Solubilization in nonionic reverse micelles in carbon dioxide, *AIChE Journal* **40** (3) (1994) 543-555.
- [25] A. Kasturirangan, C.A. Koh, A.S. Teja, Glass-Transition Temperatures in CO₂ + Polymer Systems: Modeling and Experiment, *Industrial & Engineering Chemistry Research* **50** (1) (2011) 158-162.
- [26] Y. Kamiya, Y. Naito, K. Terada, K. Mizoguchi, A. Tsuboi, Volumetric Properties and Interaction Parameters of Dissolved Gases in Poly(dimethylsiloxane) and Polyethylene, *Macromolecules* **33** (8) (2000) 3111-3119.

- [27] K. Ghosal, B.D. Freeman, Gas separation using polymer membranes: an overview, *Polymers for Advanced Technologies* **5** (11) (1994) 673-697.
- [28] W.L. Robb, Thin silicone membranes- their permeation properties and some applications, *Annals of the New York Academy of Sciences* **146** (1) (1968) 119-137.
- [29] T.C. Merkel, V.I. Bondar, K. Nagai, B.D. Freeman, I. Pinnau, Gas sorption, diffusion, and permeation in poly(dimethylsiloxane), *Journal of Polymer Science Part B: Polymer Physics* **38** (3) (2000) 415-434.
- [30] R.H.P.D.W. Green, *Perry's Chemical Engineers' Handbook, 6th Edition*, 1984.
- [31] S. Alexander Stern, Polymers for gas separations: the next decade, *Journal of Membrane Science* **94** (1) (1994) 1-65.
- [32] J.R. Royer, J.M. DeSimone, S.A. Khan, Carbon Dioxide-Induced Swelling of Poly(dimethylsiloxane), *Macromolecules* **32** (26) (1999) 8965-8973.
- [33] Y. Sato, K. Fujiwara, T. Takikawa, Sumarno, S. Takishima, H. Masuoka, Solubilities and diffusion coefficients of carbon dioxide and nitrogen in polypropylene, high-density polyethylene, and polystyrene under high pressures and temperatures, *Fluid Phase Equilibria* **162** (1-2) (1999) 261-276.
- [34] Y. Sato, T. Takikawa, S. Takishima, H. Masuoka, Solubilities and diffusion coefficients of carbon dioxide in poly(vinyl acetate) and polystyrene, *The Journal of Supercritical Fluids* **19** (2) (2001) 187-198.
- [35] S.A. Stern, V.M. Shah, B.J. Hardy, Structure-permeability relationships in silicone polymers, *Journal of Polymer Science Part B: Polymer Physics* **25** (6) (1987) 1263-1298.
- [36] A. Galia, G. Filardo, *Utilization of Dense Carbon Dioxide as an Inert Solvent for Chemical Syntheses*, Carbon Dioxide as Chemical Feedstock, Wiley-VCH Verlag GmbH & Co. KGaA, 2010, pp. 15-31.
- [37] S. Kilic, S. Michalik, Y. Wang, J.K. Johnson, R.M. Enick, E.J. Beckman, Phase Behavior of Oxygen-Containing Polymers in CO₂, *Macromolecules* **40** (4) (2007) 1332-1341.
- [38] A.I. Cooper, Polymer synthesis and processing using supercritical carbon dioxide, *Journal of Materials Chemistry* **10** (2) (2000) 207-234.
- [39] R. Fink, D. Hancu, R. Valentine, E.J. Beckman, Toward the Development of "CO₂-philic" Hydrocarbons. 1. Use of Side-Chain Functionalization to Lower the Miscibility Pressure of Polydimethylsiloxanes in CO₂, *The Journal of Physical Chemistry B* **103** (31) (1999) 6441-6444.
- [40] C.A. Mertdogan, T.P. DiNoia, M.A. McHugh, Impact of Backbone Architecture on the Solubility of Fluorocopolymers in Supercritical CO₂ and Halogenated Supercritical Solvents: Comparison of Poly(vinylidene fluoride-co-22 mol hexafluoropropylene) and Poly(tetrafluoroethylene-co-19 mol hexafluoropropylene), *Macromolecules* **30** (24) (1997) 7511-7515.
- [41] C.F. Kirby, M.A. McHugh, Phase Behavior of Polymers in Supercritical Fluid Solvents, *Chemical Reviews* **99** (2) (1999) 565-602.
- [42] S. Kilic, S. Michalik, Y. Wang, J.K. Johnson, R.M. Enick, E.J. Beckman, Effect of Grafted Lewis Base Groups on the Phase Behavior of Model Poly(dimethyl siloxanes) in CO₂, *Industrial & Engineering Chemistry Research* **42** (25) (2003) 6415-6424.
- [43] M.L. O'Neill, Q. Cao, M. Fang, K.P. Johnston, S.P. Wilkinson, C.D. Smith, J.L. Kerschner, S.H. Jureller, Solubility of Homopolymers and Copolymers in Carbon Dioxide, *Industrial & Engineering Chemistry Research* **37** (8) (1998) 3067-3079.
- [44] S. Kilic, Y. Wang, J.K. Johnson, E.J. Beckman, R.M. Enick, Influence of tert-amine groups on the solubility of polymers in CO₂, *Polymer* **50** (11) (2009) 2436-2444.
- [45] D. De Kee, Q. Liu, J. Hinestroza, Viscoelastic (Non-Fickian) Diffusion, *The Canadian Journal of Chemical Engineering* **83** (6) (2005) 913-929.
- [46] D.A. Edwards, D.S. Cohen, A mathematical model for a dissolving polymer, *AIChE Journal* **41** (11) (1995) 2345-2355.
- [47] E.C. Aifantis, On the problem of diffusion in solids, *Acta Mechanica* **37** (3) (1980) 265-296.
- [48] M.-H. Klopffer, B. Flaconneche, Transport properdines of gases in polymers: bibliographic review, *Oil & Gas Science and Technology* **56** (3) (2001) 223-244.

- [49] S.-U. Hong, Prediction of Polymer/Solvent Diffusion Behavior Using Free-Volume Theory, *Industrial & Engineering Chemistry Research* **34** (7) (1995) 2536-2544.
- [50] K.E. Polmanteer, Current Perspectives on Silicone Rubber Technology, *Rubber Chemistry and Technology* **54** (5) (1981) 1051-1080.
- [51] E.L. Warrick, O.R. Pierce, K.E. Polmanteer, J.C. Saam, Silicone Elastomer Developments 1967–1977, *Rubber Chemistry and Technology* **52** (3) (1979) 437-525.
- [52] J.S. Vrentas, C.M. Vrentas, Solvent self-diffusion in crosslinked polymers, *Journal of Applied Polymer Science* **42** (7) (1991) 1931-1937.
- [53] H. Lin, T. Kai, B.D. Freeman, S. Kalakkunnath, D.S. Kalika, The Effect of Cross-Linking on Gas Permeability in Cross-Linked Poly(Ethylene Glycol Diacrylate), *Macromolecules* **38** (20) (2005) 8381-8393.
- [54] A.R. Berens, H.B. Hopfenberg, Diffusion of organic vapors at low concentrations in glassy PVC, polystyrene, and PMMA, *Journal of Membrane Science* **10** (2) (1982) 283-303.
- [55] T. Nakagawa, H.B. Hopfenberg, V. Stannett, Transport of fixed gases in radiation-stabilized poly(vinyl chloride), *Journal of Applied Polymer Science* **15** (1) (1971) 231-245.
- [56] P. Tremblay, M.M. Savard, J. Vermette, R. Paquin, Gas permeability, diffusivity and solubility of nitrogen, helium, methane, carbon dioxide and formaldehyde in dense polymeric membranes using a new on-line permeation apparatus, *Journal of Membrane Science* **282** (1–2) (2006) 245-256.
- [57] H. Sanaeepur, A.E. Amooghin, A. Moghadassi, A. Kargari, Preparation and characterization of acrylonitrile–butadiene–styrene/poly(vinyl acetate) membrane for CO₂ removal, *Separation and Purification Technology* **80** (3) (2011) 499-508.
- [58] K. Ghosal, R.T. Chern, B.D. Freeman, W.H. Daly, I.I. Negulescu, Effect of Basic Substituents on Gas Sorption and Permeation in Polysulfone, *Macromolecules* **29** (12) (1996) 4360-4369.
- [59] P.J. Rae, D.M. Dattelbaum, The properties of poly(tetrafluoroethylene) (PTFE) in compression, *Polymer* **45** (22) (2004) 7615-7625.
- [60] R.A. Pasternak, M.V. Christensen, J. Heller, Diffusion and Permeation of Oxygen, Nitrogen, Carbon Dioxide, and Nitrogen Dioxide through Polytetrafluoroethylene, *Macromolecules* **3** (3) (1970) 366-371.
- [61] R. Gregorio, E.M. Ueno, Effect of crystalline phase, orientation and temperature on the dielectric properties of poly (vinylidene fluoride) (PVDF), *J Mater Sci* **34** (18) (1999) 4489-4500.
- [62] J.M. B. Flaconnèche, M.H. Klopffer, Permeability, Diffusion and Solubility of Gases in Polyethylene, Polyamide 11 and Poly(vinylidene fluoride), *Oil & Gas Science and Technology* **56** (3) (2001) 261-278.
- [63] H.A. Khonakdar, S.H. Jafari, R. Hässler, Glass-transition-temperature depression in chemically crosslinked low-density polyethylene and high-density polyethylene and their blends with ethylene vinyl acetate copolymer, *Journal of Applied Polymer Science* **104** (3) (2007) 1654-1660.
- [64] P. Fröbing, A. Kremmer, R. Gerhard-Multhaupt, A. Spanoudaki, P. Pissis, Relaxation processes at the glass transition in polyamide 11: From rigidity to viscoelasticity, *The Journal of Chemical Physics* **125** (21) (2006) 214701.
- [65] S.N. Leung, A. Wong, Q. Guo, C.B. Park, J.H. Zong, Change in the critical nucleation radius and its impact on cell stability during polymeric foaming processes, *Chemical Engineering Science* **64** (23) (2009) 4899-4907.
- [66] J.S. Colton, N.P. Suh, The nucleation of microcellular thermoplastic foam with additives: Part I: Theoretical considerations, *Polymer Engineering & Science* **27** (7) (1987) 485-492.
- [67] B.A. Rodeheaver, J.S. Colton, Open-celled microcellular thermoplastic foam, *Polymer Engineering & Science* **41** (3) (2001) 380-400.
- [68] M. Blander, J.L. Katz, Bubble nucleation in liquids, *AIChE Journal* **21** (5) (1975) 833-848.
- [69] X. Liao, H. Xu, S. Li, C. Zhou, G. Li, C.B. Park, The effects of viscoelastic properties on the cellular morphology of silicone rubber foams generated by supercritical carbon dioxide, *RSC Advances* **5** (129) (2015) 106981-106988.
- [70] H. Li, L.J. Lee, D.L. Tomasko, Effect of Carbon Dioxide on the Interfacial Tension of Polymer Melts, *Industrial & Engineering Chemistry Research* **43** (2) (2004) 509-514.

- [71] R.B.T. H. Park, N. Lanson, C. Tzoganakis, C. B. Park, and, and P. Chen, Effect of Temperature and Pressure on Surface Tension of Polystyrene in Supercritical Carbon Dioxide, *The Journal of Physical Chemistry B* (2007).
- [72] S.N. Leung, Mechanisms of cell nucleation, growth, and coarsening in plastic foaming: theory, simulation and experiment, PhD dissertation, University of Toronto (2009)
- [73] K. Goren, L. Chen, L.S. Schadler, R. Ozisik, Influence of nanoparticle surface chemistry and size on supercritical carbon dioxide processed nanocomposite foam morphology, *The Journal of Supercritical Fluids* **51** (3) (2010) 420-427.
- [74] M.H.N. Famili, H. Janani, M.S. Enayati, Foaming of a polymer–nanoparticle system: Effect of the particle properties, *Journal of Applied Polymer Science* **119** (5) (2011) 2847-2856.
- [75] P.M. Wilt, Nucleation rates and bubble stability in water-carbon dioxide solutions, *Journal of Colloid and Interface Science* **112** (2) (1986) 530-538.
- [76] S. Costeux, CO₂-blown nanocellular foams, *Journal of Applied Polymer Science* **131** (23) (2014) n/a-n/a.
- [77] C. Forest, P. Chaumont, P. Cassagnau, B. Swoboda, P. Sonntag, Polymer nano-foams for insulating applications prepared from CO₂ foaming, *Progress in Polymer Science* **41** (2015) 122-145.
- [78] J. Tatibouët, R. Gendron, A Study of Strain-Induced Nucleation in Thermoplastic Foam Extrusion, *Journal of Cellular Plastics* **40** (1) (2004) 27-44.
- [79] L. Chen, X. Wang, R. Straff, K. Blizard, Shear stress nucleation in microcellular foaming process, *Polymer Engineering & Science* **42** (6) (2002) 1151-1158.
- [80] L. Chen, H. Sheth, X. Wang, Effects of Shear Stress and Pressure Drop Rate on Microcellular Foaming Process, *Journal of Cellular Plastics* **37** (4) (2001) 353-363.
- [81] A. Wong, R.K.M. Chu, S.N. Leung, C.B. Park, J.H. Zong, A batch foaming visualization system with extensional stress-inducing ability, *Chemical Engineering Science* **66** (1) (2011) 55-63.
- [82] L.C. Wang, S. Leung, M. Bussmann, C.B. Park, Local pressure fluctuation around a cavity surface of a heterogeneous nucleation site.
- [83] R.J. Albalak, Z. Tadmor, Y. Talmon, Polymer melt devolatilization mechanisms, *AIChE Journal* **36** (9) (1990) 1313-1320.
- [84] S.-T. Lee, Shear effects on thermoplastic foam nucleation, *Polymer Engineering & Science* **33** (7) (1993) 418-422.
- [85] E.N. Harvey, D.K. Barnes, W.D. McElroy, A.H. Whiteley, D.C. Pease, K.W. Cooper, Bubble formation in animals. I. Physical factors, *Journal of Cellular and Comparative Physiology* **24** (1) (1944) 1-22.
- [86] N.S. Ramesh, D.H. Rasmussen, G.A. Campbell, The heterogeneous nucleation of microcellular foams assisted by the survival of microvoids in polymers containing low glass transition particles. Part II: Experimental results and discussion, *Polymer Engineering & Science* **34** (22) (1994) 1698-1706.
- [87] Y. Kim, C.B. Park, P. Chen, R.B. Thompson, Towards maximal cell density predictions for polymeric foams, *Polymer* **52** (24) (2011) 5622-5629.
- [88] X. Xu, D.E. Cristancho, S. Costeux, Z.-G. Wang, Bubble nucleation in polymer-CO₂ mixtures, *Soft Matter* **9** (40) (2013) 9675-9683.
- [89] K. Taki, Experimental and numerical studies on the effects of pressure release rate on number density of bubbles and bubble growth in a polymeric foaming process, *Chemical Engineering Science* **63** (14) (2008) 3643-3653.
- [90] C.D. Han, H.J. Yoo, Studies on structural foam processing. IV. Bubble growth during mold filling, *Polymer Engineering & Science* **21** (9) (1981) 518-533.
- [91] M.A. Shafi, J.G. Lee, R.W. Flumerfelt, Prediction of cellular structure in free expansion polymer foam processing, *Polymer Engineering & Science* **36** (14) (1996) 1950-1959.
- [92] J. Bruchon, T. Coupez, A numerical strategy for the direct 3D simulation of the expansion of bubbles into a molten polymer during a foaming process, *International Journal for Numerical Methods in Fluids* **57** (8) (2008) 977-1003.

- [93] T.R. Tuladhar, M.R. Mackley, Experimental observations and modelling relating to foaming and bubble growth from pentane loaded polystyrene melts, *Chemical Engineering Science* **59** (24) (2004) 5997-6014.
- [94] J.R. Royer, Y.J. Gay, J.M. Desimone, S.A. Khan, High-pressure rheology of polystyrene melts plasticized with CO₂: Experimental measurement and predictive scaling relationships, *Journal of Polymer Science Part B: Polymer Physics* **38** (23) (2000) 3168-3180.
- [95] P.R. Soskey, H.H. Winter, Equibiaxial Extension of Two Polymer Melts: Polystyrene and Low Density Polyethylene, *Journal of Rheology* **29** (5) (1985) 493-517.
- [96] P.G.D. Gennes, Dynamics of Entangled Polymer Solutions. II. Inclusion of Hydrodynamic Interactions, *Macromolecules* **9** (4) (1976) 594-598.
- [97] L.J. Gerhardt, C.W. Manke, E. Gulari, Rheology of polydimethylsiloxane swollen with supercritical carbon dioxide, *Journal of Polymer Science Part B: Polymer Physics* **35** (3) (1997) 523-534.
- [98] K. Taki, K. Tabata, S.-i. Kihara, M. Ohshima, Bubble coalescence in foaming process of polymers, *Polymer Engineering & Science* **46** (5) (2006) 680-690.
- [99] J.J. Feng, C.A. Bertelo, Prediction of bubble growth and size distribution in polymer foaming based on a new heterogeneous nucleation model, *Journal of Rheology* **48** (2) (2004) 439-462.
- [100] N.S. Ramesh, D.H. Rasmussen, G.A. Campbell, Numerical and experimental studies of bubble growth during the microcellular foaming process, *Polymer Engineering & Science* **31** (23) (1991) 1657-1664.
- [101] B. Krause, K. Diekmann, N.F.A. van der Vegt, M. Wessling, Open Nanoporous Morphologies from Polymeric Blends by Carbon Dioxide Foaming, *Macromolecules* **35** (5) (2002) 1738-1745.
- [102] M. Yamaguchi, M. Takahashi, Rheological properties of low-density polyethylenes produced by tubular and vessel processes, *Polymer* **42** (21) (2001) 8663-8670.
- [103] T. Takahashi, J.I. Takimoto, K. Koyama, Elongational viscosity for miscible and immiscible polymer blends. II. Blends with a small amount of UHMW polymer, *Journal of Applied Polymer Science* **72** (7) (1999) 961-969.
- [104] C. Forest, P. Chaumont, P. Cassagnau, B. Swoboda, P. Sonntag, Nanofoaming of PMMA using a batch CO₂ process: Influence of the PMMA viscoelastic behaviour, *Polymer* **77** (2015) 1-9.
- [105] S.T. Lee, C.B. Park, *Foam extrusion: Principles and Practices*, CRC Press 2000.
- [106] D. Li, Coalescence between small bubbles: Effects of surface tension gradient and surface viscosities, *Journal of Colloid and Interface Science* **181** (1996) p. 34-44.
- [107] J.M.H. Janssen, Dynamics of liquid-liquid mixing, *University of Eindhoven* (1993,) p.59-75.
- [108] C.B. Park, A.H. Behravesh, R.D. Venter, Low density microcellular foam processing in extrusion using CO₂, *Polymer Engineering & Science* **38** (11) (1998) 1812-1823.
- [109] M.-S. Kim, C.-C. Park, S.R. Chowdhury, G.-H. Kim, Physical properties of ethylene vinyl acetate copolymer (EVA)/natural rubber (NR) blend based foam, *Journal of Applied Polymer Science* **94** (5) (2004) 2212-2216.
- [110] S.K. Wason, G. Mooney, C.R. Andrews, M.E. Tarquini, J.A. Kosin, R.A. Garcia, Endothermic blowing agents compositions and applications, Google Patents, 1992.
- [111] A. Megally, R. Vossen, Multilayer thermoplastic sheet materials and thermoformed articles prepared therefrom, Google Patents, 2011.
- [112] A.H. Landrock, *5 - Miscellaneous and specialty foams: (Epoxy Foams, Polyester Foams, Silicone Foams, Urea-Formaldehyde Foams, Polybenzimidazole, Foams, Polyimide Foams, Polyphosphazene Foams, and Syntactic Foams)*, Handbook of Plastic Foams, William Andrew Publishing, Park Ridge, NJ, 1995, pp. 253-266.
- [113] E.-S. Park, Mechanical properties and antibacterial activity of peroxide-cured silicone rubber foams, *Journal of Applied Polymer Science* **110** (3) (2008) 1723-1729.
- [114] J. Gao, J. Wang, H. Xu, C. Wu, Preparation and properties of hollow glass bead filled silicone rubber foams with low thermal conductivity, *Materials & Design* **46** (2013) 491-496.
- [115] P. Hagen, Extruded foamed silicone rubber composition and method for making same, 1999, US 5985947 A

- [116] G. Marquardt, T. Naumann, H. Hurnik, Method for producing silicone foams, 2002, US6359026 B1
- [117] P. Liu, D. Liu, H. Zou, P. Fan, W. Xu, Structure and properties of closed-cell foam prepared from irradiation crosslinked silicone rubber, *Journal of Applied Polymer Science* **113** (6) (2009) 3590-3595.
- [118] B. Liu, P.-C. Wang, Y.-Y. Ao, Y. Zhao, Y. An, H.-B. Chen, W. Huang, Effects of combined neutron and gamma irradiation upon silicone foam, *Radiation Physics and Chemistry* **133** (2017) 31-36.
- [119] H.L. Sui, X.Y. Liu, F.C. Zhong, X.Y. Li, L. Wang, X. Ju, Gamma radiation effects on polydimethylsiloxane rubber foams under different radiation conditions, *Nuclear Instruments and Methods in Physics Research Section B: Beam Interactions with Materials and Atoms* **307** (2013) 570-574.
- [120] D.E. Weyer, Method of preparing siloxane resin foams, 1958, US 2833732 A
- [121] J. Bruner, Method of preparing organosiloxane elastomer foams, 1962, US 3070555A
- [122] S.V. Dubiel, G.W. Griffith, C.L. Long, G.K. Baker, R.E. Smith, Determination of reactive components in silicone foams, *Analytical Chemistry* **55** (9) (1983) 1533-1537.
- [123] D. Blanc, D. Canpont, Silicone composition for elastomer foam, 2012, WO2012032231 A1
- [124] M.-C. Dib Jawhar, PhD dissertation: "Study of the Coalescence Mechanisms During Silicone Foaming", University of Lyon (2012)
- [125] M.-C.D. Jawhar, D. Blanc, P. Chaumont, P. Cassagnau, Study of the Coalescence Mechanisms During Silicone Foaming, *Macromolecular Materials and Engineering* **299** (3) (2014) 336-343.
- [126] R. Verdejo, F. Barroso-Bujans, M.A. Rodriguez-Perez, J. Antonio de Saja, M.A. Lopez-Manchado, Functionalized graphene sheet filled silicone foam nanocomposites, *Journal of Materials Chemistry* **18** (19) (2008) 2221-2226.
- [127] R. Verdejo, F. Barroso-Bujans, M.A. Rodriguez-Perez, J. Antonio de Saja, M. Arroyo, M.A. Lopez-Manchado, Carbon nanotubes provide self-extinguishing grade to silicone-based foams, *Journal of Materials Chemistry* **18** (33) (2008) 3933-3939.
- [128] R. Verdejo, C. Saiz-Arroyo, J. Carretero-Gonzalez, F. Barroso-Bujans, M.A. Rodriguez-Perez, M.A. Lopez-Manchado, Physical properties of silicone foams filled with carbon nanotubes and functionalized graphene sheets, *European Polymer Journal* **44** (9) (2008) 2790-2797.
- [129] A. Labouriau, C. Cady, J. Gill, D. Taylor, A. Zocco, J. Stull, K. Henderson, D. Wroblewski, The effects of gamma irradiation on RTV polysiloxane foams, *Polymer Degradation and Stability* **117** (2015) 75-83.
- [130] A. Labouriau, T. Robison, L. Meincke, D. Wroblewski, D. Taylor, J. Gill, Aging mechanisms in RTV polysiloxane foams, *Polymer Degradation and Stability* **121** (2015) 60-68.
- [131] B.M. Patterson, K. Henderson, Z. Smith, Measure of morphological and performance properties in polymeric silicone foams by X-ray tomography, *J Mater Sci* **48** (5) (2013) 1986-1996.
- [132] T. Kobayashi, H. Saitoh, N. Fujii, Y. Hoshino, M. Takanashi, Porous membrane of polydimethylsiloxane by hydrosilylation cure: Characteristics of membranes having pores formed by hydrogen foams, *Journal of Applied Polymer Science* **50** (6) (1993) 971-979.
- [133] J.B. Grande, A.S. Fawcett, A.J. McLaughlin, F. Gonzaga, T.P. Bender, M.A. Brook, Anhydrous formation of foamed silicone elastomers using the Piers–Rubinsztajn reaction, *Polymer* **53** (15) (2012) 3135-3142.
- [134] M.N. Shimbo, T. On foaming process of vulcanized rubber using physical blowing agent, *Proceedings of ICAD2004* (2004).
- [135] I.-K. Hong, S. Lee, Microcellular foaming of silicone rubber with supercritical carbon dioxide, *Korean J. Chem. Eng.* **31** (1) (2014) 166-171.
- [136] L. Song, A. Lu, P. Feng, Z. Lu, Preparation of silicone rubber foam using supercritical carbon dioxide, *Materials Letters* **121** (2014) 126-128.
- [137] F. Chambon, H.H. Winter, Linear Viscoelasticity at the Gel Point of a Crosslinking PDMS with Imbalanced Stoichiometry, *Journal of Rheology* **31** (683) (1987).
- [138] H. Yan, K. Wang, Y. Zhao, Fabrication of Silicone Rubber Foam with Tailored Porous Structures by Supercritical CO₂, *Macromolecular Materials and Engineering* (2016).

- [139] Y.-W. Kim, C.B. Park, Processing of microcellular preceramics using carbon dioxide, *Composites Science and Technology* **63** (16) (2003) 2371-2377.
- [140] F. Wolff, B. Ceron Nicolat, T. Fey, P. Greil, H. Münstedt, Extrusion Foaming of a Pre ceramic Silicone Resin with a Variety of Profiles and Morphologies, *Advanced Engineering Materials* **14** (12) (2012) 1110-1115.
- [141] C.B.P. Qingfeng Wu, Nanqiao Zhou, and Wenli Zhu, Effect of Temperature on Foaming Behaviors of Homo- and Co-polymer Polypropylene/Polydimethylsiloxane Blends with CO₂, *Journal of Cellular Plastics* **45** (2009) 303-319.
- [142] W. Wang, S. Zhou, Z. Xin, Y. Shi, S. Zhao, Polydimethylsiloxane assisted supercritical CO₂ foaming behavior of high melt strength polypropylene grafted with styrene, *Frontiers of Chemical Science and Engineering* **10** (3) (2016) 396-404.
- [143] S. Siripurapu, J.M. DeSimone, S.A. Khan, R.J. Spontak, Controlled Foaming of Polymer Films through Restricted Surface Diffusion and the Addition of Nanosilica Particles or CO₂-philic Surfactants, *Macromolecules* **38** (6) (2005) 2271-2280.
- [144] P. Spitael, C.W. Macosko, R.B. McClurg, Block Copolymer Micelles for Nucleation of Microcellular Thermoplastic Foams, *Macromolecules* **37** (18) (2004) 6874-6882.
- [145] A. Strachota, M. Černý, Z. Chlup, K. Depa, M. Šlouf, Z. Sucharda, Foaming of polysiloxane resins with ethanol: A new route to pyrolytic macrocellular SiOC foams, *Ceramics International* **41** (10, Part A) (2015) 13561-13571.
- [146] J. Zhao, G. Luo, J. Wu, H. Xia, Preparation of Microporous Silicone Rubber Membrane with Tunable Pore Size via Solvent Evaporation-Induced Phase Separation, *ACS Applied Materials & Interfaces* **5** (6) (2013) 2040-2046.
- [147] M.-T. Grosse, M. Lamotte, M. Birot, H. Deleuze, Preparation of microcellular polysiloxane monoliths, *Journal of Polymer Science Part A: Polymer Chemistry* **46** (1) (2008) 21-32.
- [148] J. Normatov, M.S. Silverstein, Highly porous elastomer-silsesquioxane nanocomposites synthesized within high internal phase emulsions, *Journal of Polymer Science Part A: Polymer Chemistry* **46** (7) (2008) 2357-2366.
- [149] K. Zimny, A. Merlin, A. Ba, C. Aristégui, T. Brunet, O. Mondain-Monval, Soft Porous Silicone Rubbers as Key Elements for the Realization of Acoustic Metamaterials, *Langmuir* **31** (10) (2015) 3215-3221.
- [150] A. Kovalenko, K. Zimny, B. Mascaro, T. Brunet, O. Mondain-Monval, Tailoring of the porous structure of soft emulsion-templated polymer materials, *Soft Matter* **12** (23) (2016) 5154-5163.
- [151] H. Nazir, W. Zhang, Y. Liu, X. Chen, L. Wang, M.M. Naseer, G. Ma, Silicone oil emulsions: strategies to improve their stability and applications in hair care products, *International Journal of Cosmetic Science* **36** (2) (2014) 124-133.
- [152] M. Tebboth, Q. Jiang, A. Kogelbauer, A. Bismarck, Inflatable Elastomeric Macroporous Polymers Synthesized from Medium Internal Phase Emulsion Templates, *ACS Applied Materials & Interfaces* **7** (34) (2015) 19243-19250.
- [153] A.D. Martina, J.G. Hilborn, J. Kiefer, J.L. Hedrick, S. Srinivasan, R.D. Miller, *Siloxane Elastomer Foams*, Polymeric Foams, American Chemical Society, 1997, pp. 8-25.
- [154] M. Adam, S. Kocanis, T. Fey, M. Wilhelm, G. Grathwohl, Hierarchically ordered foams derived from polysiloxanes with catalytically active coatings, *Journal of the European Ceramic Society* **34** (7) (2014) 1715-1725.
- [155] J.P. Fuller, D. Pegg, R.M.L. Bird, T.B. Clifford, T. Clayson, Preparation of porous silicone rubber for growing cells or living tissue, 2005, US6900055 B1
- [156] H.A.I. Andrés Díaz Lantada, Beatriz Pareja Sánchez, and Josefa Predestinación García-Ruíz, Free-Form Rapid Prototyped Porous PDMS Scaffolds Incorporating Growth Factors Promote Chondrogenesis, *Advances in Materials Science and Engineering* **2014** (2014) 10.
- [157] P.K. Yuen, H. Su, V.N. Goral, K.A. Fink, Three-dimensional interconnected microporous poly(dimethylsiloxane) microfluidic devices, *Lab on a Chip* **11** (8) (2011) 1541-1544.

- [158] N. Annabi, J.W. Nichol, X. Zhong, C. Ji, S. Koshy, A. Khademhosseini, F. Dehghani, Controlling the Porosity and Microarchitecture of Hydrogels for Tissue Engineering, *Tissue Engineering. Part B, Reviews* **16** (4) (2010) 371-383.
- [159] S. Mohanty, L.B. Larsen, J. Trifol, P. Szabo, H.V.R. Burri, C. Canali, M. Dufva, J. Emnéus, A. Wolff, Fabrication of scalable and structured tissue engineering scaffolds using water dissolvable sacrificial 3D printed moulds, *Materials Science and Engineering: C* **55** (2015) 569-578.
- [160] M. Kessler, C. Roggendorf, A. Schnettler, Investigation of the physical properties of elastic syntactic foams, Electrical Insulation (ISEI), Conference Record of the 2012 IEEE International Symposium on, 2012, pp. 526-530.
- [161] D.L. Folds, Experimental Determination of Ultrasonic Wave Velocities in Plastics, Elastomers, and Syntactic Foam as a Function of Temperature, *The Journal of the Acoustical Society of America* **52** (1B) (1972) 426-427.
- [162] R. Lim, R.H. Hackman, Acoustic attenuation in syntactic foam and heavy silicone rubber composites, *The Journal of the Acoustical Society of America* **85** (S1) (1989) S131-S131.
- [163] Q. Liu, L. Shao, H. Fan, Y. Long, N. Zhao, S. Yang, X. Zhang, J. Xu, Characterization of maxillofacial silicone elastomer reinforced with different hollow microspheres, *J Mater Sci* **50** (11) (2015) 3976-3983.
- [164] P. Fahr, M.Y.a. , A. Shukla, Shock response of filled corrugated sandwich structures under extreme temperatures, *Journal of Sandwich Structures and Materials* (2016).
- [165] M. Kessler, A. Troeger, B. Heil, A. Schnettler, Investigation of the Electrical Properties of Elastic Syntactic Foam, Electrical Insulation, 2008. ISEI 2008. Conference Record of the 2008 IEEE International Symposium on, 2008, pp. 261-264.
- [166] S. Kenig, Narkis, M., Three-Phase Silicone Based Syntactic Foams, *Journal of Cellular Plastics* **20** (6) (1984) 423-429.
- [167] M.F. Yazici, P. Shukla, A., Development of a Polymer Based Syntactic Foam for High Temperature Applications, *Acta Physica Polonica A* (2014).
- [168] M. Nakanishi, Composite de caoutchouc de silicone, 1993, EP0186493 A2
- [169] L.O. Svedberg, P. AJDÉN, A method and a device for preparation of expanded thermoplastic microspheres, 2014, WO2014037361 A1
- [170] R.E. Kittle, G.M. Ronk, Method of foaming a siloxane composition using microwave energy, 1977, US4026844 A

Chapter 2: Materials and Methods

I. Materials

In this chapter the materials and the experimental methods that have been used in this work will be presented. As this thesis has been written in articles format, the materials and methods used in each one of the papers will be explained in each article. However, this chapter aims to compile the information about the materials and methods used in this study including some additional information.

I.1. Silicone polymers

A methylvinyl dimethylsiloxane elastomer, named *S*, was kindly supplied by BlueStar Silicone. Its density is about 0.97. Molar masses were determined by size exclusion chromatography (SEC) with toluene in universal calibration mode. Molar percentage of vinyl groups inside silicone backbone chain was determined by NMR in CDCl₃.

(98-99% Methyl-3,3,3-trifluoropropylsiloxane)-(1-2% methylvinyl-siloxane) elastomer (named *FS*) was purchased from ABCR (AB116651). Its density is about 1.30. The molar masses were determined by size exclusion chromatography (SEC) with THF as eluent in universal calibration mode. Molar percentage of vinyl groups inside silicone backbone chain was determined by NMR in d-THF.

S and *FS* have 10.3 and 4.1 vinyl groups per chain respectively. As a consequence, the molar mass of molecular segment between two consecutive vinyl groups, M_0 , for *S* and *FS* are equal to 37000 and 15500 g/mol respectively. Moreover, the fluorosilicone is amorphous whereas silicone is a semi-crystalline polymer. Elastomer properties are summed-up in Table 1.

Table 1: Main elastomer properties

Polymer	M_n [kg/mol] ^a	M_w [kg/mol] ^a	%mol vinyl groups ^b	T_g [°C] ^c	T_c [°C] ^c	T_f [°C] ^c
<i>S</i>	380	600	0.22	-126	-90 / -84*	-46 / -41
<i>FS</i>	63	434	1	-70	-	-

^a SEC measurements; ^b NMR results; ^c DSC measurements; *Cold crystallization

The master curves of complex shear moduli and viscosities as function of frequency for both silicone elastomers are shown in Fig. 1, $T_{ref}=30^\circ\text{C}$.

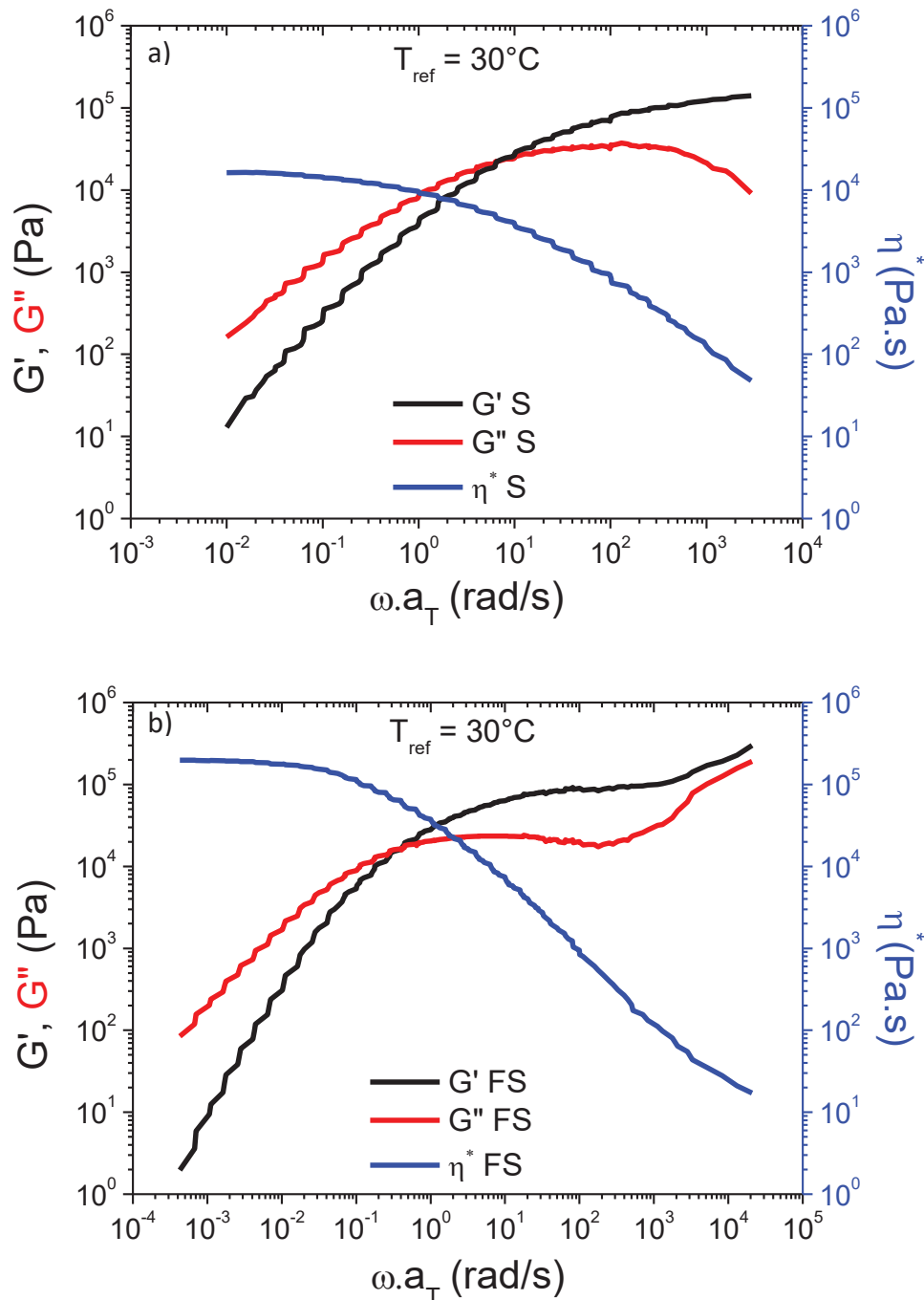


Fig. 1: Viscoelastic behavior: a) S; b) FS. Master curves at $T_{ref}=30^{\circ}\text{C}$

The zero shear viscosity was directly measured on the rheological curves at 30°C . The G' , G'' crossover defines the characteristic relaxation time, τ_c . Rheological shift factors, a_{T/T_0} , were determined using TTS module of Trios software. Flow activation energy of polymers used was modeled by an Arrhenius law of the temperature dependence of the shift factors. These three material parameters are reported in Table 2. Williams-Landel-Ferry (WLF) model fits better the data for the fluorosilicone, as it is an amorphous polymer, even if temperatures are well above $T_g+100^{\circ}\text{C}$ suggesting large flowing units. WLF parameters are as follows: $C_1=2.98$, $C_2=142.6\text{K}$ and $T_0=303\text{K}$.

The mastercurves also allow us to estimate the molar mass between entanglements. Indeed, the latter, called M_e , is usually determined from the rubbery plateau modulus G_N^0 through an equation derived from the theory of rubber elasticity [1, 2]:

$$G_N^0 = \frac{\rho RT}{M_e} \quad (1)$$

where ρ : polymer density [$\text{kg}\cdot\text{m}^{-3}$]

R : gas constant [$\text{J}\cdot\text{mol}^{-1}\cdot\text{K}^{-1}$]

T : absolute temperature [K]

In the case of S, the rubbery plateau is not well reached. However, G_N^0 is reported in literature to be about 2.4×10^5 Pa [3]. The rubbery plateau for the fluorosilicone is found to be around 1.1×10^5 Pa. The molar masses between entanglements are listed in Table 2. Thus, these values of M_e suggest there will be trapped physical entanglements during a cross-linking step in the silicone elastomer only ($M_e < M_0$) [4].

Table 2 : Rheological data of both silicone elastomers used

Polymer	η_0 (30°C) [Pa.s] $\times 10^4$	$\tau_c = 1/\omega_c$ (30°C) [s]	E_a [kJ/mol]	M_e [kg/mol]
S	2,5	0.16	14.5	10
FS	22,5	2.27	WLF	30

The fluorosilicone elastomer will be blended in the silicone elastomer to take advantage of its CO_2 -philic behavior and its lower CO_2 diffusivity in order to obtain favored heterogeneous nucleation during the foaming process of silicone elastomer (Table 3).

Table 3 : CO_2 transport properties in polymers used

Polymer	$\bar{D}(\Delta c = 0) \times 10^6$ *	$\bar{S}(P = 0) \times 10^2$ *
$[(\text{CH}_3)_2\text{SiO}]_x$	26.4	1.72
$[(\text{CF}_3\text{C}_2\text{H}_4)\text{CH}_3\text{SiO}]_x$	5.26	2.31

Units: \bar{D} [cm^2/s]; \bar{S} [cm^3 (STP)/ cm^3 (polymer)cmHg], T_g [°C]. * [5].

I.2. Peroxide

Dicumyl peroxide (DCP, $M=270$ g.mol⁻¹) was used as the free radical initiator of the crosslinking reaction in S and FS elastomers. It was purchased from Aldrich with an assay of 98% and used as received. The thermal decomposition of DCP was determined by [16, 24]:

$$\frac{d[\text{DCP}]}{dt} = -Ae^{-\left(\frac{E_a}{RT}\right)}[\text{DCP}] \quad (2)$$

With $A=7.47 \times 10^{15}$ s⁻¹; $E_a=153$ kJ/mol

I.3. Fumed silicas

Two commercial fumed silicas were used with two surface chemistries but the same specific area, 200m²/g. These fumed silica will be added in S/FS blend in order to study their stabilization effect on blend morphologies. R974 silica is a hydrophobic fumed silica after-treated with dimethyldichlorosilane while the A200 is a hydrophilic silica. A typical filler morphology is illustrated in Fig. 2. Fumed silica density is assumed to be equal to 2.2. The surface tension of each fillers are listed in Table 4.

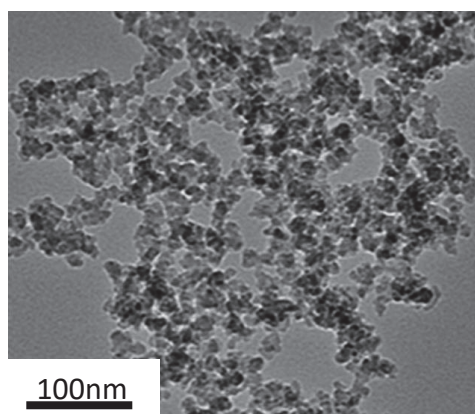


Fig. 2 : TEM image of fumed silica A200 [6].

Table 4: Surface tension data of each silica [7]

	Surface tension at 25°C (mN/m)		
	γ	γ^d	γ^p
A200	80	29.4	50.6
R974	81.7	72.3	9.4

I.4. Thermoplastic vulcaniztes (TPV) silicone components

Low-density polyethylene (LDPE) was used as thermoplastic phase ($M_n=14$ kg/mol and $M_w =107$ kg/mol [8]) while a bi-component liquid silicone rubber (LSR A/B) was used as the rubber phase. A copolymer PE grafted anhydride maleic (PE-g-AM) was used a compatibilizer using the same strategy that Prakashan et al. [9]. It contains 0.5-1%wt of AM. The main characteristics of materials and LSR parts are reported in Table 5 and in Table 6, respectively. The R972 fumed silica has a hydrophobic surface and it is used as nucleating agent. The primary particle size is 16 nm leading to a specific area of 110m²/g.

Table 5: Main properties of formulation components

Materials	Trade name	T _m [°C]	η ₀ [Pa.s]	Y _p [mN/m]	Y _d [mN/m]	Density (g.cm ⁻³)	Supplier
LDPE	LD 0304	111	17 000 ^{a)}	1.1 ^{b)}	32 ^{b)}	0.92	Total
LSR A/B	SL 7240	-40	-	1.1 ^{b)}	21.7 ^{b)}	1.12	KCC
PE-grafted Anhydride maleic	Exxelor PE 1040	132	180 000 ^{a)}	-	-	0.96	ExxonMobil
Hydrophobic silica	Aerosil R972	-	-	2 ^{c)}	30 ^{c)}	2	Evonik

Note : ^{a)}160°C; ^{b)}[4]; ^{c)}[10]

Table 6: General LSR properties

Materials	%mol Si-Vi ^{a)}	%mol Si-H ^{a)}	%wt Silica ^{b)}	M _n [kg/mol] ^{c)}	M _w [kg/mol] ^{c)}
LSR A	0.5	-	60	110	170
LSR B	0.8	1.5	40	85	140

Note : ^{a)}NMR; ^{b)}TGA ; ^{c)}SEC toluene

1.5. Chemical blowing agent used in extrusion foaming process

Pamarole BA.M4.E.MG was used as the chemical blowing agent. It is an endothermic master batch containing 40% of active material, according to specifications, embedded in LDPE carrier, T_m = 104°C from DSC measurement. From SEM/EDX analysis Fig. 3, the reactive element is sodium bicarbonate crystals with a mean size of 4.7±3.5 μm. The density of CBA is estimated at 1.42 g/cm³ by a mix law assuming that 40 wt% of reactive agent is embedded in LDPE (ρ_{LDPE}=0.9 g/cm³ and ρ_{sodium bicarbonate} =2.2 g/cm³).

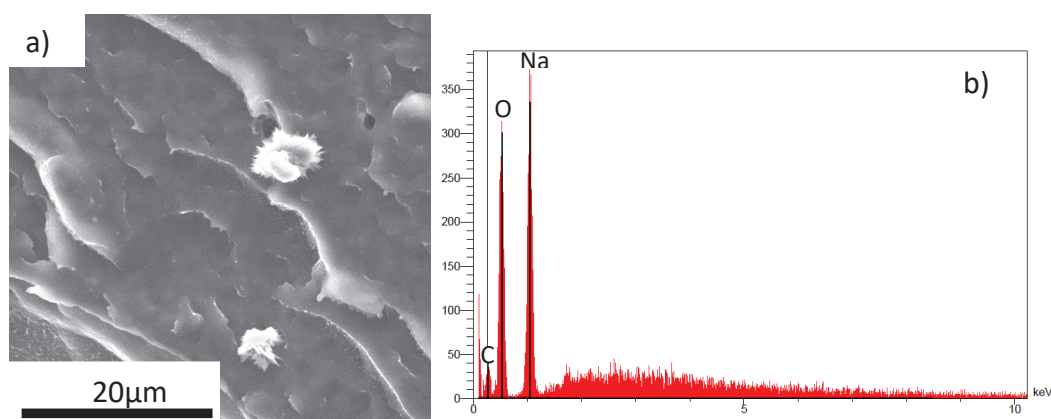
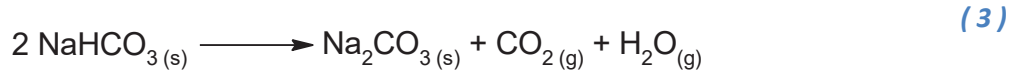


Fig. 3 : EDX analysis of the chemical blowing agent: a) Palmarole crystals dispersed in LDPE (SEM image); b) EDX measurement of a sodium bicarbonate crystal contained in palmarole.

TGA/GC measurements of palmarole were carried out to determine the amount of CO₂ produced by sodium bicarbonate at 160°C. The decomposition reaction is described in Eq. (3).



Using GC measurements, the decomposition palmarole produces approximately 0.02mol of CO_2 /g of CBA (molar volume of CO_2 at 160°C and 0.1MPa, $V_m=35.1$ L/mol). In extrusion foaming, the blowing effect should be due to both water and carbon dioxide expansion.

II. Materials processing

II.1. Premix procedures

II.1.1. Silicone/DCP blend procedure

Blends of silicone with several peroxide amounts were prepared for static and dynamic crosslinking techniques. First, S and DCP crystals are mixed in a roll mill (cylinder diameter=100 mm) at 30°C for at least 15 min to ensure good dispersion and homogenization with a gap of 0.4mm, noted as L , a roll speed of 25 rpm and a friction ratio of 0.8. Msakni et al.[11] modeled the DCP diffusion in engage copolymers and they found a diffusion coefficient at 30°C, $D_{12} \approx 6.5 \times 10^{-11} \text{m}^2 \cdot \text{s}^{-1}$. In silicone, the DCP diffusion coefficient should be of the order of magnitude of $10^{-10} \text{m}^2 \cdot \text{s}^{-1}$ because PDMS has a T_g around -120°C while Engage® copolymer's one is near -45°C [11], according to free volume theory [12]. Shear rate was estimated by analytical formulation, Eq.(4), with asymmetric roll speed in the nip region (U_1 and U_2) [13].

$$\dot{\gamma} = \frac{U_1 - U_2}{L} \quad (4)$$

We found a mean shear rate in the nip region, $\dot{\gamma} \approx 65 \text{s}^{-1}$. It is possible to estimate the time needed, t_b , to achieve a good dispersion of DCP by diffusion coupled with distributive mixing, Eq. (5) [14].

$$t_b = \sqrt{\frac{64L^2}{D_{12}\dot{\gamma}^2}} \quad (5)$$

We did not take into account elongational flow, viscoelasticity, the number of cutting of polymer blankets and local overheat in calculations. From all of these approximations, $t_b \approx 10\text{s}$ which is far below our processing time.

II.1.2. Silicone/Fluorosilicone blend procedure

Blends of silicone and fluorosilicone elastomers were prepared before the dynamic crosslinking step. First, silicone and fluorosilicone elastomers are mixed in a roll mill (cylinder diameter=100mm) at 30°C until homogenization, depending on the amount of fluorosilicone. Then, DCP crystals were added and the mixing goes on 5 min to ensure a good dispersion. The amount of DCP introduced is calculated as a function of the overall mass of both elastomers. Then if silica is used, the silica is added step by step. Once, all the content

of silica is introduced, a homogenization step is carried out for 10 min. The gap was set to 0.4mm, noted as L , a roll speed of 25 rpm and a friction ratio of 0.8.

II.2. Static crosslinking

Before crosslinking, blends are put into vacuum to avoid air bubbles at least for one day at room temperature. Then, samples are compression molded at 150°C for 2 hours using a hydraulic press with electrically heated platens, under a pressure of 100 bar. The sample thickness is 1 mm. According to thermal decomposition of DCP, Eq.(2), DCP is decomposed at 96% after 2h at 150°C (about five half-life times, $t_{1/2} \approx 25$ min). No rheological degradation occurred with silicone, without DCP, exposed to 150°C for 2 hours but some crosslinking by-products may be emitted when DCP is added.

II.3. Dynamic crosslinking

For dynamic crosslinking experiments, blends are crosslinked under shearing for 2 hours in a roll mill (or internal mixer with Banbury rotor) at constant gap, friction ratio and roll speed, the same as previously described in the blend procedure section. Temperatures are set to 150°C on each side of both rolls. Some experiments were carried out in a batch mixer with a Banbury rotor speed of 50 rpm in order to obtain torque along time for information as shown in Fig. 4. The chamber of the mixer was filled with a filling ratio of 0.7. Dynamic crosslinking tests were also performed under several atmospheres in a batch mixer (Haake Thermofischer) such as air and N₂. Each measurement was performed under the same conditions of temperature and rotor speed (145°C and 50 rpm). The N₂ was introduced at a constant flow rate directly in the chamber of the mixer. The chamber was “sealed” with a stopper while N₂ can steadily escape from a needle sunk through the stopper.

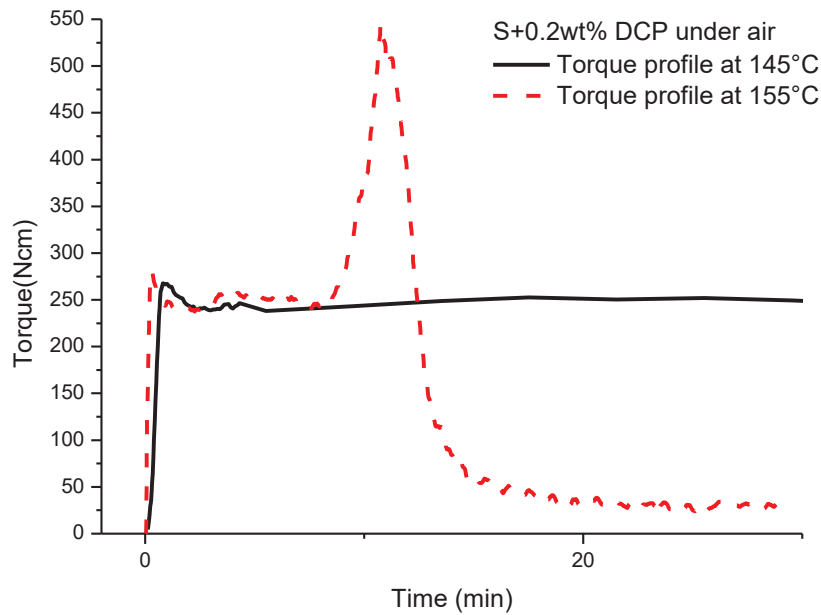


Fig. 4. Dynamic crosslinking of S+0.2wt%DCP in batch mixer (Variation of the torque and melt temperature versus shearing time). Under two different processing temperatures ($T=145$ and 155°C , set temperatures) under air, rotor speed = 50 rpm.

II.4. Twin-screw extrusion of TPV Silicone formulations

Formulations were extruded at 200°C with a screw speed of 300 rpm using a cletral twin screw extruder ($D=32$ and $L/D=52$) and dedicated pumps for LSR injections. Throughput was about 30 kg/h for LDPE and LSR output can vary from 70 to 350 g/min as a function of formulation. The LDPE, PE-g-AM pellets and silica particles were blended manually before extrusions. The ratio between LDPE/LSR was kept at 60/40 wt% for all the formulations. For TPV xB, x is the weight percentage of LSR B in the elastomeric phase in order to generate the selected gel fraction in the silicone phase. The nucleating agent (R972) amount was selected from Laguna-Gutierrez et al. work [15].

The LSR output limitation implies that TPV10B had to be extruded twice in order to be able to inject LSR A. For TPV20B, the output was increased by almost 2 in order to be able to inject LSR B. Blend compositions are summarized in Table 7. The LSR A alone is highly filled with silica (Table 6), therefore LDPE/LSRA was formulated to check the foamability of a blend between a thermoplastic and a yield stress fluid.

Table 7: Blend composition of the selected formulations (in phr)

Materials	LDPE	LDPE/LSRA	TPV 10B	TPV 20B
LDPE	100	100	100	100
LSR A	-	67	60	53
LSR B	-	-	6.7	13
PE-g-AM	-	2.5	2.5	2.5
Aerosill R972	1	1	1	1

III. Foaming processes

III.1. CO₂ batch foaming

Before the foaming experiment, a silicone/fluorosilicone formulation is compression molded, at 30°C, into a disk-shaped sample with a thickness of 1 mm using a 25 mm circular mold. Then, the circular sample is transferred in a glass Petri dish and constraints at the circular edges are added to avoid flowing during the saturation stage.

Then, this sample is placed into the autoclave at room temperature. Fig. 5 illustrates the device used for the saturation and the foaming stages which is a temperature and pressure controlled autoclave.

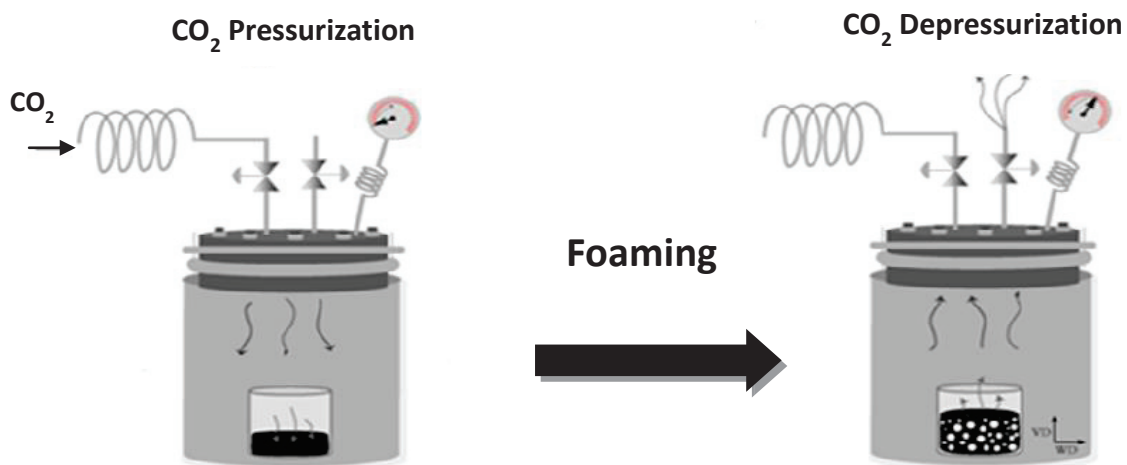


Fig. 5: One step CO₂ batch foaming system used [16] Copyright © 2012. Reproduced with permission from IOP Publishing Ltd.

Once, the temperature in the autoclave reaches the set value, CO₂ is introduced in the autoclave. Pressure ramps and iso-pressure stages are controlled manually. Pressure and temperature are recorded by computer acquisition (Fig. 6). As shown in Fig. 6, when the temperature set is lower than the ambient temperature, the pressure ramp causes a temperature increase inside the pressure vessel which quickly comes back to the set value.

The saturation time stage was selected from experiments realized at several saturation time: 1, 3, 5 hours. In the present work, foaming tests were carried out mainly with gaseous CO₂ (P=32 bar) with a saturation stage of 5 hours. Indeed, a saturation stage with gaseous CO₂ at “low” temperature requires a greater sorption time to reach the CO₂ uptake equilibrium than in supercritical conditions. CO₂ with the purity of 99.99% (N50) was used from Alphagaz.

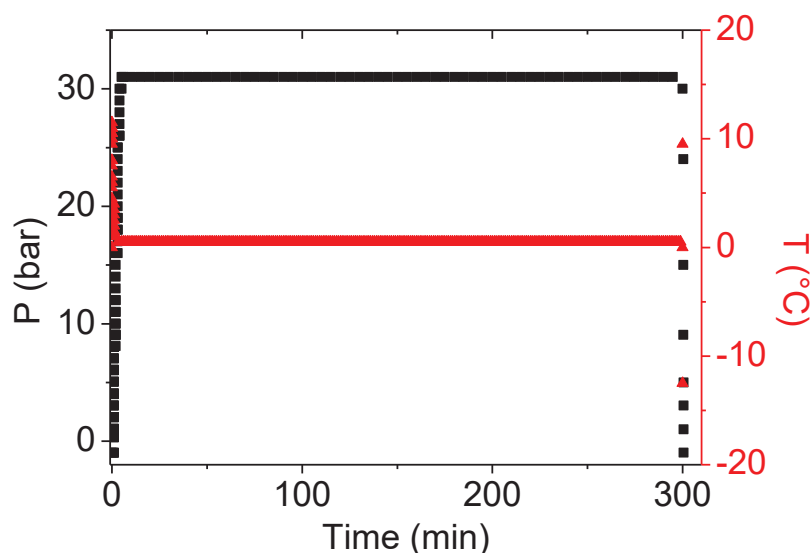


Fig. 6 : Temperature and pressure acquisition during the saturation stage.

After the saturation step, the foaming stage is triggered by opening manually a ball valve in order to achieve the highest pressure drop rate possible (Fig. 5 and Fig. 6). The pressure drop lowers the temperature inside the autoclave by Joule-Thomson effect and quickly comes back to room temperature (Fig. 6). Finally, foams are quickly removed from the autoclave and analyzed, by optical microscopy, within 15 min after foaming in order to avoid bubbles collapse (Fig. 7). Foaming experiments are reproduced twice within the same conditions to check the reliability of the results.



Fig. 7 : Example of a silicone foam which will be analyzed with a stereomicroscope.

III.2. Extrusion foaming

Formulations were extruded through a single screw extruder ($D=45$, $L/D=28$, Muller) with a screw speed of 70 rpm to produce foam as sketched in Fig. 8-a). The foam is produced at the die exit when the molten polymer/gas solution undergoes a simple difference between the pressure within the extruder and the atmospheric pressure. A gear pump was set up for output control and a static mixer was also added to improve the homogenization of the melt/gas blend and increase the pressure before the die exit. A flat die exit was used

with a width of 40 cm, B_f , a length of 25 cm and a thickness of 0.5 mm, H_f . In addition, three pressure sensors (P_1 - P_3) and two thermocouples (T_7 and T_9) were set-up to monitor the process (Fig. 8-b)).

Chemical blowing agent and the formulation pellets were first blended manually and then fed to the extruder hopper. The optimum content of chemical blowing agent was found to be equal to 3 wt%.

Fig. 8-b) shows the temperature profile used for every formulation as well as the measured temperature and pressure when LDPE was processed. In the depressurized region (blocks 4-5), the temperature is set high to ensure a fast decomposition of the CBA. Then, a compression and mixing zones (blocks 5-7) improve the distribution and dispersion of gas bubbles into the melt. Temperature is kept relatively high to ease mixing and diffusion phenomena. The static mixer allows to increase pressure, the residence time and the dissolution of the gas into the polymer melt. The temperature in this region is decreased to increase gas solubility, viscosity and melt strength before foaming at the die exit. The residence time is assumed to last several minutes.

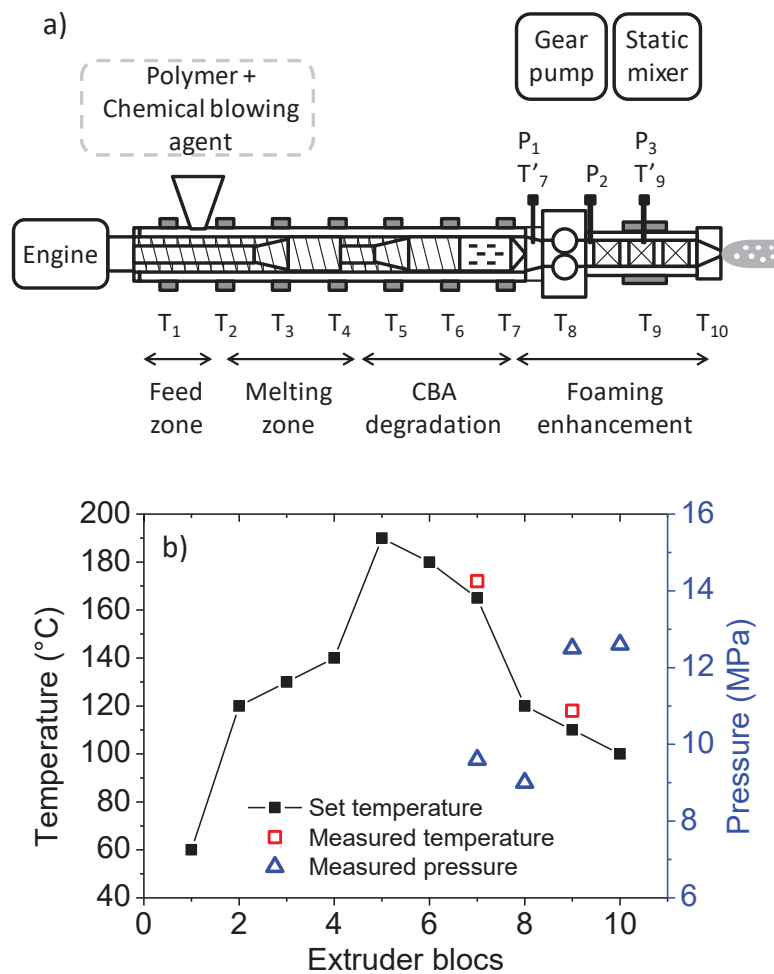


Fig. 8: Single screw extrusion foaming process: a) Extrusion set-up; b) Temperature profile. Temperature and pressure measured for LDPE.

IV. Characterization techniques

IV.1. Characterizations before foaming

Characterisation of unfoamed materials allows us to highlight the effect of blend morphologies, of the polymer rheology on cell nucleation and growth phenomena during the foaming process.

IV.1.1. Linear shear viscoelasticity

Small amplitude oscillatory shear tests were carried out on a TA INSTRUMENTS DHR2 rheometer, using the parallel-plate geometry, with 8 or 25 mm diameter disks. Frequency sweeps from 0.01 to 500 $\text{rad}\cdot\text{s}^{-1}$ were performed in the range of -20 to 150°C , under a nitrogen atmosphere, in the linear domain.

Crosslinking kinetics were followed using the parallel-plate geometry ($R=25\text{mm}$) at 0.1% of strain, 1 $\text{rad}\cdot\text{s}^{-1}$ and 150°C (DCP) or 80°C (LSR) under a nitrogen atmosphere.

IV.1.2. Extensional rheology

First, the samples were press-molded to a thickness of 0.6 mm. Then, the extensional viscosity measurements were made at 140°C on an ARES-EVF at several constant extensional rates of: 0.01, 0.1, 1 and 10s^{-1} . This temperature of 140°C was chosen to take into account the theoretical amount of dissolved carbon dioxide in the mass melted (plasticization effect) during the extrusion foaming process. With this equipment, the deformation of Hencky that can be reached is 4 so well beyond the deformation at the rupture of the samples [17].

IV.1.3. Capillary rheometry

A twin-bore capillary rheometer (RH7, Rosand, Malvern) was used to study the shear flow behavior of TPV materials. The diameter of the bore was 15 mm. Steady shear flow properties were collected from 10 s^{-1} to 10^4 s^{-1} at 140°C with a die of 1 mm in diameter, D , 20 mm in length, L , and an entry angle of 180° . No corrections were applied on the measurements. To maintain consistency between the tests, a pre-conditioning was applied before running all the experiments. Such preconditioning enables a good contact between the piston and the molten polymer, lets the whole sample reach the thermal equilibrium and removes trapped air bubbles. It consisted of two cycles of compression and soak times (5, 4 min). The compression steps were performed at a piston speed of 50 mm/min until reaching a limit pressure value at the capillary entrance.

IV.1.4. Lubricated squeezing flow (LSF)

The equibiaxial elongational measurements of S and S/FS formulations were performed using ARES-G2 by a constant area method at 30°C. The geometry has a diameter of $R=8\text{mm}$ to limit the resultant stress on the force sensor, no pin was fixed at its center. The upper geometry is controlled to set an exponential profile gap in compression in order to achieve a constant strain rate, $h(t) = h_0 e^{(-2\varepsilon_b t)}$. The sample was pre-formed in syringes of 2mL. The syringes were initially cut and lubricate to ease the removal of the sample. The lubricant used was castor oil, $\mu_L = 1\text{Pa}\cdot\text{s}$ at 30°C. Basically, ratio of lubricant to sample viscosities in LSF measurements, $\alpha = \frac{\mu_L}{\eta_0}$, is in the range $10^{-6} < \alpha < 10^{-3}$ [18, 19]. In our case, $1.2 \times 10^{-5} < \alpha < 6.5 \times 10^{-5}$ so we can assume pure bi-elongational flow and a “perfect” slip at the interface during our experiments. If lubricant viscosity is too low, it results in a fast lubricant squeezing out; if its viscosity is too high therefore, shear stress will arise to the sample [20, 21]. Lubricant is dropped off on the lower plate. Gap is then set to $2\delta = 0.3\text{mm}$ to spread the castor oil on each plate. The upper plate goes up and a thin layer of lubricant remains on each plate. The castor oil is not miscible with silicone and ensures then a good lubrication to avoid shear stress during the compression. Lubrication is believed to be lost at small Hencky strain for constant strain rate experiments, $\varepsilon_b \approx 1$ [18]. To keep the assumption that the stress in the sample can be deduced from the force applied at larger Hencky strain, Venerus et al. [18] developed a continuous lubricated squeezing flow apparatus. We used samples with a height of at least $2h_0 = 7\text{mm}$. As $h_0 \gg \delta$ and assuming a uniform deformation for an incompressible material, Hencky strain and Hencky strain rate can be expressed as:

$$\varepsilon_b = -\frac{1}{2} \ln \left(\frac{h(t)}{h_0} \right) \quad (6)$$

$$\dot{\varepsilon}_b = \frac{d\varepsilon_b(t)}{dt} \quad (7)$$

Bi-axial stress is defined from the compression force, $F(t)$. We neglected here instrument compliance, inertia and surface tension forces.

$$\sigma_B(t) = \frac{F(t)}{\pi R^2} \quad (8)$$

Therefore, bi-elongational viscosity, $\eta_B^+(t, \dot{\varepsilon}_B)$, is defined as followed:

$$\eta_B^+(t, \dot{\varepsilon}_B) = \frac{\sigma_B}{\dot{\varepsilon}_B} \quad (9)$$

The transient bi-axial viscosity, η_b , for PDMS-based copolymers with lubricant for several strain rate is plotted in Fig. 9. The solid line represents $6\eta^+$, where η^+ is the shear viscosity in the linear viscoelastic region. With lubrication, η_b was nearly equal to $6\eta^+$ in the steady state, at a high strain. This behavior is expected in the case of linear viscoelastic

regime for linear polymers in biaxial flow, Trouton law. η_b also tends to follow the linear viscoelastic rule independently of strain rates. As a consequence, this result validates the experimental lubrication for our LSF tests and the robustness of this technique. When Hencky strain is greater than 1.5, the viscosity rapidly increases suggesting a loss of lubrication. Data will not be analyzed for $\epsilon > 1.5$. Results are reliable until a Hencky strain of 1.5 and for a maximum strain rate of 0.5s^{-1} .

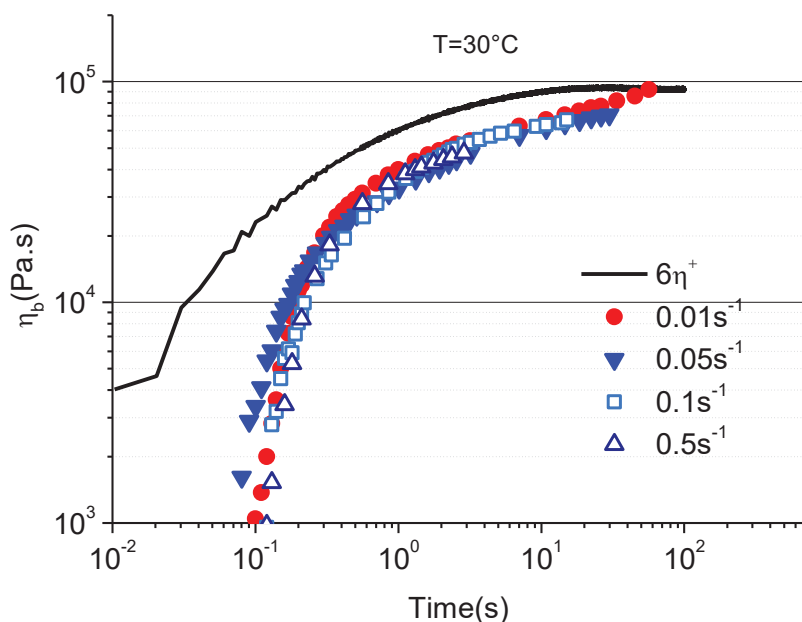


Fig. 9. Experimental validation for several strain rate, S and $T=30^\circ\text{C}$: Bi-elongational viscosity versus time

IV.1.5. Differential scanning calorimetry (DSC)

A TA INSTRUMENTS DSC Q200 apparatus was used to measure phase transitions and oxidation. Sealed pans were used to measure phase transitions with a heating rate of $10^\circ\text{C}/\text{min}$, a sample mass of 10 mg under a flow rate of 25 mL/min of Helium.

Drilled aluminum pans were used in oxidation experiments to measure enthalpy of oxidation reaction. Thermal analysis was performed under N_2 and air at a flow rate of 25 mL/min. The mass of the samples is about 10 mg. A heating rate $10^\circ\text{C}/\text{min}$ under N_2 was applied until 150°C . An isotherm was then triggered for 5 min, followed by a gas switch N_2/Air at the same temperature for 2 hours.

IV.1.6. Proton nuclear magnetic resonance (H-NMR)

H-NMR spectra were recorded with a NMR Bruker Avance III operating at 400 MHz at room temperature (RMN polymer platform of Institut de Chimie de Lyon). Solution had a concentration of 60 mg/ml in CDCl_3 or d-THF without TetraMethylSiloxane (TMS).

IV.1.7. Swelling test

The silicone rubber network was characterized only by the soluble fraction (ω_s). Tetrahydrofuran (THF) was used as good solvent at room temperature. Specimens taken from the vulcanized sheet were immersed in THF ($V=30\text{mL}$) for 72 h at 25°C . Swollen samples at equilibrium were taken out from the solvent, blotted with filter paper, and weighted immediately. Samples were subsequently dried in a vacuum oven for 24 h at 70°C and reweighed. The soluble fraction was then directly measured.

IV.1.8. Size exclusion chromatography (SEC)

Triple detection SEC was carried out on a TDA300-EXD apparatus from Viscotek, equipped with three detectors connected in series, i.e. light scattering, refractometer and viscosimeter detectors. The temperature of analysis, 35°C , was set both in columns and in the detector chamber to ensure better reproducibility, as well as a stable baseline throughout the characterization. Two linear GMHHR-H columns and a HHR-H Guard precolumn (both from Viscotek) were used. Toluene was chosen as eluent, at a flow rate of $1\text{ mL}\cdot\text{min}^{-1}$, without a need for a flow marker. The sample concentration is $4\text{ mg}\cdot\text{mL}^{-1}$ in toluene. Data acquisition and treatment were performed using Viscotek OmniSEC software version 4.1. Absolute molar mass of the samples were recalculated according to the mass of the sample injected.

A Waters 515 SEC instrument equipped with a differential refractometer (R401) and a UV detector (model 440) were used to analyze the molecular weight distributions of the fluorosilicone. The solvent was tetrahydrofuran (THF) and the flow rate was $1\text{ mL}\cdot\text{min}^{-1}$. The sample concentration is $4\text{ mg}\cdot\text{mL}^{-1}$ in THF.

IV.1.9. Blend morphologies characterization

Silicone/fluorosilicone blends

First, blend morphologies are characterized with an optical microscope Olympus BX41 in transmission mode with a phase contrast filter. The mean domain size is measured for, at least, 100 domains manually with ImageJ and its ellipsoidal tool. The mean domain size corresponds, here, to the mean Feret diameter. If blend morphologies are too fine for optical microscopy, we used a cryo-SEM, FEI QUANTA 250 FEG. First, samples were frozen in liquid nitrogen. Then, samples are transferred in the SEM equipped with a cold stage. Samples were fractured and coated with gold prior to observation.

TPV Silicone

The morphologies are taken using a FEI QUANTA 250 FEG (High vacuum) in E-T detector (5kV) and BSE detector (10kV). First, samples were frozen in liquid nitrogen and fractured. If necessary, LSR phases were extracted in THF after the cryo-fracturation. Surfaces are then covered with a thin layer of carbon by plasma metallization. The average

nodule size (diameter) is measured using the ellipse tool in ImageJ software for at least 50 droplets.

IV.1.10. Deformed droplet retraction method

According to Deyrail et al. [24, 25], measurements of interfacial tension were carried out on S/FS blend at 150°C. Diluted S/FS blends were proceeded in roll mill at 30°C in order to get the coarsest morphology, for magnification limitations, by playing with the surface tension and viscosity ratio between both polymers. Using the Linkam device, a step deformation is imposed to melt drops of FS embedded in the silicone matrix. The relaxation phenomenon is then monitored by optical microscopy until the drop returned from an ellipsoidal to an equilibrium spherical shape (Fig. 10). The interfacial tension between both polymers may be deduced by knowing the viscosity for each polymer and the variation of the deformed drop as a function of the relaxation time. Experiments were repeated on different droplets. FS nodules have a mean size of 11 μm, the film thickness used for the measurements were of 500 μm to avoid wall effects. Since Talyor's work [26], the relaxation of a viscous deformed drop in a melt matrix is known to be only driven by interfacial surface tension. As temperature is constant during the shape recovery, components rheological behavior remains unchanged. From Bousmina et al. work [27], interfacial tension may be predicted from deformed drop retraction, following the deformability, D .

$$D = D_0 \exp \left[- \frac{40(p+1)}{(2p+3)(19p+16)} \frac{\gamma_{12}}{\eta_m R_0} t \right] \quad (10)$$

$$D = D_0 \exp \left[- \frac{t}{\tau_d} \right] = \frac{L-B}{L+B}$$

Where D_0 is the deformability, R_0 is the initial spherical radius at the initial time, p is the zero shear viscosity ratio, L and B are respectively the major and minor axis of the ellipsoid, η_m is the matrix viscosity, γ_{12} is the interfacial tension and the corresponding relaxation time is defined as:

$$\tau_d = \frac{(2p+3)(19p+16)}{40(p+1)} \frac{\eta_m R_0}{\gamma_{12}} \quad (11)$$

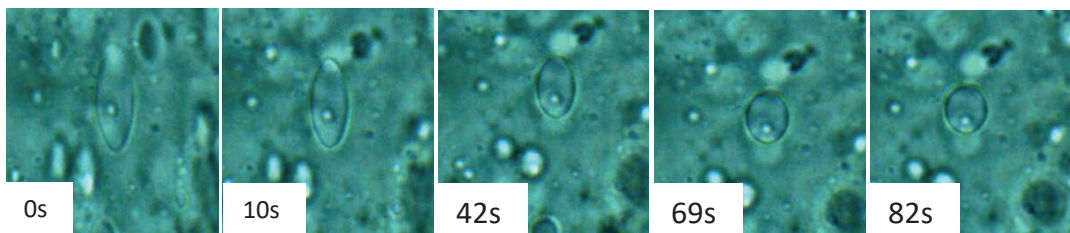


Fig. 10: Retraction of a fluorosilicone ellipsoidal droplet immersed in the silicone matrix at 150°C for successive times. $R_0 = 13\mu\text{m}$

IV.1.11. Thermogravimetric analysis (TGA)

A TGA Q500 TA Instrument was used to verify the amount of silica dispersed in the silicone/fluorosilicone blend. Samples were heated from 30 °C up to 800 °C at a heating rate of 10 °C/min.

IV.2. Foam characterization

IV.2.1. Foam density

TPV foams

Foam density was calculated by dividing the sample weight by its volume. To that end, samples were weighted on a high precision balance and their volume was estimated with a calliper. As foamed samples were often not flat on their entire surface, their density was estimated from cut smaller flat surfaces. The density measurements are done for three samples for reliability reasons.

Silicone foams

For density measurements, the samples were weighted before foaming and the measurements of the foam sample size enable us to estimate the volume by optical microscopy. The samples, for density measurements only, were set on Teflon paper and free to flow. As flow is symmetric and the mass and volume are kept constant, we can estimate a foam density, even if the sample thickness will change during the saturation stage.

IV.2.2. Image analysis

Foam samples were frozen in liquid nitrogen and fractured to protect their microstructure. TPV foam surfaces were then covered with a thin layer of carbon by plasma metalization before analyzing the surface with a FEI QUANTA 250 FEG (High vacuum) in E-T detector (5kV) and BSE detector (10kV). A Leica MDG41 stereomicroscope was used to characterize silicone foams morphologies.

Foams are then characterized with ImageJ software. At least 50 bubbles are measured, for each foam, to average cell size. The average cell size (diameter) is measured using the ellipse tool in ImageJ software. The coalesced bubbles are not taken into account in the measurements.

Cell densities, d_{cell} , were calculated from obtained micrographs such as [22]

$$d_{cell} \approx \left(\frac{nM^2}{A}\right)^{3/2} \quad (12)$$

where n : number of cells observed in a micrograph

A : area of the micrograph

M : magnification factor

The following equation was used to determine the cell density of the original un-foamed material d_o corresponding to the initial cell concentration before cell expansion:

$$d_o = \frac{d_{cell}}{1 - V_f} \quad (13)$$

where V_f : void fraction = $1 - \rho/\rho_s$ with ρ the foam density and ρ_s the solid phase density

References

- [1] C. Liu, J. He, E.v. Ruymbeke, R. Keunings, C. Bailly, Evaluation of different methods for the determination of the plateau modulus and the entanglement molecular weight, *Polymer* **47** (13) (2006) 4461-4479.
- [2] P. Lomellini, Effect of chain length on the network modulus and entanglement, *Polymer* **33** (6) (1992) 1255-1260.
- [3] M. Gottlieb, C.W. Macosko, G.S. Benjamin, K.O. Meyers, E.W. Merrill, Equilibrium modulus of model poly(dimethylsiloxane) networks, *Macromolecules* **14** (4) (1981) 1039-1046.
- [4] J.E. Mark, *Physical Properties of Polymers Handbooks*, Springer, 2007.
- [5] S.A. Stern, V.M. Shah, B.J. Hardy, Structure-permeability relationships in silicone polymers, *Journal of Polymer Science Part B: Polymer Physics* **25** (6) (1987) 1263-1298.
- [6] Y. Yue, H. Zhang, Z. Zhang, Y. Chen, Polymer–filler interaction of fumed silica filled polydimethylsiloxane investigated by bound rubber, *Composites Science and Technology* **86** (2013) 1-8.
- [7] A. Taguet, P. Cassagnau, J.M. Lopez-Cuesta, Structuration, selective dispersion and compatibilizing effect of (nano)fillers in polymer blends, *Progress in Polymer Science* **39** (8) (2014) 1526-1563.
- [8] C. Peiti, J.-M. Haudin, B. Vergnes, Modification of rheological properties of branched polyethylenes by a thermomechanical treatment, *AIP Conference Proceedings* **1664** (1) (2015) 170002.
- [9] K. Prakashan, A.K. Gupta, S.N. Maiti, Effect of compatibilizer on micromechanical deformations and morphology of dispersion in PP/PDMS blend, *Journal of Applied Polymer Science* **105** (5) (2007) 2858-2867.
- [10] W. Tong, Y. Huang, C. Liu, X. Chen, Q. Yang, G. Li, The morphology of immiscible PDMS/PIB blends filled with silica nanoparticles under shear flow, *Colloid and Polymer Science* **288** (7) (2010) 753-760.
- [11] A. Msakni, P. Chaumont, P. Cassagnau, Diffusion of the dicumyl peroxide in molten polymer probed by rheology, *Rheol Acta* **46** (7) (2007) 933-943.
- [12] J.S. Vrentas, J.L. Duda, Diffusion in polymer–solvent systems. I. Reexamination of the free-volume theory, *J. Polym. Sci. Polym. Phys.* **15** (3) (1977) 403-416.
- [13] S.-H. Park, S. Lee, D. Moreira, P.R. Bandaru, I. Han, D.-J. Yun, Bioinspired superhydrophobic surfaces, fabricated through simple and scalable roll-to-roll processing, *Scientific Reports* **5** (2015) 15430.
- [14] Z. Tadmor, C.G. Gogos, *Principles of Polymer Processing* John Wiley & Sons, 1979.
- [15] E. Laguna-Gutierrez, C. Saiz-Arroyo, J.I. Velasco, M.A. Rodriguez-Perez, Low density polyethylene/silica nanocomposite foams. Relationship between chemical composition, particle dispersion, cellular structure and physical properties, *European Polymer Journal* **81** (Supplement C) (2016) 173-185.
- [16] G. Gedler, M. Antunes, V. Realinho, J.I. Velasco, Novel polycarbonate-graphene nanocomposite foams prepared by CO₂ dissolution, *IOP Conference Series: Materials Science and Engineering* **31** (1) (2012) 012008.
- [17] J.R. Royer, J.M. DeSimone, S.A. Khan, High-pressure rheology and viscoelastic scaling predictions of polymer melts containing liquid and supercritical carbon dioxide, *Journal of Polymer Science Part B: Polymer Physics* **39** (23) (2001) 3055-3066.
- [18] D.C. Venerus, T.-Y. Shiu, T. Kashyap, J. Hostteler, Continuous lubricated squeezing flow: A novel technique for equibiaxial elongational viscosity measurements on polymer melts, *Journal of Rheology* **54** (5) (2010) 1083-1095.
- [19] S. Chatraei, C.W. Macosko, H.H. Winter, Lubricated Squeezing Flow: A New Biaxial Extensional Rheometer, *Journal of Rheology* **25** (4) (1981) 433-443.
- [20] A.C. Papanastasiou, C.W. Macosko, L.E. Scriven, Analysis of lubricated squeezing flow, *International Journal for Numerical Methods in Fluids* **6** (11) (1986) 819-839.

Chapter 2: Materials and Methods

[21] A. Nishioka, Y. Takagi, T. Takahashi, Y. Masubuchi, J.-i. Takimoto, K. Koyama, Measurement of Biaxial Elongational Viscosity of Polymer Melts Using Lubricated Squeezing Flow Method, *Journal of the Society of Materials Science, Japan* **47** (12) (1998) 1296-1300.

[22] V. Kumar, N.P. Suh, A process for making microcellular thermoplastic parts, *Polymer Engineering & Science* **30** (20) (1990) 1323-1329.

Part II

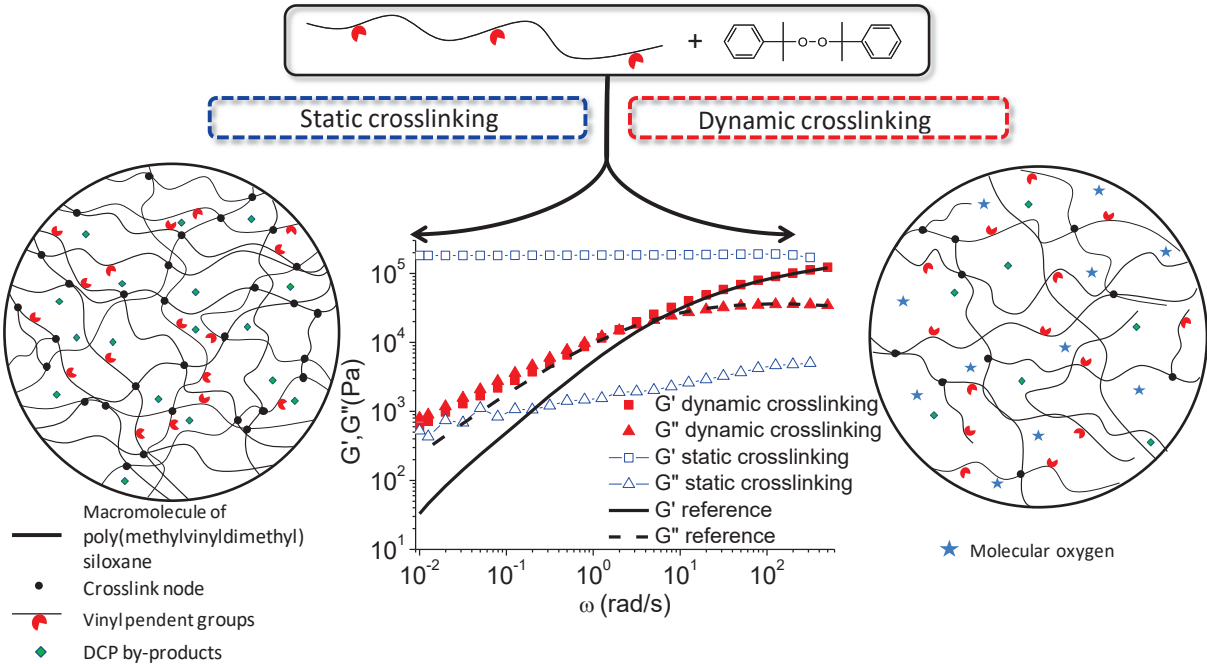
Chapter 3 : Mechanisms of dynamic crosslinking of silicone elastomer

ABSTRACT

Methylvinyl dimethylsiloxane copolymer elastomer was crosslinked under static and dynamic conditions with several amounts of peroxide. For samples crosslinked in static conditions, the insoluble fractions and the shear equilibrium moduli have been observed in a good agreement with theories of network elasticity. As regards the dynamically crosslinked samples, the rheological and SEC analysis have revealed that the crosslinking reaction gives rise to multi-scale branched structures with molecular structures achieving 10^7 g/mol and proved that these samples remain soluble and processable. Moreover, dynamic crosslinked samples also show a strain hardening behavior even in bi-elongational flows. Furthermore, experiments under nitrogen and air atmospheres were carried out to better understand the mechanisms of the formation of these branched structures. The results suggest that molecular oxygen lowers the consumption of vinyl groups inhibiting the crosslinking reaction. Finally, the rheological behavior may be explained by the original microstructure composed of un-crosslinked chains playing the role of the matrix while the miscible and branched structures of macromolecules act as reinforcement agent.

Reformatted version of paper originally published in European Polymer Journal

GRAPHICAL ABSTRACT



Dynamic cross-linking of silicone elastomer: Radical branching controlled by thermo-oxidation under shearing

T. Métivier^a, E. Beyou^a, P. Cassagnau^{a,*}

^a Univ Lyon, University of Lyon, Ingénierie des Matériaux Polymères, CNRS UMR 5223, 15 Bd Latarjet, 69622 Villeurbanne, France

Introduction

Generally speaking, crosslinking reactions transform a liquid viscoelastic polymer into a viscoelastic solid in converting polymer chains into a 3D network [1]. Their distinct mechanical properties depend on the topological network structure formed by crosslinking reaction, i.e. the density and distribution of crosslinking nodes, the chain length between each crosslinking nodes, the thermal stability of the network nodes, the density of entanglements and the network flaws [2, 3].

At first, silicone elastomer crosslinking can be carried out at various temperatures by a hydrosilylation reaction in which a Si-H group adds to a vinyl group to form a Si-C bond [4]. The reaction is mostly catalysed by a platinum complex such as Karstedt's catalyst [4]. In comparison to peroxide cured silicone, the molar mass of the silicone used for liquid silicone rubber (LSR) is six times lower which allows the use of pump or injection processes [5]. Besides, addition cure silicone rubbers give generally more perfect crosslinking networks and were widely studied to check the relationship between the network topology and the theory of rubber elasticity [6, 7]. Additionally, the LSRs are preferably used for medical applications as there are no by-product residues [8]. For anti-misting applications in coating industries, the hydrosilylation reaction is used to branch vinyl-PDMS based copolymers in order to improve their elongational rheology [9].

Radiation curing such as UV [10], electron beam [11] or γ -radiation [12] are also alternative routes. Radiation curing is an easy and quick process without any formation of harmful chemical products. However, it is mainly restricted to membranes or coatings with a thickness adapted to the penetration of the radiation beam. Radiation curing of silicone may also be used in medical applications allowing for example to effectively control the crosslinking density within the sample. Thus, gradient crosslinking structures may reproduce systems with a gradient elastic modulus [10].

Regarding the linear poly(dimethylsiloxane), the radical crosslinking by hydrogen abstraction was found inefficient even by using highly reactive peroxides such as bis(2,4-dichloro)benzoyl and benzoyl peroxides [13-15]. However, the addition of

methylvinylsiloxane in the backbone, at low content such as 0.1 or 0.2mol%, increases the crosslinking efficiency by a factor of 4 with the highest content of methylvinylsiloxane [13]. The crosslinking of silicone elastomer with diacyl and dialkyl peroxides were widely studied [14-19]. Actually, the diacyl peroxides were found sufficiently reactive to react with both methyl and vinyl groups whereas the dialkyl peroxides are assumed to react more specifically with vinyl groups. As similar mechanical properties may be achieved with dialkyl peroxides, they became more frequently used because they entail less process constraints such as long post cure to remove the acidic by-product remaining after the decomposition of diacyl peroxide [20, 21]. Generally, peroxide cured silicone rubbers exhibit low compression set, high-processing temperature stability and enhanced Young modulus [20].

Besides, crosslinking reactions under shearing are widely studied for thermoplastic vulcanizates (TPV) materials. The elastomeric phase is supposed to be crosslinked in the same experimental conditions than in static crosslinking process [22, 23]. The crosslinking is carried out only in the dispersed phase while the elongational and shear flows during the blending reduce the size of the elastomeric phase as the crosslinking reaction goes on. Msakni et al. [24] was the first to study the dynamic crosslinking of a polymer alone in bulk conditions. They achieved to produce hyperbranched structures of ethylene-based copolymers which are still processable in presence of 1wt% of DCP.

Usually, the addition of long chain branched polymers [25], high molar mass chains [25] or miscible crosslinked polymers [26] have shown to be an effective route in the improvement of the elongational properties of the matrix by enhancing the strain hardening for blowing applications. For example, the addition of only 1wt% of crosslinked LLDPE (gel content 75%) in the LLDPE matrix enables to increase the melt strength by a factor of 10 and increase the foam expansion by almost 50% without any effect on the shear viscosity [26]. In the case of PE [27], the addition of peroxides at concentration below 3500ppm is used to link polymer chains while staying below the gel point. The introduction of vinyl groups within the macromolecules brings forth higher branching reaction leading to complex branched structures with high flow activation energy.

As shown by Msakni et al. [24], static and dynamic crosslinking lead to far different rheological behavior. However, dynamic crosslinking remains not well understood. The main objective of this study is to bring new insights in the field of dynamic crosslinking of silicone bulk polymers. The effect of dynamic crosslinking on the shear and bi-elongational rheologies is thoroughly described. The influence of atmospheric conditions are also investigated because it is well known that thermo-oxidative conditions lead to a drop in crosslinking efficiency in presence of peroxide [28].

I. Experimental part

I.1. Materials

Silicone polymer: A methylvinyl dimethylsiloxane copolymer elastomer, called SR, was kindly supplied by BlueStar Silicone. Its density is about 0.97. Molar masses were determined by size exclusion chromatography (SEC) with toluene in universal calibration mode ($M_n=380$ kg/mol, $M_w=600$ kg/mol). Molar percentage of vinyl groups inside silicone backbone chain was determined by NMR in $CDCl_3$, 0.22mol%, which represents 10.3 vinyl groups per chain. The molar mass of molecular segment between two consecutive vinyl groups, M_0 , is equal to 37000 g/mol while the molar mass between entanglements at 25°C, $M_e \approx \frac{\rho RT}{G_N^0}$ is 10 000 g/mol setting the rubbery plateau modulus, G_N^0 , of the Vinyl-PDMS about 2.4×10^5 Pa [6]. Thus, it suggests there will be trapped physical entanglements during a crosslinking step [29].

Free-radical cross-linking: Dicumyl peroxide (DCP, $M=270$ g.mol⁻¹) was used as the free radical initiator of the cross-linking reaction. It was purchased from Aldrich with an assay of 98% and used as received. The thermal decomposition of DCP was determined by [16, 24]:

$$\frac{d[DCP]}{dt} = -Ae^{-\left(\frac{E_a}{RT}\right)}[DCP] \quad (1)$$

With $A=7.47 \times 10^{15} \text{ s}^{-1}$; $E_a=153 \text{ kJ/mol}$

I.2. Methods

I.2.1. Blend procedure

Blends of silicone with several peroxide amounts were prepared for static and dynamic vulcanization techniques. First, SR and DCP crystals are mixed in a roll mill (cylinder diameter=100 mm) at 25°C for at least 15 min to ensure good dispersion and homogenization with a gap of 0.3mm, noted as L , a roll speed of 25 rpm and a friction ratio of 0.8. Msakni et al.[30] modeled the DCP diffusion in engage copolymers and they found a diffusion coefficient at 25°C, $D_{12} \approx 6.5 \times 10^{-11} \text{ m}^2 \cdot \text{s}^{-1}$. In silicone, the DCP diffusion coefficient should be of the order of magnitude of $10^{-10} \text{ m}^2 \cdot \text{s}^{-1}$ because PDMS has a T_g around -120°C while engage copolymer's one is near -45°C [30], according to free volume theory [31]. Shear rate was estimated by analytical formulation, eq.(2), with asymmetric roll speed in the nip region (U_1 and U_2) [32].

$$\dot{\gamma} = \frac{U_1 - U_2}{L} \quad (2)$$

We found a mean shear rate in the nip region, $\dot{\gamma} \approx 65s^{-1}$. It is possible to estimate the time needed, t_b , to achieve a good dispersion of DCP by diffusion coupled with distributive mixing, eq. (3) [33].

$$t_b = \sqrt{\frac{64L^2}{D_{12}\dot{\gamma}^2}} \quad (3)$$

We did not take into account elongational flow, viscoelasticity, the number of cutting of polymer blankets and local overheat in calculations. From all of these approximations, $t_b \approx 10s$ which is far below our processing time.

I.1.1. Static cross-linking

Before cross-linking, blends are put into vacuum to avoid air bubbles at least for one day at room temperature. Then, samples are compression molded at 150°C for 2 hours using a hydraulic press with electrically heated platens, under a pressure of 100 bar. Based on thermal decomposition of DCP, eq.(1), DCP is decomposed at 96% after 2h at 150°C (about five half-life times, $t_{1/2} \approx 25$ min). No rheological degradation occurred with silicone, without DCP, exposed to 150°C for 2 hours but some cross-linking by-products may be emitted when DCP is added.

I.1.2. Dynamic cross-linking

For dynamic cross-linking experiments, blends are cross-linked under shearing for 2 hours in a roll mill (or internal mixer with Banbury rotor) at constant gap, friction ratio and roll speed, the same as previously described in the blend procedure section. Temperatures are set to 150°C on each side of both rolls. Some experiments were carried out in a batch mixer with a Banbury rotor speed of 50rpm in order to obtain torque along time for information as shown in Fig. 1-a. The chamber of the mixer was filled with a filling ratio of 0.7. Dynamic cross-linking tests were also performed under several atmospheres in a batch mixer (Haake Thermofischer) such as air and N₂. Torque measurements are detailed in Fig. 1-b, each measurement was performed under the same conditions of temperature and rotor speed (145°C and 50rpm). These Figures will be discussed in the Result section.

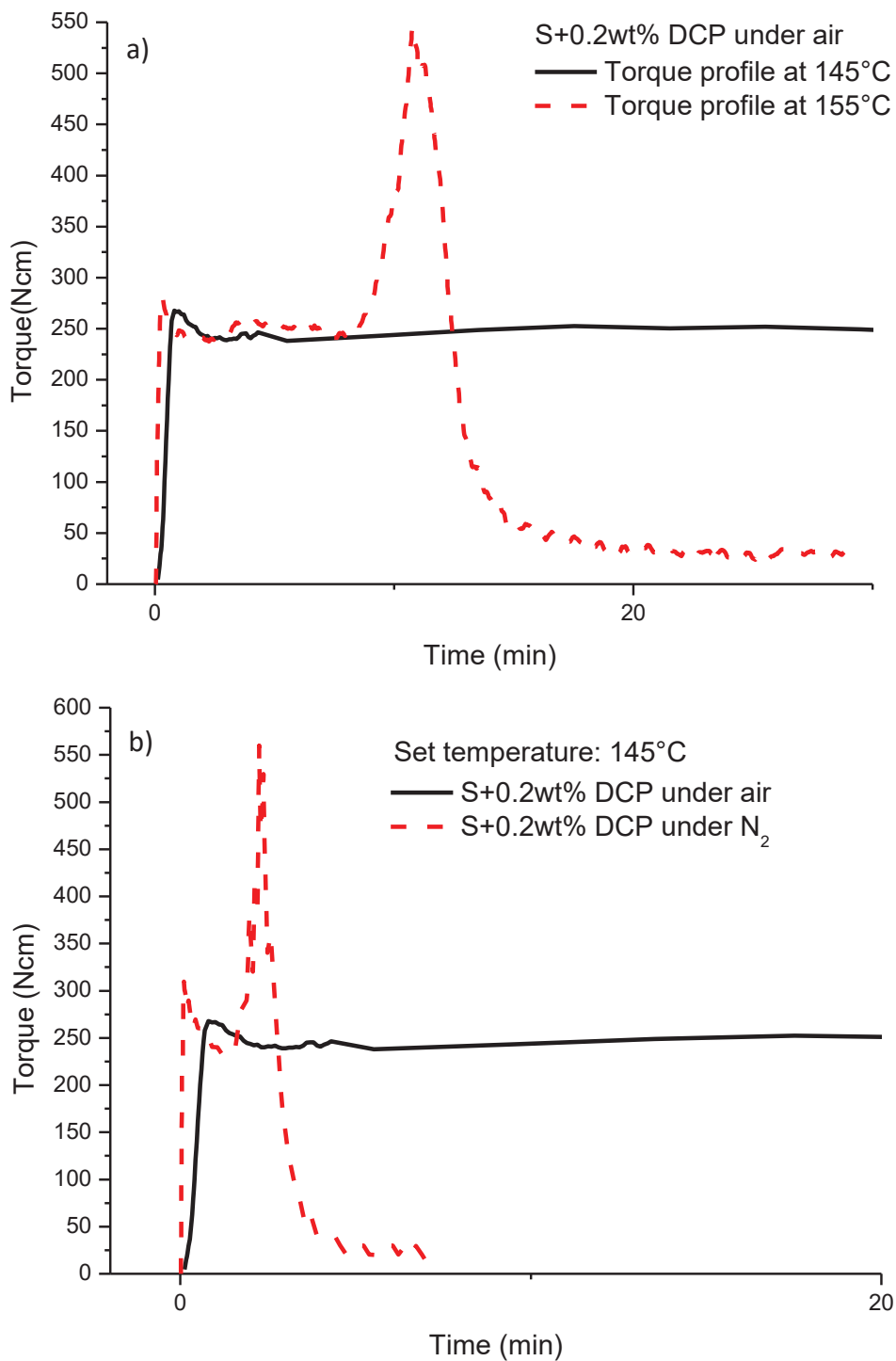


Fig. 1. Dynamic cross-linking of S+0.2wt%DCP in batch mixer (Variation of the torque and melt temperature versus shearing time). a) Under two different processing temperatures ($T=145$ and 155°C , set temperatures) under air, rotor speed = 50rpm ; b) Comparison of experiments carried out in a batch mixer under air and N_2 , $T = 145^{\circ}\text{C}$, rotor speed = 50rpm.

I.2. Characterization

Linear shear viscoelasticity:

Small amplitude oscillatory shear tests were carried out on a TA INSTRUMENTS DHR2 rheometer, using the parallel-plate geometry, with 8 or 25 mm diameter disks. Frequency sweeps from 0.01 to 500 rad.s⁻¹ were performed at room temperature. Cross-linking kinetics were followed using the parallel-plate geometry (R=25mm) at 0.1% of strain, 1 rad.s⁻¹ and 150°C, under a nitrogen atmosphere.

Lubricated Squeezing Flow (LSF):

The equibiaxial elongational measurements were performed using ARES-G2 by a constant area method at 30°C. The geometry has a diameter of $R=8\text{mm}$ to limit the resultant stress on the force sensor, no pin was fixed at its center. The upper geometry is controlled to set an exponential profile gap in compression in order to achieve a constant strain rate, $h(t) = h_0 e^{(-2\varepsilon_b t)}$. The sample was pre-formed in syringes of 2mL. The syringes were initially cut and lubricate to ease the removal of the sample. The lubricant used was castor oil, $\mu_L = 1\text{Pa}\cdot\text{s}$ at 25°C. Basically, ratio of lubricant to sample viscosities in LSF measurements, $\alpha = \frac{\mu_L}{\eta_0}$, is in the range $10^{-6} < \alpha < 10^{-3}$ [34, 35]. In our case, $1.2 \times 10^{-5} < \alpha < 6.5 \times 10^{-5}$ so we can assume pure bi-elongational flow and a “perfect” slip at the interface during our experiments. If lubricant viscosity is too low, it results in a fast lubricant squeezing out; if its viscosity is too high therefore, shear stress will arise to the sample [36, 37]. Lubricant is dropped off on the lower plate. Gap is then set to $2\delta = 0.3\text{ mm}$ to spread the castor oil on each plate. The upper plate goes up and a thin layer of lubricant remains on each plate. Castor oil is not miscible with silicone and ensure a good lubrication to avoid shear stress during the compression. Lubrication is believed to be lost at small Hencky strain for constant strain rate experiments, $\varepsilon_b \approx 1$ [34]. To keep the assumption that the stress in the sample can be deduced from the force applied at larger Hencky strain, Venerus et al. [34] developed a continuous lubricated squeezing flow apparatus. We used samples with a height of at least $2h_0 = 7\text{mm}$. As $h_0 \gg \delta$ and assuming a uniform deformation for an incompressible material, Hencky strain and Hencky strain rate can be expressed as:

$$\varepsilon_b = -\frac{1}{2} \ln \left(\frac{h(t)}{h_0} \right) \quad (4)$$

$$\dot{\varepsilon}_b = \frac{d\varepsilon_b(t)}{dt} \quad (5)$$

Bi-axial stress is defined from the compression force, $F(t)$. We neglected here instrument compliance, inertia and surface tension forces.

$$\sigma_B(t) = \frac{F(t)}{\pi R^2} \quad (6)$$

Therefore, bi-elongational viscosity, $\eta_B^+(t, \dot{\varepsilon}_B)$, is defined as followed:

$$\eta_B^+(t, \dot{\varepsilon}_B) = \frac{\sigma_B}{\dot{\varepsilon}_B} \quad (7)$$

The transient bi-axial viscosity, η_b , for PDMS-based copolymers with lubricant for several strain rate is plotted in Fig. 2. The solid line represents $6\eta^+$, where η^+ is the shear viscosity in the linear viscoelastic region. With lubrication, η_b was nearly equal to $6\eta^+$ in the steady state, at a high strain. This behavior is expected in the case of linear viscoelastic regime for linear polymers, Trouton law. η_b also tends to follow the linear viscoelastic rule independently of strain rates. As a consequence, this result validates the experimental lubrication for our LSF tests and the robustness of this technique. When Hencky strain is greater than 1.5, the viscosity rapidly increases suggesting a loss of lubrication. Data will not be analyzed for $\varepsilon > 1.5$. Results are reliable until a Hencky strain of 1.5 and for a maximum strain rate of 0.5s^{-1} .

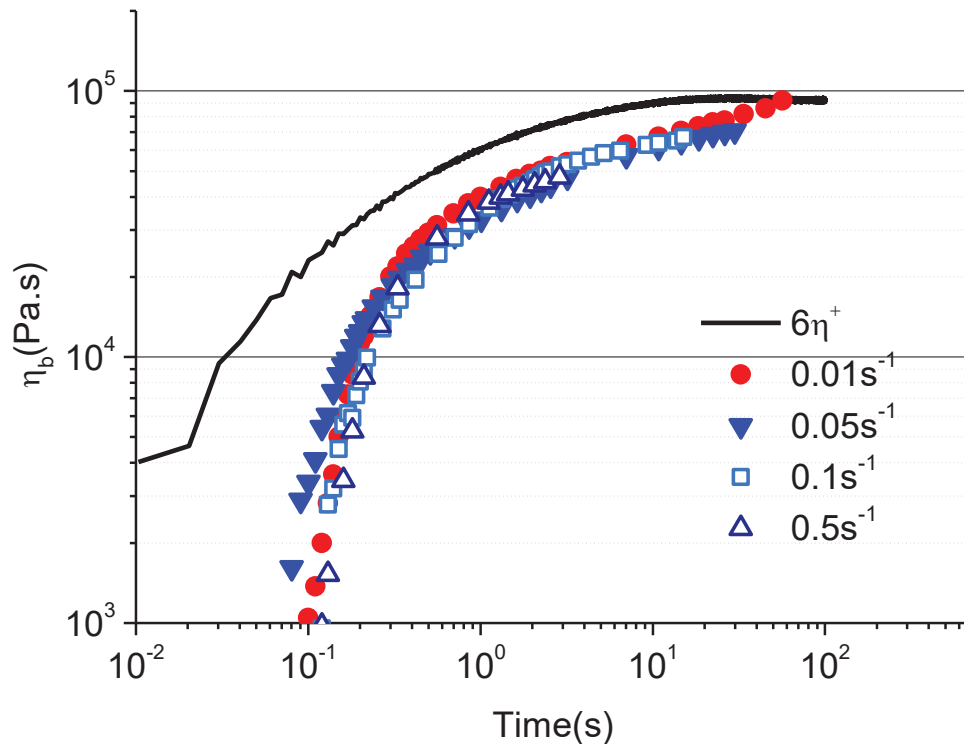


Fig. 2. Experimental validation for several strain rate, S and $T=25^\circ\text{C}$: Bi-elongational viscosity versus time

Differential Scanning Calorimetry (DSC):

A TA INSTRUMENTS DSC Q200 apparatus was used. Drilled aluminium pans were used in oxidation experiments to measure enthalpy of oxidation reaction. Thermal analysis was performed under N_2 and air at a flow rate of 25 mL/min for oxidation experiments. The mass of the samples is about 10 mg . For oxidation experiment, a heating rate 10°C/min

under N₂ was applied until 150°C. An isotherm was then triggered for 5 min, followed by a gas switch N₂/Air at the same temperature for 2 hours.

Proton Nuclear Magnetic Resonance (H-NMR):

H-NMR spectra were recorded with a NMR Bruker Avance III operating at 400 MHz at room temperature (RMN polymer platform of Institut de Chimie de Lyon). CDCl₃ was used as solvent.

Swelling Test:

The silicone rubber network was characterized only by the soluble fraction (ω_s). Tetrahydrofuran (THF) was used as good solvent at room temperature. Specimens taken from the vulcanized sheet were immersed in THF (V=30mL) for 72 h at 25°C. Swollen samples at equilibrium were taken out from the solvent, blotted with filter paper, and weighted immediately. Samples were subsequently dried in a vacuum oven for 24 h at 70°C and reweighed. The soluble fraction was then directly measured. We corrected the soluble fraction by removing the polymerization/depolymerization by-product fraction present into the rubber because it should not contribute to the cross-linking network. This fraction was determined with an isotherm of 2 hours at 150°C in TGA under an inert atmosphere. The ramp to achieve the isotherm was set to 10°C/min. Depolymerization reactions (cyclization) occur at temperature above 290°C under air [38] unless in presence of oxygen, moisture and basic or acidic contaminants lowering the degradation temperature to 150°C [39-41]. From this experiment, we found a by-product fraction equal to 1.9% in weight. During static cross-linking, this fraction cannot be evaporated because of the pressure set by the hot press (P=100bar).

Size Exclusion Chromatography (SEC):

Triple detection SEC was carried out on a TDA300-EXD apparatus from Viscotek, equipped with three detectors connected in series, i.e. light scattering, refractometer and viscosimeter detectors. The temperature of analysis, 35°C, was set both in columns and in the detector chamber to ensure better reproducibility, as well as a stable baseline throughout the characterization. Two linear GMHHR-H columns and a HHR-H Guard precolumn (both from Viscotek) were used. Toluene was chosen as eluent, at a flow rate of 1 mL.min⁻¹, without a need for a flow marker. Data acquisition and treatment were performed using Viscotek OmniSEC software version 4.1. Absolute molar mass of the samples were recalculated according to the mass of the sample injected.

II. Results and discussion

II.1. Static cross-linking

Dicumyl peroxide was chosen in this study because it is assumed to lead to a more homogeneous topological cross-linking network in comparison to diaryl peroxides. The acidic residues coming from the diaryl peroxide decomposition are also avoided and replaced by more harmless ketones or alcohols [21]. The cross-linking mechanism of silicone elastomer with dialkyl peroxide such as dicumyl peroxide is illustrated in Fig. 3.

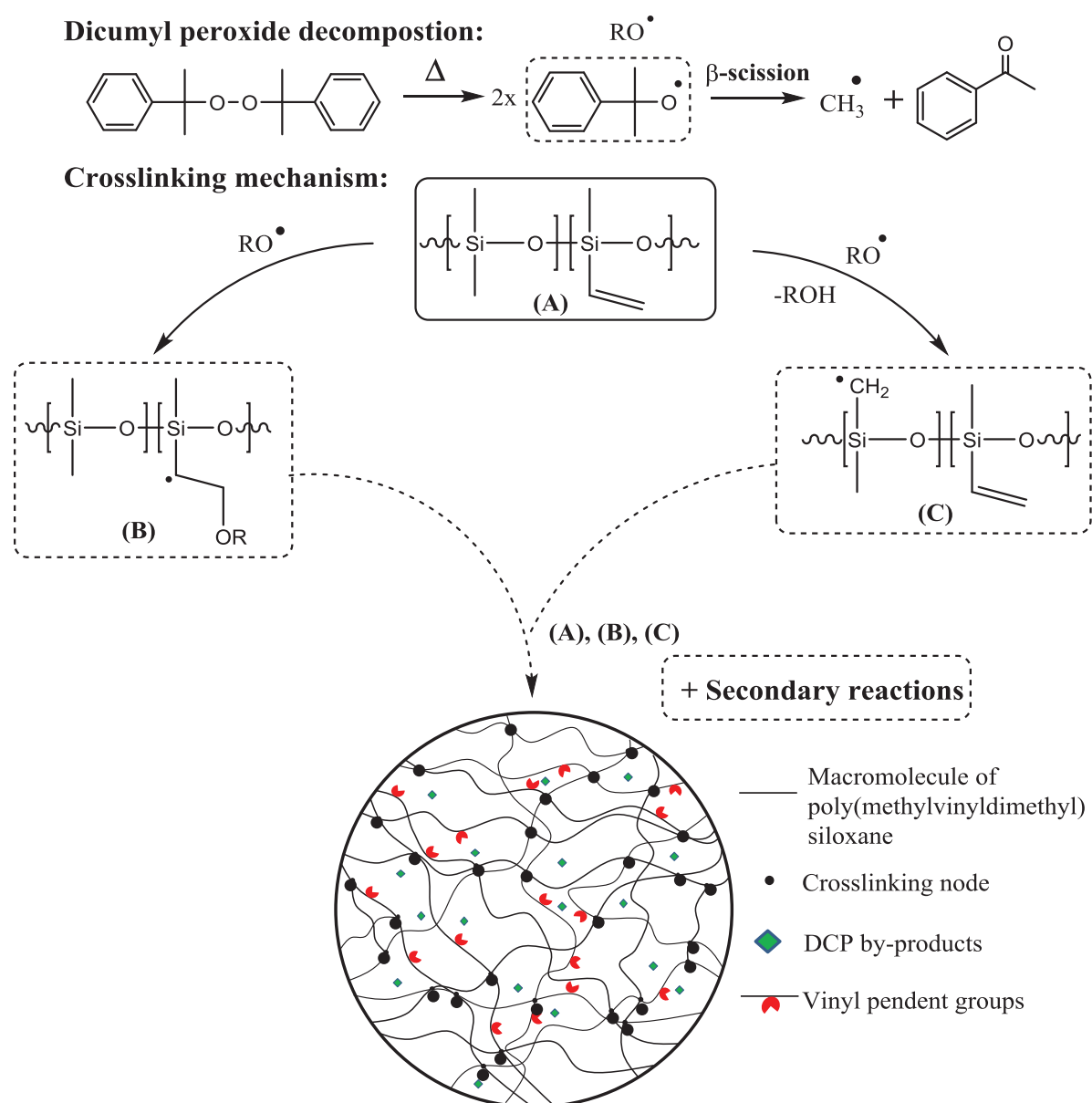


Fig. 3. DCP decomposition and free radical cross-linking mechanisms of poly(methylvinyl dimethyl) siloxane

This cross-linking mechanism was first assumed by Dunham et al. [14]. Baquey et al. [18, 19] used siloxane oligomers with molar mass lower than 700g/mol to effectively prove

these assumptions. First, two cumyloxy radicals are formed by thermolysis of the DCP and the β -scission reaction constitutes already 63% of the decomposition at 150°C [42]. Then, the cumyloxy or methyl radicals may react with Si-methyl or pendent vinyl groups of the silicone chain (A) to form macro-radicals (B) and (C)[18]. However, the cumyloxy radical addition on pendent vinyl group is more favorable over the hydrogen abstraction from the Si-methyl group [14]. On the one hand, the silylalkyl radicals generated from hydrogen abstraction of Si-methyl may react with an unsaturated group to form a trimethylene adduct radical. On the other hand, the silylalkyl radicals created from cumyloxy reaction with the vinyl group may also form an adduct radical. Thus, these adduct radicals may terminate by hydrogen transfer or couple with another radical. In parallel, termination reactions between macroradicals also lead to the formation of cross-links. Therefore, these simultaneous cross-linking reactions lead to a complex topological network structure as illustrated in Fig. 3.

However, the radical cross-linking reactions are controlled by the radical diffusion which is dependent on the medium viscosity. In silicones, several vinyl groups are present in the same macromolecule or macro-radicals. If some groups are linked, it will lower the diffusion of the newly formed macromolecules. Therefore, some radical reactions may be promoted considering the high medium viscosity of silicone elastomers. Indeed, Mani et al. [17] successfully modeled the rheological cross-linking kinetic data by considering only a termination reaction between two radicals obtained from the addition of cumyloxy radical to the vinyl group.

During cross-linking reaction, silicone chain mobility is greatly reduced leading to enhanced moduli which can be monitored by kinetic rheology studies as presented in Fig. 4-a. The DCP conversion, depicted in Fig. 4-a, is derived from eq. (1). During the cross-linking reaction, chain branching occurs leading to a wide molar mass distribution and numerous molecular structures. At gel point, a macromolecular chain cross the whole sample [43]. In this paper, we made the assumption that the gel point of a cross-linking polymer coincides with the G' - G'' crossover. In other words, we suppose that, at this point, G' and G'' are equal over the whole range of frequencies and proportional to the square of the angular frequency. Above gel point, a 3D network is formed and the number of cross-links increases with time leading to a steady state value of storage modulus at the end of the reaction, reported in Table 1. Loss modulus has an inflexion point; this is explained by the fact that at first molar mass increases in wide distribution non-homogeneously. After gel point, as the network gets denser, the molar mass distribution between cross-linking points gets finer and more homogeneous leading to a decrease of loss modulus. The gel time is 180s which gives a DCP conversion at 150°C of 8.3%. According to the viscoelastic behavior obtained at the end of the cross-linking time shown in Fig. 4-b, both samples act as viscoelastic solid since the elastic modulus is over the loss modulus on the whole frequency range explored. When 0.1wt% of DCP is added, the silicone rubber is not fully cross-linked as G' is not constant on the frequency range studied and $\tan \delta = \frac{G''}{G'}$ remains close to 0.1.

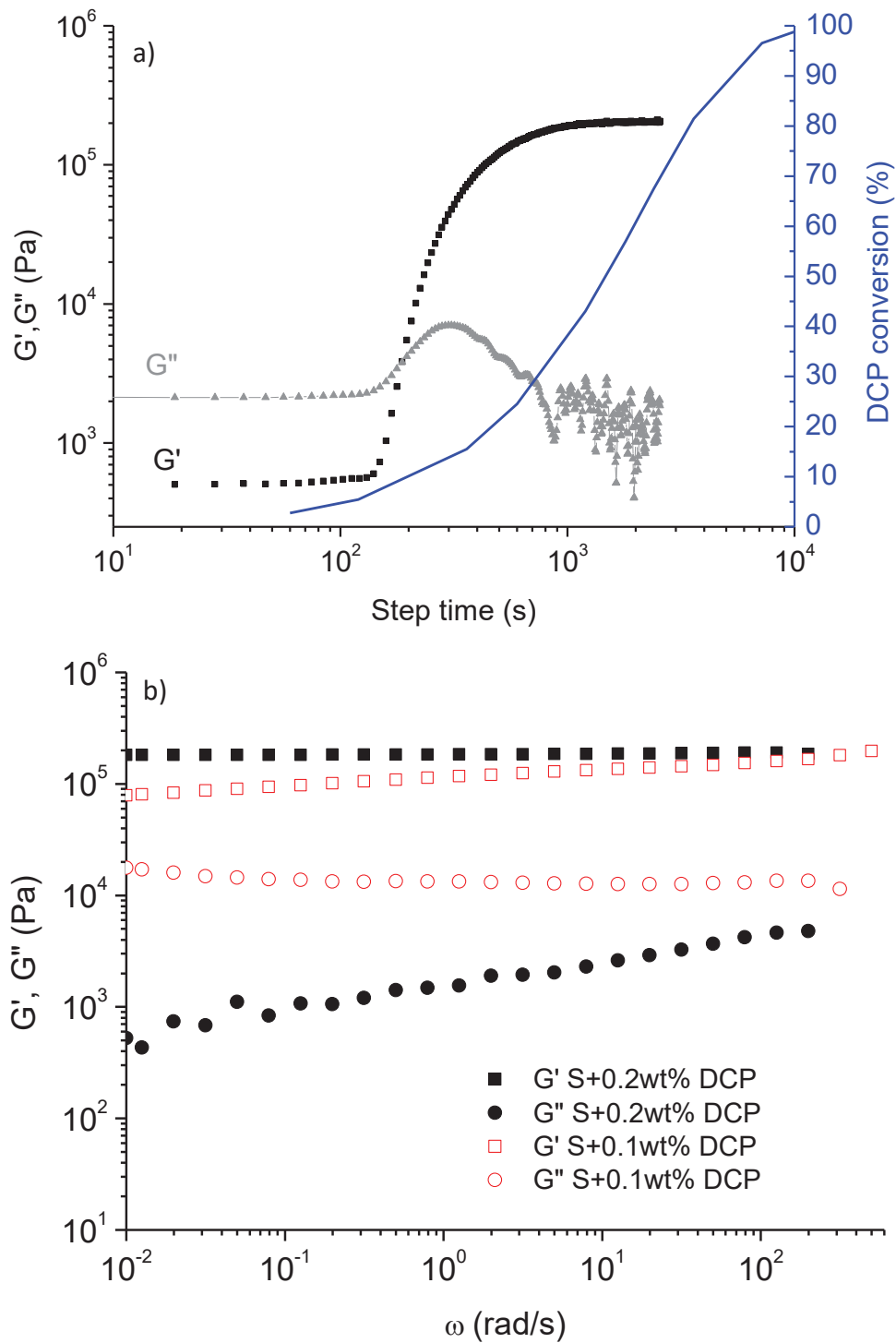


Fig. 4. Cross-linking of S samples under static conditions. a) Variation of the complex shear moduli as a function of time at 150°C , $\omega=1\text{rad/s}$. b) Viscoelastic behavior of samples at the end of the cross-linking reactions ($T=150^\circ\text{C}$). Variations of the Storage and Loss moduli at $T=30^\circ\text{C}$, $\varepsilon=0.1\%$, with different amounts of DCP.

In this study, the phenomenological model of Langley [2], Dossin and Graessley [3], eq.(8), was used to predict the shear equilibrium modulus, G_e . This model takes into account

the input of chemical cross-links, $(\nu - h\mu)RT$, and also entrapped entanglements of chains by the newly formed cross-linking network, $T_e G_N^0$. T_e defines the ratio of entanglements contributing to shear modulus and G_N^0 is the rubbery plateau modulus, which depends on the entangled molar mass, $G_N^0 = \frac{\rho RT}{M_e}$. According to Gottlieb et al. [6], G_N^0 is 2.4×10^5 Pa at room temperature for PDMS. For chemical cross-links input, h is an empirical parameter often set to 0. ν and μ are, respectively, the density of active elastic strands and the density of cross-link bonds.

$$G_e^{Langley-Grassley} = (\nu - h\mu)RT + T_e G_N^0 \quad (8)$$

With $G_N^0 = 2.4 \times 10^5$ Pa ; $h = 0$; $R = 8.314$ J/(mol.K); $T = 303$ K

According to the theory developed by Pearson and Grassley [44], all the parameters: ν, μ, T_e , the extent of the reaction, p , and cross-link functionality, f , are determined from the measurements of the soluble fraction, ω_s , as reported in Table 1. According to the cross-linking mechanism described in Fig. 3, the extent of the reaction is assumed to be mostly correlated to the vinyl consumption. Experimental and predicted shear moduli show good agreements, Table 1 and Fig. 4-b.

Table 1: Topological parameters computed from Pearson and Graessley model

	ω_s	p	T_e	ν [mol.m ⁻³]	μ [mol.m ⁻³]	f	$G_e^{Langley-Grassley}$ x10 ⁵ [Pa]	$G_e^{0 rheo}$ x10 ⁵ [Pa]
S + 0.1wt% DCP	0.09	0.26	0.20	3.53	2.12	3.3	0.57	0.80
S + 0.2wt% DCP	0.02	0.56	0.48	11.5	6.48	3.5	1.45	1.84

II.2. Dynamic cross-linking

As shown in Fig. 1-a, the processing temperature range is very narrow. Regarding the sample cross-linked at 155°C, after introduction, the torque quickly and drastically increase followed by a drop of torque. During the torque increases, the silicone network becomes more and more cross-linked until it becomes brittle. Under high shear, the cross-linked S turns into powder. This behavior was already observed for EVA by Verbois et al. [22]. When the same experiment is carried out at 145°C, the torque profile remains almost constant which means that the S sample does not turn into powder and remains processable along the whole cross-linking reaction. As torque variation is typical of bulk variation of viscosity, we may expect little modification of rheological behavior of dynamically cross-linked rubbers from torque measurements. The dynamic cross-linked samples remain also soluble in THF and behave like viscoelastic liquid, as shown in Fig. 5. Actually, we qualitatively obtained similar results that Msakni et al. [24] for ethylene octene copolymers. From their study, it is

assumed that the no-cross-linked chains play the role of the matrix, embedding large clusters of macromolecules.

Further, viscoelastic behavior of dynamically and statically cross-linked samples are far different. Indeed, statically cross-linked samples have a viscoelastic solid-like behavior whereas dynamically cross-linked samples still behave as viscoelastic liquid-like fluids. However, an onset in the terminal zone in the rheological response of the dynamic cross-linked samples can be identified as compared to the neat elastomer. The following discussion is focused on the understanding of why there is such difference of rheological behavior between both while the elastomer has the same amount of peroxide.

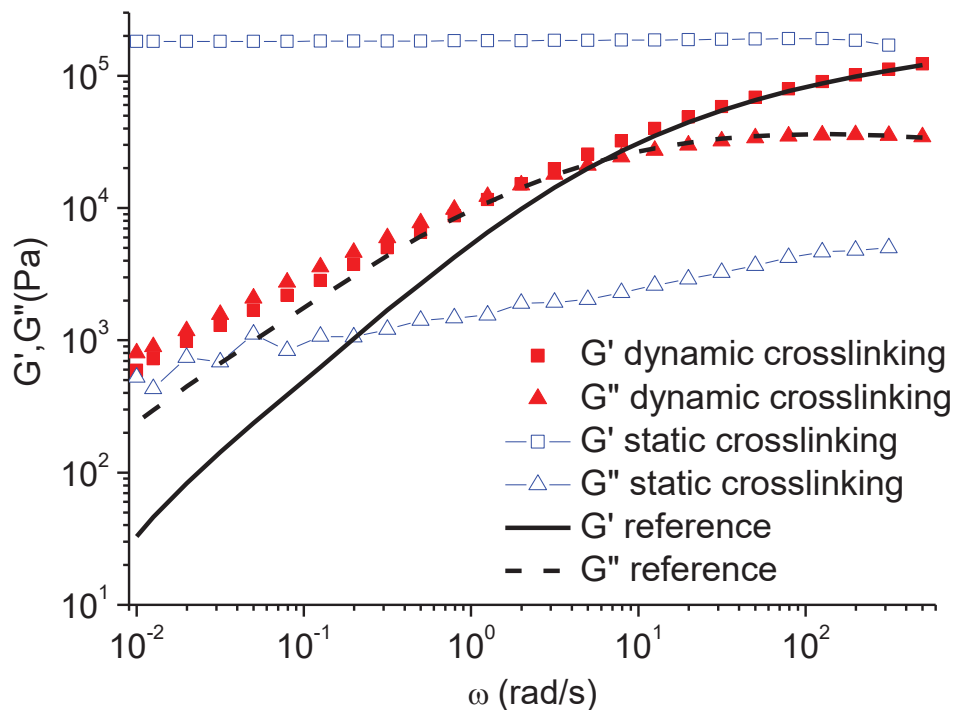


Fig. 5. Viscoelastic behavior at $T=30^{\circ}\text{C}$ of silicone elastomers cross-linked (0.2wt%DCP) under different processing conditions. Static conditions ($T=150^{\circ}\text{C}$) and dynamic conditions ($T_{\text{haake}}=145^{\circ}\text{C}$; $N=50\text{rpm}$)

Actually, the dynamic cross-linking experiments were conducted under N_2 and air atmospheres, as shown in Fig. 1-b. The sample made under nitrogen turns into powder in few minutes whereas under air, the torque is stable along the whole reaction time. It is well known that radicals can be trapped by free radical species such as molecular oxygen, leading to the formation of unstable hydroperoxides [45], or nitroxide [17]. Cross-linking reaction defines the creation of a bond between two polymer chains. The creation of this covalent bond is exothermic, like also oxidation, and it may be followed by DSC. Oxidation induction time (OIT) measurements were performed in order to quantify the overall oxidation and cross-linking phenomena. Isothermal DSC scans were performed, first under N_2 , to determine the overall exothermic heat of the reaction of homolytic decomposition of DCP and C-C bond formation (Fig. 6). Here, it is assumed that no exothermic side reactions occur, none oxidation reactions for instance. As shown in Fig. 6, the overall cross-linking reaction

was followed by DSC and the heat flow was fitted, curve with hollow circles. Integration of the fitting function was performed to estimate the enthalpy of reaction, ΔH_c . We found $\Delta H_c = 5.34 \text{ J/g}$, also reported in Table 2.

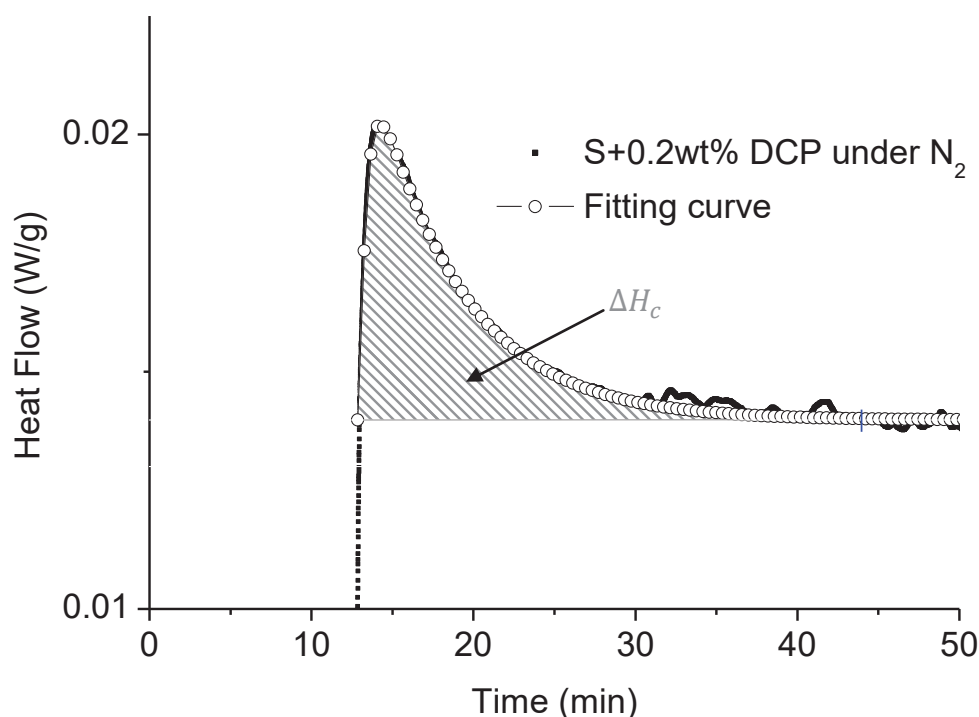


Fig. 6. DSC measurement showing the total heat of cross-linking reaction obtained under N₂. Sample S+0.2wt%DCP at 150°C for 120 minutes. Integration of the curve to calculate the enthalpy of cross-link C-C bonds, ΔH_c .

Then, scans were performed under N₂ until reaching 150°C followed by an isothermal step for 5 min on drilled capsules. N₂ was switched to air as gas carrier which enables us to follow oxidation reactions (Fig. 7). Instantly after air was introduced in the chamber, a large peak emerges which may be attributed to oxidation of the sample. The fact that the oxidation peak occurs directly after oxygen introduction suggests a fast and easy oxidation. Molecular oxygen is relatively permeable into PDMS. It has a solubility of $0.18 \text{ cm}^3 \text{ (STP)/}(\text{cm}^3 \cdot \text{atm})$ and can diffuse easily in PDMS, $D_{O_2} = 34 \times 10^{-10} \text{ m}^2/\text{s}$ at 35°C [46]. A modified pulse function was used to fit the new evolution of the heat flow measurement before air injection. According to Fig. 6, this fitting curve also takes into account that the fit function must tend to zero after 35 min of reaction. Integration was performed to the whole heat measurements and the fitted part. Then, it was deduced enthalpies of the overall cross-linking, ΔH_t , and oxidation reactions, ΔH_{oxy} , reported in Table 2. About 65% of the overall enthalpy of reaction is attributed to the oxidation reactions. Moreover, as a lower content of vinyl groups should form cross-links under air, ΔH_c has a lower value under air as compared to the trials carried out under N₂.

The oxidation reaction should contribute even more in case of dynamic cross-linking because a continuous amount of O₂ is incorporated. For molecular oxygen, the radical

trapping rate constants, in solution, is diffusion controlled ($>10^9 \text{ M}^{-1}\cdot\text{s}^{-1}$) [47]. The rate constants of cumyloxy radical grafting onto vinyl groups is assumed to be in the range of 10^6 to $10^7 \text{ M}^{-1}\cdot\text{s}^{-1}$ and the rate constant of C-C bond creation is calculated around $0.8 \text{ M}^{-1}\cdot\text{s}^{-1}$ [48]. Therefore, the radical trapping rate of molecular oxygen is substantially faster than the rate of C-C bond formation. In most cases, during the cross-linking step, uncontrolled thermo-oxidation leads generally to surface tackiness. However during dynamic cross-linking, a constant amount of molecular oxygen is introduced, dispersed and contribute to the inhibition of the cross-linking reaction in the bulk by quenching the cumyloxy radical or generating unstable hydroperoxides species [49].

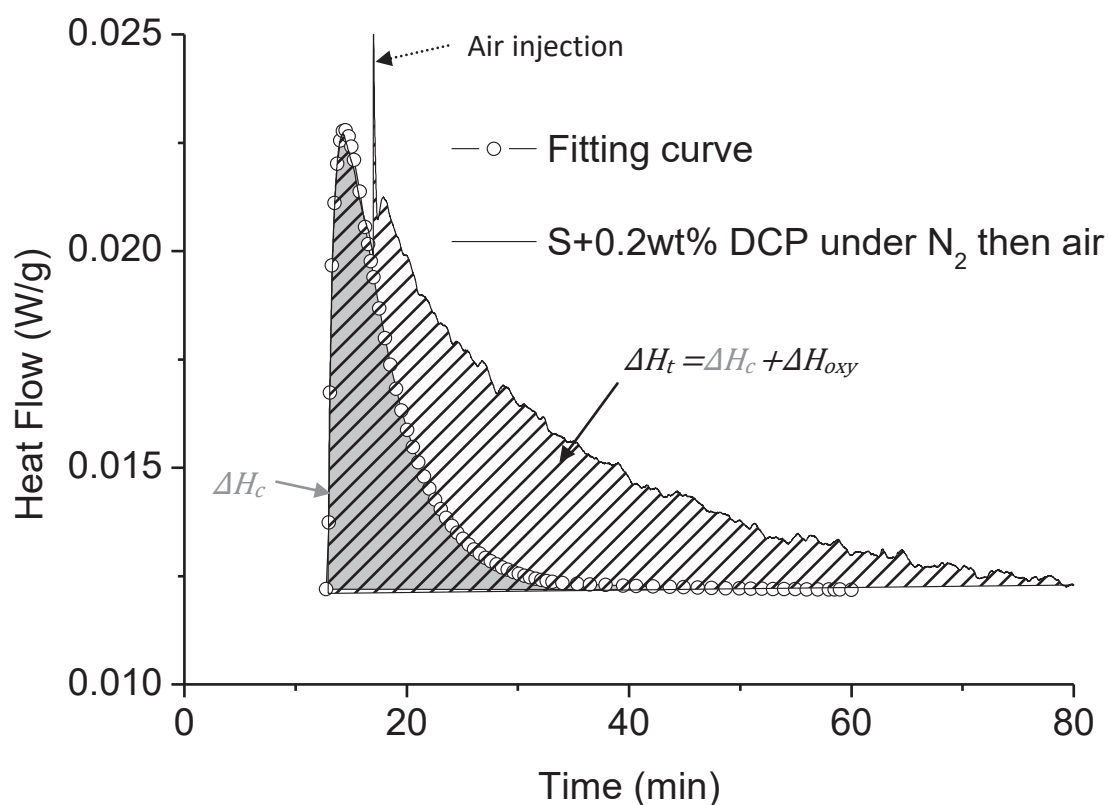


Fig. 7. DSC measurement showing the total heat of cross-linking reaction obtained under thermo-oxidative atmosphere. Sample S+0.2wt%DCP at 150°C under N₂ for 5 minutes then under air for 115 minutes. Integration of the curves to calculate the enthalpy of homolytic decomposition of DCP and C-C bond formation, ΔH_c , and the enthalpy of oxidation, ΔH_{oxy} .

Table 2: Enthalpies of reaction determined by integration of the heat flow measured by DSC.

	ΔH_c [J/g]	ΔH_{oxy} [J/g]	ΔH_t [J/g]
Under N ₂	5.34	-	5.34
Under N ₂ and Air	3.8	8.0	11.8

NMR experiments were performed in order to quantify the grafting reactions of DCP on macromolecules during the dynamic cross-linking, under thermo-oxidative atmosphere. The ^1H spectra of silicone elastomer and dynamically cross-linked silicone rubber are shown in Fig. 8 a) and b) respectively.

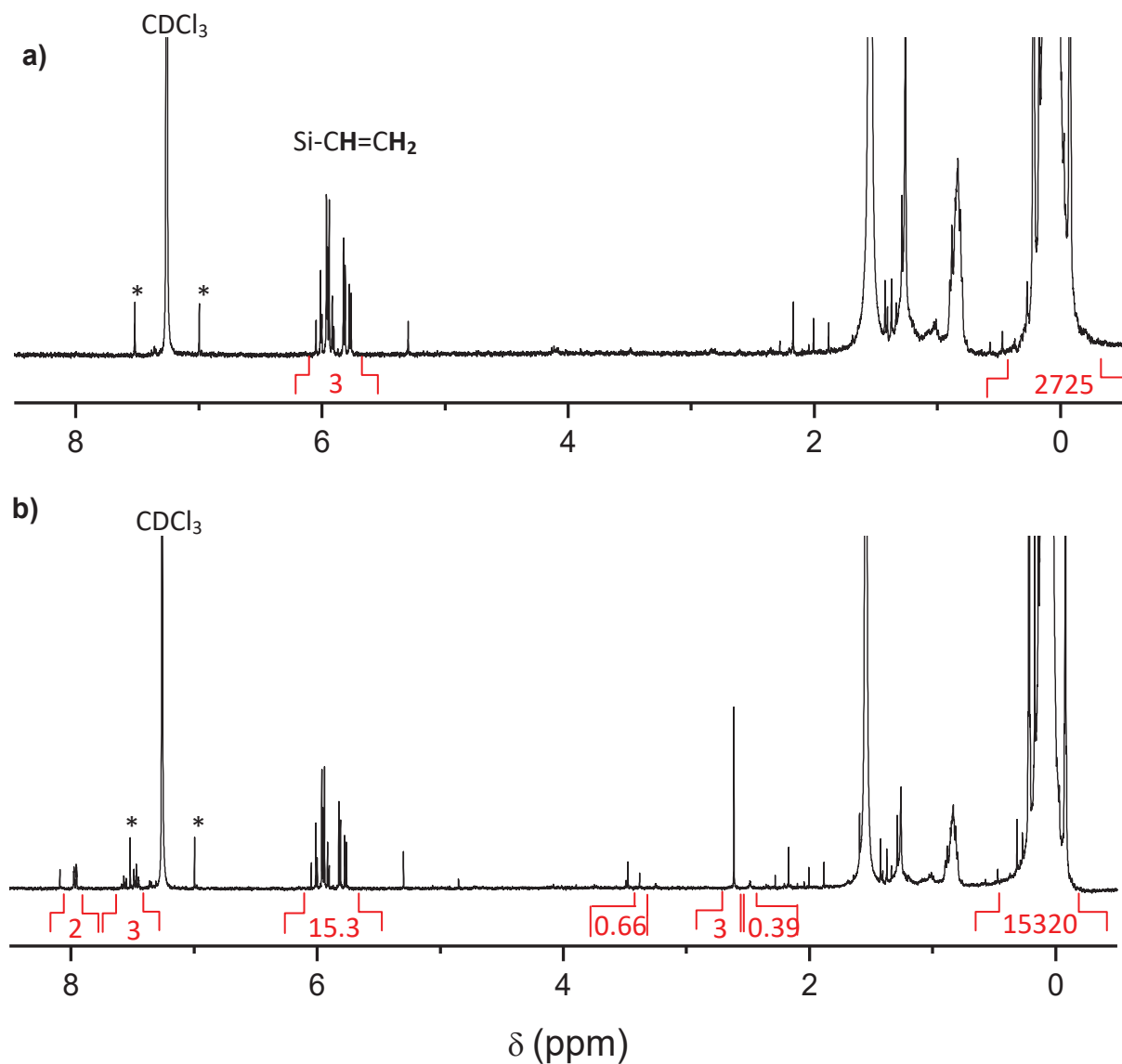


Fig. 8. ^1H NMR Spectra: a) virgin S; b) Dynamically cross-linked S (0.2wt%DCP, $T=145\text{ }^\circ\text{C}$, $N=50\text{ rpm}$)

The ^1H NMR spectra display a broad signal at 0.2 ppm corresponding to the protons of Si-CH_3 [50]. The signals at 0.8 and 1.2 ppm may be correlated to the Si-CH_3 protons of silicone oligomers such as hexamethylcyclotrisiloxane (D_3) [50]. These remaining oligomers may be evaporated during the dynamic cross-linking ($T_b(\text{D}_3) = 134^\circ\text{C}$ [51]) which could explain the decrease in signal intensity between the neat and the dynamically cross-linked sample analysis. The multiplet signal corresponding to vinylic protons is located between 5.7 and 6.2 ppm [50]. In the case of the spectrum of soluble fraction of the dynamically cross-linked rubber, we can clearly observe the emergence of a new signal at 2.6 ppm (Fig. 8b)

which can be attributed to the protons in alpha position of the ketone in acetophenone [52] ($T_b = 202^\circ\text{C}$), according to the mechanism in Fig. 3.

Further, the presence of new signals near 2.45 and 3.55 ppm may be attributed to DCP grafting onto the vinyl group forming RO-CH and RO-CH₂ groups, respectively [16]. This is confirmed by the presence of multiplets in the 7.3 and 8.0 ppm range which may be attributed to aromatic protons.

The vinyl consumption can be deduced by comparing the integration of the signals at 5.7-6.2 ppm in both spectra. As a matter of fact, we calculated that the vinyl concentration represents 0.22 mol% in the neat silicone elastomer. However, due to the small conversion value (14 %) of the vinyl group after the dynamic cross-linking step, we found that the vinyl concentration represents only 0.19 mol% in the dynamically cross-linked silicone rubber. Then, it was also possible to check the conversion of DCP into acetophenone by comparing the integral of the signal of the acetophenone at 2.6 ppm and the signals of the DCP grafting at 2.45 and 3.55 ppm. Hence, it was found that only 35% of the DCP effectively participate in the cumyloxy grafting. Therefore, the formation of methyl radicals through a β -scission reaction should represent 65% of the dicumyl peroxide content. By comparison, in the case of static cross-linking, the vinyl group consumption is about 60% (Table 1). The presence of molecular oxygen during the dynamic cross-linking decreases effectively the vinyl consumption by a factor of 4.

The subsequent analyses will be only carried out on dynamically crosslinked samples under air. In this section, we will detail the impact of this radical inhibition on the chain structure. Fig. 9 shows the molar mass distribution of S for several levels of DCP incorporated and processed in a dynamic mode. A strong broadening of the molecular weight distribution is detected in the high molecular weights until 10^7 g/mol. This broadening increases with the amount of DCP used. Average molecular weights are reported in Table 3. As most of the vinyl groups are not in telechelic positions, these results confirm that the dynamic cross-linking of SR enables to create branched structure with a broad molecular weight distribution via a peroxidic route.

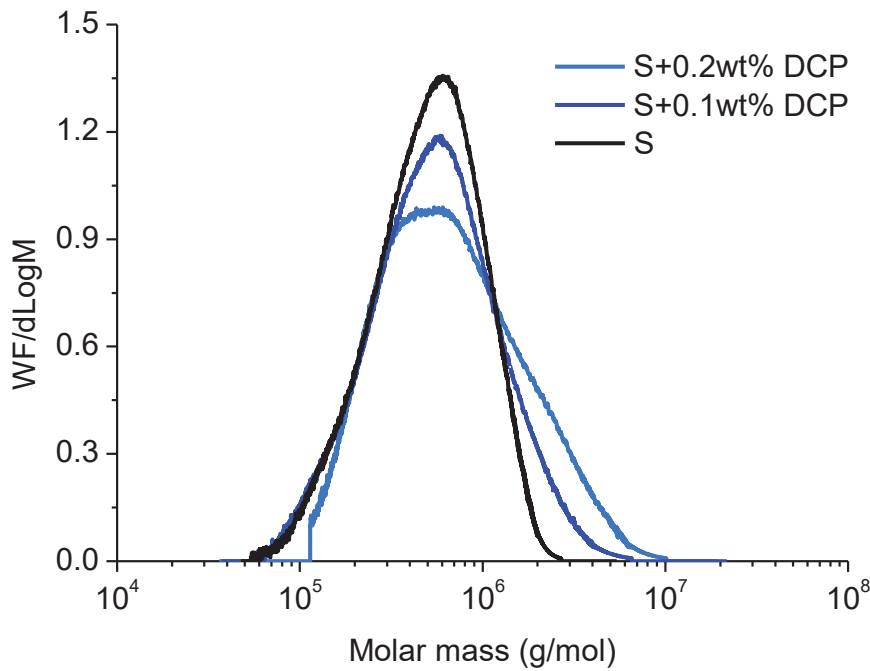


Fig. 9. Molar mass distribution of samples dynamically cross-linked (0,1wt% and 0.2wt%DCP, $T=145$ °C, $N=50$ rpm) compared with the neat sample reference.

Table 3: Molar masses of neat and dynamic cross-linked samples

Sample	M_n [kg/mol]	M_w [kg/mol]	M_z [kg/mol]	$I_p (M_w/M_n)$
S	350	600	840	1.7
S + 0.1wt%DCP	400	740	1330	1.9
S + 0.2wt%DCP	480	1000	2130	2.1

The viscoelastic behavior of samples dynamically cross-linked was characterized as shown in Fig. 11 a,b). As compared to neat S, the variations of $G'(\omega)$ (Fig 11 a) and $G''(\omega)$ (Fig 11b) shows a strong modification of the terminal relaxation zone with an increase of the relaxations times. Note that for sample cross-linked under static conditions this terminal relaxation does not exist anymore as the storage modulus exhibits an equilibrium modulus. The amount of DCP plays a significant role on the rheological responses of dynamically cross-linked samples. By increasing the amount of DCP, relaxation time and the moduli in the low frequency increase, Fig. 11 a), b) and Table 4. These results are in complete agreement with the molar mass distribution curves and M_w and M_z data reported in Fig. 9 and Table 3.

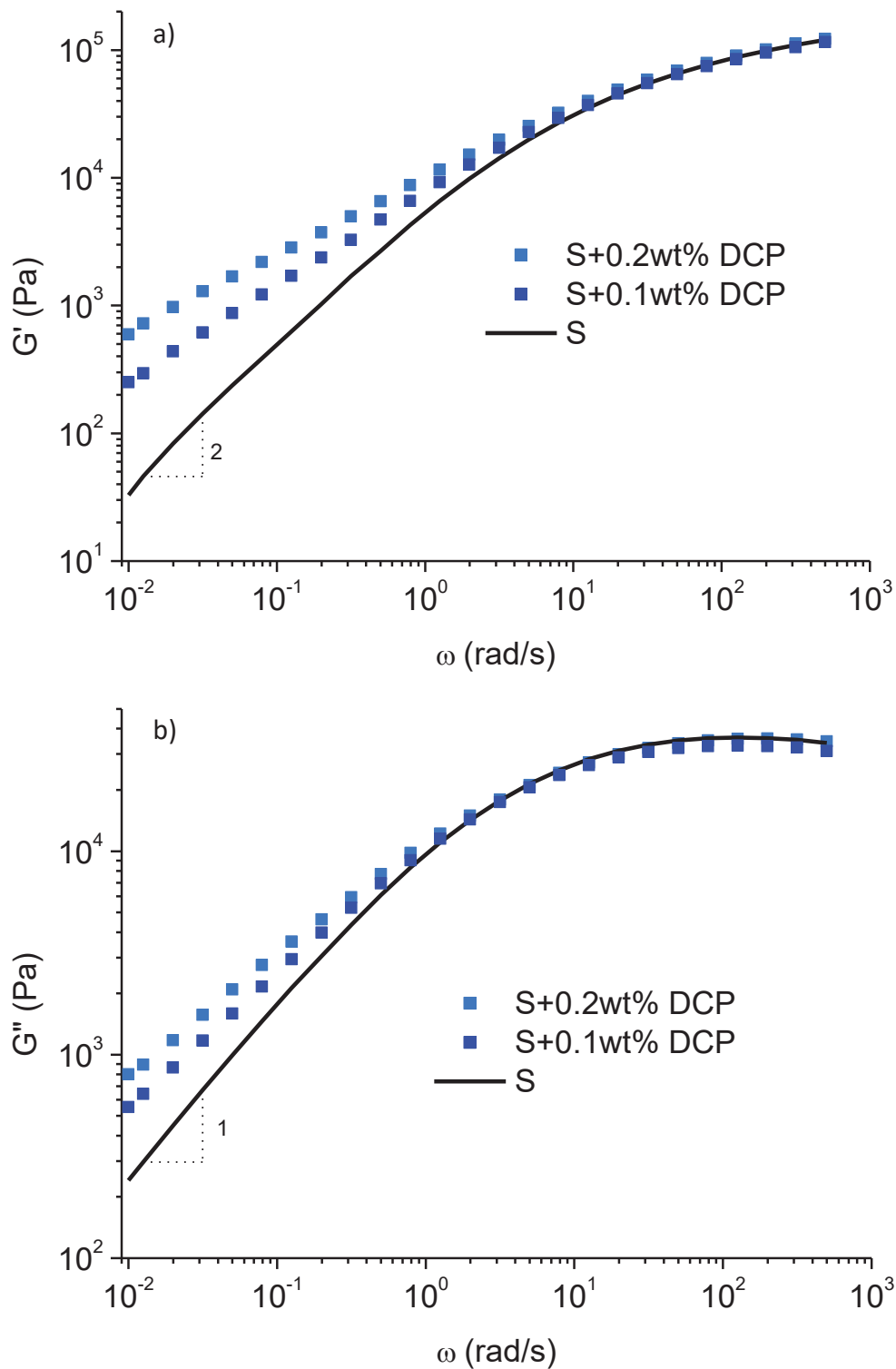


Fig. 10. Influence of DCP concentration on the viscoelastic behavior of dynamic cross-linked samples: a) Storage moduli b) Loss moduli

From the experimental linear viscoelastic response it can be fitted the multi-mode parameters of the Maxwell model [50]. The dynamic material parameters are described by a continuous set of parameters G_i, λ_i forming the continuous spectrum of relaxation, $H(\lambda)$. The frequencies available experimentally by dynamic rheology enable to scope out

intermediate and long time scale molecular dynamics i.e. entanglement and flow behaviors. Analysis and modeling of the terminal relaxation spectra is of first interest to characterize branching of long molecular chain. Relaxation spectra were calculated from experimental data by Trios software and plotted in Fig. 11. Zero shear viscosities were calculated from modeled parameters as reported in

Table 4. It is clear that the dynamic cross-linked brings forth a modification of the molecular structure which is mainly observed, as measured by SEC measurements, in the longer relaxation times so concerning large scale molecular structures. The chain structure is modified at a multi-scale as sets of parameters, from $\lambda=1$ to 500 s, have changed after dynamic cross-linking attesting that a complex blend of multi-scale branched structures is produced. As the amount of peroxide increases, the large scale molecular structure modification becomes greater. For short relaxation times, the relaxation spectra remain unchanged which confirms that only structure modification occurs at large scales during the dynamic cross-linking.

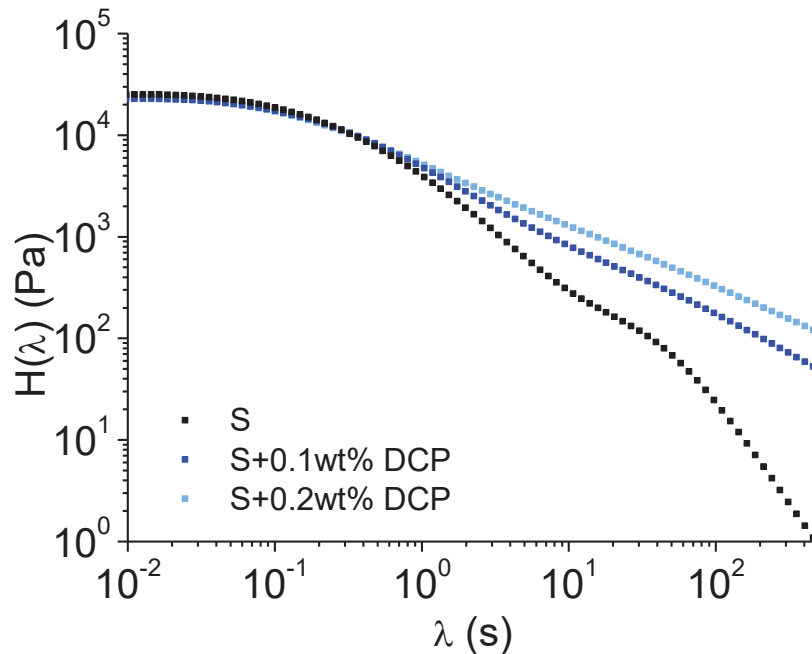


Fig. 11. Relaxation spectra of each formulation obtained from fitting of the dynamic data at $T=30^{\circ}\text{C}$

Table 4: Viscoelastic parameters of dynamic cross-linked samples at $T=30^{\circ}\text{C}$

Sample	$\tau_c^a)$	$\eta_0 = \int_0^{+\infty} H(\lambda)\lambda d\ln\lambda$ [Pa.s] $\times 10^4$
S	0.16	2.50
S + 0.1wt%DCP	0.30	8.34
S + 0.2wt%DCP	0.57	14.5

a) G' , G'' crossover at 30°C

Most of the studies are focused on rheological uni-axial characterization to predict elongational flow behavior. Indeed, bi-axial measurements are difficult to set up, not always

reliable or accurate. Nevertheless, it was found that strain hardening may be present in both uni-axial and bi-axial flow though strain hardening in bi-axial flow is found to be much weaker [53]. In the following section, lubricated squeezing flow (LSF) measurements will be discussed characterizing the bi-axial behavior of our formulations. However, LSF technique is limited to strain rate of $0.5s^{-1}$ and Hencky strain of 1.5 as previously explained in the experimental section. It is important to note, in the case of HMS-PP, strain hardening may be limited to a small deformation rate only [25] which might lead to errors if extrapolation to higher deformation rates are desired. Fig. 12 summarizes the LSF experiments for all the formulations at a strain rate of $0.1s^{-1}$. Even if strain hardening is very weak in bi-axial flow, it becomes obvious that dynamic cross-linking improves elongational properties as compared to a neat elastomer. For the neat elastomer, the stress achieves almost a steady state for $\varepsilon_b=0.2-1.5$ whereas if a small amount of peroxide is introduced, the stress keeps increasing when the strain increases. As observed in SEC measurements before, the distribution of multi-scale branched structures get larger and towards larger structures with the amount of DCP used. The corresponding relaxation times and moduli increase which in turn increase the bi-elongational response upon compression because the presence of this branched structures limit the flow behavior of the remaining linear chains inducing an upward deviation from the Troutonian regime.

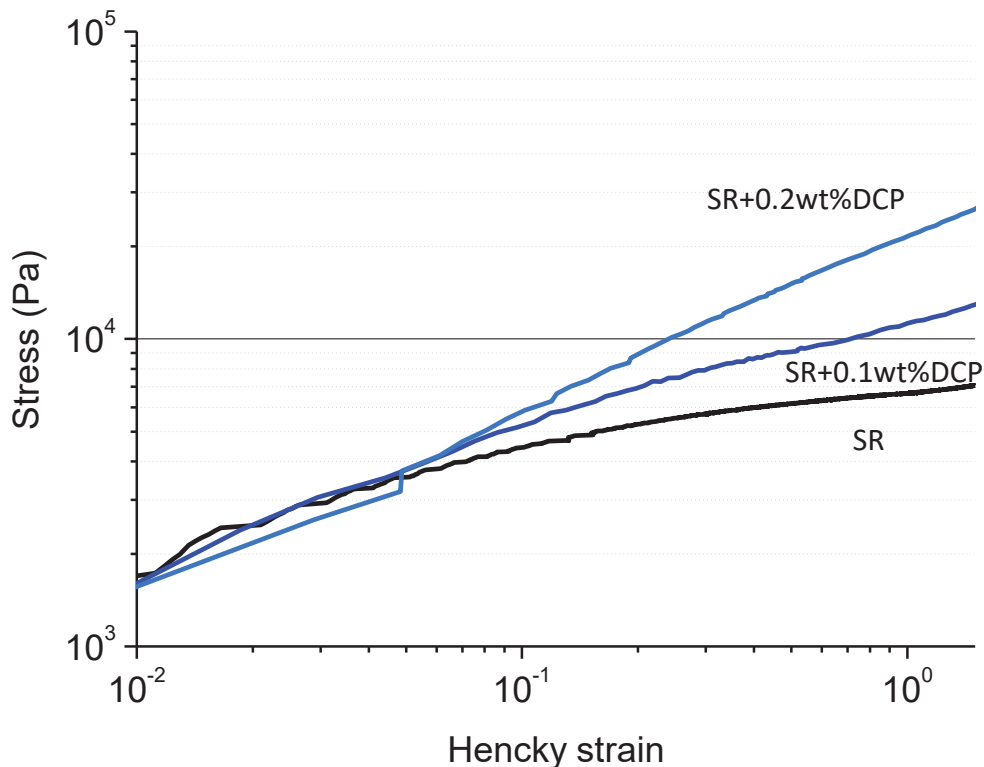


Fig. 12. Bi-elongational behavior (lubricated squeezing flow) of cross-linked samples under dynamic conditions, $\dot{\varepsilon}_b = 0.1s^{-1}$ and $T=25^\circ C$.

Conclusion

The static and dynamic cross-linking of vinyl-PDMS based copolymer were studied in the present work with the main objective to bring new insights in the field of dynamic crosslinking of bulk polymers. Although static cross-linking of silicone rubber have already been investigated, our results define the stand for the dynamic cross-linking study. Static cross-linking results are quantitatively in good agreements with theory of network elasticity and cross-linking chemical mechanisms.

Even though the sample should be fully cross-linked under static conditions, it was found that under dynamic conditions the cross-linked samples remain processable and totally soluble. Rheological and SEC analysis revealed that the cross-linking reaction gives rise to multi-scale branched structures with molecular structures achieving 10^7 g/mol. As a result, the dynamic cross-linked samples showed a strain hardening behavior in bi-elongational flow. It must be pointed out that such rheological behavior is greatly favorable for blowing applications. Furthermore, dynamic cross-linking experiments were carried out under thermo-oxidative and inert atmosphere. It was then proved that molecular oxygen inhibited the cross-linking reaction inducing a low consumption of vinyl groups within the molten medium. Thanks to these results, we may imagine the following mechanism for the cross-linking in a dynamic mode. First, the macromolecules generate cross-link bonds and form primary branched structures. As the number of bonds increases, branched macromolecules tend to agglomerate to form hyperbranched at the micro-scale. Simultaneously, the molecular oxygen delays the cross-linking kinetic which enables to leave free macromolecules. The un-cross-linked chains play the role of the matrix while the miscible hyperbranched structures act as reinforcement agent. However, further works should be conducted to evidence the presence of hyperbranched or gel structures by AFM and light scattering techniques. One can imagine using this process to graft functional groups with nitroxide compounds in order to control the grafting efficiency.

Acknowledgements: The authors are grateful to the FUI SMOUSSIF for the financial support of this work.

References

- [1] F. Ignatz Hoover, B.H. To, *Vulcanization*, Rubber Compounding: Chemistry and Applications, CRC Press, 2004.
- [2] N.R. Langley, Elastically Effective Strand Density in Polymer Networks, *Macromolecules* **1** (4) (1968) 348-352.
- [3] L.M. Dossin, W.W. Graessley, Rubber Elasticity of Well-Characterized Polybutadiene Networks, *Macromolecules* **12** (1) (1979) 123-130.
- [4] B. Marciniac, *Comprehensive Handbook on hydrosilylation*, Pergamon press, 1992.
- [5] L.M. Lopez, A.B. Cosgrove, J.P. Hernandez-Ortiz, T.A. Osswald, Modeling the vulcanization reaction of silicone rubber, *Polymer Engineering & Science* **47** (5) (2007) 675-683.
- [6] M. Gottlieb, C.W. Macosko, G.S. Benjamin, K.O. Meyers, E.W. Merrill, Equilibrium modulus of model poly(dimethylsiloxane) networks, *Macromolecules* **14** (4) (1981) 1039-1046.
- [7] E.M. Valles, C.W. Macosko, Properties of Networks Formed by End Linking of Poly(dimethylsiloxane), *Macromolecules* **12** (4) (1979) 673-679.
- [8] J. Heiner, B. Stenberg, M. Persson, Crosslinking of siloxane elastomers, *Polymer Testing* **22** (3) (2003) 253-257.
- [9] J. Clark, R. Ekeland, M. Owens, D.P. Van, Silicone coatings containing silicone mist suppressant compositions, 2001, WO 2001098418 A2
- [10] A. Stricher, R.G. Rinaldi, G. Machado, G. Chagnon, D. Favier, L. Chazeau, F. Ganachaud, Light-Induced Bulk Architecturation of PDMS Membranes, *Macromolecular Materials and Engineering* **301** (10) (2016) 1151-1157.
- [11] M. Frounchi, S. Dadbin, F. Panahinia, Comparison between electron-beam and chemical crosslinking of silicone rubber, *Nuclear Instruments and Methods in Physics Research Section B: Beam Interactions with Materials and Atoms* **243** (2) (2006) 354-358.
- [12] D.J.T. Hill, C.M.L. Preston, D.J. Salisbury, A.K. Whittaker, Molecular weight changes and scission and crosslinking in poly(dimethyl siloxane) on gamma radiolysis, *Radiation Physics and Chemistry* **62** (1) (2001) 11-17.
- [13] W.J. Bobear, Crosslink Densities in Peroxide-Cured Silicone Gum Vulcanizates, *I&EC Product Research and Development* **3** (4) (1964) 277-281.
- [14] M.L. Dunham, D.L. Bailey, R.Y. Mixer, New Curing System for Silicone Rubber, *Industrial & Engineering Chemistry* **49** (9) (1957) 1373-1376.
- [15] K.E. Polmanteer, Silicone Rubber, Its Development and Technological Progress, *Rubber Chemistry and Technology* **61** (3) (1988) 470-502.
- [16] S. Mani, P. Cassagnau, M. Bousmina, P. Chaumont, Cross-Linking Control of PDMS Rubber at High Temperatures Using TEMPO Nitroxide, *Macromolecules* **42** (21) (2009) 8460-8467.
- [17] S. Mani, P. Cassagnau, M. Bousmina, P. Chaumont, Rheological modelling of the free-radical crosslinking of PDMS rubber in the presence of TEMPO nitroxide, *Polymer* **51** (17) (2010) 3918-3925.
- [18] G. Baquey, L. Moine, O. Babot, M. Degueil, B. Maillard, Model study of the crosslinking of polydimethylsiloxanes by peroxides, *Polymer* **46** (17) (2005) 6283-6292.
- [19] G. Baquey, L. Moine, M. Degueil-Castaing, J.C. Lartigue, B. Maillard, Decomposition of Di-tert-butyl Peroxide in Siloxane: An Approach of the Free Radical Cross-Linking of Silicones, *Macromolecules* **38** (23) (2005) 9571-9583.
- [20] D.K. Thomas, The crosslinking of methylvinyl silicones with organic peroxides, *Polymer* **7** (5) (1966) 243-250.
- [21] L.D. Loan, Mechanism of Peroxide Vulcanization of Elastomers, *Rubber Chemistry and Technology* **40** (1) (1967) 149-176.
- [22] A. Verbois, P. Cassagnau, A. Michel, J. Guillet, C. Raveyre, New thermoplastic vulcanizate, composed of polypropylene and ethylene-vinyl acetate copolymer crosslinked by tetrapropoxysilane: evolution of the blend morphology with respect to the crosslinking reaction conversion, *Polymer International* **53** (5) (2004) 523-535.

- [23] G. Martin, C. Barres, P. Sonntag, N. Garois, P. Cassagnau, Morphology development in thermoplastic vulcanizates (TPV): Dispersion mechanisms of a pre-crosslinked EPDM phase, *European Polymer Journal* **45** (11) (2009) 3257-3268.
- [24] A. Msakni, P. Chaumont, P. Cassagnau, Crosslinking of ethylene–octene copolymers under dynamic conditions: A new way to access polymeric hyperbranched structure, *Polymer Engineering & Science* **46** (11) (2006) 1530-1540.
- [25] J. Stange, H. Münstedt, Rheological properties and foaming behavior of polypropylenes with different molecular structures, *Journal of Rheology* **50** (6) (2006) 907-923.
- [26] M. Yamaguchi, K.-I. Suzuki, Rheological properties and foam processability for blends of linear and crosslinked polyethylenes, *Journal of Polymer Science Part B: Polymer Physics* **39** (18) (2001) 2159-2167.
- [27] C.J. Pérez, G.A. Cassano, E.M. Vallés, M.D. Failla, L.M. Quinzani, Rheological study of linear high density polyethylenes modified with organic peroxide, *Polymer* **43** (9) (2002) 2711-2720.
- [28] P.R. Dluzeski, Peroxide Vulcanization of Elastomers, *Rubber Chemistry and Technology* **74** (3) (2001) 451-492.
- [29] J.E. Mark, *Physical Properties of Polymers Handbooks*, Springer, 2007.
- [30] A. Msakni, P. Chaumont, P. Cassagnau, Diffusion of the dicumyl peroxide in molten polymer probed by rheology, *Rheol Acta* **46** (7) (2007) 933-943.
- [31] J.S. Vrentas, J.L. Duda, Diffusion in polymer–solvent systems. I. Reexamination of the free-volume theory, *J. Polym. Sci. Polym. Phys.* **15** (3) (1977) 403-416.
- [32] S.-H. Park, S. Lee, D. Moreira, P.R. Bandaru, I. Han, D.-J. Yun, Bioinspired superhydrophobic surfaces, fabricated through simple and scalable roll-to-roll processing, *Scientific Reports* **5** (2015) 15430.
- [33] Z. Tadmor, C.G. Gogos, *Principles of Polymer Processing* John Wiley & Sons, 1979.
- [34] D.C. Venerus, T.-Y. Shiu, T. Kashyap, J. Hosttetter, Continuous lubricated squeezing flow: A novel technique for equibiaxial elongational viscosity measurements on polymer melts, *Journal of Rheology* **54** (5) (2010) 1083-1095.
- [35] S. Chatraei, C.W. Macosko, H.H. Winter, Lubricated Squeezing Flow: A New Biaxial Extensional Rheometer, *Journal of Rheology* **25** (4) (1981) 433-443.
- [36] A.C. Papanastasiou, C.W. Macosko, L.E. Scriven, Analysis of lubricated squeezing flow, *International Journal for Numerical Methods in Fluids* **6** (11) (1986) 819-839.
- [37] A. Nishioka, Y. Takagi, T. Takahashi, Y. Masubuchi, J.-i. Takimoto, K. Koyama, Measurement of Biaxial Elongational Viscosity of Polymer Melts Using Lubricated Squeezing Flow Method, *Journal of the Society of Materials Science, Japan* **47** (12) (1998) 1296-1300.
- [38] S. Hamdani, C. Longuet, D. Perrin, J.-M. Lopez-cuesta, F. Ganachaud, Flame retardancy of silicone-based materials, *Polymer Degradation and Stability* **94** (4) (2009) 465-495.
- [39] M. Kučera, J. Láníková, Thermal stability of polydimethylsiloxane. I. Deactivation of basic active centers, *Journal of Polymer Science* **54** (160) (1961) 375-384.
- [40] N. Grassie, I.G. Macfarlane, The thermal degradation of polysiloxanes—I. Poly(dimethylsiloxane), *European Polymer Journal* **14** (11) (1978) 875-884.
- [41] T.H. Thomas, T.C. Kendrick, Thermal analysis of polydimethylsiloxanes. I. Thermal degradation in controlled atmospheres, *Journal of Polymer Science Part A-2: Polymer Physics* **7** (3) (1969) 537-549.
- [42] Y. Watanabe, H. Ishigaki, H. Okada, S. Suyama, Temperature Dependence of Initiation Reactions of Oxygen-Centered Radicals, *Polym J* **29** (8) (1997) 693-696.
- [43] F. Chambon, H.H. Winter, Linear Viscoelasticity at the Gel Point of a Crosslinking PDMS with Imbalanced Stoichiometry, *Journal of Rheology* **31** (683) (1987).
- [44] D. Pearson, W. Graessley, Elastic Properties of Well-Characterized Ethylene-Propylene Copolymer Networks, *Macromolecules* **13** (4) (1980) 1001-1009.
- [45] A.G. Ferradino, Antioxidant Selection for Peroxide Cure Elastomer Applications, *Rubber Chemistry and Technology* **76** (3) (2003) 694-718.

- [46] T.C. Merkel, V.I. Bondar, K. Nagai, B.D. Freeman, I. Pinnau, Gas sorption, diffusion, and permeation in poly(dimethylsiloxane), *Journal of Polymer Science Part B: Polymer Physics* **38** (3) (2000) 415-434.
- [47] B. Maillard, K.U. Ingold, J.C. Scaiano, Rate constants for the reactions of free radicals with oxygen in solution, *Journal of the American Chemical Society* **105** (15) (1983) 5095-5099.
- [48] S. Mani, Fundamentals aspects of crosslinking control of PDMS rubber at high temperatures using TEMPO nitroxide, PhD, University of Lyon (2011)
- [49] S.C. Ligon, B. Husár, H. Wutzel, R. Holman, R. Liska, Strategies to Reduce Oxygen Inhibition in Photoinduced Polymerization, *Chemical Reviews* **114** (1) (2014) 557-589.
- [50] A.B. Birkefeld, R. Bertermann, H. Eckert, B. Pfeleiderer, Liquid- and solid-state high-resolution NMR methods for the investigation of aging processes of silicone breast implants, *Biomaterials* **24** (1) (2003) 35-46.
- [51] S.E. Denmark, C.R. Butler, *Hexamethylcyclotrisiloxane*, Encyclopedia of Reagents for Organic Synthesis, John Wiley & Sons, 2001.
- [52] S. Wang, C. Miao, W. Wang, Z. Lei, W. Sun, A Salen–Co³⁺ Catalyst for the Hydration of Terminal Alkynes and in Tandem Catalysis with Ru–TsDPEN for the One-Pot Transformation of Alkynes into Chiral Alcohols, *ChemCatChem* **6** (6) (2014) 1612-1616.
- [53] M. Sugimoto, Y. Masubuchi, J. Takimoto, K. Koyama, Melt Rheology of Polypropylene Containing Small Amounts of High-Molecular-Weight Chain. 2. Uniaxial and Biaxial Extensional Flow, *Macromolecules* **34** (17) (2001) 6056-6063.

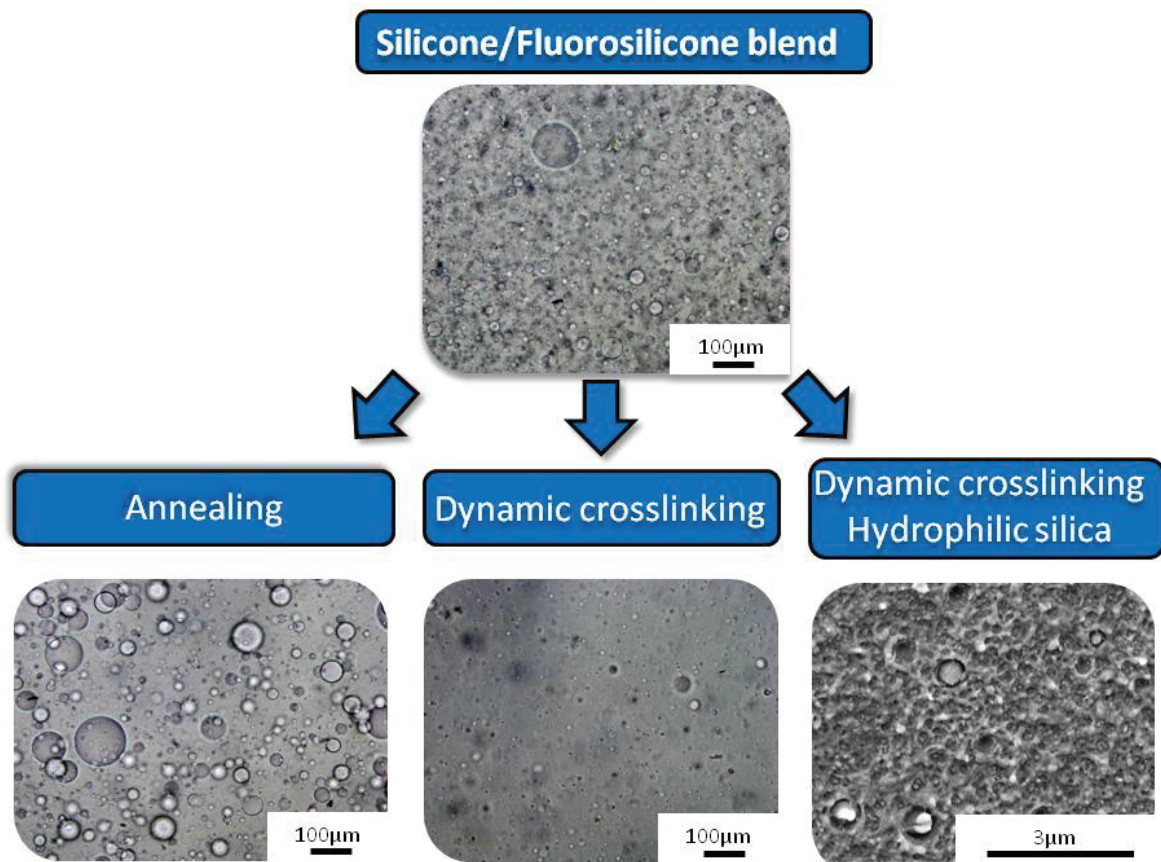
Chapter 4: Compatibilization of Silicone/Fluorosilicone blends by dynamic crosslinking and fumed silica addition.

ABSTRACT

The aim of this work is to study the compatibility of silicone / fluorosilicone blends by exploring two compatibilization strategies. First, the crosslinking of the blend under shearing conditions leads to a reduction in the size of the fluorosilicone domain and hence to an effective stabilization of the morphology under shear and long time annealing. The refinement of the morphology in the dynamic crosslinking step is most likely due to a decrease in the viscosity ratio coming from preferential crosslinking of the fluorosilicone phase. However, the formation of a copolymer between silicone and fluorosilicone at the blend interface cannot be totally excluded. Secondly, the silicone/fluorosilicone blend was compatibilized by the addition of silica particles whose surface is hydrophilic or hydrophobic. Fumed hydrophilic silica allows reducing the size of the fluorosilicone phase up to 500 nm while its hydrophobic counterpart is ineffective. This observation has been attributed to the specific hydrogen and dipolar interactions of the silicone and the CF₃ group with the silanol present on the surface of the hydrophilic silica. The compatibilization mechanism is supposed to be due to a decrease in the interfacial tension and to a reduction of the coalescence phenomenon

Reformatted version of paper originally published in Polymer

GRAPHICAL ABSTRACT



Compatibilization of Fluorosilicone/Silicone blends by dynamic crosslinking and fumed silica addition.

T. Métivier^a, P. Cassagnau^{a,*}

^a Univ Lyon, Université Lyon1, Ingénierie des Matériaux Polymères, CNRS UMR 5223, 15 Bd Latarjet, 69622 Villeurbanne, France

Introduction

From its intrinsic structure, poly (dimethylsiloxane) (PDMS) is of great interest in the industry. Indeed, it has excellent low temperature flexibility, heat resistance, dielectric and weathering properties [1]. It is widely used in medical applications because of its hydrophobicity, biocompatibility and high gas permeability [2]. Silicone chemistry is also widespread which gives access to a large panel of molar masses, chemical functionalities and structures [3]. As for fluorosilicone, the addition of trifluoropropyl groups increases resistance to fuels, oils and solvents especially non-polar such as hydrocarbons [4]. Fluorosilicone also exhibits low temperature flexibility and may serve as seals in the automotive industry because of its wide service temperature range from -50°C to 300°C [5].

The first approach to exploit the properties of both polymers is to tailor a high molar mass copolymer [6]. Xu et al. [7] achieved to manufacture a random copolymer with fine and homogeneous morphology and improved mechanical properties in comparison to the silicone/fluorosilicone blend. Copolymer was found to swell less in lubricating and sealing oil but it swells more in kerosene and gasoline than the blend depending on the difference between the interaction parameters of the copolymers and the tested solvent. Bhuvaneswari et al. [8] studied the silicone blends based on fluorosilicone and silicone rubber for seal applications in aeronautical fuel systems. They finally showed that such blends are promising for such applications.

Actually, polymer blending is an attractive way to take advantages of both polymers properties while reducing the cost [6, 9]. Unmodified silicone/polymer blends are known to be difficult leading to unstable and coarse morphology with poor mechanical properties [10]. Li et al. [11] blended silicone and a random fluorosilicone oils and silicone resin to achieve an enhanced oil resistant composite with limited drawbacks in the mechanical properties. According to Kobayashi et al. [12], the fluorosilicone and silicone elastomers are difficult to blend because of their different solubility parameters leading to low surface adhesion and poor mechanical properties. They tailored random and block copolymers to successfully improve mechanical properties of the blend. The block copolymer was found to be the most effective, with 5wt% of copolymers incorporated, in increasing by three the tensile strength.

Liu et al. [13] studied the fluorosilicone/silicone blend in which a low molecular weight poly(methylsiloxane-co-fluorosiloxane) was used as an interfacial agent in order to improve phase morphology. The mechanical properties were improved by 10% by adding 4 phr of their copolymer. As expected, the oil-aging properties of the blend were improved when high fluorosilicone content is used. Industrially, fluorocarbon polymer and silicone rubber are blended and in situ compatibilized with hydroxyl end blocked methylvinylsiloxane oligomers [14] or vinyltris(t-butyl peroxy)silane [15]. Guo et al [16] developed blends of fluoro-rubber and silicone rubber which has been compatibilized by using 2,2,2-trifluoroethyl methacrylate grafted silicone rubber as a compatibilizer. Furthermore, the incorporation of fumed silica at different contents proved to be efficient for the improvement of the mechanical properties (tear and tensile strength, hardness and elongation at break).

Size reduction of the nodular phase is generally carried out by the addition of a compatibilizer by decreasing the interfacial tension but inorganic nanoparticles are recently used to effectively compatibilize a polymer blend [17, 18]. When the particles are located at the interface between two polymers, coalescence and/or interfacial tension may be reduced [19, 20]. The localization of the particles may be predicted by thermodynamics; however, blend compositions, melt viscosity, the shearing, the time and the sequence of mixing may prevent to reach this predicted equilibrium [17, 18].

This article deals with two strategies of compatibilization of fluorosilicone/silicone blends. Firstly, the neat fluorosilicone/silicone blend morphology will be studied and the influence of crosslinking under shearing on the blend morphology will be discussed. Secondly, the addition of fumed silica, with two surface chemistries, on the blend morphology development will be also studied. Fumed silica was selected because of its wide use as reinforcement agent in the silicone industry.

I. Experimental part

I.1. Materials

Silicone polymers: A methylvinyl dimethylsiloxane elastomer, named S, was kindly supplied by BlueStar Silicone. Its density is about 0.97 g.cm⁻³. Molar masses were determined by size exclusion chromatography (SEC) with toluene in universal calibration mode. Molar percentage of vinyl groups inside silicone backbone chain was determined by NMR in CDCl₃. (98-99% Methyl-3,3,3-trifluoropropylsiloxane)-(1-2% methylvinyl-siloxane) elastomer (named FS) was purchased from ABCR (AB116651). Its density is about 1.30 g.cm⁻³. The molar masses were determined by size exclusion chromatography (SEC) with THF. Molar percentage of vinyl groups inside silicone backbone chain was determined by NMR in d-THF. S and FS have 10.3 and 4.1 vinyl groups per chain respectively. As a consequence, the molar weight of molecular segment between two consecutive vinyl groups, M_0 , for S and FS are equal to 37000 and 15500 g/mol respectively. The fluorosilicone is amorphous whereas silicone is a semi-crystalline polymer. Elastomer properties are summed-up in Table 1.

Table 1: Main elastomer properties

Polymer	M_n [kg/mol] ^a	M_w [kg/mol] ^a	%mol vinyl groups ^b	T_g [°C] ^c	T_c [°C] ^c	T_f [°C] ^c
S	380	600	0.22	-126	-90 / -84*	-46 / -41
FS	63	434	1	-70	-	-

^a SEC measurements; ^b NMR results; ^c DSC measurements; *Cold crystallization

Two fumed silica were used with two surface chemistries with the same specific area, 200m²/g, fumed silica R974 and A200. R974 silica is hydrophobic fumed silica after-treated with dimethyldichlorosilane while the A200 is hydrophilic silica [21]. It was added several content of silica in S+10wt%FS+0.2wt%DCP blend as listed in Table 2. Filler contents were verified by TGA and reported in Table 2.

Table 2: Filler contents measured by TGA

Blend	Experimental filler content (wt%) ^a	Experimental filler content (vol%)
5A200	5.4	2.5
5R974	4	1.8
10A200	8.3	3.9
15A200	14.5	7.0
15R974	14.4	7.0

The master curves of complex shear moduli and viscosities as function of frequency for both silicone elastomers are shown in Fig.1, $T_0 = 30^\circ\text{C}$.

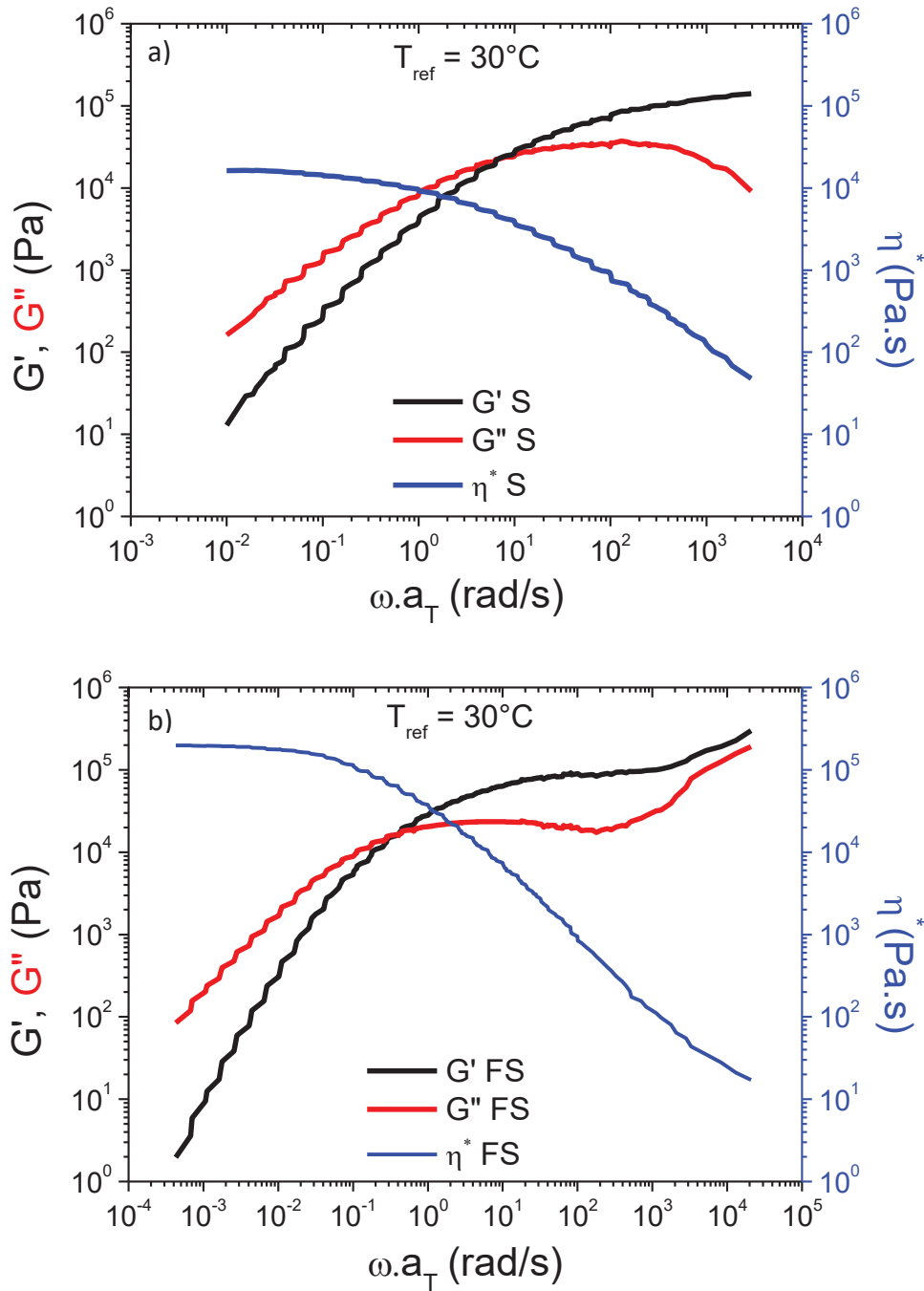


Fig. 1: Viscoelastic behavior: a) S; b) FS. Master curves at $T_{ref}=30^\circ\text{C}$

The zero shear viscosity was directly measured on the rheological curves at 30°C . The G' , G'' crossover defines the characteristic relaxation time, τ_c . Rheological shift factors, a_{T/T_0} , were determined using TTS module of Trios software. Flow activation energy of polymers used was modeled by an Arrhenius law of the temperature dependence of the shift factors. These three material parameters are reported in Table 3. Williams-Landel-Ferry (WLF) model fits better the data for the fluorosilicone, as it is an amorphous polymer, even if temperatures

are well above $T_g+100^\circ\text{C}$ suggesting large flowing units. WLF parameters are as follows: $C_1=2.98$, $C_2=142.6$ K and $T_0=303$ K.

Table 3: Rheological data of both silicone elastomers used

Polymer	$\eta_0(30^\circ\text{C})$ [Pa.s] $\times 10^4$	$\tau_c = 1/\omega_c$ (30°C) [s]	E_a (kJ/mol)
S	2,5	0.16	14.5
FS	22,5	2.27	WLF $C_1=2.98$ $C_2=142.6\text{K}$

Free-radical crosslinking: Dicumyl peroxide (DCP, $M=270$ g.mol⁻¹) was used as the free radical initiator of the crosslinking reaction. It was purchased from Aldrich with an assay of 98% and used as received. The thermal decomposition of DCP was determined by [22, 23]:

$$\frac{d[DCP]}{dt} = -Ae^{-\left(\frac{E_a}{RT}\right)} * [DCP] \quad (1)$$

With $A=7.47 \times 10^{15} \text{ s}^{-1}$; $E_a=153.5$ kJ/mol

I.2. Samples preparation

I.2.1. Pre-mix procedure

Blends of silicone and fluorosilicone elastomers were prepared before the dynamic vulcanization step. First, silicone and fluorosilicone elastomers are mixed in a roll mill (cylinder diameter=100 mm) at room temperature until homogenization, depending of the amount of fluorosilicone. Then, DCP crystals were added and the mixing goes on 5 min to ensure a good dispersion. Then if silica is used, the silica is added step by step. Once, all the content of silica is introduced, a homogenization step is carried out for 10 min. The gap was set to 0.4 mm, noted as L , a roll speed of 25 rpm and a friction ratio of 0.8. We estimated the shear rate between the two rolls with asymmetric rolls speed (U_1 and U_2) as follows [24] :

$$\dot{\gamma} = \frac{U_1 - U_2}{L} = 65 \text{ s}^{-1} \quad (2)$$

I.2.2. Dynamic Crosslinking

The premix blends are crosslinked under shearing for 2 hours in a roll mill at constant gap, friction ratio and roll speed, the same as previously described in the pre-mix procedure section. The dynamic crosslinking process was studied in details in our previous publication [25]. Temperatures are set to 150°C on each side of both rolls. Based on thermal decomposition of DCP [20, 21], DCP is decomposed at 96% after 2h at 150°C (about five half-

life times, $t_{1/2} \approx 25$ min). Before characterization, blends are put into vacuum to avoid air bubbles at least for one day at room temperature.

I.3.Characterizations

Linear Shear Rheology

Small amplitude oscillatory shear tests were carried out on a TA INSTRUMENTS DHR2 rheometer, using the parallel-plate geometry, with 25 mm diameter disks. Frequency sweeps from 0.01 to 500 $\text{rad}\cdot\text{s}^{-1}$ were performed in the range of -20 to 150°C, under a nitrogen atmosphere, in the linear domain.

Microscopy

First, blend morphologies are characterized with an optical microscope Olympus BX41 in transmission mode with a phase contrast filter. The mean domain size is measured for, at least, 100 domains manually with ImageJ and its ellipsoidal tool. The mean domain size corresponds, here, to the mean Feret diameter. If blend morphologies are too fine for optical microscopy, we used a cryo-SEM, FEI QUANTA 250 FEG. First, samples were frozen in liquid nitrogen. Then, samples are transferred in the SEM equipped with a cold stage. Samples were fractured and coated with gold prior to observation.

Deformed Droplet Retraction Method

According to Deyrail et al. [26, 27], measurements of interfacial tension were carried out on S/FS blend at 150°C. Diluted S/FS blends were proceeded in roll mill at room temperature in order to get the coarsest morphology, for magnification limitations, by playing with the surface tension and viscosity ratio between both polymers. Using the Linkam device, a step deformation is imposed to melt drops of FS embedded in the silicone matrix. The relaxation phenomenon is then monitored by optical microscopy until the drop returned from an ellipsoidal to an equilibrium spherical shape. The interfacial tension between both polymers may be deduced by knowing the viscosity for each polymer and the variation of the deformed drop as a function of the relaxation time. Experiments were repeated on different droplets. FS nodules have a mean size of 11 μm , the film thickness used for the measurements were of 500 μm to avoid wall effects. Since Talyor's work [28], the relaxation of a viscous deformed drop in a melt matrix is known to be only driven by interfacial surface tension. As temperature is constant during the shape recovery, components rheological behavior remains unchanged. From Xing et al. work [29], interfacial tension may be predicted from deformed drop retraction, following the deformability, D .

$$D = D_0 \exp \left[- \frac{40(p+1)}{(2p+3)(19p+16)} \frac{\gamma_{12}}{\eta_m R_0} t \right] \quad (3)$$

$$D = D_0 \exp \left[- \frac{t}{\tau_d} \right] = \frac{L-B}{L+B}$$

Where D_0 is the deformability, R_0 is the initial spherical radius at the initial time, p is the zero shear viscosity ratio, L and B are respectively the major and minor axis of the ellipsoid, η_m is the matrix viscosity, γ_{12} is the interfacial tension and the corresponding relaxation time is defined as:

$$\tau_d = \frac{(2p+3)(19p+16)\eta_m R_0}{40(p+1)\gamma_{12}} \quad (4)$$

Fig. 2 shows the retraction of a droplet of fluorosilicone embedded in the silicone matrix at 150°C as a function of time with the initial radius, $R_0 = 13\mu m$.

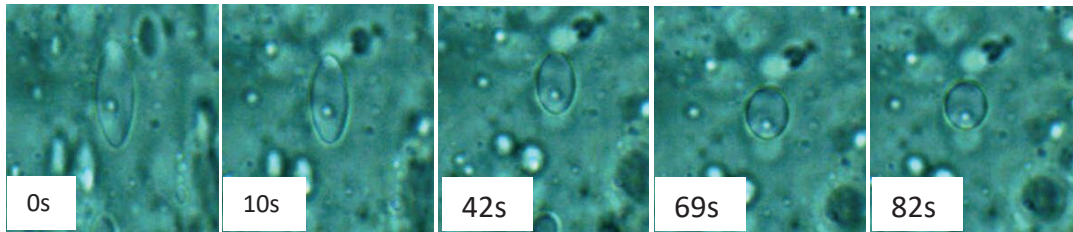


Fig. 2: Retraction of a fluorosilicone ellipsoidal droplet immersed in the silicone matrix at 150°C for successive times.

According to the time dependence of the deformability of a fluorosilicone droplet embedded in a silicone matrix and the Eq. (3), droplet relaxation time can be determined by fitting experimental data as shown in Fig. 3. Then interfacial tension is then calculated to be: $\gamma_{12}=3.5mN/m$.

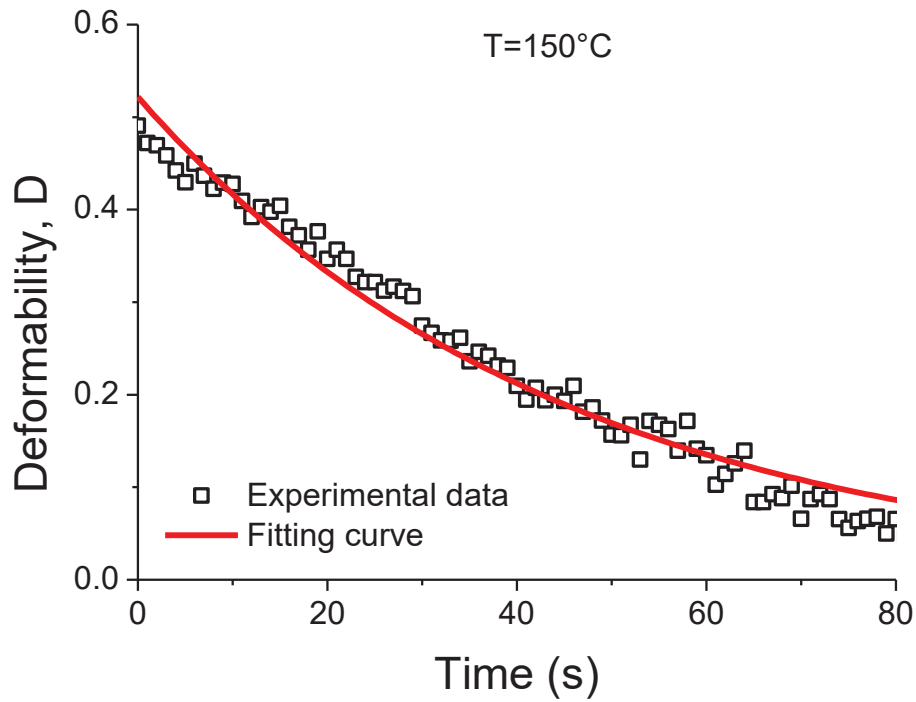


Fig. 3: Time evolution of droplet deformability for a fluorosilicone droplet at 150°C and the corresponding fitting curve.

Thermogravimetric analysis (TGA)

A TGA Q500 TA Instrument was used to verify the amount of silica dispersed in the blend. Samples were heated from 30 °C up to 800 °C at a heating rate of 10 °C/min.

II. Results and discussion

II.1. Morphologies of silicone/fluorosilicone blends

The Fig.4 a-d shows the optical images of S/FS blends for several fluorosilicone contents. S and FS are not compatible as their interfacial tension is 3.5 ± 0.5 mN/m. Fluorosilicone domains correspond to the clear dispersed phase surrounded by a darker perimeter for contrast reasons. A broad distribution of nodule size is noticed, especially for a high content of fluorosilicone (Fig.4-d).

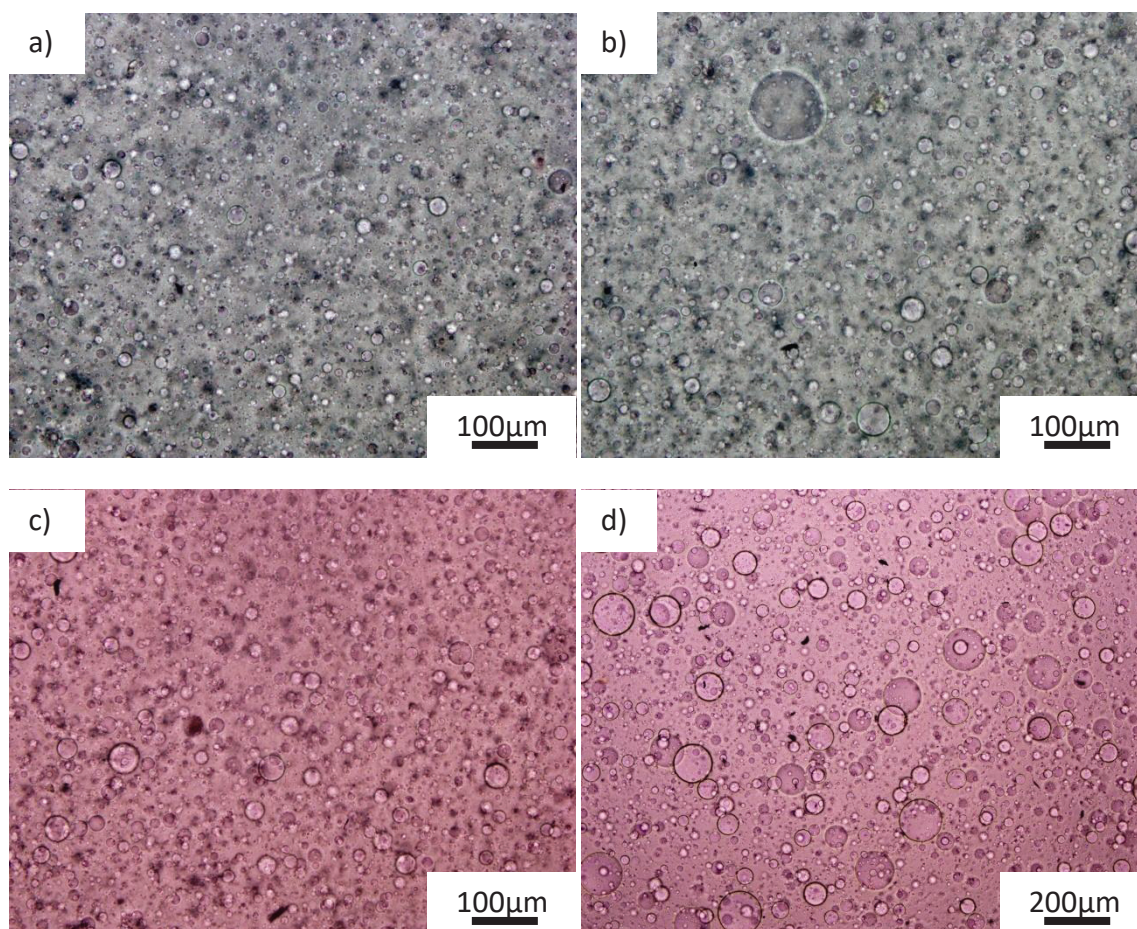


Fig. 4: Optical images of a) S+5wt%FS; b) S+10wt%FS; c) S+15wt%FS; d) S+20wt%FS. Samples were blended at 150°C in a roll mill.

From optical images, fluorosilicone nodule sizes are shown in Fig.4, as a function of fluorosilicone content. The nodule size increases with increasing fluorosilicone content. This result may be due to coalescence and insufficient shear to break the dispersed phase droplets. Coalescence should dominate at high content of fluorosilicone which explains the broad size morphology obtained when 20wt% of fluorosilicone is added.

The blend morphology was predicted using a Serpe's model [30]. As the viscosity ratio $p > 1$ for the mean shear rate calculated and the set temperature, the Serpe's model is defined as follows:

$$A_n = \frac{4\gamma_{12}}{\dot{\gamma}\eta_m p^{0.84} F(\phi_{FS}, \phi_S)} \quad (5)$$

Where ϕ_{FS} , ϕ_S are the volume fraction of fluorosilicone and silicone, $F(\phi_{FS}, \phi_S)$ is an empirical function in order to take into account the coalescence phenomenon and A_n is the average diameter of the dispersed phase. We modified the exponent from 0.8 to 0.7 in the function $F(\phi_{FS}, \phi_S)$ to fit the experimental size of fluorosilicone domains.

$$F(\phi_{FS}, \phi_S) = (1 - 4(\phi_{FS}\phi_S)^{0.7}) \quad (6)$$

Thanks to the analytical calculation of shear rate and rheological data listed in Table 4, the average diameter of the fluorosilicone phase is calculated according to Eq. 5. Mean nodule size of the FS phase was quantitatively predicted by the modified Serpe's model as shown in Fig. 5.

Table 4: Modified Serpe model parameters used for S/FS blends, $T=150^\circ\text{C}$

$\dot{\gamma}$ [s^{-1}]	γ_{12} [mN/m]	η_m [Pa.s]*	η_d [Pa.s]*	p^*
65	3.5	650	800	1.2

Note: *Taken at 65 s^{-1}

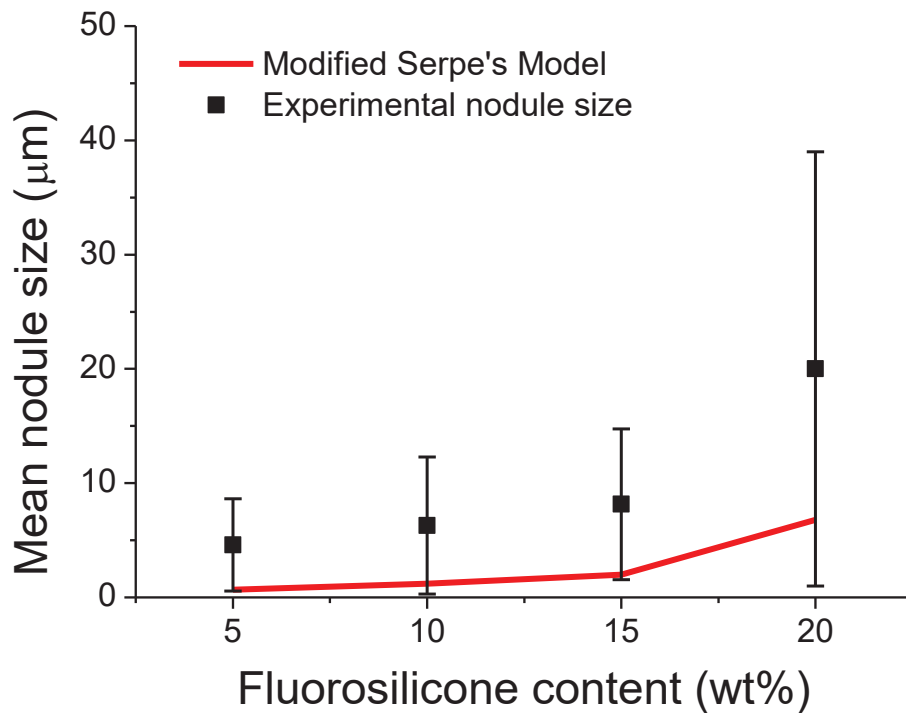


Fig. 5: Mean nodule size and predicted nodule size of fluorosilicone as a function of fluorosilicone content. The nodule size predictions were made using a modified Serpe's model.

II.2. Compatibilization by Dynamic Crosslinking

The optical microscope images of a neat and a dynamically crosslinked S+10wt%FS blends are shown in Fig.6a and 6b respectively. The mean nodule size of fluorosilicone measures $7\pm 6.0\ \mu\text{m}$ when silicone and fluorosilicone are blended at 150°C . However, the nodule size decreases to $3.5\pm 2.0\ \mu\text{m}$ under the dynamic crosslinking step with 0.2wt% DCP. The mean nodule size as well, as the standard deviation, decreases with the dynamic crosslinking. This result means that a finer and a narrower distribution of FS domain size is obtained by dynamic crosslinking.

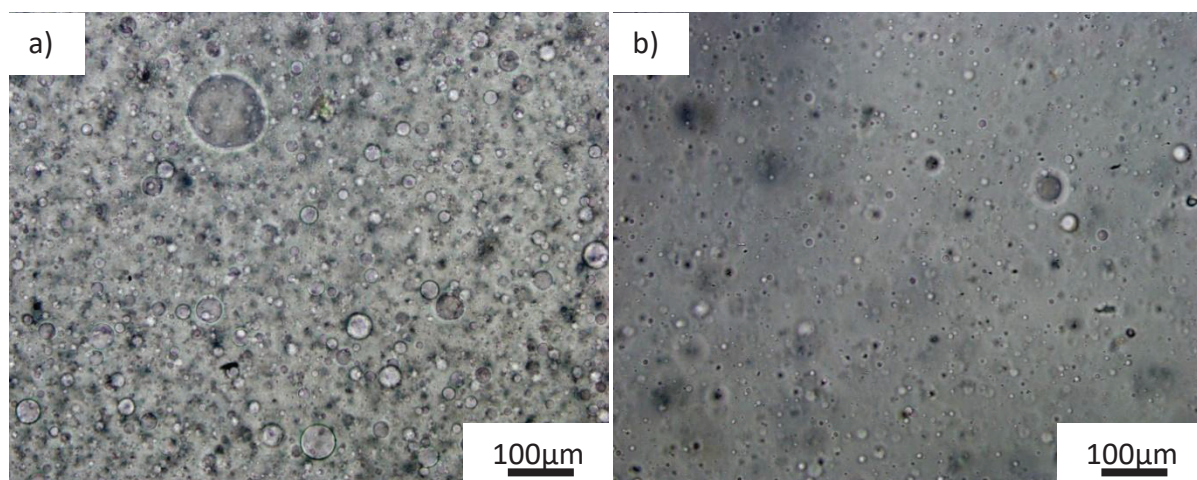


Fig. 6: Optical microscope images of blends: a) S+10wt% FS (blended at 150°C); b) S+10wt%FS +0.2wt%DCP (dynamically crosslinked)

The nodule size reduction may be explained by two mechanisms: the reduction of the interfacial tension and/or the reduction of the viscosity ratio. First, it may be assumed that, during dynamic crosslinking, macro-radicals of both silicone and fluorosilicone chains may be recombined at the interface leading to the formation of an in situ block copolymer S-g-FS with the ability to reduce the interfacial tension. But, the recombination of both radical coming from both polymers is unlikely or at least very difficult to prove from an experimental point of view. The amount of the resulting copolymer is extremely low and NMR experiments, after selective extractions, did not enable us to conclude about their existence. Shape droplet relaxation method was used for the blend dynamically crosslinked with 0.1wt%DCP in order to measure the interfacial tension. Similar blend morphologies can be observed in Fig.7a. The fluorosilicone domains are spherical at equilibrium but they can be deformed similarly as illustrated in Fig.2. Therefore fluorosilicone domains should have an enhanced elasticity but they probably stay below their gel point after the dynamic crosslinking step [27].

As the number of vinyl groups in the fluorosilicone chains is 2.5 times lower than in the silicone chains; the matrix viscosity should increase more rapidly than the fluorosilicone phase viscosity, lowering the viscosity ratio. As a consequence, we made the assumption

Chapter 4: Compatibilization of Fluorosilicone/silicone blends by dynamic crosslinking and fumed silica addition

that the viscosity ratio will be divided by 2.5. With this assumption and the experimental data, interfacial tension is reported Table 5. The interfacial tension does not decrease significantly as it varies from 3.5 to 2.8 mN/m between the neat blend and the dynamically crosslinked blend. However, the former assumption is really crude because we cannot know precisely the viscosity ratio. Indeed, as explained in our previous work [25], molecular oxygen effectively lower the crosslinking efficiency of the neat matrix during dynamic crosslinking process to achieve multi-branched structure and this mechanism should be still valid in the present case. In addition, we do not know the DCP solubility/concentration in each phase.

Table 5: Experimental data and assumption used to calculate interfacial tension between fluorosilicone and silicone elastomers dynamically crosslinked.

τ_d [s]	R_0 [μm]	p (150°C)	η_m [Pa.s] (150°C)	γ_{12} [mN/m] (150°C)
26	7	0.92*	5500	$3 \pm 0,5$

Note:* Assumption

Using the droplet relaxation data and assuming a constant interfacial tension ($\gamma_{12}=3.5$ mN/m), we obtained a viscosity ratio of 1.3. The viscosity ratio is effectively lowered which will ease the dispersion of the fluorosilicone. Meanwhile, both viscosities will be increased by the crosslinking reaction which in turn lowers coalescence of the fluorosilicone nodules. This predicted viscosity ratio is higher than the theoretical viscosity ratio (0.92) because the extent of crosslinking, during the dynamic crosslinking, should be lower due to the presence of oxygen in different concentrations as a function of the materials. As a matter of fact, we cannot determine which mechanisms prevail. In fact, it is more likely that a combination of interfacial tension and viscosity ratio reductions is at the origin of the compatibilization mechanism.

Both mechanisms as detailed before should stabilize the morphology along time and shearing. Fig.7 shows the morphologies of two blends made without (Fig.7a, b) and with dynamic crosslinking (Fig.7c, d) which undergo a roll blending at room temperature. As the blending is carried out at room temperature, interfacial tension and viscosity ratio increase which is not in favor of the blending of fluorosilicone. Therefore, under shearing, the coalescence will be speeded up. The morphology of the blend that undergone a dynamic crosslinking step before changed slightly whereas the fluorosilicone domains, for the un-crosslinked sample, are far larger. Indeed, the morphology of dynamic crosslinked sample changes from $4 \pm 2.5 \mu\text{m}$ to $8.3 \pm 5 \mu\text{m}$ whereas the morphology of the unmodified blend varies from $7 \pm 6.0 \mu\text{m}$ to $17 \pm 15 \mu\text{m}$ after the room temperature blending. According to this experiment, we confirm that the morphology is stabilized.

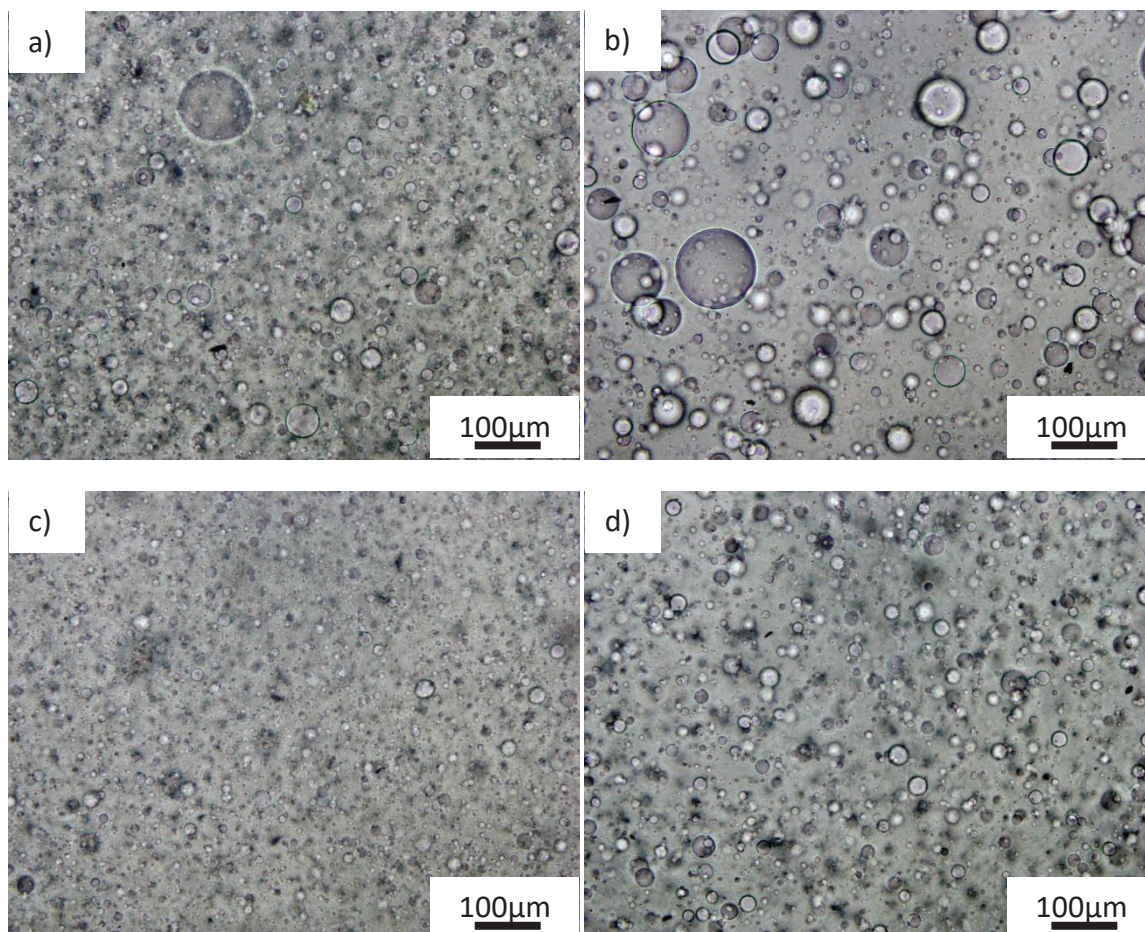


Fig. 7 : Optical microscope images of blends: a) S+10wt%FS blended at 150°C; b) S+10wt%FS blended at 150°C then blended at room temperature; c) S+10wt%FS+0.1wt%DCP; d) S+10wt%FS+0.1wt%DCP then blended at room temperature.

As both polymers are in the melt state at room temperature, coalescence should also take place without any stress applied to the blend but for a longer time range. Fig.8 shows optical images of blends made with 15%wt of FS which underwent none stimulus for several months, simulating an annealing step. In Fig.8-a exhibiting the virgin blend, the FS nodules are far larger than the dynamic crosslinked blend, Fig.8-b. According to this annealing step, the blend stabilization is also confirmed.

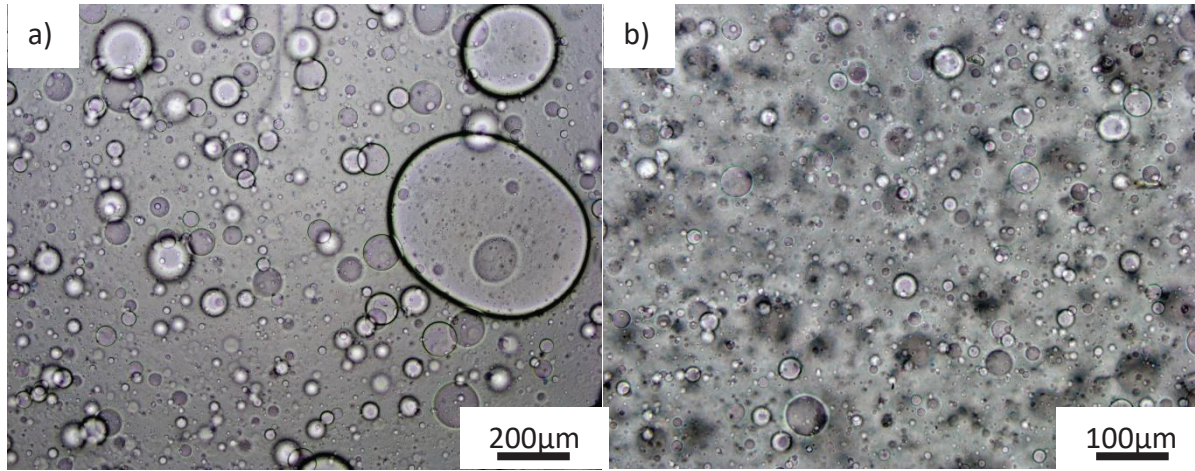


Fig. 8: Optical images of blend morphologies after 1 year without any stress applied :a) S+15wt%FS b) S+15wt%FS+0.1wt%DCP.

II.3. Addition of silica

In this section, the effect of the addition of silica with two different surface chemistries on the blend morphology was investigated. As explained in the materials section, a hydrophilic (A200) and a hydrophobic (R974) fumed silica were selected with similar specific surface. The interaction between polymers and fillers are of great interest in determining the morphology after the mixing step. Indeed, the localization of the silica in the blend may influence the blend morphology. Two cases may occur: the particles may be dispersed mainly in one of the two phases or at the interface between both phases. The two situations may be predicted in analyzing the surface tension of the components used. The wetting parameter defines the equilibrium localization of silica by thermodynamics calculation through Eq.(7).

$$\omega = \frac{\gamma_{Si-2} - \gamma_{Si-1}}{\gamma_{12}} \quad (7)$$

Where γ_{Si-i} is the interfacial tension between the silica particle and the polymer, i . When $\omega < -1$, the silica particles should be at the equilibrium in the polymer 2. If $\omega > 1$, the silica particles should be at the equilibrium in the polymer 1. When $-1 < \omega < 1$, filler particles should be located at the interface. The interfacial tension between dispersive components such as polymers is generally calculated using the Wu model [31], Eq. 8, and surface tension data listed in Table 6. Due to a lack of surface tension reported data as a function temperature for the FS polymer, we calculated interfacial tension and wetting parameters at room temperature only (Table 6).

$$\gamma_{12} = \gamma_1 + \gamma_2 - 4\left(\frac{\gamma_1^d \gamma_2^d}{\gamma_1^d + \gamma_2^d} + \frac{\gamma_1^p \gamma_2^p}{\gamma_1^p + \gamma_2^p}\right) \quad (8)$$

Table 6: Surface tension data of each component of the blend [15, 32]

	Surface tension at 25°C (mN/m)			ω
	γ	γ^d	γ^p	
S	22.8	21.7	1.1	-
FS	13.6	10.8	2.8	-
A200	80	29.4	50.6	0.65
R974	81.7	72.3	9.4	3.5

According to data listed in Table 6, the interfacial tension between both polymers was checked. We found an interfacial tension between silicone and fluorosilicone, at room temperature, $\gamma_{12}=4.4\text{mN/m}$ which is in agreement with our previous measurement at 150°C ($\gamma_{12}=3.5\text{mN/m}$).

The wetting parameters were calculated using the data listed in Table 6, at equilibrium hydrophilic silica should be preferentially located at the interface whereas the hydrophobic silica should stay in the silicone matrix. The equilibrium location of the hydrophilic silica may be due to the strong electron withdrawing effect of fluorine atom present in the fluorosilicone which should bring forth specific interactions with the silanol group on the surface of the hydrophilic silica [11].

However, the final localization of a filler particle may be different from the predicted localization by the wetting parameter. Indeed, due to the high viscosity of a melt polymer, the particle diffusion is extremely low and it is strongly dependent on the mixing sequence and time [17, 20, 33]. According to the experimental section, the polymers are first blended, then the filler particles are added at room temperature. Afterwards, the blend is dynamically crosslinked for two hours, therefore and it can be then expected that it reaches a metastable equilibrium.

First, cryo-SEM images of a blend made from S+10wt%FS with 5wt%A200 dynamically crosslinked with 0.2wt% DCP are shown in Fig.9a, b. The most interesting observation from these images is the interface between the matrix and the fluorosilicone domains: In Fig. 9-a, it can be observed silica particles on the surface of FS domains. The same results can be clearly observed in Fig. 9-b. These images confirm the prediction made from the thermodynamic calculations for the hydrophilic silica.

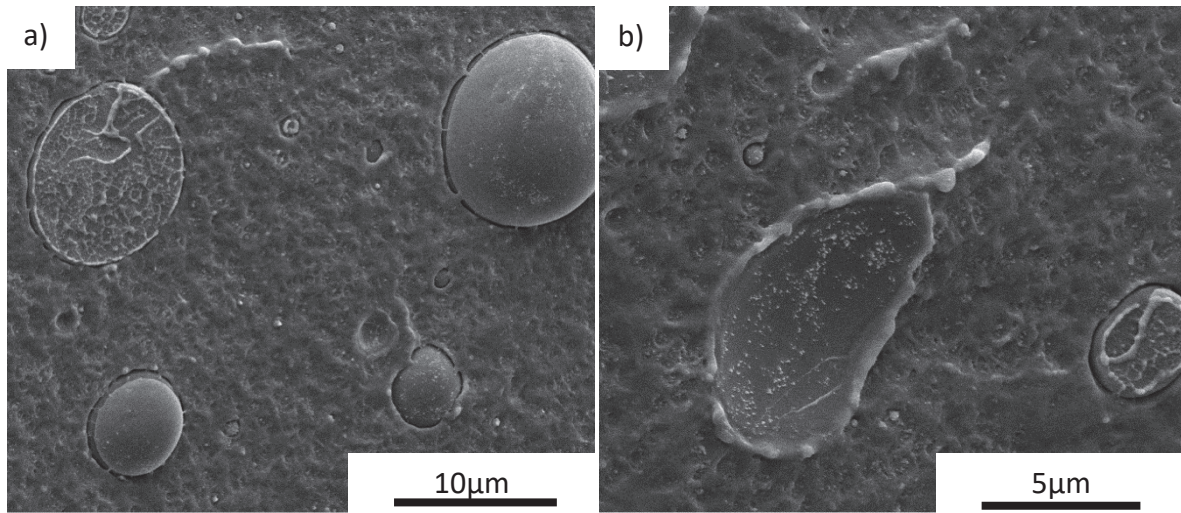


Fig. 9: Cryo-SEM images of S+10wt%FS with 5wt%A200 dynamically crosslinked with 0.2wt% DCP.

In addition, the effect of surface chemistry of the silica on the blend rheology was investigated in Fig.10. As expected from Aranguren et al. [34], the reinforcement effect of the hydrophobic silica is much less efficient than the one of the hydrophilic silica. It is well known that hydrophilic silica is good reinforcing filler in silicone blend because of the hydrogen bonding between the silanol at the surface of the silica particle and the silicone backbone [34]. As the R974 silica has almost no silanol groups the affinity with both polymers should be low [21]. By increasing the filler content, filler-filler and filler-polymer-filler interactions are enhanced which in turn increases the viscosity [34].

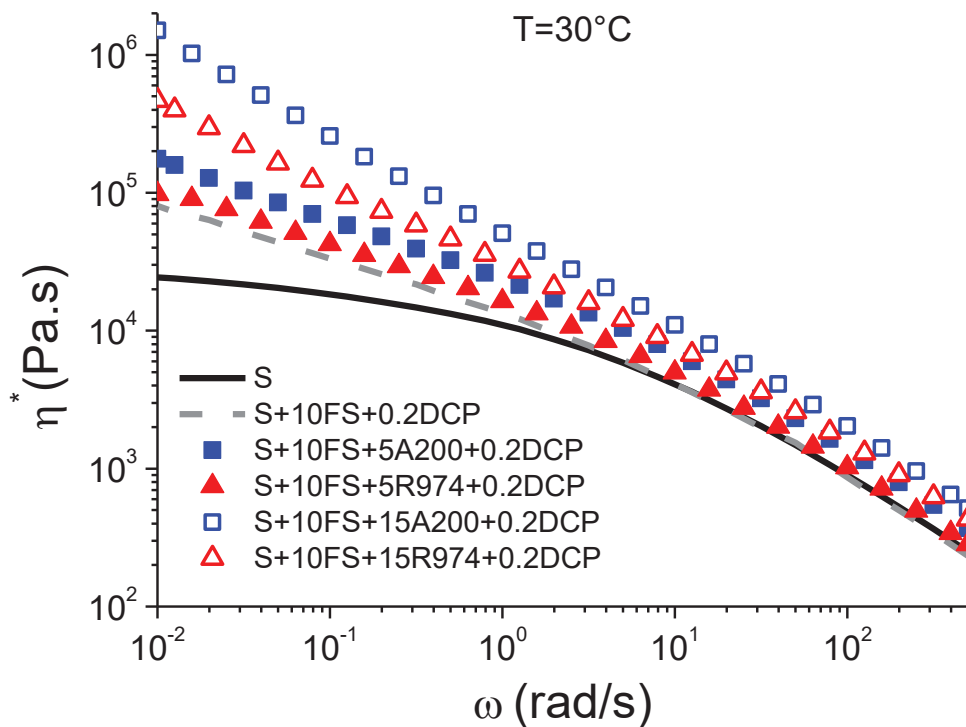


Fig. 10: Complex viscosity as a function of frequency of crosslinked samples under dynamic conditions, $\epsilon=0.1\%$ and $T=30^\circ\text{C}$. Samples filled with fumed silica at two filler ratios and two surface chemistries (A200: hydrophilic; R974: hydrophobic).

Blend morphologies are shown in Fig.11 a-e as function of filler content and for both silica used. The corresponding image analysis is reported in Table 7. On the one hand, as the filler content increases from 5wt% to 15wt% of hydrophobic silica, the nodule size is only divided by two. On the other hand, the blend with hydrophilic silica, the nodule size is reduced steadily until the silica volume fraction is close to 7vol%. In this specific case, the nodule size drops to 500 nm.

As the R974 silica has low interactions with silicone backbone, it induces a limited viscosity increase of the matrix (Fig.10). Therefore, the coalescence phenomenon and viscosity ratio are not strongly decreased inducing a small nodule size reduction. However, the hydrophilic silica has a greater effect on the blend morphology which may be explained by several mechanisms.

First, as additional interactions occur with the fluorosilicone, we may assume that some hydrophilic silica will migrate into the fluorosilicone domains which will modify the viscoelasticity of the nodular phase and enhance the droplet stability [35]. However, the fluorosilicone has already a high viscosity which will imply that only a small amount of silica will migrate within the nodule [36]. In addition, Fig.10 shows that the hydrophilic silica greatly increases the viscosity of the silicone phase. Therefore, with the increasing viscosity of both polymers, the coalescence phenomenon should be reduced by limiting the drainage of the thin film between two approaching fluorosilicone droplets.

Moreover, hydrophilic silica has specific interactions with both polymers therefore we may assume that it is necessary to introduce larger amount of filler to distribute silica particles in each phase and at the interface. Particle migration is known to be filler loading dependent which may explain the filler loading threshold to achieve sub-micronic nodule. Once sufficient amount of silica is dispersed at the interface between the two phases, silica particles can then play the role of interfacial stabilizing system by building a solid layer around the fluorosilicone nodules as assumed from Fig.9 and the wetting parameter calculation [19].

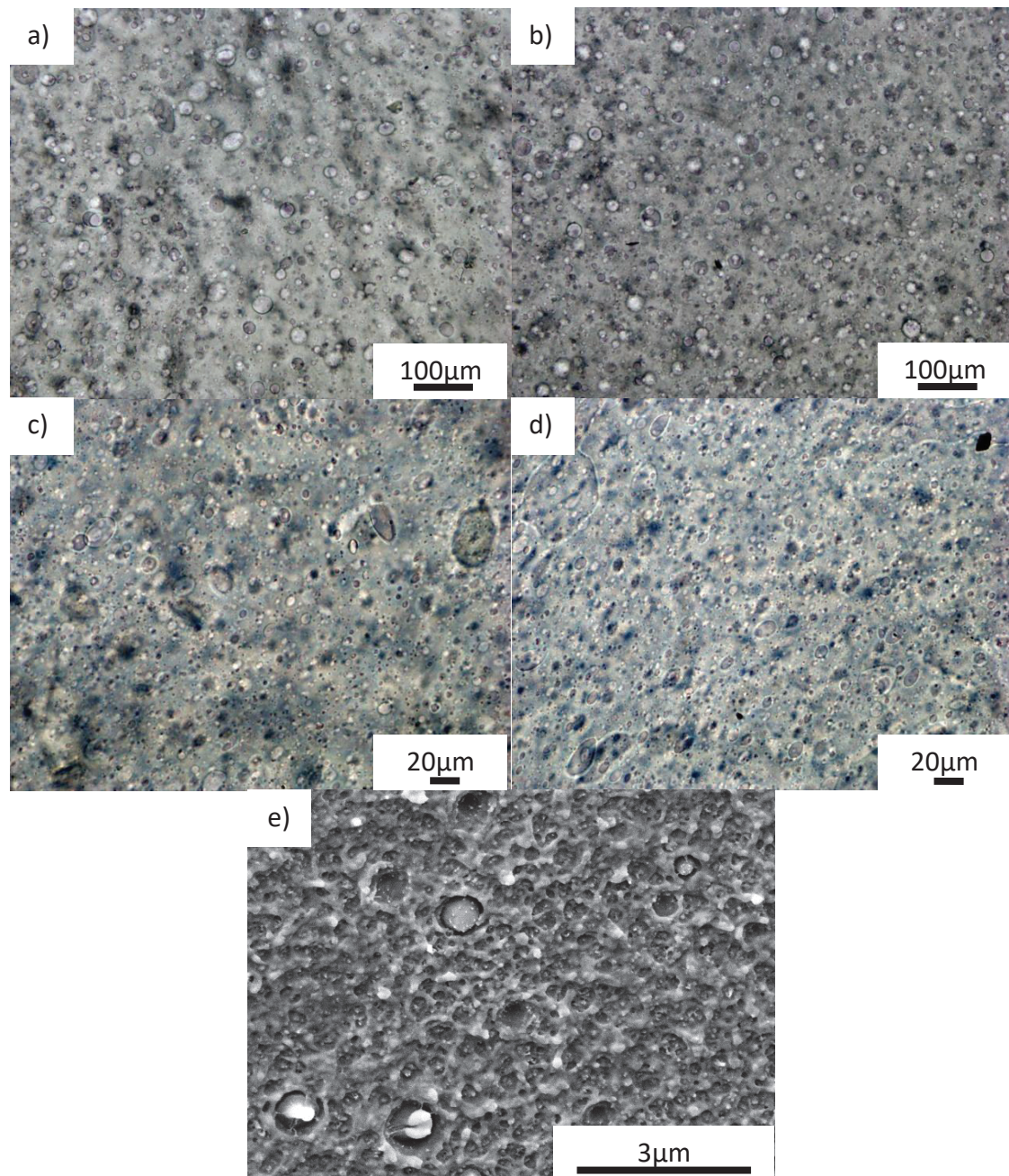


Fig. 11: Images of S+10wt%FS+0.2wt%DCP blend with various amounts of silica: a) 5wt% A200; b) 5wt% R974; c) 10wt% A200 ; d) 15wt% R974; e) Cryo-SEM image of 15wt% A200

Table 7 : Image analysis of S+10wt%FS+0.2wt%DCP blend with various content of silica.

Blend	Fluorosilicone nodule size [μm]
5A200	5.7 ± 5.1
5R974	5.3 ± 4.4
10A200	2.9 ± 2.0
15A200	$0.5 \pm 0,16$
15R974	2.9 ± 1.9

Conclusion

In this paper, we have explored two compatibilization pathways of silicone/fluorosilicone elastomers. First, the interfacial tension of the blend ($\approx 3.5\text{mN/m}$) was determined from the droplet relaxation method. Following, the Serpe's model was developed in order to predict the blend morphology. As a result, a quantitative prediction of the blend morphology was predicted for this unreactive system.

The first compatibilization strategy was based on the crosslinking of the two elastomers under shearing conditions. The dynamic crosslinking process was found to be an effective way to compatibilize and to stabilize the blend morphology (fluorosilicone dispersed phase) under shearing and annealing (One year). The mechanisms of compatibilization, i.e. the reduction of the interfacial tension by the in situ formation of graft copolymer or the modification of the viscosity ratio could not be totally differentiated or excluded.

The second way of compatibilization has been to add during mixing fumed silica particles having a hydrophilic or a hydrophobic surface. The hydrophilic silica enabled us to effectively reduce the size of the dispersed fluorosilicone phase while its hydrophobic counterpart seems to be ineffective. This observation was attributed to the specific hydrogen and dipolar interactions of the silicone backbone, the CF_3 group with the silanol present at the surface of the hydrophilic silica. The hydrophilic silica compatibilization mechanisms were assumed to be due to its location at the interface of both phases preventing the coalescence phenomenon. This compatibilization of the fluorosilicone/silicone blends could be an original way for specific properties such as oil resistance and sealing applications.

References

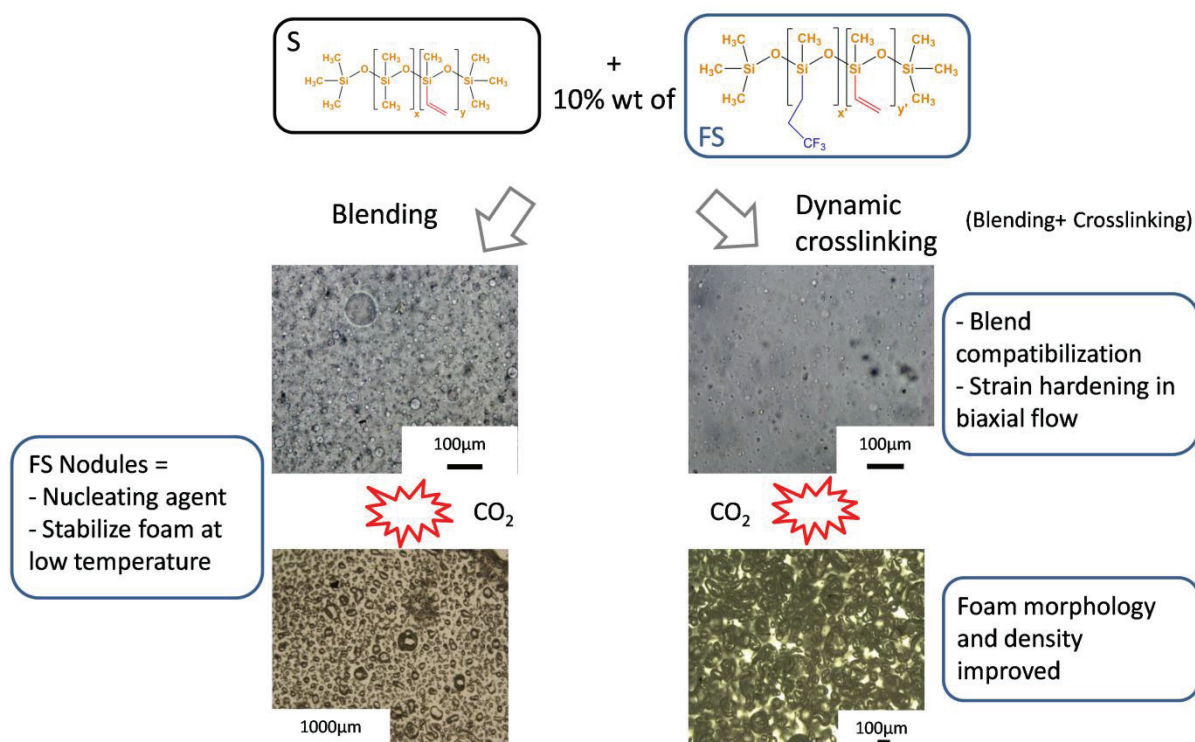
- [1] E. Yilgör, I. Yilgör, Silicone containing copolymers: Synthesis, properties and applications, *Progress in Polymer Science* **39** (6) (2014) 1165-1195.
- [2] P.K. Yuen, H. Su, V.N. Goral, K.A. Fink, Three-dimensional interconnected microporous poly(dimethylsiloxane) microfluidic devices, *Lab on a Chip* **11** (8) (2011) 1541-1544.
- [3] R.G. Jones, W. Ando, J. Chojnowsk, Silicon Containing Polymers: The Science and Technology of Their Synthesis and Applications, *Silicon Chemistry* **1** (4) (2002) 185-212.
- [4] D.J. Cornelius, C.M. Monroe, The unique properties of silicone and fluorosilicone elastomers, *Polymer Engineering & Science* **25** (8) (1985) 467-473.
- [5] M. Dawir, Sealing in the automotive industry with liquid fluoro-silicone elastomers, *Sealing Technology* **2008** (7) (2008) 10-14.
- [6] J.A. Manson, L.H. Sperling, *Polymer Blends and composites*, Plenum Press, New York, 1976.
- [7] X. Xu, Z. Xu, P. Chen, X. Zhou, A. Zheng, Y. Guan, Preparation of Fluorosilicone Random Copolymers with Properties Superior to Those of Fluorosilicone/Silicone Polymer Blends, *Journal of Inorganic and Organometallic Polymers and Materials* **25** (5) (2015) 1267-1276.
- [8] BhuvaneshwariCM, Dhanasekaran R, Chakravarthy SKR, Kale S, Gouda G Evaluation of Fluorosilicone Silicone Elastomer Blend for Aeronautical Fuel System, *Progress in Rubber Plastics and Recycling Technology*, **31**(3), (2015) 207-217
- [9] D.R. Paul, S. Newman, *Polymer blends*, Academic Press, 1978.
- [10] P. Lucas, J.-J. Robin, *Silicone-Based Polymer Blends: An Overview of the Materials and Processes*, Functional Materials and Biomaterials, Springer Berlin Heidelberg, Berlin, Heidelberg, 2007, pp. 111-147.
- [11] B. Li, S. Chen, J. Zhang, Improvement in oil resistance of room temperature-vulcanized polysiloxane rubber via blending with self-synthetic fluorosilicone, *Journal of Elastomers & Plastics* **46** (8) (2014) 695-709.
- [12] H. Kobayashi, W. Nishiumi, Preparation and characterization of poly(methyl-3,3,3-trifluoropropylsiloxane-co-dimethylsiloxane), *Die Makromolekulare Chemie* **194** (5) (1993) 1403-1410.
- [13] Y. Liu, H. Liu, R. Zhang, C. Zhou, S. Feng, Preparation and properties of heat curable blended methylfluorosilicone rubber, *Polymer Engineering & Science* **53** (1) (2013) 52-58.
- [14] G. Gornowicz, I. Chorvath, L. Tonge, Y. Kim, D. Romenesko, K. Kwan, S. Warren, Fluorocarbon elastomer silicone vulcanizates, 2007, US 7,173,092 B2
- [15] S.S. Badesha, C.O. Eddy, A.W. Henry, G.A. Campbell, Compatibilized blend of fluoroelastomer and polysiloxane useful for printing machine component, 2000, US 6035780 A
- [16] Guo J, Zeng X, Li H, Luo Q, Compatibilization of Fluororubber/Silicone Rubber Blends by the Incorporation of 2,2,2-Trifluoroethyl Methacrylate Grafted Silicone Rubber, *Journal of elastomers and plastics*. **42** (2010) 539-560
- [17] A. Taguet, P. Cassagnau, J.M. Lopez-Cuesta, Structuration, selective dispersion and compatibilizing effect of (nano)fillers in polymer blends, *Progress in Polymer Science* **39** (8) (2014) 1526-1563.
- [18] F. Fenouillot, P. Cassagnau, J.C. Majesté, Uneven distribution of nanoparticles in immiscible fluids: Morphology development in polymer blends, *Polymer* **50** (6) (2009) 1333-1350.
- [19] S. Vandebriel, J. Vermant, P. Moldenaers, Efficiently suppressing coalescence in polymer blends using nanoparticles: role of interfacial rheology, *Soft Matter* **6** (14) (2010) 3353-3362.

- [20] L. Elias, F. Fenouillot, J.C. Majeste, P. Cassagnau, Morphology and rheology of immiscible polymer blends filled with silica nanoparticles, *Polymer* **48** (20) (2007) 6029-6040.
- [21] J. Mathias, G. Wannemacher, Basic characteristics and applications of aerosil: 30. The chemistry and physics of the aerosil Surface, *Journal of Colloid and Interface Science* **125** (1) (1988) 61-68.
- [22] S. Mani, P. Cassagnau, M. Bousmina, P. Chaumont, Cross-Linking Control of PDMS Rubber at High Temperatures Using TEMPO Nitroxide, *Macromolecules* **42** (21) (2009) 8460-8467.
- [23] A. Msakni, P. Chaumont, P. Cassagnau, Crosslinking of ethylene–octene copolymers under dynamic conditions: A new way to access polymeric hyperbranched structure, *Polymer Engineering & Science* **46** (11) (2006) 1530-1540.
- [24] S.-H. Park, S. Lee, D. Moreira, P.R. Bandaru, I. Han, D.-J. Yun, Bioinspired superhydrophobic surfaces, fabricated through simple and scalable roll-to-roll processing, *Scientific Reports* **5** (2015) 15430.
- [25] T.Métivier, P. Cassagnau, Mechanisms of dynamic cross-linking of silicone elastomer: Radical cross-linking controlled by thermo-oxidation under shearing, *European Polymer Journal* (2018).
- [26] Y. Deyrail, R. Fulchiron, P. Cassagnau, Morphology development in immiscible polymer blends during crystallization of the dispersed phase under shear flow, *Polymer* **43** (11) (2002) 3311-3321.
- [27] Y. Deyrail, P. Cassagnau, Phase deformation under shear in an immiscible polymer blend: Influence of strong permanent elastic properties, *Journal of Rheology* **48** (3) (2004) 505-524.
- [28] G.I. Taylor, The formation of emulsions in definable fields of flow, *Proc. R. Soc. Lond.* (1934).
- [29] P. Xing, M. Bousmina, D. Rodrigue, M.R. Kamal, Critical Experimental Comparison between Five Techniques for the Determination of Interfacial Tension in Polymer Blends: Model System of Polystyrene/Polyamide-6, *Macromolecules* **33** (21) (2000) 8020-8034.
- [30] G. Serpe, J. Jarrin, F. Dawans, Morphology-processing relationships in polyethylene-polyamide blends, *Polymer Engineering & Science* **30** (9) (1990) 553-565.
- [31] S. Wu, Calculation of interfacial tension in polymer systems, *Journal of Polymer Science Part C: Polymer Symposia* **34** (1) (1971) 19-30.1
- [32] J.E. Mark, *Physical Properties of Polymers Handbooks*, Springer, 2007.
- [33] F. Gubbels, R. Jerome, E. Vanlathem, R. Deltour, S. Blacher, F. Brouers, Kinetic and Thermodynamic Control of the Selective Localization of Carbon Black at the Interface of Immiscible Polymer Blends, *Chemistry of Materials* **10** (5) (1998) 1227-1235.
- [34] M.I. Aranguren, E. Mora, J.V.D. Jr., C.W. Macosko, Effect of reinforcing fillers on the rheology of polymer melts, *Journal of Rheology* **36** (6) (1992) 1165-1182.
- [35] M. Kong, Y. Huang, G. Chen, Q. Yang, G. Li, Retarded relaxation and breakup of deformed PA6 droplets filled with nanosilica in PS matrix during annealing, *Polymer* **52** (22) (2011) 5231-5236.
- [36] M. Liebscher, L. Tzounis, P. Pötschke, G. Heinrich, Influence of the viscosity ratio in PC/SAN blends filled with MWCNTs on the morphological, electrical, and melt rheological properties, *Polymer* **54** (25) (2013) 6801-6808.

Chapter 5: Fluorosilicone/Silicone blends: Foaming behavior.

ABSTRACT

An alternative approach, based on vinyl-PDMS/Fluorosilicone blends, has been developed to improve the CO₂ foaming behavior of silicone elastomers. For this purpose, a dynamic crosslinking process has been used to compatibilize these silicone blends and to improve their strain hardening behavior under biaxial deformation. As a result, fine cells (65 μm) have been achieved using gaseous CO₂ in a one-step batch foaming process. Actually, the dispersed fluorosilicone domains act as nucleating sites allowing the formation of higher nuclei densities which reduce the overall bubble size by competitive nuclei growth. This new formulation strategy has allowed us to develop silicone foams with equivalent properties (cell and foam densities) to foams prepared by supercritical CO₂.



Reformatted version of paper originally published in Polymer.

Fluorosilicone/Silicone blends: Foaming behavior.

T. Métivier^a, P. Cassagnau^{a,*}

^a Univ Lyon, Université Lyon1, Ingénierie des Matériaux Polymères, CNRS UMR 5223, 15 Bd Latarjet, 69622 Villeurbanne, France

Introduction

Poly(methylvinyl-dimethyl)siloxane (vinyl-PDMS) has excellent thermal, dielectric and weathering properties [1]. It is widely used in medical applications because of its hydrophobicity, biocompatibility and high gas permeability [2]. Silicone foams take advantages of the interesting properties of silicone combined with foam properties. Thus, its high thermal stability and elasticity combined with a good resilience and low density enable the silicone foams to be used in challenging applications (aerospace, aeronautic, ...), where other organic foams are inadequate, such as shock or vibration absorbing supports at high temperature or very low temperature, thermal shielding, fireproof applications or medical prostheses [3,4].

First, silicone foaming is mainly carried out by chemical means. Indeed, the chemical foaming may be performed by thermal degradation of organic or inorganic foaming agents which release N₂, CO₂ and/or other gases [5-7]. Generally, it remains undesirable, sometimes harmful, by-products inside the foam. The second chemical foaming strategy consists in hydrosilylation/condensation reactions between Si-H, Si-C≡C and an alcohol [4, 8-11]. The foaming is triggered by H₂ production therefore it may be hazardous in confined environments or industries. In both methods, crosslinking and foaming are often achieved simultaneously. Thus, the control of balance between both reactions kinetics is the main challenge.

Since 1987, the Montreal protocol has banned widely used physical foaming agents such as chlorofluorocarbons (CFCs) and hydrochlorofluorocarbons (HCFCs) in order to protect the ozone atmospheric layer. As a consequence, carbon dioxide, in its supercritical or gaseous states, has become one of the most widely studied foaming agents in the academic and industrial fields [12, 13]. Indeed, CO₂ does not leave any by-products after foaming and it has a low critical point. However, it has a lower solubility in polymers in comparison to CFCs and HCFCs [14]. In academic studies, CO₂ foaming is typically performed in a batch process but it can also be transferable to industrial processes such as extrusion or injection foaming [15, 16].

Few studies are focused on the CO₂ foaming of silicone even though CO₂ has a good solubility in silicone elastomers. In most studies, the silicone elastomer is generally partially

crosslinked before foaming since crosslinking cannot be controlled simultaneously to foaming in batch-foaming experiments. Indeed, Shimbo, Nomura, Muratani & Fukumura [17] were the first to discuss the competition between crosslinking and foaming. Hong & Lee [18] refined the previous study and gave a narrow foaming window, for silica filled silicone rubbers, around $\tan \delta = G''/G' \sim 0.2$. Moreover, most of the studies are focused on the effect of various silica contents on the foaming behavior of partially crosslinked silicone elastomers [18-21]. By playing with the silica content, Yan, Wang & Zhao [21] achieved foams with cell size in the range between 8 and 120 μm , cell density between 105 -108 cells/cm³ and density between 0.45 and 0.9 g.cm⁻³.

To date, the addition of fillers such as silica [19], carbon nanotubes [4] or graphene [10] into silicone elastomers is the usual way of investigations to control nucleation and viscoelastic properties. None studies are dealing with the improvement of the foaming behavior of silicone by a polymer blend strategy. Therefore, we propose, in this work, to blend a methylvinyl dimethylsiloxane elastomer with a highly CO₂-philic silicone, namely a fluorosilicone elastomer. The influence of the blend composition on the nucleation and on the foam development (cell and foam densities) will be discussed. In addition, the effects of a dynamic crosslinking process on the blend morphologies, the shear and biaxial deformation behaviors will be correlated to foaming behavior and final foam morphology. Note that the complete studies about the blend morphology of silicone/fluorosilicone and the dynamic crosslinking process of a silicone elastomer are detailed in our previous publications [22, 23].

I. Experimental part

I.1. Materials

Silicone polymers: A methylvinyl dimethylsiloxane copolymer elastomer, named S, was kindly supplied by BlueStar Silicone. Its density is 0.97 g.cm^{-3} at room temperature (98-99% Methyl-3,3,3-trifluoropropylsiloxane)-(1-2% methylvinylsiloxane) elastomer (named FS) was purchased from ABCR (AB116651). Its density is 1.30 g.cm^{-3} . Elastomer properties can be found in our previous publication [22].

Free-radical crosslinking: The organic peroxide used was dicumyl peroxide (DCP, 98% purity), supplied by Aldrich.

I.2. Samples preparation

I.2.1. Silicone blending

Blends of silicone and fluorosilicone elastomers with DCP were prepared at various ratios. First, silicone and fluorosilicone elastomers are mixed in a roll mill (cylinder diameter=100mm) at room temperature until homogenization, depending of the content of fluorosilicone introduced. Then, DCP crystals were added and the mixing goes on 10 min to ensure a good dispersion. The gap was set to 0.4mm, noted as L , a roll speed of 25 rpm and a friction ratio of 0.8. Finally, the blends are put into vacuum at least for one day at room temperature.

I.2.2. Dynamic and Static Crosslinking

The blends are crosslinked under shearing (dynamic crosslinking), for 2 h in a roll mill at a constant gap, friction ratio and roll speed, the same as previously described in silicone blending section. Temperatures are set to 150°C on each side of both rolls. The dynamic crosslinking process was thoroughly studied in our previous publications [22, 23]. Based on the thermal decomposition of DCP [24, 25], DCP is decomposed at 96% after 2 h at 150°C (about five half-life times, $t_{1/2} \approx 25 \text{ min}$).

For static crosslinking, samples are compression molded at 120°C for 25 min using a hydraulic press with electrically heated platens, under a pressure of 5 MPa. Then, the samples are rapidly quenched into cold water in order to stop the crosslinking reactions.

Before characterization, the samples are put into a vacuum for one day at least at room temperature in order to avoid air bubbles.

1.2.3. Foaming Experiments

Before the foaming experiments, the sample is compression molded, at 30°C, into a disk-shaped sample with a thickness of 1 mm using a 25 mm circular mold. Then, this sample is transferred into a glass Petri dish. Constraints at the circular edges are also added to avoid flowing during the saturation stage. Then, this sample is placed into an autoclave at room temperature. Fig. 1 illustrates the foaming strategy used for the saturation and the foaming stages in the temperature and pressure controlled autoclave.

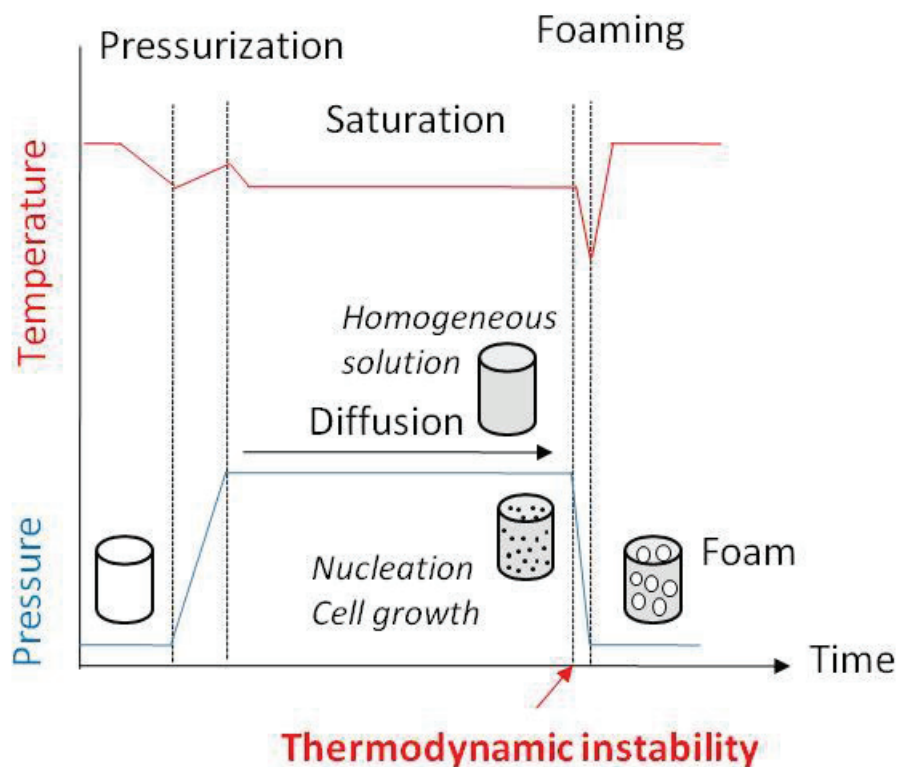


Fig. 1 : One step CO₂ batch foaming strategy used

Once, the temperature in the autoclave reaches the set value (0°C), CO₂ is introduced in the autoclave. Pressure ramps and isopressure stages are controlled manually with valves. Pressure and temperature are recorded by computer acquisition (Fig. 1). As shown in Fig. 1, when the temperature set is lower than the ambient temperature, the pressure ramp causes a temperature increase inside the pressure vessel which quickly comes back to the set value.

In the present work, foaming tests were carried out mainly with gaseous CO₂ (P = 3 MPa, T=0°C) with a saturation stage which lasts 5 h in order to obtain a homogeneous polymer/CO₂ solution by gas diffusion. From Garg, Gulari & Manke [26] data, the CO₂ concentration at equilibrium should be close to 10% wt.

After the saturation step, the foaming stage is triggered by opening a ball valve in order to achieve the highest pressure drop rate possible (Fig. 1). The pressure drop lowers

the temperature inside the autoclave by Joule-Thomson effect which quickly comes back to room temperature (Fig. 1). Foaming experiments are reproduced twice within the same conditions to check the reliability of the results. CO₂ with the purity of 99.99% (N50) was used from Alphagaz.

I.3.Characterization

Linear Shear rheology

Small amplitude oscillatory shear tests were carried out on a TA INSTRUMENTS DHR2 rheometer, using the parallel-plate geometry, with 25 mm diameter disks. Frequency sweeps from 0.01 to 500 rad.s⁻¹ were performed between -20 and 60°C, under a nitrogen atmosphere.

Lubricated Squeezing Flow (LSF)

The equibiaxial elongational measurements were performed using ARES-G2 by a constant area method at room temperature. The upper geometry ($R=8\text{mm}$) is controlled to set an exponential profile gap in compression in order to achieve a constant strain rate, $h(t) = h_0 e^{(-2\varepsilon_b t)}$. The lubricant used was castor oil, $\eta = 1\text{Pa}\cdot\text{s}$ at 25°C which is not miscible with PDMS. Basically, ratio of lubricant to sample viscosities in LSF measurements, $\alpha = \frac{\mu_L}{\eta_0}$, is in the range $10^{-6} < \alpha < 10^{-3}$ [28, 29]. In our case, $1.2 \times 10^{-5} < \alpha < 6.5 \times 10^{-5}$ so we can assume pure bi-elongational flows and a “perfect” slip at the interface during our experiments. To keep the assumption that the stress in the sample can be deduced from the force applied, data for $\varepsilon_b > 1.5$ will not be analyzed. Experimental validation and details of the method can be found in our previous publication [24].

Optical Microscopy

Blend morphologies are characterized with an optical microscope Olympus BX41 in transmission mode with an optic filter. The mean nodule size is measured for, at least, 100 nodules manually with ImageJ and its ellipsoidal tool. The mean nodule size corresponds, here, to the mean Feret diameter. Then, the nodule density is calculated from the nodule size, its volume and the volume fraction of fluorosilicone in the blend.

As no post-curing treatment was carried out, foam images are taken using a Leica MDG41 stereomicroscope within 15 min after foaming experiments in order to prevent post-relaxation phenomenon. Foams remain enough thin and transparent to enable the foam characterization by light transmission directly without any further preparation. If needed, as the depth of the field of optical microscope is limited, foam morphologies may be the result of z-stacking of several images. However, for foam characterization (cell size and cell density), foam images are not z-stacked. At least 50 non-merged bubbles are measured

manually with ImageJ software and its ellipsoidal tool, for each foam, to average cell size. The mean cell size corresponds, here, to the mean Feret diameter.

Cell densities, N_{cell} , were calculated from obtained micrographs such as [30]

$$N_{cell} \approx \left(\frac{nM^2}{A}\right)^{3/2} \quad (1)$$

where n : number of cells observed in a micrograph

A : area of the micrograph

M : magnification factor

Density measurements

The samples were weighted before foaming and the measurements of sample size enable us to estimate the volume by optical microscopy. The samples, for density measurements only, were set on Teflon paper and free to flow. As flow is symmetric and the volume is kept, we can estimate a foam density, even if the sample thickness will change during the saturation stage.

II. Results and discussion

II.1. Foaming behavior of Silicone/Fluorosilicone blends

For foaming applications, the content of CO₂ dissolved within the polymer should be as high as possible to bring forth a high nucleation rate. Therefore, the main strategies used in literature are to choose a CO₂-philic polymer alone or a blend of a CO₂-philic polymer in a matrix to also take advantage of heterogeneous nucleation. According to Kirby and McHugh [30], CO₂ solubility in poly(dimethyl)siloxane is high in comparison to usual thermoplastic polymers because of its high free volume available leading also to its extremely high gas diffusivities. One of the highest CO₂ solubilities was found in the silicone elastomer with fluorine groups, poly(trifluoropropylmethyl siloxane) because its fluorinated side-group produces specific interaction with the penetrant gas [31]. It is assumed that fluorine atoms play the role of a Lewis base with the electron-deficient carbon of CO₂. For these properties, we chose to blend a fluorosilicone into a silicone matrix. Gas transport properties of the selected polymers are listed in Table 1. The addition of fluorosilicone nodules in the silicone matrix should increase locally the CO₂ concentration dissolved leading to a higher overall CO₂ uptake during the saturation stage. Moreover, fluorosilicone has a higher T_g than silicone, therefore CO₂ diffusivity is lower, according to free volume theory [32].

Table 1 : CO₂ transport properties in polymers used

Polymer	T _g [*]	$\bar{P}(\Delta P = 0) \times 10^8$ ^{**}	$\bar{D}(\Delta c = 0) \times 10^6$ ^{**}	$\bar{S}(P = 0) \times 10^2$ ^{**}
$[(CH_3)_2SiO]_x$	-123	45.7	26.4	1.72
$[(CF_3C_2H_4)CH_3SiO]_x$	-70	12.1	5.26	2.31

Units: \bar{P} [cm³ (STP) cm/scm²cmHg]; \bar{D} [cm²/s]; \bar{S} [cm³ (STP)/cm³ (polymer)cmHg], T_g [°C].

*Measured by DSC, **Experimental data taken from [32]

Blends with several fluorosilicone contents were processed in a roll mill then observed by optical microscopy. Blends morphology may be found in our previous publication [22] but the respective mean FS nodule size and nodule densities are reported as a function of fluorosilicone content in Fig. 2. The nodule size remains almost constant in increasing FS content till 15 wt% FS. As coalescence should dominate at high content of fluorosilicone, it explains the large standard deviation of the mean nodule size obtained when 20 wt% FS is added. The resulting nodule density also remains almost constant till 15 wt% FS added, around 5×10^{10} cm⁻³, then as coalescence dominates for 20 wt% FS nodule density falls to 1.6×10^9 cm⁻³.

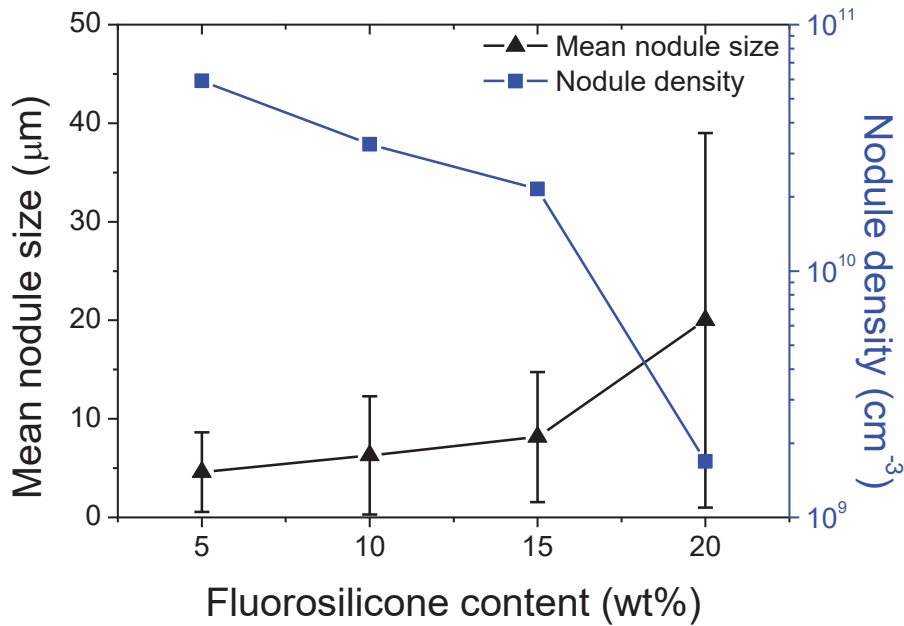
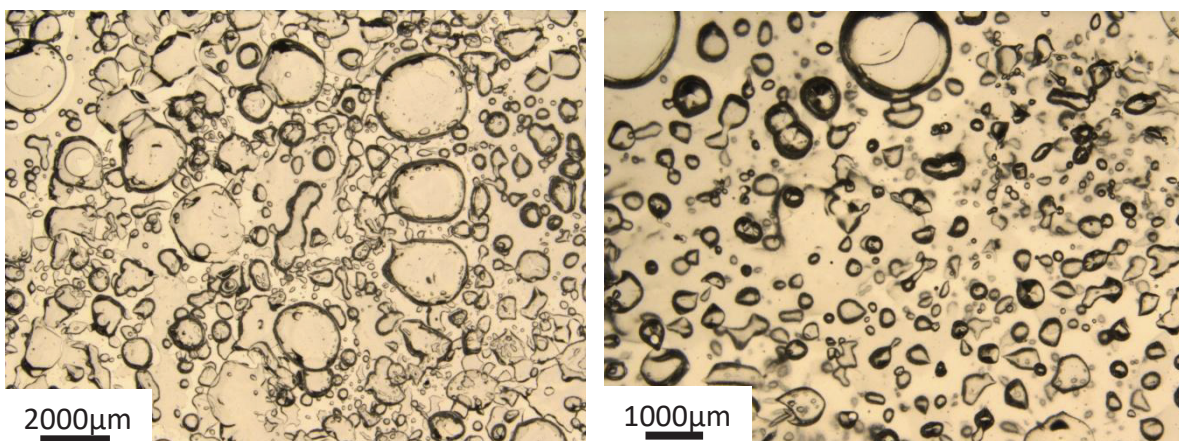


Fig. 2: Volume density and mean size of fluorosilicone nodules as a function of fluorosilicone content.

As shown in Fig. 3-a, the neat silicone foam has a high density around 0.8 because there are large unfoamed areas. Bubbles have a large size distribution with a mean cell size of $670 \pm 550 \mu\text{m}$ and a cell density of 600 cells/cm^3 . The foaming of S/FS blends was then investigated as a function of fluorosilicone content (Fig. 3 b-d), and compared with the neat S foam, considered as reference. By introducing fluorosilicone elastomer into formulations, cell sizes get lower until 10 wt% of FS. The finest homogeneous morphology ends up with S+10 wt%FS foam. In increasing the content of fluorosilicone till 20 wt%, the foam becomes non-homogeneous. The initial morphology containing a wide size distribution of fluorosilicone domains may give rise of this non-homogeneous structure. Indeed, larger domains are less efficient in terms of heterogeneous nucleation because their volume density is lower even though they have a larger curvature radius [33]. Incidentally, the dispersion of higher content of fluorosilicone is difficult because of its strong immiscibility with PDMS ($\gamma \approx 3.5 \text{ mN/m}$ determined in our previous paper [22]).



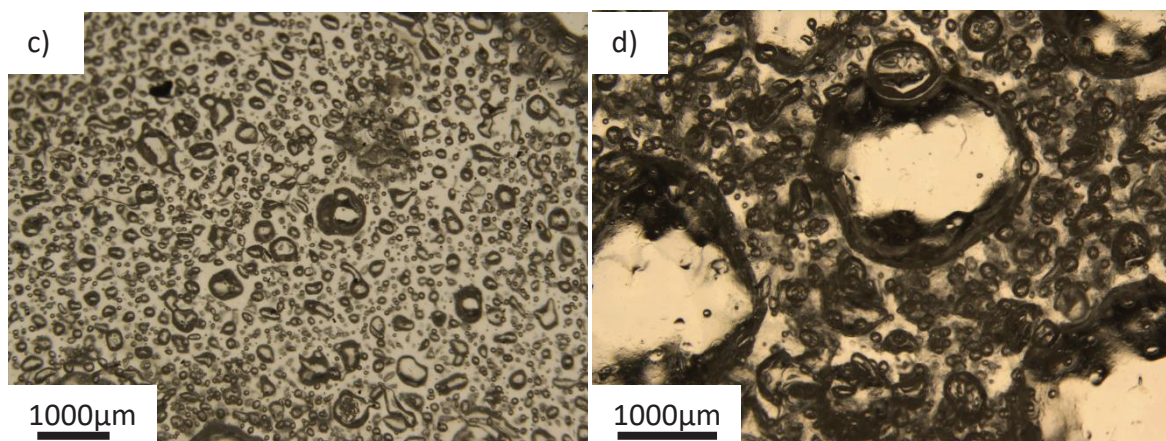


Fig. 3: Foam morphologies as a function of fluorosilicone content : a) S; b) S+5wt% FS; c) S+10wt% FS; d) S+20wt% FS. Foaming conditions: 3 MPa, 0°C for 5h and $dP/dt_{mean} = -0.36\text{MPa/s}$

Stereological analyses of the optical images enable us to measure the mean cell size and cell density of foam samples. Concerning the S+20 wt%FS foams, the measurements of the cell size and cell density included the whole foam morphology (large standard deviation of cell size). Fig. 4 shows the average cell size and cell density as a function of fluorosilicone content. The average cell size and standard deviation decrease with the addition of fluorosilicone until 10 wt%. The mean cell size decreases strongly from 670 ± 550 to 120 ± 70 μm when 10wt% FS is added. Then, the overall mean cell size remains almost constant for higher content. Regarding cell density results, the cell density increases with the fluorosilicone content. The highest cell density is obtained with 10 wt% of fluorosilicone added, $5 \times 10^6 \text{ cm}^{-3}$, corresponding to an increase of four decades in comparison to the neat silicone elastomer, $6 \times 10^2 \text{ cm}^{-3}$ in the same foaming conditions (saturation pressure of 3 MPa and saturation temperature of 0°C). Foam densities also decrease with the addition of fluorosilicone till 0.53 g.cm^{-3} then step up again as the foam morphologies become non-homogeneous.

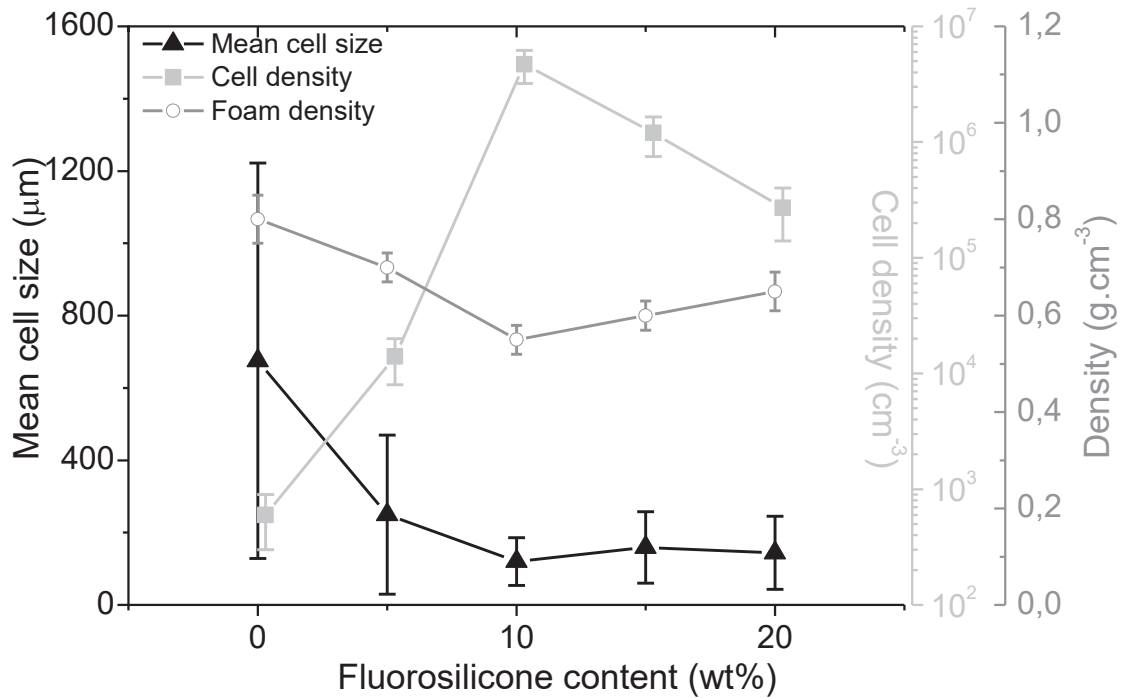


Fig. 4: Cell size and density as a function of fluorosilicone content. Foaming conditions: 3 MPa, 0°C for 5h and $dP/dt_{mean} = -0.36\text{MPa/s}$

From Fig.4, the incorporation of a small amount of fluorosilicone into a vinyl PDMS matrix allows the increase in the cell density along with a cell size reduction. These results may be explained by the fact that the fluorosilicone nodules act as potential heterogeneous nucleation sites. Indeed, a possible mechanism of nucleation is that the gas-rich volume that represents the fluorosilicone nodules serve as a CO₂ tank. CO₂ diffuses out more slowly from fluorosilicone nodules than in the matrix (table 1). Then, this little amount of carbon dioxide might contribute a longer time to the nucleation at the interface between both elastomers which is a low nucleation energy level area since the interfacial tension is low ($\gamma \approx 3.5 \text{ mN/m}$). In addition, the fluorosilicone nodules may also decrease the global surface tension then lower the nucleation energy level [34]. In situ visualization should be carried out to validate these assumptions. As a consequence, the bubble growth is reduced indirectly by the competitive growth of a larger number of nuclei.

However, if we compared the cell density d_{cell} and the nodule density of fluorosilicone in our best case, S+10 wt%FS, there is a difference of four decades. This low nucleation efficiency might be the result of the intrinsic properties of the matrix, namely its high gas permeability. Indeed, the gas loss to the surroundings increases with the diffusivity which implies that only a small fraction of dissolved gas contributes to nucleation in our samples. In addition, from numerical simulation results, as the gas diffusivity increases the cell collapse rate also gets faster [35] and cell growth increases [36] leading to a coarser foam morphology. From these reasons, all literature results concerning silicone foaming obtained cell density around $10^6\text{-}10^9 \text{ cm}^{-3}$ and cell size of 4 μm at best, which seems to be the upper limit for this material [19, 21].

In the following section, we studied the influence of the saturation temperature on the foaming behavior of the blend S+10wt% FS. Samples were saturated at 0°C, 20°C, 40°C and 60°C under a saturation pressure of 3 MPa. The cell morphologies and their respective analyses are reported in Fig. 5 and Table 2. Results point out cell size gets larger, cell size distribution becomes non-uniform and coalescence is more pronounced when temperature is increased. The mean cell size increases largely and cell density drops when the temperature is increased by only 20°C. With an increase of temperature the gas solubility is known to be reduced which in turn lowers the gas concentration dissolved and the nucleation rate. Based on classical nucleation theory, the nucleation rate should also be limited because the increase of temperature will enhance the nucleation energy level. Matrix viscosity is also reduced (η_m (30°C) =19 000 Pa.s and η_m (60°C) =16 000 Pa.s) inducing more extended cell growth and coalescence phenomena. However, these arguments cannot fully explain these results.

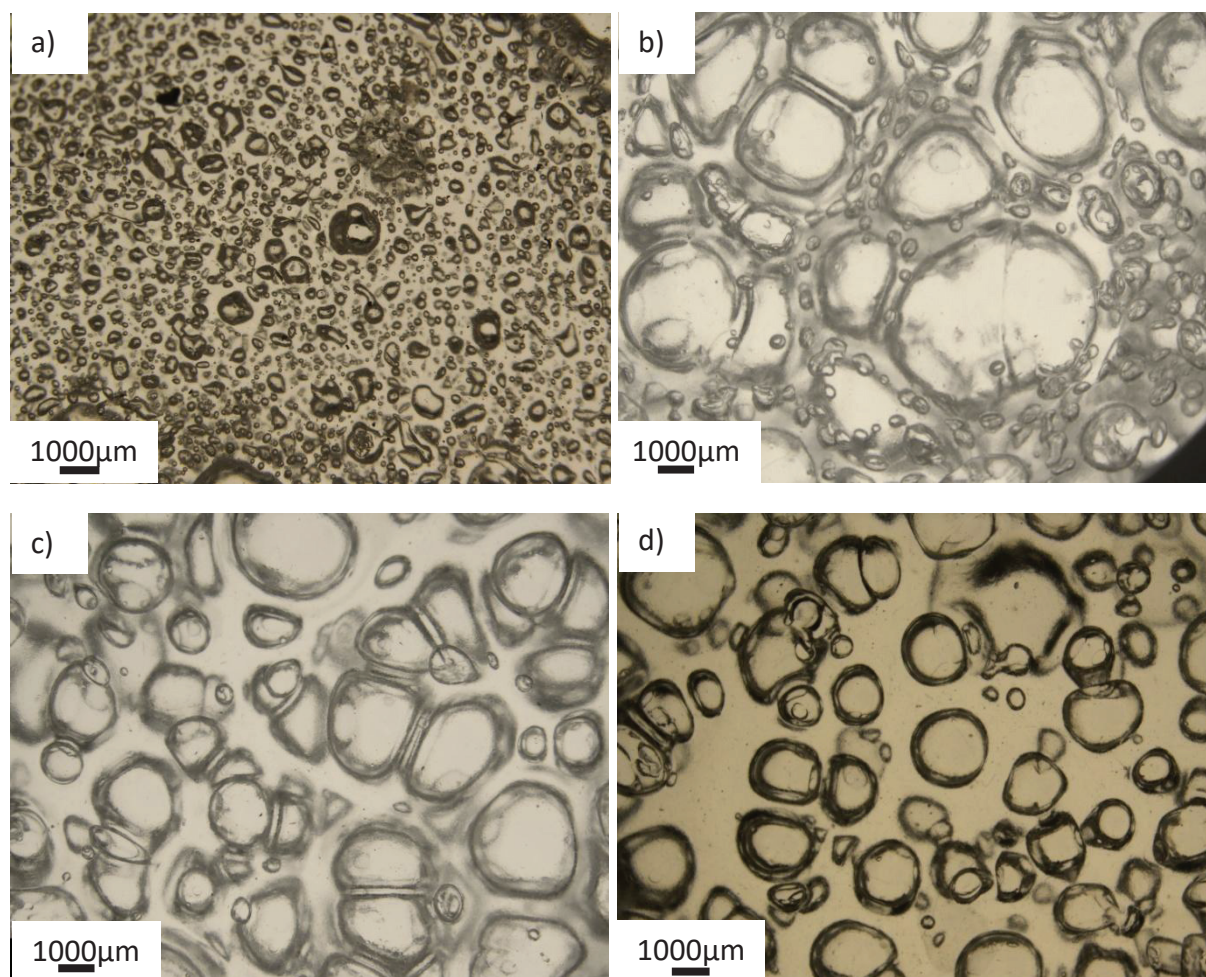


Fig. 5 : Foam morphologies of S+10wt% FS as a function of saturation temperature : a) 0°C; b) 20°C; c) 40°C; d) 60°C. Foaming conditions: 3 MPa for 5h and $dP/dt_{mean} = -0.36$ MPa/s

Table 2: Cell density and mean cell size of S+10wt% FS foams as function of saturation temperature.

T [°C]	Cell size [μm]	Cell density (cells/cm ³)
0	120 \pm 66	4.7 \times 10 ⁶
20	890 \pm 800	350
40	1490 \pm 840	82
60	1260 \pm 620	66

Furthermore, due to the Joule-Thomson effect, the measured temperature within the batch process reached -20°C at the end of the decompression in the case of an initial saturation temperature of 0°C [37]. To further discuss this, rheological tests were carried out at sub-ambient temperatures to characterize the rheological behavior of both polymers at low temperature. Viscosity ratios are plotted as function of temperatures and angular frequencies in Fig. 6. When the temperature decreases, viscosity ratios increase in low-frequency range because of the difference in flow activation energies between both polymers. Therefore, we may assume that the nodular phase would stabilize the foam when the sample temperature decreases explaining the results illustrated in Fig. 5. However, it is important to keep in mind that nucleation and cell growth should be almost completed only after few seconds reducing the cooling effect on the inner surface of bubbles and in the closest neighborhood of bubbles as the thermal conduction of PDMS, $\lambda_{PDMS} \approx 0.15 \text{ W} \cdot \text{m}^{-1} \cdot \text{K}^{-1}$, is low [38].

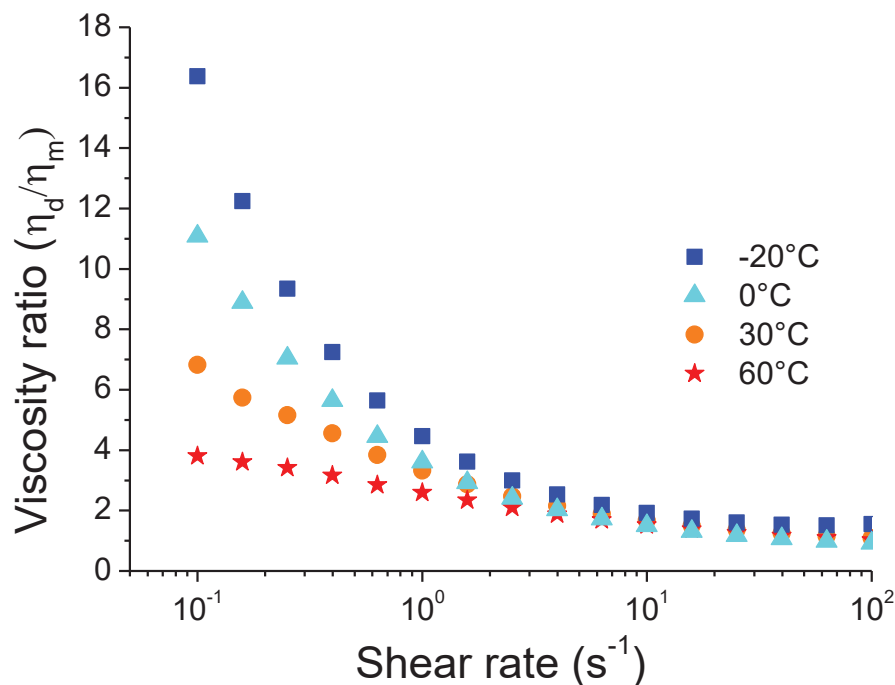


Fig. 6: Viscosity ratio between silicone and fluorosilicone as function of shear rate obtained from linear shear viscoelasticity measurements ($\epsilon=0.1\%$) and Cox-Merz law. Shear viscosities were measured between -20°C and 60°C .

II.2. Foaming Behavior of Silicone/Fluorosilicone Blends Staticly Crosslinked

Shimbo et al. [17] proved that there is a correlation between the network elasticity of a crosslinked silicone rubber and its final foam morphology. On the one hand, if the crosslinking density has a low value, the resulting cell morphology is coarse because the network elasticity cannot constrain the cell growth and coalescence. On the other hand, if the crosslinking exceeds a certain value, the network elasticity prevents the formation of bubbles. As a matter of fact, there is a narrow foaming window in which the network elasticity is strong enough to limit cell growth and hinder cell coalescence while allowing the foam expansion. Hong & Lee [18] refined this former study by giving viscoelastic data and obtained their best foam morphology for $\tan \delta = G''/G' \approx 0.2$. In this section, the aim was to monitor the influence of the viscoelastic properties on the foaming behavior.

According to crosslinking kinetics measured by rheology, S and S/10 wt%FS blends were crosslinked with 1 wt% DCP under a press at 120°C for 25 minutes. Then, the viscoelastic behavior of the partially crosslinked silicone rubbers were characterized as illustrated in Fig. 7. The viscoelastic properties of these samples are found to be close to the foaming window as $\tan \delta = 0.28$ (at 30°C, 1 rad/s) after 25 minutes of curing at 120°C.

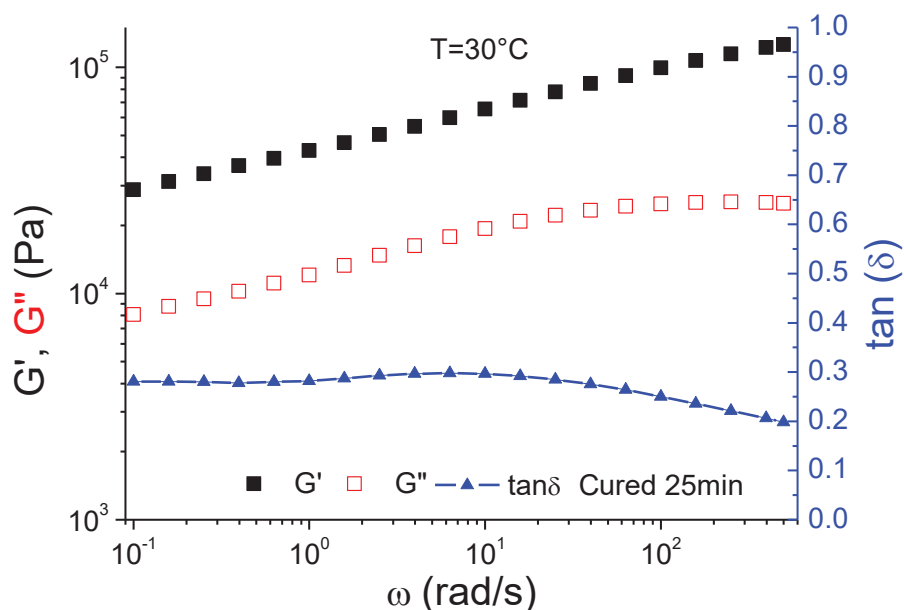


Fig. 7: Crosslinking of SR samples under static conditions: Viscoelastic behavior of samples after 25 minutes of curing time. Variations of Storage, Loss moduli and $\tan \delta$ as a function of frequency at 30°C, $\epsilon=0.1\%$. Silicone elastomer (S) cured with 1wt% DCP at 120°C for 25 min and quenched into cold water to stop the crosslinking reaction.

Fig. 8 a) and b) show the foam morphologies of neat silicone rubber and S+10 wt%FS blend cured after 25 min at 120°C. From image analyses of Fig. 8 a) and b), foam density, cell size and cell density are reported in Table 3. First, in the case of neat silicone rubber (Fig. 8-

a), the cell size is decreased by almost a factor of three while the cell density is increased by a factor of three as compared to the neat silicone elastomer foam. As for the S+10 wt%FS cured samples, the cell size is further decreased by a factor of two and the cell density is also increased by two orders of magnitude in comparison to the partially cured silicone rubber. However, the foam density remains almost constant. Once more, these results proved that the fluorosilicone nodules act as nucleating agents. Nevertheless, the foam morphology of the cured S+10 wt% FS blend is very similar to the foam morphology of the same blend uncured suggesting that the first order effect is the nucleation. In fact, the blend viscosity increases by only a factor of two when the blend is cured for 25 min at 120°C (Fig. 7) whereas in Hong & Lee work [18], the viscosity was increased by almost a factor of ten for their optimum conditions.

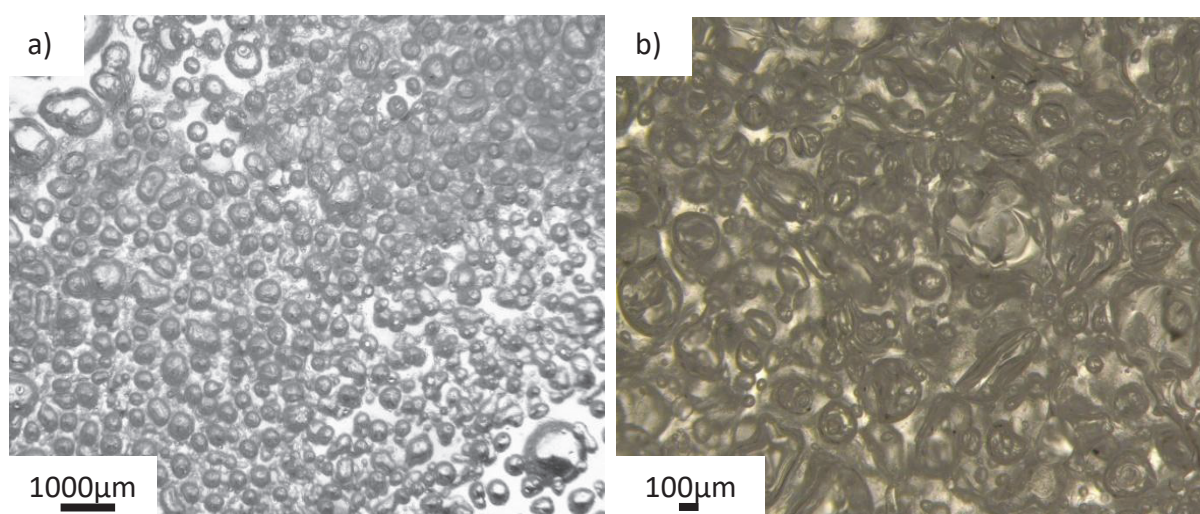


Fig. 8: Foam morphologies of partially crosslinked samples: a) S+1wt%DCP and c) S+10FS+1wt% DCP crosslinked under press at 120°C during 25 min ($\tan \delta=0.28$). Foaming conditions: 3 MPa, 0°C for 5h and $dP/dt_{mean} = -0.36$ MPa/s.

Table 3: Foam properties of partially crosslinked samples: Crosslinked under press at 120°C during 25 min ($\tan \delta=0.28$)

Sample	Cell size [μm]	Cell density (cells/cm^3)
S+1wt% DCP	265 ± 150	2.2×10^4
S+10wt% FS+ 1wt% DCP	125 ± 80	8×10^6

However, these samples cannot be fully understood as their elongational behavior is difficult to characterize. In the next section, we will develop an alternative approach based on the dynamic crosslinking of silicone/fluorosilicone blends. The effects of a dynamic crosslinking process on the initial blend morphologies, the shear and biaxial deformation behaviors will be correlated to the foaming behavior and final foam morphology of formulations.

II.3. Foaming Behavior of Silicone/Fluorosilicone Blends Dynamically Crosslinked

Fig. 9 a) and b) show the optical microscope images of S+10 wt%FS blend and the same blend dynamically crosslinked with 0.2 wt% DCP respectively. On the one hand, the mean FS nodule size is $7 \pm 6.0 \mu\text{m}$ when silicone and fluorosilicone are blended at 150°C . On the other hand, the addition of 0.2 wt% of DCP brings forth the mean fluorosilicone domain size to reduce till $3.5 \pm 2.0 \mu\text{m}$ [22]. The volumetric density of the dispersed phase increases along with the nodule size reduction. The volumetric density of fluorosilicone domain, acting as nucleating agents, varies from $2.5 \times 10^{10} \text{ cm}^{-3}$ to $1.8 \times 10^{11} \text{ cm}^{-3}$. Therefore, the increase in the nodule density should favour foaming experiments through more heterogeneous nucleation sites available.

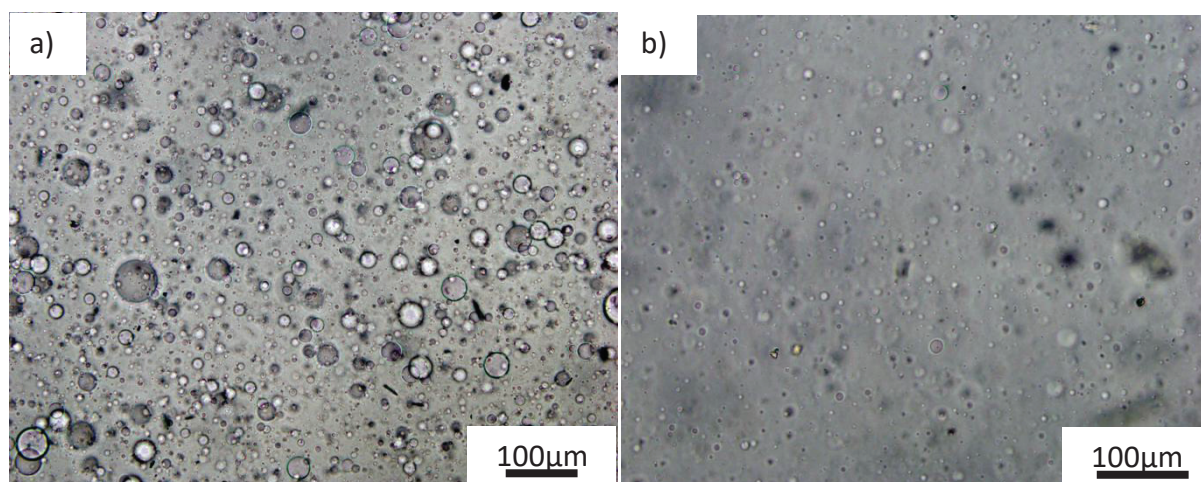


Fig. 9: Optical microscope images of blends: a) S+10wt%FS (blended at 150°C); b) S+10wt%FS+0.2wt%DCP dynamically crosslinked at 150°C for 2 hours.

The variation of absolute complex viscosity of the dynamically crosslinked blends, η^* at $T=30^\circ\text{C}$, versus angular frequency are shown in Fig. 10. Neat silicone shows the expected rheological behavior of a viscoelastic liquid. The blend of silicone with 10 wt% of fluorosilicone shows the same rheological behavior as the neat matrix because of the immiscibility between both polymers ($\gamma \approx 3.5 \text{ mN/m}$). The increase of complex viscosity in the low frequency region was attributed to the formation of hyperbranched structures of high molar masses in the neat silicone elastomer dynamically crosslinked in our previous work [23]. Similar results are obtained when the S/FS blends are dynamically crosslinked but the shift in low frequency is lower. This suggests that some content of DCP is involved into the crosslinking of the fluorosilicone phase. Zero shear viscosity estimations calculated from relaxation spectra can be found in our previous publication [23]. The corresponding characteristic relaxation times, defined as the crossover of G' , G'' , are reported in Table 4. In agreement with our previous results, the characteristic relaxation times increase with the extent of chemical modification.

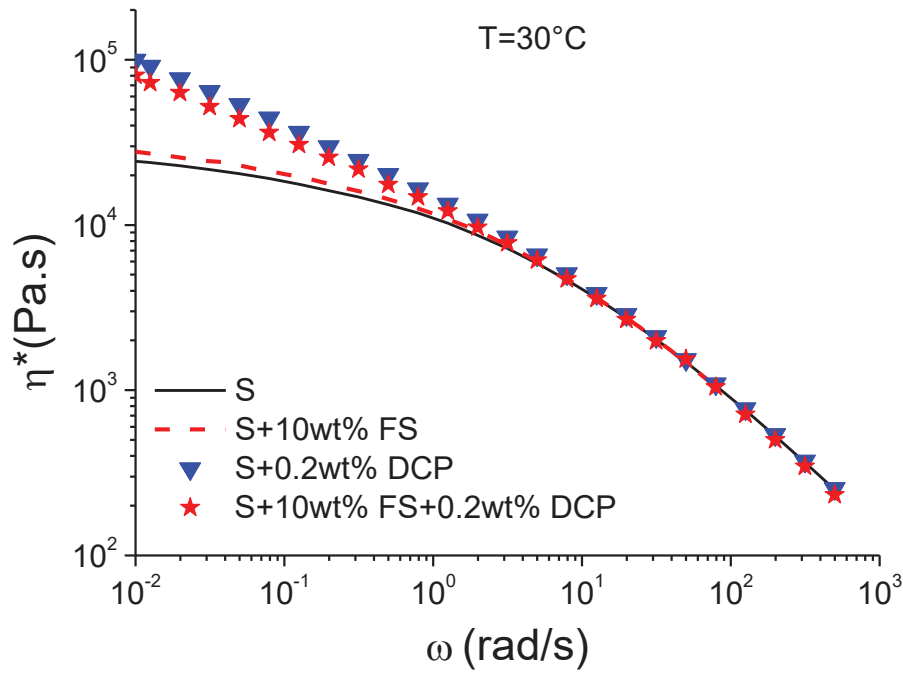


Fig. 10: Complex viscosity as a function of frequency of crosslinked samples under dynamic conditions, $\epsilon=0;1\%$ and $T=30^\circ\text{C}$.

Table 4: Viscoelastic parameters of neat and dynamic crosslinked samples

Sample	$\tau_c = 1/\omega_c [s]^a$
S	0.16
S+0.2wt% DCP	0.57
S+10wt% FS+0.2wt% DCP	0.43

^a Rheology measurements

From numerical simulations, zero shear viscosity and characteristic relaxation time seem to be critical parameters to control cell growth and stability in the early stage of the foaming [36, 39]. A longer relaxation time is a synonym to an enhanced melt elasticity inducing an improved stability during the bubble growth. In other words, an increase in zero shear viscosity and relaxation time may be viewed as using polymers with higher molar mass. Stange & Münstedt [40] foamed linear PP with several molar masses. They experimentally validated that linear PPs with increasing molar masses allow higher expansion ratios because of the melt strength enhancement. However, the improvement of foaming behavior by only considering the increase of molar mass is inefficient. The introduction of strain hardening behavior in elongation, with the addition of branched polymer structures, greatly improves the foamability of the polymer [40]. As a consequence, the rheological behavior of our blends in biaxial flows will be discussed in the following section.

During the foam expansion, the cell walls undergo a biaxial stretching. Consequently, Lubricated Squeezing Flow (LSF) experiments were carried out to characterize the biaxial deformation behavior of our formulations. Fig. 11 summarizes the biaxial properties of the samples at the constant strain rate of 0.1 s^{-1} at room temperature. In the cases of the neat

elastomer and the S+ 10wt% FS blend, stresses remain close to the Troutonian regime of the matrix and the fluorosilicone nodules do not seem to play any role in the biaxial deformation behavior. Though strain hardening is weak under biaxial deformation, the dynamic crosslinking step improves obviously biaxial properties in comparison to the neat elastomer. When the samples are dynamically crosslinked, there is an upward strain hardening deviation from the Troutonian regime. Actually, the dynamic crosslinking process enables the formation of multi-scale branched structures [23].

Numerical simulations have shown that strain hardening have almost no influence of cell growth rate and a moderate impact on the cell growth stability when considering a uniform deformation field i.e. at the early stage of foaming. However, strain hardening becomes determining in a non-uniform deformation field i.e. when bubbles approach to each other [36, 39].

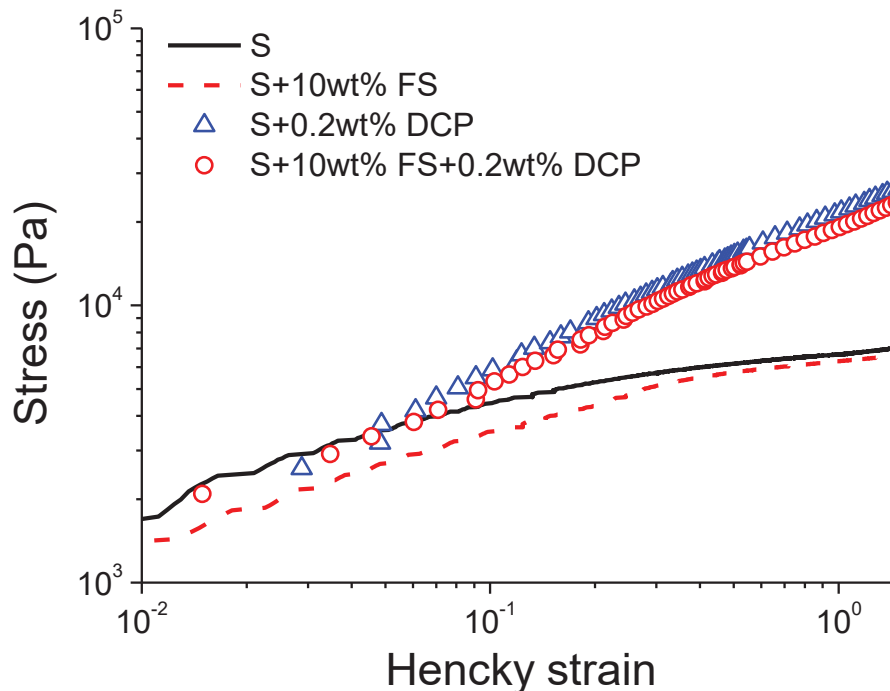


Fig. 11: Bi-elongational behavior (lubricated squeeze flow) of crosslinked samples under dynamic conditions, $\dot{\epsilon} = 0.1s^{-1}$ and $T=25^{\circ}C$.

However, the rheological behaviors, described in Fig. 10 and Fig. 11, are different in the case of sample/ CO_2 systems. Through the addition of CO_2 , entangled polymer chains will be diluted and the free volume will be increased. Zero shear viscosity is strongly dependent of the fractional free volume. An increase in fractional free volume will reduce zero shear viscosity. If we assumed an overall CO_2 concentration within our sample of about 10wt%, according to our operating conditions and experimental data from Garg, Gulari & Manke [26], the zero shear viscosity of the matrix may be reduced by almost two [41]. Equivalent results were also found by rheological measurements made on silica filled silicone rubber/ CO_2 systems [19]. Bi/Uniaxial viscosities should also be reduced [42]. However, the

change of fractional free volume in the presence of branched structure in the matrix is supposed to be lower. The stiffness modification of the polymer chains gives a lower specific volume to the branched polymer/CO₂ system in comparison to the linear polymer/CO₂ system [43]. Therefore, viscosity reduction is assumed to be lower in the case of dynamically crosslinked samples.

Foaming experiments were carried out on dynamically crosslinked samples with and without fluorosilicone. In all cases as shown in Fig. 12 and Table 5, the morphologies get finer and more homogeneous when formulations are dynamically crosslinked as compared to the uncrosslinked blends.

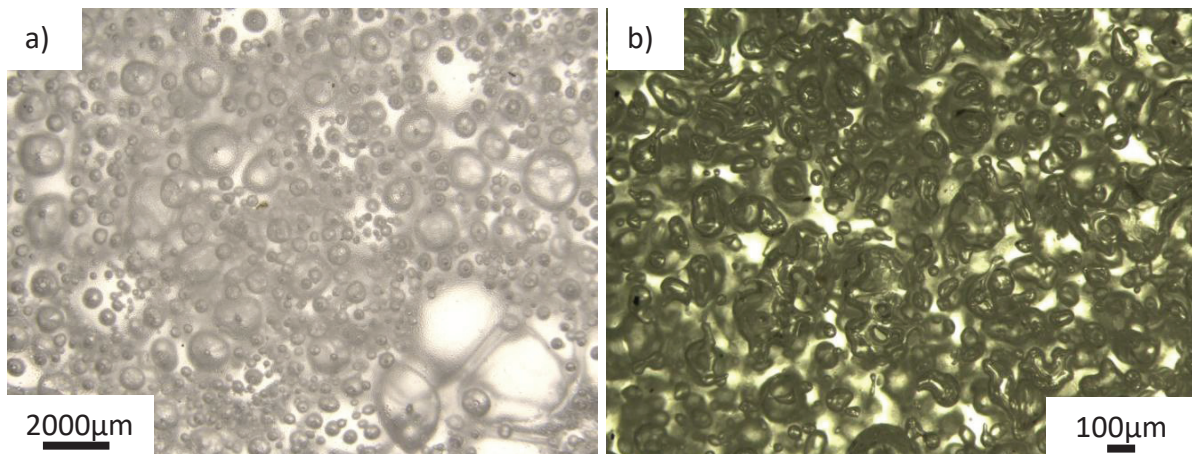


Fig. 12: Optical microscope images of foams: a) S+0.2wt%DCP; b) S+10wt%FS+0.2wt%DCP. Foaming conditions: 3 MPa, 0°C for 5h and $dp/dt_{mean} = -0.36$ MPa/s

Without fluorosilicone, when the material has not strain hardening behavior, namely S, the resulting foam is poorly expanded and a lot of bubbles have burst as previously discussed (Fig. 3-a). As the amount of DCP increases up to 0.2 wt%, the cell density increases by almost a factor of four compared to a neat silicone elastomer. In the meantime, the mean cell size is reduced by almost a factor of two. As the zero shear viscosity, relaxation time and strain hardening increase with the use of DCP, the cell growth and coalescence get limited leading to more homogeneous foams with lower mean cell size and more uniform cell wall thickness. Without any nucleating agents, this morphology is due to the improvement of viscoelastic and biaxial deformation behaviors only.

When considering the formulation with fluorosilicone, the dynamic crosslinking step further improves the foam morphology as compared to S+10 wt% FS. Indeed, the combination of the nodule size reduction of fluorosilicone and improvement of rheological behavior enable us to achieve a low mean cell size of 65µm with a cell density of 2.7×10^8 cells/cm⁻³ under gaseous conditions.

Table 5: Foam properties as a function of fluorosilicone content and dynamic crosslinking

Formulation	Cell size (μm)	Cell density ($\text{cells}/\text{cm}^{-3}$)	Foam density
<i>S</i>	670 ± 550	600	0.8
<i>S+0.2wt%DCP</i>	420 ± 300	2300	0.52
<i>S+10wt%FS</i>	120 ± 70	5×10^6	0.55
<i>S+10wt%FS+0.2wt%DCP</i>	65 ± 40	3×10^8	0.47

In addition, foam morphologies between the dynamically crosslinked neat matrix with 0.2 wt% DCP (Fig. 12-b) and the neat matrix crosslinked in static mode (Fig. 8-a) are very similar. However, their microstructure and viscoelasticity are far different between samples crosslinked in dynamic/static modes, $\tan \delta=1.16$ and 0.28 respectively (at 1 rad/s, 30°C, $\epsilon=0.1\%$). Intriguingly, a solid viscoelastic foams as well as a melt branched polymer. In order to answer to this observation, additional works must be done to characterize the elongational behavior of samples crosslinked in static mode.

Conclusion

A substitute silicone foaming strategy, based on the microstructuration of a highly CO₂-philic polymer, is proposed through the study of the foaming behavior of silicone/fluorosilicone blends.

Cell structures with a mean cell size of 120 μm were obtained from silicone/fluorosilicone blends using a one-step batch foaming process under gaseous CO₂. The fluorosilicone nodules were found to be effective nucleating agents. Their presence does not affect the rheological behavior of the matrix but they allow the formation of higher nuclei densities which reduce the overall bubble size by competitive nuclei growth. The cell density is improved by four decades and the cell size is divided by five in comparison to the neat matrix when considering the S+10 wt% FS formulation. The influence of the saturation temperature was also investigated, as expected the lower the saturation temperature is, the higher nucleation rate will be. The nodules of fluorosilicone seem to stabilize the foam morphology when the temperature decreases because of the difference in flow activation energies between both polymers.

The dynamic crosslinking process was found to be an effective way to compatibilize silicone and fluorosilicone leading to higher volume density of potential nucleating agents. The viscoelasticity and biaxial deformation behavior of the dynamically crosslinked samples are also improved. As a consequence, the cell density is improved by six decades; cell size is divided by ten in comparison to the neat matrix under gaseous conditions.

Similar results as literature in terms of viscoelasticity-foamability relation were obtained for the neat matrix crosslinked in static mode. However, the neat matrix crosslinked in dynamic or static modes seem to foam in the same way which cannot be explained with the set of data in our possession and suggest a complex relationship between viscoelasticity, elongational behavior, crosslinking microstructure and foamability.

References

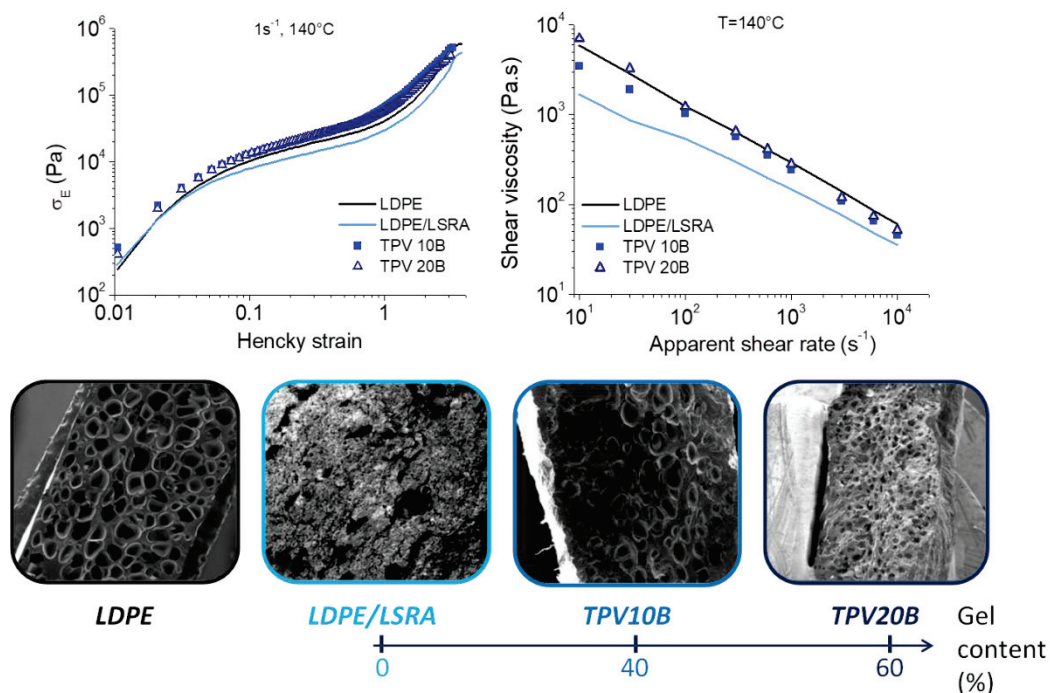
- [1] E. Yilgör, I. Yilgör, Silicone containing copolymers: Synthesis, properties and applications, *Progress in Polymer Science* **39** (6) (2014) 1165-1195.
- [2] P.K. Yuen, H. Su, V.N. Goral, K.A. Fink, Three-dimensional interconnected microporous poly(dimethylsiloxane) microfluidic devices, *Lab on a Chip* **11** (8) (2011) 1541-1544.
- [3] P. Fahr, M.Y.a. , A. Shukla, Shock response of filled corrugated sandwich structures under extreme temperatures, *Journal of Sandwich Structures and Materials* (2016).
- [4] R. Verdejo, F. Barroso-Bujans, M.A. Rodriguez-Perez, J. Antonio de Saja, M. Arroyo, M.A. Lopez-Manchado, Carbon nanotubes provide self-extinguishing grade to silicone-based foams, *Journal of Materials Chemistry* **18** (33) (2008) 3933-3939.
- [5] P. Liu, D. Liu, H. Zou, P. Fan, W. Xu, Structure and properties of closed-cell foam prepared from irradiation crosslinked silicone rubber, *Journal of Applied Polymer Science* **113** (6) (2009) 3590-3595.
- [6] J. Gao, J. Wang, H. Xu, C. Wu, Preparation and properties of hollow glass bead filled silicone rubber foams with low thermal conductivity, *Materials & Design* **46** (2013) 491-496.
- [7] E.-S. Park, Mechanical properties and antibacterial activity of peroxide-cured silicone rubber foams, *Journal of Applied Polymer Science* **110** (3) (2008) 1723-1729.
- [8] M.-C.D. Jawhar, D. Blanc, P. Chaumont, P. Cassagnau, Study of the Coalescence Mechanisms During Silicone Foaming, *Macromolecular Materials and Engineering* **299** (3) (2014) 336-343.
- [9] D. Blanc, D. Canpont, Silicone composition for elastomer foam, 2012, WO2012032231 A1
- [10] R. Verdejo, F. Barroso-Bujans, M.A. Rodriguez-Perez, J. Antonio de Saja, M.A. Lopez-Manchado, Functionalized graphene sheet filled silicone foam nanocomposites, *Journal of Materials Chemistry* **18** (19) (2008) 2221-2226.
- [11] R. Verdejo, C. Saiz-Arroyo, J. Carretero-Gonzalez, F. Barroso-Bujans, M.A. Rodriguez-Perez, M.A. Lopez-Manchado, Physical properties of silicone foams filled with carbon nanotubes and functionalized graphene sheets, *European Polymer Journal* **44** (9) (2008) 2790-2797.
- [12] C. Forest, P. Chaumont, P. Cassagnau, B. Swoboda, P. Sonntag, Polymer nano-foams for insulating applications prepared from CO₂ foaming, *Progress in Polymer Science* **41** (2015) 122-145.
- [13] M. Sauceau, J. Fages, A. Common, C. Nikitine, E. Rodier, New challenges in polymer foaming: A review of extrusion processes assisted by supercritical carbon dioxide, *Progress in Polymer Science* **36** (6) (2011) 749-766.
- [14] Y. Sato, K. Fujiwara, T. Takikawa, Sumarno, S. Takishima, H. Masuoka, Solubilities and diffusion coefficients of carbon dioxide and nitrogen in polypropylene, high-density polyethylene, and polystyrene under high pressures and temperatures, *Fluid Phase Equilibria* **162** (1-2) (1999) 261-276.
- [15] F. Wolff, B. Ceron Nicolat, T. Fey, P. Greil, H. Münstedt, Extrusion Foaming of a Pre-ceramic Silicone Resin with a Variety of Profiles and Morphologies, *Advanced Engineering Materials* **14** (12) (2012) 1110-1115.
- [16] L.J.M. Jacobs, M.F. Kemmere, J.T.F. Keurentjes, Sustainable polymer foaming using high pressure carbon dioxide: a review on fundamentals, processes and applications, *Green Chemistry* **10** (7) (2008) 731-738.
- [17] M.N. Shimbo, T. On foaming process of vulcanized rubber using physical blowing agent, *Proceedings of ICAD2004* (2004).
- [18] I.-K. Hong, S. Lee, Microcellular foaming of silicone rubber with supercritical carbon dioxide, *Korean J. Chem. Eng.* **31** (1) (2014) 166-171.
- [19] X. Liao, H. Xu, S. Li, C. Zhou, G. Li, C.B. Park, The effects of viscoelastic properties on the cellular morphology of silicone rubber foams generated by supercritical carbon dioxide, *RSC Advances* **5** (129) (2015) 106981-106988.
- [20] L. Song, A. Lu, P. Feng, Z. Lu, Preparation of silicone rubber foam using supercritical carbon dioxide, *Materials Letters* **121** (2014) 126-128.
- [21] H. Yan, K. Wang, Y. Zhao, Fabrication of Silicone Rubber Foam with Tailored Porous Structures by Supercritical CO₂, *Macromolecular Materials and Engineering* (2016).

- [22] T.Métivier, P. Cassagnau, Fluorosilicone/Silicone blends. Compatibilization by dynamic crosslinking and fumed silica, *Polymer* (2018).
- [23] T.Métivier, P. Cassagnau, Mechanisms of dynamic cross-linking of silicone elastomer: Radical cross-linking controlled by thermo-oxidation under shearing, *European Polymer Journal* **101** (2018) 37-45.
- [24] S. Mani, P. Cassagnau, M. Bousmina, P. Chaumont, Cross-Linking Control of PDMS Rubber at High Temperatures Using TEMPO Nitroxide, *Macromolecules* **42** (21) (2009) 8460-8467.
- [25] A. Msakni, P. Chaumont, P. Cassagnau, Crosslinking of ethylene–octene copolymers under dynamic conditions: A new way to access polymeric hyperbranched structure, *Polymer Engineering & Science* **46** (11) (2006) 1530-1540.
- [26] A. Garg, E. Gulari, C.W. Manke, Thermodynamics of polymer melts swollen with supercritical gases, *Macromolecules* **27** (20) (1994) 5643-5653.
- [27] D.C. Venerus, T.-Y. Shiu, T. Kashyap, J. Hosttler, Continuous lubricated squeezing flow: A novel technique for equibiaxial elongational viscosity measurements on polymer melts, *Journal of Rheology* **54** (5) (2010) 1083-1095.
- [28] S. Chatraei, C.W. Macosko, H.H. Winter, Lubricated Squeezing Flow: A New Biaxial Extensional Rheometer, *Journal of Rheology* **25** (4) (1981) 433-443.
- [29] V. Kumar, N.P. Suh, A process for making microcellular thermoplastic parts, *Polymer Engineering & Science* **30** (20) (1990) 1323-1329.
- [30] C.F. Kirby, M.A. McHugh, Phase Behavior of Polymers in Supercritical Fluid Solvents, *Chemical Reviews* **99** (2) (1999) 565-602.
- [31] S.A. Stern, V.M. Shah, B.J. Hardy, Structure-permeability relationships in silicone polymers, *Journal of Polymer Science Part B: Polymer Physics* **25** (6) (1987) 1263-1298.
- [32] J.S. Vrentas, J.L. Duda, Diffusion in polymer–solvent systems. I. Reexamination of the free-volume theory, *J. Polym. Sci. Polym. Phys.* **15** (3) (1977) 403-416.
- [33] N. Fletcher, Size effect in heterogeneous nucleation, *The Journal of chemical physics* **29** (3) (1958) 572-576.
- [34] K. Goren, L. Chen, L.S. Schadler, R. Ozisik, Influence of nanoparticle surface chemistry and size on supercritical carbon dioxide processed nanocomposite foam morphology, *The Journal of Supercritical Fluids* **51** (3) (2010) 420-427.
- [35] S.N. Leung, A. Wong, Q. Guo, C.B. Park, J.H. Zong, Change in the critical nucleation radius and its impact on cell stability during polymeric foaming processes, *Chemical Engineering Science* **64** (23) (2009) 4899-4907.
- [36] Y. Otsuki, T. Kanai, Numerical simulation of bubble growth in viscoelastic fluid with diffusion of dissolved foaming agent, *Polymer Engineering & Science* **45** (9) (2005) 1277-1287.
- [37] H. Sovova, A. Nistor, M. Topiar, J. Kosek, Vitrification conditions and porosity prediction of CO₂ blown polystyrene foams, *The Journal of Supercritical Fluids* **127** (2017) 1-8.
- [38] P. Yi, R.A. Awang, W.S.T. Rowe, K. Kalantar-zadeh, K. Khoshmanesh, PDMS nanocomposites for heat transfer enhancement in microfluidic platforms, *Lab on a Chip* **14** (17) (2014) 3419-3426.
- [39] Y. Li, Z. Yao, Z.-h. Chen, K. Cao, S.-l. Qiu, F.-j. Zhu, C. Zeng, Z.-m. Huang, Numerical simulation of polypropylene foaming process assisted by carbon dioxide: Bubble growth dynamics and stability, *Chemical Engineering Science* **66** (16) (2011) 3656-3665.
- [40] J. Stange, H. Münstedt, Rheological properties and foaming behavior of polypropylenes with different molecular structures, *Journal of Rheology* **50** (6) (2006) 907-923.
- [41] L.J. Gerhardt, A. Garg, C.W. Manke, E. Gulari, Concentration-dependent viscoelastic scaling models for polydimethylsiloxane melts with dissolved carbon dioxide, *Journal of Polymer Science Part B: Polymer Physics* **36** (11) (1998) 1911-1918.
- [42] D. Ladin, C.B. Park, S.S. Park, H.E. Naguib, S.W. Cha, Study of Shear and Extensional Viscosities of Biodegradable PBS/CO₂ Solutions, *Journal of Cellular Plastics* **37** (2) (2001) 109-148.
- [43] Y.G. Li, C.B. Park, Effects of Branching on the Pressure–Volume–Temperature Behaviors of PP/CO₂ Solutions, *Industrial & Engineering Chemistry Research* **48** (14) (2009) 6633-6640.

Chapter 6: Rheology and Extrusion Foaming of Partially Crosslinked Thermoplastic Vulcanizates Silicone

ABSTRACT

The present work is focused on the foaming behavior of Thermoplastic Vulcanizates (TPV) silicone in which partially crosslinked silicone nodules are dispersed. In TPVs, the silicone nodules dispersed in a low-density polyethylene (LDPE) phase have a mean size around 1 μm . The crosslinking densities of the elastomer phase were selected according to their viscoelasticity. Surprisingly, the linear and non-linear shear rheology were more sensitive to formulations than extensional rheology. Indeed, every formulation has similar extensional rheological behavior than the neat LDPE and reaches prerequisites for foaming applications in terms of elongation at break and melt strength. In agreement with non-linear shear rheology, the foaming behavior of these formulations may be correlated to the extrusion foaming parameters which are known to control the nucleation i.e. the pressure before the die and the depressurization rate at the die exit. With a proper crosslinking density of the silicone nodules, the TPV foamability tends to the foamability of the neat LDPE achieving a foam density of 0.54 with mean cell size of $140 \pm 50 \mu\text{m}$ and a cell density of $3 \times 10^5 \text{ cells/cm}^3$. As the partially crosslinked silicone nodules cannot foam, they are assumed to improve nucleation while allowing a sufficient expansion of the LDPE phase.



**Reformatted version of paper originally submitted in International Polymer
Processing**

Rheology and Extrusion Foaming of Partially Crosslinked Thermoplastic Vulcanizates Silicone

T. Métivier^a, P. Cassagnau^{a,*}, C. Forest^b, G. Martin^b, N. Garois^b

^aUniv Lyon, Université Lyon1, Ingénierie des Matériaux Polymères, CNRS UMR 5223, 15 Bd Latarjet, 69622 Villeurbanne, France

^bHUTCHINSON Research Centre, Rue Gustave Nourry - B.P. 31, 45120 Chalette sur Loing, France

Introduction

The thermoplastic elastomers, TPEs, have generally a hetero-phasic morphology with a hard phase and a soft phase, respectively the thermoplastic phase and the elastomer phase [1]. TPE possesses the properties of thermoset rubber with the processability of thermoplastic polymers. The in-situ crosslinking of an elastomer phase under melt mixing (dynamic crosslinking) with a thermoplastic leads to the synthesis of thermoplastic vulcanizates (TPV) which is a special group within TPE class. Since their invention by Gessler et al. [2], they have been of great interest for industries leading to a broadening of TPV material properties in tailoring the structure and nature of the TPV blend. The most widespread TPV is made from PP/EPDM blend since its development by Coran et al. [3] and Abdou-Sabet and Fath [4]. These TPVs combine generally the thermoset rubber properties such as heat, oil, weathering, wearing resistance, soft touch and good mechanical properties with the thermoplastic processability and recyclability [1, 5, 6]. Nowadays, TPVs are mainly used in automotive, appliances, medical and electronics applications. However, this conventional TPV found limited applications in automotive under hood purposes where the contact with oil under high temperature conditions (135 to 170°C) are standard [1, 5, 6]. To fulfill these requirements, super-TPVs were tailored based on vulcanized silicone rubber and engineering thermoplastics (TPVSi) [7-11]. These TPVSi surpass the performance of conventional TPVs in extreme conditions and may replace some specific thermoset rubbers.

If a closed cell structure is achieved, the foaming of these TPVSi may bring forth interesting new properties for sealing applications such as a low density, improved compression properties,... However, the extrusion of low density TPV foam remains very difficult and not fully understood because of their recent introduction on the market and their strong complexity in terms of formulation, rheology and processing. Indeed, Kropp et al. [12] compared the foaming behavior of several TPEs with CO₂ such as a thermoplastic urethane (TPU), a styrene base TPE (SEBS) and a PP/EPDM TPV. The TPV foaming was the most difficult because only the thermoplastic phase foamed and the elastomeric phase

restricted the expansion process leading to a foam density of 0.76 and an inhomogeneous cell structure.

Moreover, the TPV foaming depends primarily on the blend composition [13, 14]. Indeed, the softer grades of TPV were the most difficult to foam due to their high content of crosslinked rubber. However, the foamability of TPV can be improved by adjusting the crosslinking density of the elastomeric phase or by lowering the content of crosslinked rubber [13-15]. Indeed, it was found that the degree of foamability of PP/EPDM TPV decreases linearly with an increase of the degree of cure in the rubber phase [15].

By comparing several physical blowing agents on the foaming behavior of a commercial TPV, Kim et al. [16] found that $n\text{-C}_4\text{H}_{10}$ and CO_2 achieved the best results because of their high solubility. With CO_2 , it was achieved a fine cell density around 3×10^7 cells/cm³ with mean cell size around 20-80 μm and a foam density of 0.21. By contrast, using water as blowing agent, Sahnoune et al. [17] achieved a very low foam density close to 0.15 with cell size around 200 μm and cell density of an order of magnitude of 10^5 cells/cm³. DSM also claims to have foam EPDM/PP TPV (100/60) with a density of 0.25 by adding alumina trihydrate (ATH), a water releasing agent at 220°C [18]. However, in the case of water foaming, water is not solubilized in the polymer, but it is dispersed as fine droplets in the polymer melt [14].

To our knowledge, none study deals with TPV Silicone foaming while silicone exhibits high CO_2 solubility and low surface tension which are advantages according to the classical nucleation theory [19, 20]. Therefore, we propose in this publication to study the extrusion foaming process of a TPV Silicone made from LDPE and Liquid Silicone Rubber (LSR) with a chemical blowing agent releasing water and carbon dioxide by thermal decomposition. First, the viscoelastic behavior of neat silicone with several crosslinking densities was studied. Consequently, the foamability of TPV Silicone with the selected gel contents was correlated with their shear and elongational rheology and process conditions.

I. Experimental part

I.1. Materials

Polymers and additives: Low-density polyethylene (LDPE) was used as thermoplastic phase ($M_n=14$ kg/mol and $M_w =107$ kg/mol [21]) and a bi-component liquid silicone rubber (LSR A/B) was used as the rubber phase. A copolymer PE grafted anhydride maleic (PE-g-AM) was used a compatibilizer using the same strategy as Prakashan et al. [22]. According to suppliers, it contains 0.5-1%wt of AM. The main characteristics of materials and LSR parts are reported in Table 1 and Table 2, respectively.

Table 1: Main properties of formulation components

Materials	Trade name	T_m [°C]	η_0 [Pa.s]	Y_p [mN/m]	Y_d [mN/m]	Density (g.cm ⁻³)	Supplier
LDPE	LD 0304	111	17 000 ^{a)}	1.1 ^{b)}	32 ^{b)}	0.92	Total
LSR A/B	SL 7240	-40	-	1.1 ^{b)}	21.7 ^{b)}	1.12	KCC
PE-grafted Anhydride maleic	Exxelor PE 1040	132	180 000 ^{a)}	-	-	0.96	ExxonMobil
Hydrophobic silica	Aerosil R972	-	-	2 ^{c)}	30 ^{c)}	2	Evonik

Note : ^{a)}160°C; ^{b)} [23]; ^{c)} [24]

Table 2: General LSR properties

Materials	%mol Si-Vi ^{a)}	%mol Si-H ^{a)}	%wt Silica ^{b)}	M_n [kg/mol] ^{c)}	M_w [kg/mol] ^{c)}
LSR A	0.5	-	60	110	170
LSR B	0.8	1.5	40	85	140

Note : ^{a)}NMR; ^{b)}TGA; ^{c)} SEC

Fumed silica R972 was chosen for thermodynamic and foaming strategy reasons. From interfacial tension data [25] and Wu model calculations [26], the wetting parameter is equal to -0.64 therefore the fumed silica is assumed to be located at equilibrium at the interface between PE and silicone phases. These silica nanoparticles (primary particle size=16nm) with a high specific area (110m²/g) should therefore enhance foaming behavior at the interface between both polymers or at least in the PE domain since the silica is first blended with PE and extrusion times are short.

Foaming agents : Pamarole BA.M4.E.MG was used as chemical blowing agent (CBA). It is an endothermic master batch containing 40% of active material, according to specifications, embedded in LDPE carrier, $T_m = 104^\circ\text{C}$ (DSC measurement). Commercial chemical blowing agents like palmarole, hydrocerol,... are widely used for extrusion and injection foaming [27-29]. A blend of LDPE and palmarole was processed in a roll mill to estimate the size and

dispersion of CBA particles. From SEM/EDX analysis (Fig. 1), the reactive element is sodium bicarbonate crystals with a mean size of $4.7 \pm 3.5 \mu\text{m}$. The resulting volume of a CBA particle, assuming a spherical particle, is equal to $4.35 \times 10^{-10} \text{ cm}^3$. The density of CBA is estimated at 1.42 g/cm^3 by a mix law assuming that 40 wt% of reactive agent is embedded in LDPE ($\rho_{\text{LDPE}} = 0.9 \text{ g/cm}^3$ and $\rho_{\text{sodium bicarbonate}} = 2.2 \text{ g/cm}^3$). Therefore, the mass of reacting agent is $5.9 \times 10^{-10} \text{ g}$. The overall mass of palmarole incorporated in the blend is 0.41 g (3 wt%) which leads to 0.165 g of reactive agent. Finally, the number of particles of reactive agent, N_p , is calculated by the ratio between the overall mass of reactive agent introduced and the average mass of one reactive agent particle: $N_p = 0.165 / 5.9 \times 10^{-10} = 2.80 \times 10^8 \text{ particles/cm}^3$ of polymer.

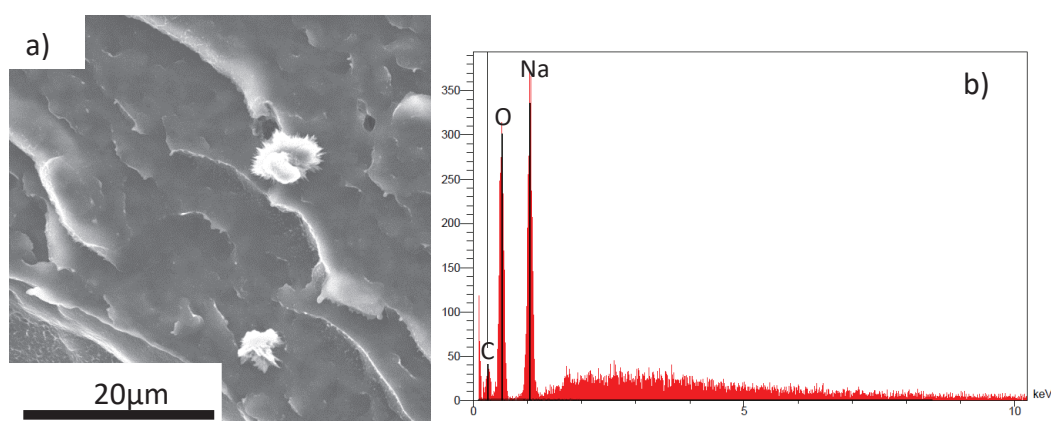
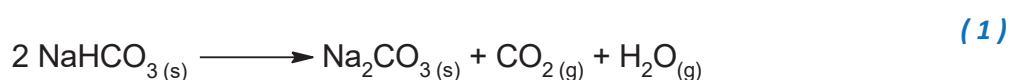


Fig. 1: EDX analysis of the chemical blowing agent: a) Palmarole crystals dispersed in LDPE (SEM image); b) EDX measurement of a sodium bicarbonate crystal contained in palmarole.

TGA/GC measurements of palmarole were carried out to determine the amount of CO_2 produced by sodium bicarbonate at 160°C (Fig. 2). The decomposition reaction is described in Eq. (1).



Using GC measurements, the decomposition palmarole produces approximately $0.02 \text{ mol of CO}_2 / \text{g of CBA}$ as illustrated in Fig. 2 (molar volume of CO_2 at 160°C and 0.1 MPa , $V_m = 35.1 \text{ L/mol}$). In extrusion foaming, the blowing effect should be due to both water and carbon dioxide expansion (Eq. 1).

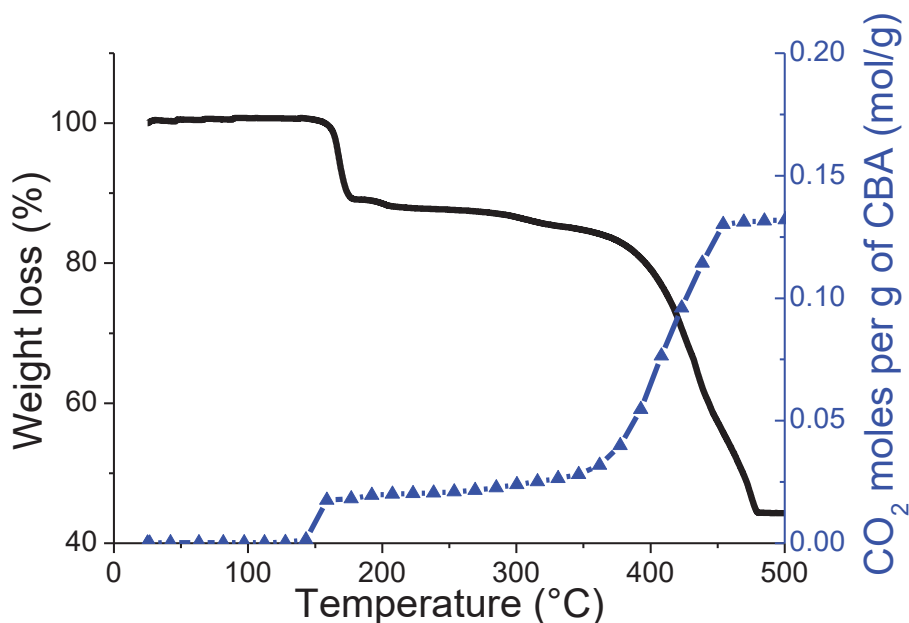


Fig. 2 : CO₂ yield during the thermal decomposition of palmarole. Black line: Weight loss, Blue line: CO₂ yield. Temperature ramp: 10°C/min until 500°C (ATG-GC)

I.2. Sample preparation

I.2.1. Static crosslinking of LSR blends

When mixed together and heated, LSRA and LSRB form a thermoset rubber by hydrosilylation crosslinking reactions [30]. LSR A/B compounds with several A/B mixing ratios were blended then put into vacuum to avoid air bubbles at least for 1h at 30°C. Then, samples are compression molded at 80°C for 30 min using a hydraulic press with electrically heated platens, under a pressure of 10 MPa. The crosslinking time was determined by kinetic rheology measurements detailed in the linear shear rheology section. Before extrusion foaming experiments, these tests were performed to select the interesting gel content of the silicone phase which will be dispersed within the TPVs.

I.2.2. Extrusion of Formulations

Formulations were extruded at 200°C using a clextral twin screw extruder D=32 and L/D=52 and dedicated pumps for LSR injections. Throughput was about 30 kg/h for LDPE and the overall LSR flow rate was kept constant in order to keep the ratio between LDPE/LSR at 60/40 wt% for all the formulations. In addition, LSRA and LSRB flow rates can vary independently from 70 to 350 g/min as a function of formulation. Blend compositions are summarized in Table 3. The LSR A alone is highly filled with silica (Table 2), therefore LDPE/LSRA was formulated to check the foamability of a blend between a thermoplastic and a yield stress fluid. For TPV xB, x is the weight percentage of LSR B in the elastomeric phase

in order to generate the selected crosslinking densities in the silicone phase. The nucleating agent amount was selected from Laguna-Gutierrez et al. work [31].

Blend compositions are summarized in Table 3. The LSR A alone is highly filled with silica (Table 2), therefore LDPE/LSRA was formulated to check the foamability of a blend between a thermoplastic and a yield stress fluid.

Table 3: Blend composition of the selected formulations (in phr)

Materials	LDPE	LDPE/LSRA	TPV 10B	TPV 20B
LDPE	100	100	100	100
LSR A	-	67	60	53
LSR B	-	-	6.7	13
PE-g-AM	-	2.5	2.5	2.5
Aerosill R972	1	1	1	1

I.3. Characterization

Linear Shear Rheology

Small amplitude oscillatory shear tests were carried out on a TA INSTRUMENTS DHR2 rheometer, using the parallel-plate geometry, with 25 mm diameter disks. Frequency sweeps from 0.01 to 500 rad.s⁻¹ were performed in the linear domain at 30°C (LSRs) and 160°C (TPVs), under a nitrogen atmosphere. Crosslinking kinetics of LSRA/B blends were followed using a parallel-plate geometry (R=25mm) at 0.1% of strain, 1 rad.s⁻¹ and 80°C under a nitrogen atmosphere.

Extensional Rheology

First, the samples were press-molded to a thickness of 0.6 mm. Then, the extensional viscosity measurements were made at 140 ° C on an ARES-EVF at several constant extensional rates of: 0.01, 0.1, 1 and 10s⁻¹. This temperature of 140 ° C was chosen to take into account the theoretical amount of dissolved carbon dioxide in the mass melted (plasticization effect) during the extrusion foaming process. With this equipment, the deformation of Hencky that can be reached is 4 so well beyond the deformation at the rupture of the samples [32].

Capillary Rheometry

A twin-bore capillary rheometer (RH7, Rosand, Malvern) was used to study the shear flow behavior of TPV materials. The diameter of the bore was 15 mm. Steady shear flow properties were collected from 10 s⁻¹ to 10⁴ s⁻¹ at 140°C with a die of 1 mm in diameter, D, 20 mm in length, L, and an entry angle of 180°.

Swelling Test

The silicone rubber network was characterized only by the soluble fraction (ω_s). Tetrahydrofuran (THF) was used as good solvent at 25°C. Specimens taken from the crosslinked sheet were immersed in THF ($V=30\text{mL}$) for 72 h at 25°C. Swollen samples at equilibrium were taken out from the solvent, blotted with filter paper, and weighted immediately. Samples were subsequently dried in a vacuum oven for 24 h at 70°C and reweighed. The soluble fraction was then directly measured.

Scanning Electron Microscopy (SEM)

Initial morphologies and foam images are taken using a FEI QUANTA 250 FEG (High vacuum) in E-T detector (5kV) and BSE detector (10kV). First, samples were frozen in liquid nitrogen and cryo-fractured. Surfaces are then covered with a thin layer of carbon by plasma metallisation. Foam is then characterized with ImageJ software. At least 50 bubbles are measured, for each foam, to average cell size. If necessary, LSR phases were extracted in THF after the cryo-fracturation.

Cell densities, d_{cell} , were calculated from obtained micrographs such as [33]

$$d_{cell} \approx \left(\frac{nM^2}{A}\right)^{3/2} \quad (2)$$

where n : number of cells observed in a micrograph
 A : area of the micrograph
 M : magnification factor

The following equation was used to determine the cell density of the original unfoamed material d_o corresponding to the initial cell concentration before cell expansion:

$$d_o = \frac{d_{cell}}{1 - V_f} \quad (3)$$

I.4. Extrusion foaming process

I.4.1. Extrusion foaming set-up

Formulations were extruded through a single screw extruder ($D=45$; $L/D=28$, Muller) with a screw speed of 70 rpm to produce foam as sketched in Fig. 3-a [34]. A gear pump was set up for output control and a static mixer was also added to improve the homogenization of the melt/gas blend. A flat die exit was used with a width of 40 cm, B_f , a length of 25 cm

and a thickness of 0.5 mm, H_f . In addition, three pressure sensors (P_1 - P_3) and two thermocouples (T_7 and T_9) were set-up to monitor the process (Fig. 3-b).

Chemical blowing agent and the formulation pellets were first dry blended and then fed to the extruder hopper. The optimum content of chemical blowing agent was found to be equal to 3 wt%.

Fig. 3-b shows the temperature profile used for every formulation as well as the measured temperature and pressure when LDPE was processed. In the depressurized region (blocks 4-5), the temperature is set high to ensure a fast decomposition of the CBA. Then, a compression and mixing zones (blocks 5-7) improve the distribution and dispersion of gas bubbles into the melt. Temperature is kept relatively high to ease mixing and diffusion phenomena. The static mixer allows increasing pressure, the residence time and the dissolution of the gas into the polymer melt. The temperature in this region is decreased to increase gas solubility, viscosity and melt strength before foaming at the die exit.

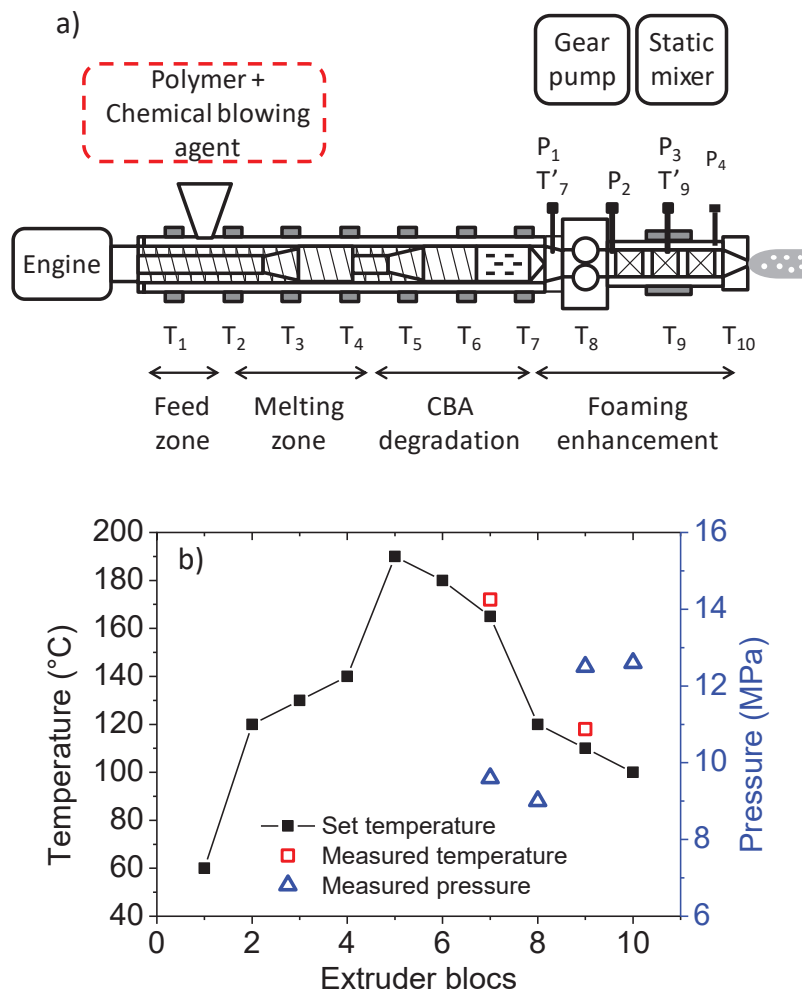


Fig. 3 : Single screw extrusion foaming process: a) Extrusion set-up; b) Temperature profile. Temperature and pressure measured for LDPE.

I.4.2. CO₂ solubility in TPV

No measurements of carbon dioxide diffusivity and solubility were done for TPVs. Therefore, we propose to use data published for PDMS [35] and HDPE [36] to assess the gas solubility in TPVs, since gas properties for LDPE and HDPE are close. Assuming that specific volume of the blends exhibited volume additivity of neat polymer melt, Henry's law may follow additivity rule based on Flory-Huggins theory [37], Eq. (4).

$$\ln\left(\frac{1}{K_{p1b}}\right) = \Phi_{02} \ln\left(\frac{1}{K_{p12}}\right) + \Phi_{03} \ln\left(\frac{1}{K_{p13}}\right) + \Phi_{02}\Phi_{03}\chi_{23} \quad (4)$$

Where K_i are Henry's constants and $\Phi_{02} + \Phi_{03} = 1$ with Φ_{0i} the volume fraction of component i without gas (1). However, Henry's law was found to follow a linear function of the composition in the molten state, i.e. $\chi_{23} = 0$ [37].

Moreover, Henry's law constant may be correlated as a function of temperature, Eq.(5), with law parameters listed in Table 4.

$$1/K_i = \exp\left[-\left(A + B\left(\frac{T_c}{T}\right)^2\right)\right] \quad (5)$$

With $T_c(\text{CO}_2) = 304.1\text{K}$

Table 4: Temperature dependence parameters of Henry law and Henry's law constant at 160°C for both materials

Materials	A	B	$1/K_i$ [cm ³ /kg-pol.atm] at 160°C
HDPE [36]	6.571	2.764	279
PDMS [35]	-6.298	2.545	309

Henry's law constant of the blend at the molten state with a volume fraction $\Phi_{02} = \Phi_{\text{PE}} = 0.66$ is equal to 286 cm³/(kg-pol.atm) at 160°C. Consequently, the solubility of TPVs should remain close to solubility of PE in the CBA degradation zone.

Using the calculated Henry's law constant of the blend, the amount of carbon dioxide dissolved in the extrusion condition may be predicted thanks to iso-concentration profile as follows:

$$P_{\text{sol}} = C \frac{1}{K_i} = C \exp\left[-\left(A + B * \left(\frac{T_c}{T}\right)^2\right)\right] \quad (6)$$

Iso-concentration profiles are reported for HDPE in Fig. 4. According to these theoretical results and experimental pressure and temperature profile at the extruder exit, at least 7%wt of CO₂ could be dissolved into formulations (Fig. 3-b).

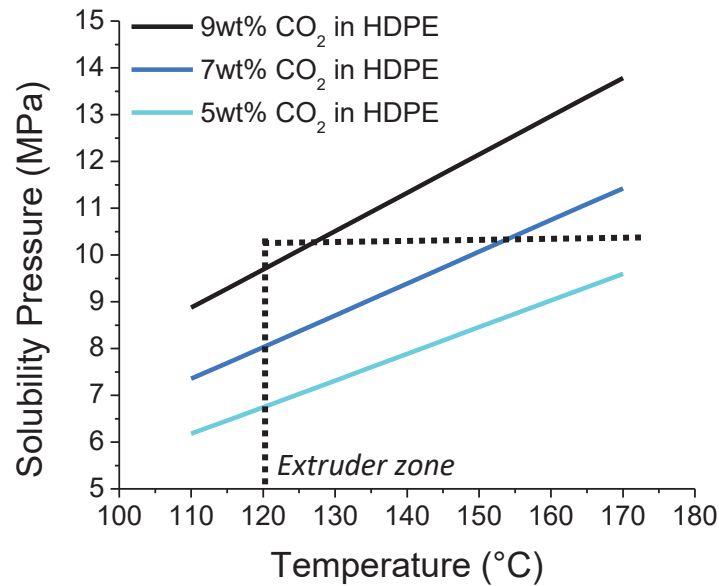


Fig. 4: Iso-concentration profiles as function of temperature for HDPE. Represents the extrusion condition limits (Pressure and temperature) reached when LDPE was extruded within the extruder.

1.4.3. CO₂ dissolution

In the following section, the homogenization time is estimated in order to determine if the molten polymers/gas mixture is homogeneous within the residence time of the process. The calculations are based on the work done by Park et al.[38]. The shear field produced by a single screw with a screw radius, $r_s = 2.7 \times 10^{-2} \text{m}$, is limited but the addition of a mixing zone in the head of the screw and a static mixer at the end of the process should greatly enhance the convective diffusion and therefore reduce the diffusion time (Fig. 3-a). First, an approximate shear strain rate is calculated according to Eq.(7). The shear field reported is calculated for the transport section assuming a constant screw channel.

$$\dot{\gamma} \approx r_s \left(\frac{2\pi\Omega}{60} \right) / b \quad (7)$$

Assuming a screw speed of 70 rpm, Ω , and a screw channel depth, b , of 2 mm, the shear strain rate should be close to 100 s^{-1} .

As the dissolution of a gaseous/supercritical phase in molten polymers in dynamic conditions is extremely difficult to model, the estimation of homogenization time is based on the estimation of the striation thickness of the polymer/gas mixture through equations (9) to (11). The striation thickness, s , defined the periodic average thickness in which composition is identical. This striation thickness is directly linked to the interfacial area developed by the mixing process between two immiscible polymers [39].

$$s \approx \frac{d_b}{\Phi_v \lambda_g} \quad (8)$$

The striation thickness is dependent on the bubble size in a shear field, d_b , the volume fraction of gas which has to be dissolved, Φ_v , and the stretching ratio of the bubble, λ_g , or the effectiveness of breaking the bubbles into smaller ones. The material properties and assumptions for the model are reported in Table 5. The volume fraction of gas dissolved (Φ_v) was estimated based on previous calculation and pressures measured in extruder, setting that around 7%wt of CO₂ is dissolved in the matrix.

Table 5: Materials properties and assumptions used to model the homogenization time

Materials	CO ₂ diffusivity ^a (D) [m ² /s]	Density [g/cm ³]	Viscosity ^c [Pa.s]	Surface tension ^b (σ) [N/m]	CO ₂ solubility ^d [g-gas/g-polym]	Volume fraction (Φ _v) [%]
LDPE	4.4x10 ⁻⁹	0.92	500	0.026[40]	0.07 [36]	0.75
CO ₂	-	0.147 ^d [41]	3x10 ⁻⁵	-	-	0.25

Note : ^a at 150°C; ^b at 160°C ; ^c at 160°C and 100s⁻¹; ^d 160°C and 10MPa.

The size of the bubbles in a shear field is defined as follows.

$$d_b = \frac{\dot{\gamma} \eta_m f(\eta_m, \eta_g) Ca}{2\sigma} \quad (9)$$

Indeed, the bubble size depends on the viscosity ratio between the matrix and the gas, $f(\eta_m, \eta_g)$, as well as the surface tension, σ , the shear field, $\dot{\gamma}$, and the capillary number, Ca . Regarding the viscosity ratio, Eq. (10), the critical capillary number for which the bubbles disintegrated should be around 1000, according to Grace curve [42].

$$f(\eta_m, \eta_g) = \frac{19(\eta_g/\eta_m)+16}{16(\eta_g/\eta_m)+16} = 1 \quad \text{and} \quad \eta_g/\eta_m = 6 \times 10^{-8} \quad (10)$$

According to assumptions, the predicted bubble size, d_b , is supposed to be around 1 mm. From literature, the stretching ratio was set to 100 [38]. Therefore, striation thickness was found equal to 40 microns and the gas dissolution into the striation thickness should be done in 0.5 seconds according to Eq.(11).

$$t_d \approx s^2/D \quad (11)$$

This estimation gives only an order of magnitude of the time needed to generate a homogeneous gas/polymer solution. In comparison to process residence time, which is several minutes, we may assume that a complete gas dissolution is achieved.

II. Results and discussion

II.1. Viscoelasticity of LSR A/B blends without LDPE

The viscoelasticity of the rubber phase which will be later dispersed in TPV formulation is first characterized. Complex viscosities, $|\eta^*|$, of uncrosslinked parts LSR A and LSR B are depicted in line in Fig. 5. These components have a high fraction of silica which explained their yield stress behavior (Table 2).

Fig. 5 shows also the complex viscosities of crosslinked LSR A/B blends, prepared according to the method detailed in the static crosslinking section. The amount of LSR B was increased to model several crosslinking densities. As the amount of B increases, $|\eta^*|$ increases over the whole frequency range studied as well as the gel fraction which starts from $40 \pm 2\%$ till $90 \pm 1\%$ according to swelling tests. Concerning the blends LSR A/B with ratio 70/30 and 60/40, the samples are strongly crosslinked with gel content of $80 \pm 2\%$ and $90 \pm 1\%$ respectively. The upper limit of $|\eta^*|$ and their gel content tell us that these ratios are not interesting for foaming applications because the crosslinking network will prevent any TPV expansion. Consequently, the LSRA/B ratio 90/10 and 80/20, with a gel fraction of $40 \pm 2\%$ and $60 \pm 2\%$ respectively, were selected for the formulation of TPV. By the way, these gel contents are close to those used by Cakmak et al. [15] when they improved the foaming behavior of soft grades PP/EPDM TPV.

Moreover, some research works observed that the addition of silicone into PP improves its foaming behavior which is greatly encouraging for our TPVs [43, 44].

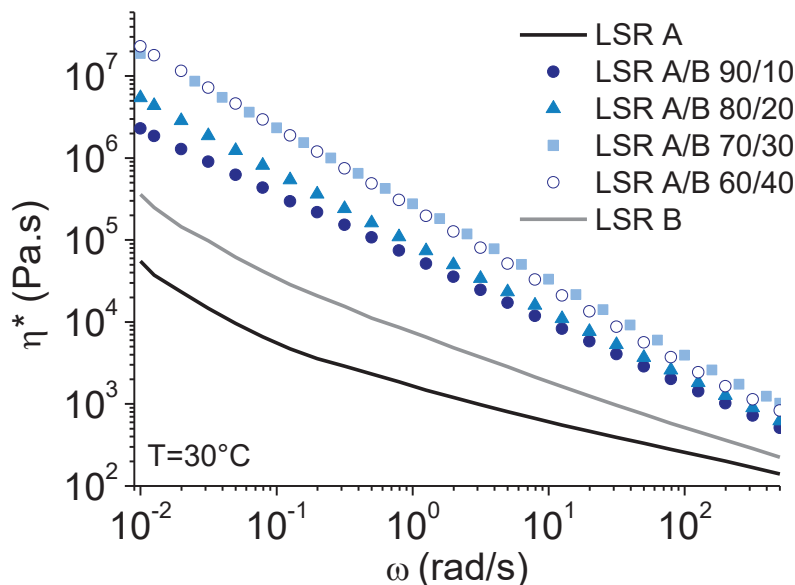
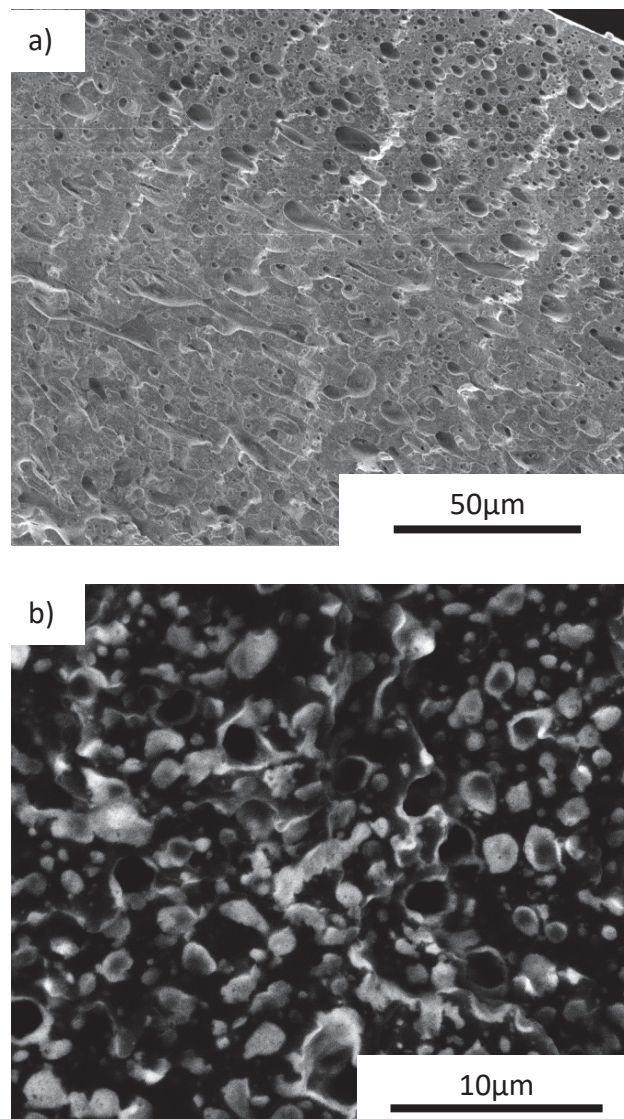


Fig. 5 : Viscoelastic data of LSR A-B with several mixing ratios cured at 80°C for 30 min. The lines represent the uncrosslinked LSR parts. Complex viscosity as a function of frequency at 30°C and $\epsilon=0.1\%$.

II.2. TPV Characterization

The LDPE/LSRA and TPVs blend morphologies are shown in Fig. 6. These morphologies were obtained from samples injected and cryo-fractured. The LSR content was extracted by THF overnight for the LDPE/LSRA blend. The images were taken in BSED mode for TPVs morphologies. The white phase corresponds to LSR domains and the black phase represents the LDPE phase which was confirmed by EDX measurements. The LDPE/LSRA blend has co-continuous morphology which is expected from the blend composition (Fig. 6-a). TPV 10B has a homogeneous nodular morphology with a mean nodule size $1.4 \mu\text{m} \pm 0.7$ while TPV20B has mean nodule size in the homogeneous region of $1.0 \mu\text{m} \pm 0.5$ (Fig. 6-b and c). The presence of large clusters of LSR ($24 \mu\text{m} \pm 15$) in TPV20B may be the results of flow instabilities as the extruder and injection pumps were used in their limits to process this blend (Fig. 6-c).



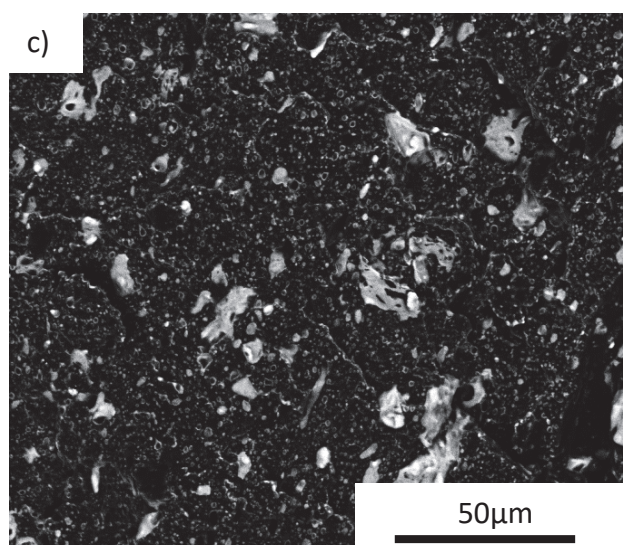
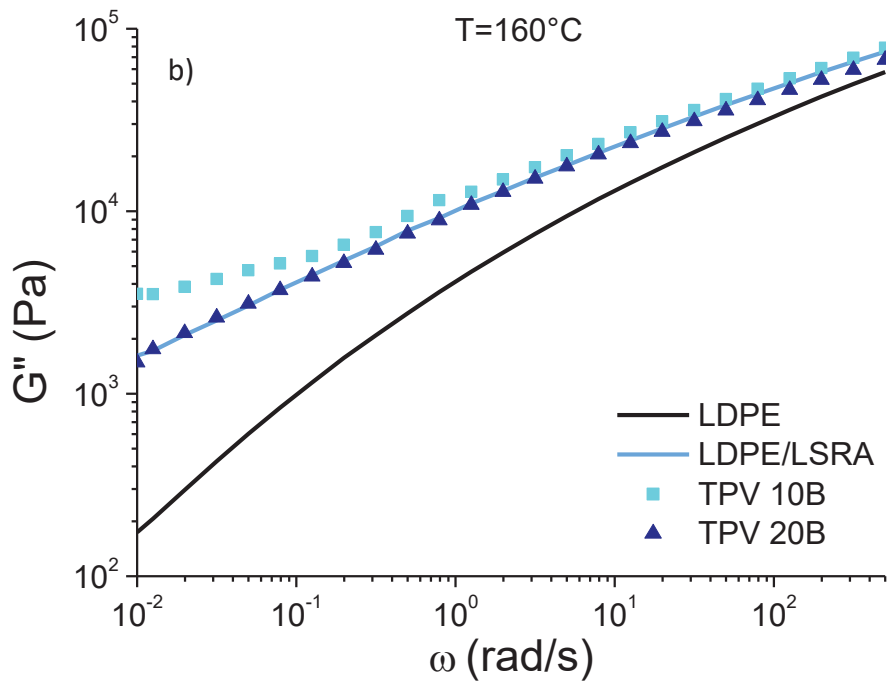
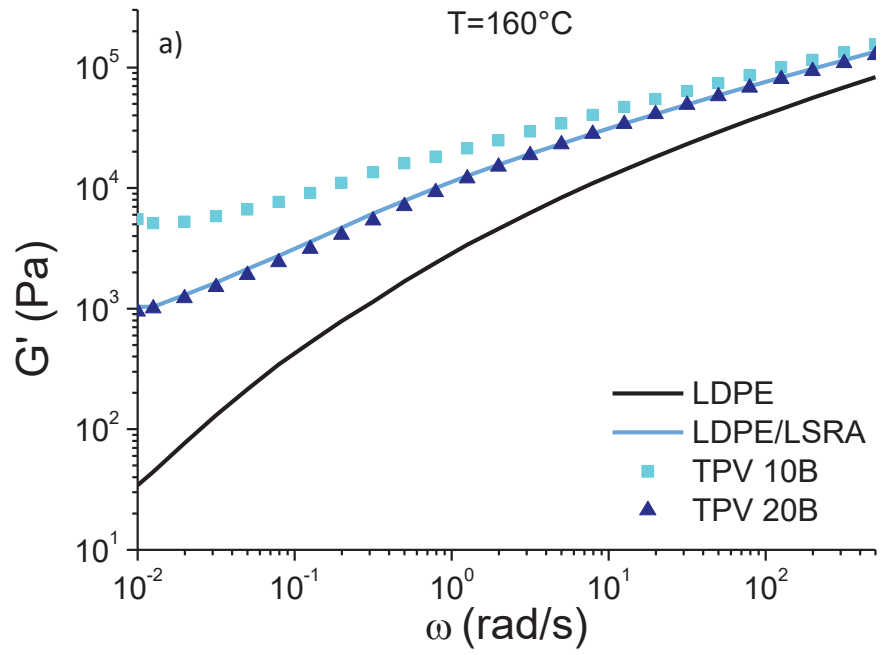


Fig. 6 : SEM images of formulations morphologies: a) LSR extracted LDPE/LSRA blend; b) TPV10B; c) TPV20B. TPVs SEM images are in BSED mode. All these samples were injected prior to observation.

Fig. 7-a and b exhibit the storage and the loss moduli versus frequency for the studied materials at 160°C. LDPE shows a standard behavior of a molten viscoelastic polymer. LDPE/LSRA blend behavior is not comparable to LDPE as a substantial increase of G' and G'' appears especially in the low frequency region. As LSRA is highly filled with silica and LDPE/LSRA blend has a co-continuous morphology, we may attribute this rheological behavior to the response of a three-dimensional network of uncured LSRA in LDPE.

Moreover, TPV10B exhibits a strong increase in both moduli and G' tends to form a plateau at low frequency. This behavior may be correlated to the relaxation and friction of a network of well dispersed crosslinked rubber nodules. Intriguingly, TPV20B should behave similarly to TPV10B but the presence of coarse silicone nodules may weaken the material explaining its lower moduli. Even at high frequency, reinforcement can be observed suggesting rubber particles-matrix interactions.

Fig. 7-c shows the complex viscosity as a function of angular frequency. A strong upturn of the complex viscosity is observed at low frequency. At low frequency, TPV10B behaves like an elastic network of rubber particles having a yield stress. This behavior is correlated to the good state of dispersion of the rubber particles within TPV10B. At intermediate frequency, PE/LSRA and TPVs behave like a LDPE melt filled with particles. At higher frequency, the rheological properties of the LDPE matrix become dominant. Similar behaviors can be found for other TPV systems [45-48].



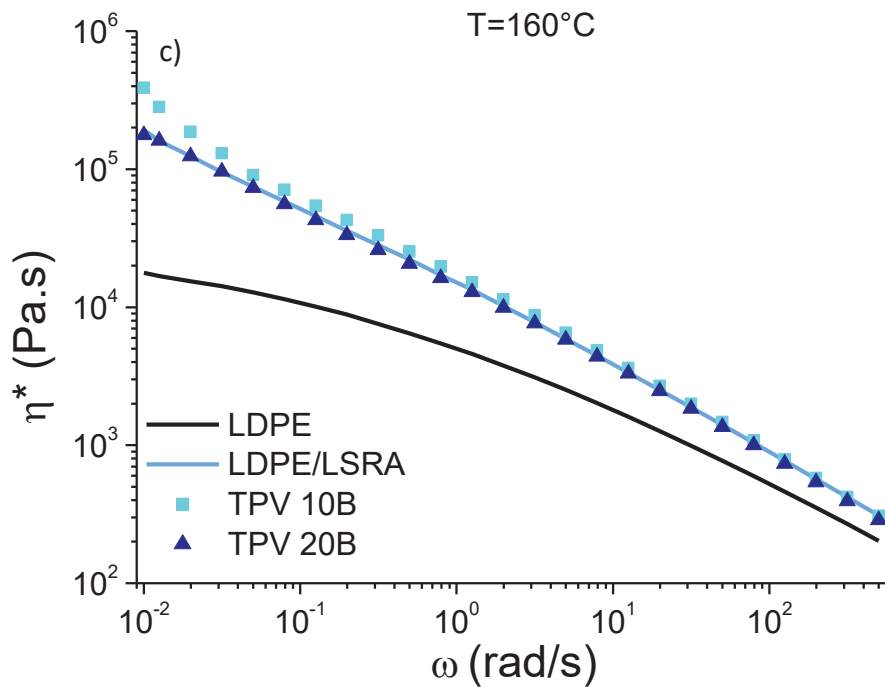


Fig. 7 : Viscoelastic behavior of the studied formulations: a) Storage moduli; b) Loss moduli; c) Complex viscosities as a function of frequency. The lines represent the matrix (LDPE), in black, and the LDPE/LSRA blend, in blue. Tests performed at 160°C and $\epsilon=0.1\%$.

Fig. 8 summarizes the steady-state experiments conducted at 140°C on each formulation with the flow curve of the LDPE matrix depicted by the line. Within the shear rates range studied, the shear thinning behavior appears for all the materials.

TPVs exhibit the similar behavior at high shear rate than the matrix which is in agreement with literature [48]. However, the LDPE/LSRA blend has a shear viscosity three times lower than the matrix which might come from the co-continuous morphology and a migration at the extrudate surface of un-crosslinked silicone phase acting as a lubricant at high shear rate. A possible evidence of a wall slip phenomenon might be found in SEM morphology of an injected PE/LSRA blend because the skin layer has a different morphology than the core (Fig. 6-a). In a lower extent, similar trends are obtained for TPVs results as their shear viscosities become slightly lower than the neat LDPE. These results contrast with the frequency sweeps in which wall slips are likely absent (Fig. 7-c).

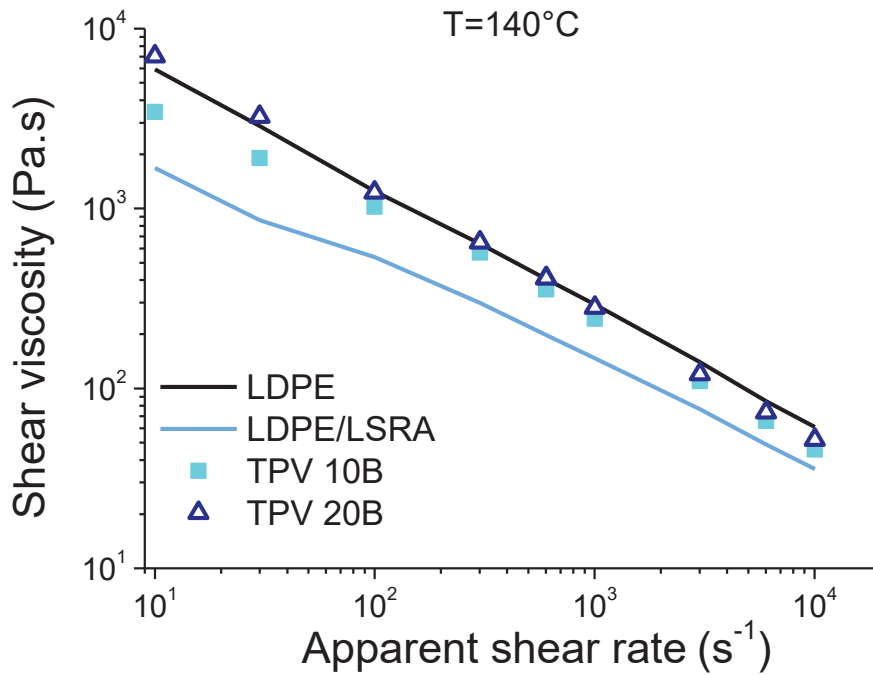


Fig. 8 : Steady state viscosity as function of apparent shear rate for each formulation. The lines represent the matrix (LDPE), in black, and the LDPE/LSRA blend, in blue. Tests performed at 140°C, L/D=20/1.

Usually, the elongational rheology is used to predict the cell growth because bi-elongational deformation occurs during bubble expansion [49]. Fig. 9 shows the elongational viscosities of the formulations at several extension rates and 140°C. The black lines are the 3-fold linear viscosity $3\eta^+(t)$, representing the linear viscoelastic regime. An up-ward deviation of η_E^+ from the linear viscoelastic regime, namely the Troutonian regime, is referred as strain hardening behavior. As expected, LDPE shows a strain hardening behavior because of its intrinsic branched structure [50]. LDPE/LSRA and TPV10B show similar strain hardening behavior that the neat matrix whereas TPV 20B has a lower extent of deviation from the viscoelastic regime. In addition, the strain hardening behavior is decreasing as the crosslinking extent increases in the LSR phase.

Moreover, a slight reinforcement in the linear viscoelastic regime under uniaxial elongation can be observed for TPVs as compared to LDPE. However, higher reinforcements in elongation flow were observed for PP/EPDM (50/50) TPV or for particles filled compounds [48, 51]. Further works should be carried out to explain the correlation between the deformability of the silicone nodules and the elongational behavior of the blend.

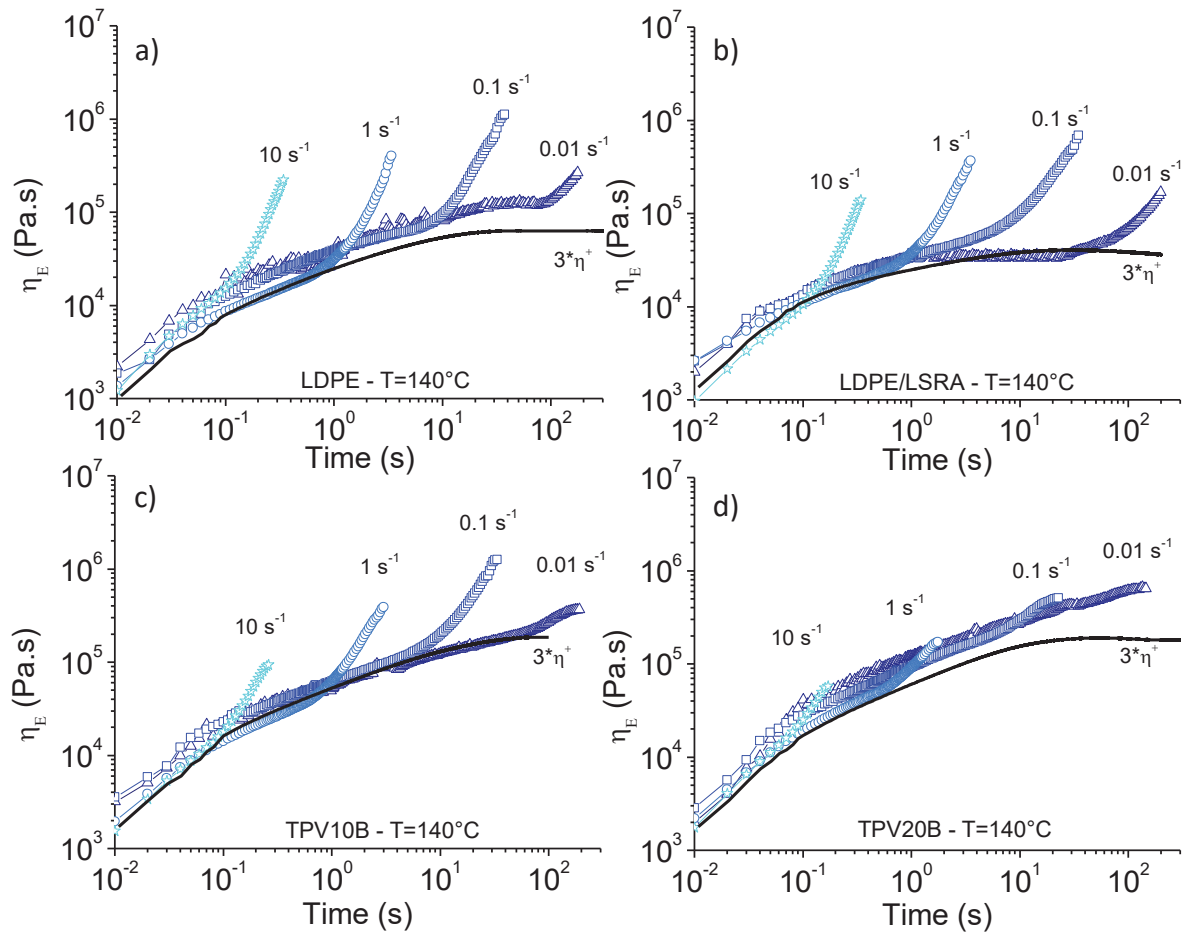


Fig. 9: Variation of elongational viscosity as function of time for several strain rates: a) PE-ref; b) PE/LSRA; c) TPV10B; d) TPV20B. The black line represents the Troutonian regime. Test performed at 140°C .

The stress-Hencky deformation curve is shown in Fig. 10 at a constant elongation rate of 1 s^{-1} for every formulation. The extensional rate was selected in reference to the foaming window ($\varepsilon = [3; 4]$, $\dot{\varepsilon} = [1; 5]\text{ s}^{-1}$) [49]. Every formulation exhibits the same behavior as the neat matrix i.e. elongation at break and maximum elongation stress (also called melt strength) and achieve foaming prerequisites. Therefore, during the gas expansion, the cell wall of every formulation should behave equivalently.

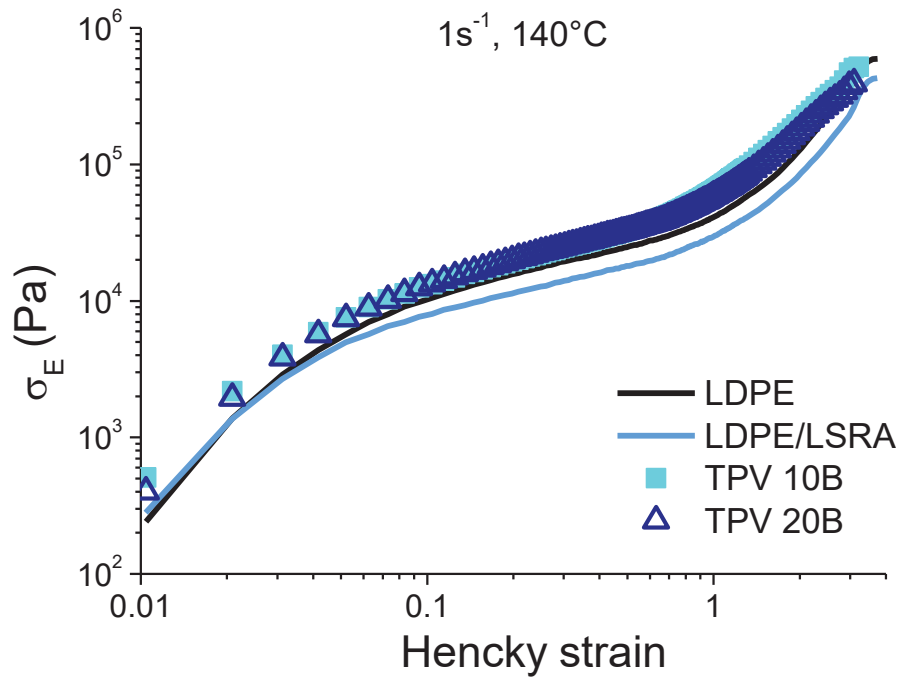


Fig. 10: Elongational stress as a function of Hencky strain for every formulation. The lines represent the matrix (LDPE), in black, and the LDPE/LSRA blend, in gray. Test performed at 140°C and 1 s-1.

Intriguingly, the addition of 40wt% of LSR (cured or uncured) induces almost no elongational flow modification of the materials as compared to the neat matrix. Spitael et al. [52] were also able to measure the strain hardening behavior of TPV blend with branched PPs but the details about the formulation or morphology are unknown. According to Yamaguchi et al. [53], the introduction of immiscible crosslinked nodules should not modify the elongational behavior of the matrix but they introduced only 3wt% of immiscible crosslinked nodules whereas in our formulations there are 40 wt% of crosslinked nodules.

In our case, the shear rheology seems more sensitive to the formulations than elongational viscosity which is usually the opposite. Similar results were found for HIPS and LDPE/PS blends systems without any explanations [54, 55].

II.3. Extrusion Foaming

The aim of this section is to show the foamability of each formulation with the same extrusion conditions i.e. temperature profile, screw speed and equipment. The foam morphologies of each formulation are represented in Fig. 11. The LDPE/LSRA foam has a very low content of bubbles and these bubbles are generally collapsed (Fig. 11-b). For TPV foams, as the amount of LSR B increases, the foam morphology tends to a homogeneous and well-defined cell structure close to the morphology of the LDPE.

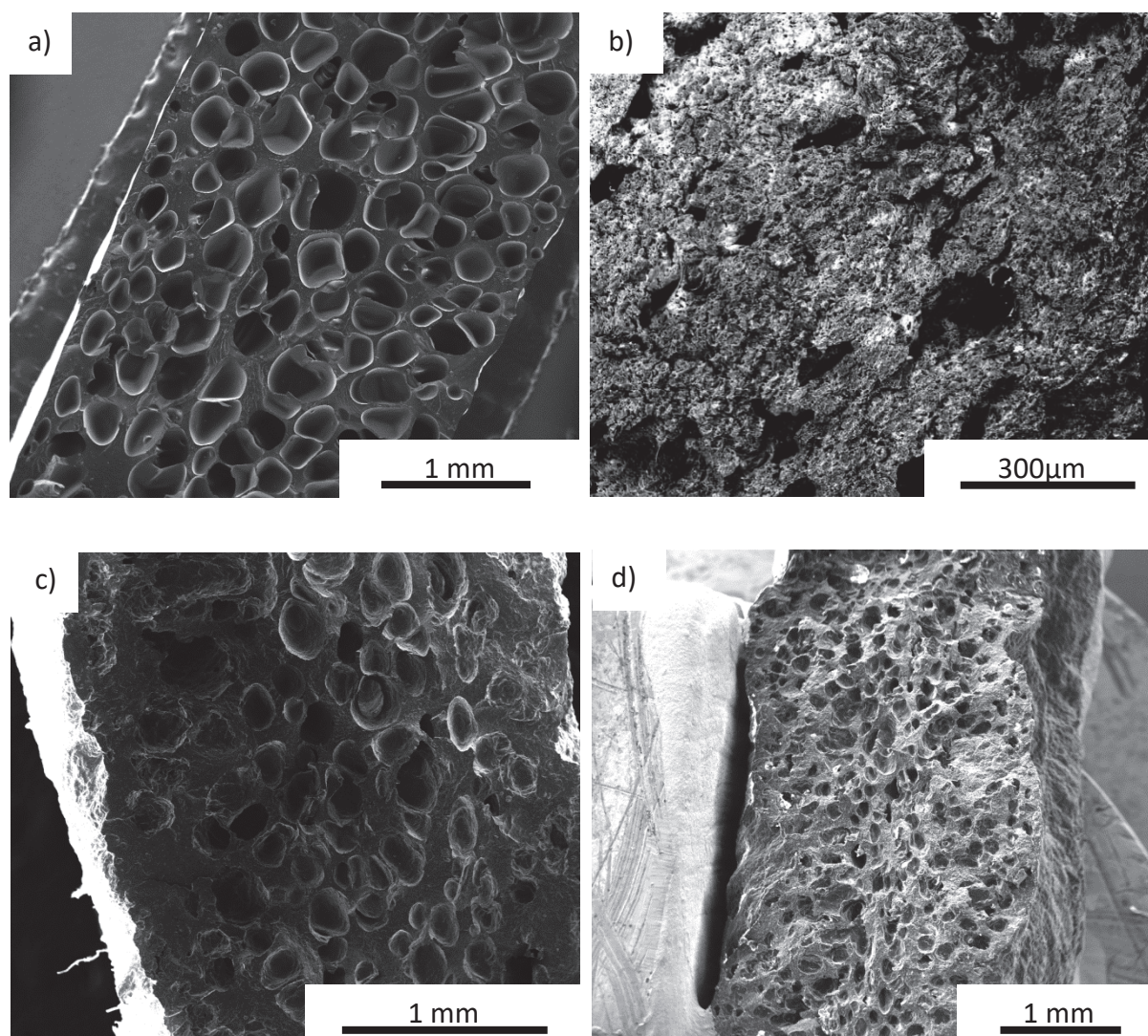


Fig. 11 : Foam morphologies of each formulation obtained with 3wt% of palmarole: a) LDPE; b) LDPE/LSRA; c) TPV10B; d) TPV20B.

These morphologies were analyzed and the corresponding results are listed in Table 6. Analysis of LDPE/LSRA foam was not performed because few bubbles were formed during the process leading to a high foam density of 0.8.

Table 6 : Foam analysis for each formulation studied. Extrusion foaming with 3wt% of palmarole.

	LDPE	LDPE/LSRA	TPV10B	TPV20B
Mean cell size (μm)	235 \pm 80	-	210 \pm 50	145 \pm 50
d_{cell} (cell/cm^3)	9 $\times 10^4$	-	1 $\times 10^5$	3 $\times 10^5$
Void fraction	0.59	-	0.42	0.45
d_0 (cell/cm^3)	2 $\times 10^5$	-	2 $\times 10^5$	6 $\times 10^5$
Density	0.40 \pm 0.02	0.8 \pm 0.02	0.57 \pm 0.04	0.54 \pm 0.03

As expected from the elongational rheology of the LDPE, the LDPE foam exhibits a foam density of 0.4 \pm 0.02 with a homogeneous cell structure (Fig. 11-a). The mean cell size

and cell density are $235\pm 80 \mu\text{m}$ and $9\times 10^4 \text{ cell/cm}^3$, respectively. Regarding the initial particle density of CBA (determined in the materials section), the initial cell density, d_0 , in the LDPE foam is three decades lower suggesting a relatively low nucleation efficiency of the CBA.

Now if we consider the TPV foam results (Fig. 11-c and d). On the one hand, the addition of partially crosslinked silicone nodules in LDPE increases the foam density to 0.54 ± 0.03 . On the other hand, the mean cell size reduces from $235\pm 80 \mu\text{m}$ to $145\pm 50 \mu\text{m}$ while cell density increases slightly from 9×10^4 to $3\times 10^5 \text{ cell/cm}^3$. The void fraction is also decreased in TPVs in comparison to the LDPE foam.

The foam density increase is first due to the lower content of the LDPE phase (60wt%) which limits the foam expansion i.e. reduce the void fraction. Moreover, It is important to consider that the addition of silicone in the formulations will also enhance the depletion of gas molecules at the foam surface because of its high gas permeability [56]. According to the classical nucleation theory, this local desorption phenomenon limits the cell nucleation and growth leading to thick foam skin or cell walls which will further increase the foam density [57].

The cell size reduction and the cell density obtained for TPV foams are explained by taking into account the extrusion pressures and the depressurization rate achieved at the die exit which are two important parameters controlling the nucleation [49, 58].

First, the steady state shear data are used to model the materials with a simple power law model, Eq.(12), in the shear rate range studied in Fig. 8. As wall slip phenomena probably occur during the capillary measurements, the modeling is only qualitative. Nevertheless, wall slip phenomena should also occur when the melt goes through the extrusion die.

$$\eta = k_p \dot{\gamma}^{n-1} \quad (12)$$

With k_p , the consistency and n , the shear thinning index.

A direct correlation is obtained between the consistency of the material and the pressure before the die. As expected, a high consistency blend will bring forth a high pressure within the static mixer (Table 7). According to nucleation theory, the nucleation energy barrier is substantially lowered with an increase of the pressure difference between the saturation pressure and the atmospheric pressure which in turn induces a higher nucleation rate. Moreover, an higher saturation pressure enables to dissolve a higher content of gas which is also beneficial for nucleation [57].

To further understand the foaming behavior of the materials studied, the depressurization rates, $\frac{dP}{dt}$, through the flat die used was estimated using Eq. (13) and reported in Table 7 [59, 60]. From literature, the highest the depressurization rate is, the highest the cell density and the lowest the cell size will be [58]. In agreement with literature, LDPE and TPV20B undergo the highest depressurization rate and have the finest cell structure.

$$\frac{dP}{dt} = \frac{2^{n+1}k_p(2 + \frac{1}{n})^n Q^{n+1}}{B_f^{n+1}H_f^{2n+2}} \quad (13)$$

With Q is the melt flow rate set to 20 kg/h. B_f , H_f are the flat die geometries defined in the experimental section.

Table 7: Sum up of extrusion process parameters (experimental pressure before the flat die and estimated depressurization rate through the flat die). Power law parameters used to model the high shear rate behavior of the materials and the depressurization rate at 140°C.

	LDPE	LDPE/LSRA	TPV 10B	TPV 20B
n	0.34	0.45	0.37	0.29
k_p	27000	6500	18000	36000
$\frac{dP}{dt}$ [MPa.s ⁻¹]	29	13	18	29
Experimental pressure in the static mixer (P_3) [MPa]	12	8	13	15

As no significant modification was measured in the elongational behavior in the PE/LSRA blend in comparison to the neat LDPE, the combination of the low pressure inside static mixer and the low depressurization rate clarifies the poor foamability of the LDPE/LSRA blend. Moreover, the blend structuration of the LDPE/LSRA is not in favor of foaming. Indeed, there is a co-continuous network of a highly permeable silicone leading to a strong depletion of gas to the surroundings.

However in TPVs, the initial cell density, d_o , remains almost constant as compared to LDPE foams while the weight fraction of the LDPE phase in TPVs represents 60wt% and only this phase can foam. These results may be justified according to two mechanisms.

First, the sum of the high pressure within the static mixer and the high depressurization rate undergone at the die exit effectively enhance the nucleation rate which in turns decrease the bubbles size by competitive cell growth.

Secondly, the blend structuration of TPV20B may increase the nuclei density by adding heterogeneous nucleation sites brought by the silicone nodules. The presence of nodules does not modify the cell growth as the rheological behavior remains unchanged (Fig. 10). But the bubble growth is reduced indirectly by the competitive growth of a larger number of nuclei. A possible mechanism of nucleation is that the gas-rich volume that represents the LSR nodules act as effective nucleating agents. Indeed, silicone exhibits high CO₂ solubility and low surface tension which are advantages according to the classical nucleation theory.

Conclusion

The present work is devoted to the foaming behavior of TPV silicone in which partially crosslinked silicone nodules are dispersed. The main objective of this study is to bring more insights in the correlation between process conditions, TPV foam morphologies and the shear and elongational rheology of the formulations.

First, several crosslinking densities of the rubber phase alone were selected from linear shear experiments. Then, TPVs were tailored with the preferred gel contents leading to fine morphologies with silicone nodule sizes around 1 μm .

Regarding the linear shear and elongational rheology data, TPV formulations exhibit unusual rheological behavior. Indeed, the addition of high content of crosslinked or uncrosslinked silicone induces significant rheological modification only in shear flow.

Even though neat LDPE, LDPE/LSRA blend and TPVs have similar elongational flow behavior, their foamability is far different. These intriguing results were clarified thanks to the microstructure and the rheological behavior at high shear rate of the formulations. Indeed, the steady state rheology governed the extruder pressure and the depressurization rate undergone by the molten formulations at the die exit which in turns control the nucleation. Therefore, with a proper gel content of the silicone nodules, the TPV foamability tends to the foamability of the neat LDPE achieving a foam density of 0.54 with mean cell size of $140 \pm 50 \mu\text{m}$ and a cell density of $3 \times 10^5 \text{ cells/cm}^3$. As the silicone nodules cannot foam, they are assumed to improve nucleation while allowing a sufficient expansion.

References

- [1] J.G. Drobny, *Thermoplastic Elastomers Prepared by Dynamic Vulcanization*, Handbook of Thermoplastic Elastomers, William Andrew Publishing, Norwich, NY, 2007, pp. 179-190.
- [2] A.M. Gessler, J.W.H. Haslett, Process for preparing a vulcanized blend of crystalline polypropylene and chlorinated butyl rubber, 1962, U.S. Patent 3037954 A
- [3] A.Y. Coran, B. Das, R.P. Patel, Thermoplastic vulcanizates of olefin rubber and polyolefin resin, 1978, U.S. Patent 4130535 A
- [4] S. Abdou-Sabet, M.A. Fath, Thermoplastic elastomeric blends of olefin rubber and polyolefin resin, 1982, U.S. Patent 4311628 A
- [5] B.J. Cail, R. D.DeMarco, New Heat and Oil Resistant Thermoplastic Vulcanizate (TPV) for Demanding Underhood Applications, SAE International, 2003.
- [6] K.E. Kear, *Developments in thermoplastic elastomers*, Rapra Publishing, 2003.
- [7] S. Mani, P. Cassagnau, M. Bousmina, P. Chaumont, Morphology Development in Novel Composition of Thermoplastic Vulcanizates Based on PA12/PDMS Reactive Blends, *Macromolecular Materials and Engineering* **296** (10) (2011) 909-920.
- [8] T. Chatterjee, S. Wießner, K. Naskar, G. Heinrich, Novel Thermoplastic Vulcanizates (TPVs) Based on Silicone Rubber and Polyamide Exploring Peroxide Cross-linking, *eXPRESS Polymer Letters* **8** (4) (2014) 220-231.
- [9] C.M. Brewer, I. Chorvath, F.M. Fournier, C.S. Gross, M.K.J. Lee, D. Li, R.L. Rabe, Thermoplastic silicone elastomers from compatibilized polyamide resins, 2003, W.O. Patent 2002008335 A2
- [10] N. Garois, P. Sonntag, S. Hong, G. Martin, D. Galpin, Thermoplastic elastomer vulcanizate and process for preparing same, 2014, U.S. Patent 8648145 B2
- [11] G.A. Gornowicz, K.E. Lupton, D.J. Romenesko, K. Struble, H. Zhang, Thermoplastic silicone elastomers, 2000, U.S. Patent 6013715A
- [12] D. Kropp, W. Michaeli, T. Herrmann, O. Schröder, Foam Extrusion of Thermoplastic Elastomers Using CO₂ as Blowing Agent, *Journal of Cellular Plastics* **34** (4) (1998) 304-311.
- [13] A. Dutta, M. Cakmak, Influence of Composition and Processing History on the Cellular Morphology of the Foamed Olefinic Thermoplastic Elastomers, *Rubber Chemistry and Technology* **65** (5) (1992) 932-955.
- [14] I. Pesneau, M. Champagne, R. Gendron, M. Huneault, Foam Extrusion of PP-EMA Reactive Blends, *Journal of Cellular Plastics* **38** (5) (2002) 421-440.
- [15] A. Dutta, M. Cakmak, Foaming of Vulcanized PP/EPDM Blends Using Chemical Blowing Agents, *Rubber Chemistry and Technology* **65** (4) (1992) 778-791.
- [16] S.G. Kim, C.B. Park, M. Sain, Foamability of Thermoplastic Vulcanizates Blown with Various Physical Blowing Agents, *Journal of Cellular Plastics* **44** (1) (2008) 53-67.
- [17] A. Sahnoune, Foaming of Thermoplastic Elastomers with Water, *Journal of Cellular Plastics* **37** (2) (2001) 149-159.
- [18] A.O. Dozeman, Y. Wang, Thermoplastic vulcanisate, the thermoplastic vulcanisate containing a foaming agent and foam of the thermoplastic vulcanisate, 2004, U.S. Patent 6750292 B2
- [19] A. Garg, E. Gulari, C.W. Manke, Thermodynamics of Polymer Melts Swollen with Supercritical Gases, *Macromolecules* **27** (20) (1994) 5643-5653.
- [20] P. Spitael, C.W. Macosko, R.B. McClurg, Block Copolymer Micelles for Nucleation of Microcellular Thermoplastic Foams, *Macromolecules* **37** (18) (2004) 6874-6882.

- [21] C. Peiti, J.-M. Haudin, B. Vergnes, Modification of rheological properties of branched polyethylenes by a thermomechanical treatment, *AIP Conference Proceedings* **1664** (1) (2015) 170002.
- [22] K. Prakashan, A.K. Gupta, S.N. Maiti, Effect of compatibilizer on micromechanical deformations and morphology of dispersion in PP/PDMS blend, *Journal of Applied Polymer Science* **105** (5) (2007) 2858-2867.
- [23] J.E. Mark, *Physical Properties of Polymers Handbooks*, Springer, 2007.
- [24] W. Tong, Y. Huang, C. Liu, X. Chen, Q. Yang, G. Li, The morphology of immiscible PDMS/PIB blends filled with silica nanoparticles under shear flow, *Colloid and Polymer Science* **288** (7) (2010) 753-760.
- [25] D.W. Van Krevelen, K. Te Nijenhuis, *Interfacial Energy Properties, Properties of Polymers* (Fourth Edition), Elsevier, Amsterdam, 2009, pp. 229-244.
- [26] S. Wu, Calculation of interfacial tension in polymer systems, *Journal of Polymer Science Part C: Polymer Symposia* **34** (1) (1971) 19-30.
- [27] Q. Li, L.M. Matuana, Foam extrusion of high density polyethylene/wood-flour composites using chemical foaming agents, *Journal of Applied Polymer Science* **88** (14) (2003) 3139-3150.
- [28] E.M. Chang, M; Li, X; Mohebbi, A; Park CB, Optimizing chemical blowing agent content in foam injection molding process of PP, SPE ANTEC, Anaheim, 2017.
- [29] A.K. Bledzki, O. Faruk, Microcellular Injection Molded Wood Fiber-PP Composites: Part I - Effect of Chemical Foaming Agent Content on Cell Morphology and Physico-mechanical Properties, *Journal of Cellular Plastics* **42** (1) (2006) 63-76.
- [30] L.M. Lopez, A.B. Cosgrove, J.P. Hernandez-Ortiz, T.A. Osswald, Modeling the vulcanization reaction of silicone rubber, *Polymer Engineering & Science* **47** (5) (2007) 675-683.
- [31] E. Laguna-Gutierrez, C. Saiz-Arroyo, J.I. Velasco, M.A. Rodriguez-Perez, Low density polyethylene/silica nanocomposite foams. Relationship between chemical composition, particle dispersion, cellular structure and physical properties, *European Polymer Journal* **81** (Supplement C) (2016) 173-185.
- [32] J.R. Royer, J.M. DeSimone, S.A. Khan, High-pressure rheology and viscoelastic scaling predictions of polymer melts containing liquid and supercritical carbon dioxide, *Journal of Polymer Science Part B: Polymer Physics* **39** (23) (2001) 3055-3066.
- [33] V. Kumar, N.P. Suh, A process for making microcellular thermoplastic parts, *Polymer Engineering & Science* **30** (20) (1990) 1323-1329.
- [34] N. Garois, P. Sonntag, S. Hong, G. Martin, D. Galpin, Elastomère réticulé à transformation thermoplastique et son procédé de préparation, 2011, E.P. Patent 2380933 A1
- [35] V.M. Shah, B.J. Hardy, S.A. Stern, Solubility of carbon dioxide, methane, and propane in silicone polymers: Effect of polymer side chains, *Journal of Polymer Science Part B: Polymer Physics* **24** (9) (1986) 2033-2047.
- [36] Y. Sato, K. Fujiwara, T. Takikawa, Sumarno, S. Takishima, H. Masuoka, Solubilities and diffusion coefficients of carbon dioxide and nitrogen in polypropylene, high-density polyethylene, and polystyrene under high pressures and temperatures, *Fluid Phase Equilibria* **162** (1-2) (1999) 261-276.
- [37] Y. Sato, T. Takikawa, M. Yamane, S. Takishima, H. Masuoka, Solubility of carbon dioxide in PPO and PPO/PS blends, *Fluid Phase Equilibria* **194-197** (2002) 847-858.

- [38] C.B. Park, N.P. Suh, Rapid Polymer/Gas Solution Formation for Continuous Production of Microcellular Plastics, *Journal of Manufacturing Science and Engineering* **118** (4) (1996) 639-645.
- [39] W.D. Mohr, R.L. Saxton, C.H. Jepson, Mixing in Laminar-Flow Systems, *Industrial & Engineering Chemistry* **49** (11) (1957) 1855-1856.
- [40] A. Falsafi, S. Mangipudi, M.J. Owen, *Surface and Interfacial Properties*, in: J.E. Mark (Ed.), *Physical Properties of Polymers Handbook*, Springer New York, New York, NY, 2007, pp. 1011-1020.
- [41] R. Span, W. Wagner, A New Equation of State for Carbon Dioxide Covering the Fluid Region from the Triple-Point Temperature to 1100 K at Pressures up to 800 MPa, *Journal of Physical and Chemical Reference Data* **25** (6) (1996) 1509-1596.
- [42] H.P. Grace[†], Dispersion phenomena in high viscosity immiscible fluid systems and application of static mixers as dispersion devices in such systems, *Chemical Engineering Communications* **14** (3-6) (1982) 225-277.
- [43] M. Wang, J. Ma, R. Chu, C.B. Park, Z. Nanqiao, Effect of the introduction of polydimethylsiloxane on the foaming behavior of block-copolymerized polypropylene, *Journal of Applied Polymer Science* **123** (5) (2012) 2726-2732.
- [44] W. Wang, S. Zhou, Z. Xin, Y. Shi, S. Zhao, Polydimethylsiloxane assisted supercritical CO₂ foaming behavior of high melt strength polypropylene grafted with styrene, *Frontiers of Chemical Science and Engineering* **10** (3) (2016) 396-404.
- [45] P. Cassagnau, G. Martin, C. Barrès, *Reactive Systems and Thermoplastic Vulcanizates*, Applied Polymer Rheology, John Wiley & Sons, Inc., 2011, pp. 241-261.
- [46] L.A. Goettler, J.R. Richwine, F.J. Wille, The Rheology and Processing of Olefin-Based Thermoplastic Vulcanizates, *Rubber Chemistry and Technology* **55** (5) (1982) 1448-1463.
- [47] F. Goharpey, H. Nazockdast, A.A. Katbab, Relationship between the rheology and morphology of dynamically vulcanized thermoplastic elastomers based on EPDM/PP, *Polymer Engineering & Science* **45** (1) (2005) 84-94.
- [48] P.K. Han, J.L. White, Rheological Studies of Dynamically Vulcanized and Mechanical Blends of Polypropylene and Ethylene-Propylene Rubber, *Rubber Chemistry and Technology* **68** (5) (1995) 728-738.
- [49] S.T. Lee, C.B. Park, *Foam extrusion: Principles and Practices*, CRC Press 2000.
- [50] H. Münstedt, T. Steffl, A. Malmberg, Correlation between rheological behaviour in uniaxial elongation and film blowing properties of various polyethylenes, *Rheology acta* **45** (1) (2005) 14-22.
- [51] H. Tanaka, J.L. White, Experimental investigations of shear and elongational flow properties of polystyrene melts reinforced with calcium carbonate, titanium dioxide, and carbon black, *Polymer Engineering & Science* **20** (14) (1980) 949-956.
- [52] P. Spitael, C. W Macosko, A. Sahnoune, Extensional rheology of polypropylene and its effect on foaming of thermoplastic elastomers, Proceedings of the Annual Technical Conference (ANTEC '02), 2002.
- [53] M. Yamaguchi, H. Miyata, Strain Hardening Behavior in Elongational Viscosity for Binary Blends of Linear Polymer and Crosslinked Polymer, *Polymer Journal* **32** (2000) 164.
- [54] V.C. Barroso, S.P. Ribeiro, J.M. Maia, Unusual extensional behavior of a polystyrene/HIPS blend, *Rheol Acta* **42** (5) (2003) 483-490.
- [55] L.A. Utracki, P. Sammut, On the uniaxial extensional flow of polystyrene/polyethylene blends, *Polymer Engineering & Science* **30** (17) (1990) 1019-1026.

- [56] S.A. Stern, V.M. Shah, B.J. Hardy, Structure-permeability relationships in silicone polymers, *Journal of Polymer Science Part B: Polymer Physics* **25** (6) (1987) 1263-1298.
- [57] C. Forest, P. Chaumont, P. Cassagnau, B. Swoboda, P. Sonntag, Polymer nano-foams for insulating applications prepared from CO₂ foaming, *Progress in Polymer Science* **41** (2015) 122-145.
- [58] Q. Guo, J. Wang, C.B. Park, M. Ohshima, A Microcellular Foaming Simulation System with a High Pressure-Drop Rate, *Industrial & Engineering Chemistry Research* **45** (18) (2006) 6153-6161.
- [59] W. Michaeli, *Extrusion dies for plastics and rubber*, Hanser, 1983.
- [60] H. Zhang, Scale-Up of Extrusion Foaming Process for Manufacture of Polystyrene Foams Using Carbon Dioxide, University of Toronto (2010)

Conclusions

In this dissertation, fundamental works were conducted to understand the formation mechanisms of silicone elastomer foams (cell nucleation, bubble growth and coalescence...) and to find relations between the cell structure, the process parameters, the initial blend morphologies and the rheology of these formulations. In terms of industrial applications, the final objective was to study the foaming behavior of ThermoPlastic Vulcanizates (TPV) silicone in the framework of the FUI project SMOUSSIF.

In the first part, a theoretical study was carried out on the batch-foaming behavior of a silicone elastomer. Carbon dioxide was selected as the blowing agent because of its high solubility in poly(dimethyl siloxane) copolymers (PDMS). The first foaming attempts of the neat silicone elastomer lead to bad aspects foams with big and collapse bubbles. These results are mainly due to the intrinsic high gas permeability and viscoelasticity of silicone elastomer. Therefore, the main objective of this first part was to improve the foaming behavior of the neat silicone elastomer.

In silicone foaming, crosslinking and foaming process should be synchronized to achieve well-defined foam structure. However in batch foaming experiments, the set saturation temperature prevent the crosslinking reaction to occur. Therefore the traditional strategy to improve the silicone foaming behavior is to partially crosslink the silicone elastomer before the foaming step. But the pre-curing process has to be adjusted along with material and specimen size, which is really inconvenient. In this context, an alternative approach was developed based on the enhancement of the viscoelasticity and elongational rheology by chain branching. Indeed, a strain hardening behavior in bi-elongational flow was effectively added to the neat elastomer in order to reduce the cell size and coalescence while allowing a higher foam expansion. The strain hardening behavior was brought by the dynamic crosslinking of the neat elastomer (crosslinking under shearing conditions i.e. in a roll mill) which gives rise to multi-scale branched structures. However, the branching topology remains uncontrolled and unknown. Moreover, the dynamically crosslinked samples undergo longer post-relaxation phenomena allowing a potential post-crosslinking step to stabilize the foam.

The high gas permeability of silicone elastomer induces that most of the dissolved gas escapes to the surroundings resulting in a low nucleation. Therefore, the bubble nucleation in neat silicone elastomer was improved thanks to the microstructuration of the fluorosilicone elastomer. Indeed, the addition of fluorosilicone nodules in the silicone matrix should increase the overall CO₂ uptake during the saturation stage and it also allows the formation of higher nuclei densities by heterogeneous nucleation which in turns reduces the overall bubble size by competitive nuclei growth. Nonetheless, the blend morphology is not

Conclusions

stabilized along time and fluorosilicone domains remain large therefore it is necessary to compatibilize this blend.

Furthermore, the dynamic crosslinking process was carried out on silicone/fluorosilicone blends to take advantage of the improved elongational rheology from the dynamic crosslinking and the enhanced nucleation efficiency from the microstructuration of the fluorosilicone. Otherwise, the dynamic crosslinking of this blend turns out to be an efficient compatibilization strategy. Therefore, the alliance of the fluorosilicone domain size reduction, the reduction of the interfacial surface tension and the improvement of the viscoelasticity and bi-elongational rheology brought by the dynamic crosslinking enables to substantially improve the foaming behavior of the blend. Finally, this foaming route gives similar results under gaseous conditions, in terms of cell size and cell density, as highly filled silicone rubber under supercritical conditions. Nevertheless, this strategy remains difficult to extend in the industry because of its time-consuming aspect but it might give fundamental tools to improve foaming behavior for other systems.

In the second part, the foaming of ThermoPlastic Vulcanizates (TPV) silicone has been carried out in a single screw process with commercial chemical blowing agent releasing safe gases i.e. carbon dioxide and water. From literature, it is known that fully crosslinked elastomeric phase prevent the expansion of TPV. Therefore, blends of LDPE and partially crosslinked Liquid Silicone Rubber (LSR) were foamed. The results showed that their foaming behavior is correlated to their high shear rheology and the extrusion foaming parameters which are known to control the nucleation i.e. the pressure before the die and the depressurization rate at the die exit. Moreover, the partially crosslinked LSR nodules are assumed to improve nucleation by heterogeneous nucleation while allowing a sufficient expansion of the LDPE phase. With the proper conditions (not optimized), the TPV foams achieves similar foaming behavior as neat LDPE while the LSR content represents 40wt% of the formulation.

Perspectives

This study clears up a part of the mystery concerning the dynamic crosslinking on silicone elastomer. However, further characterizations may be carried out to fully characterize the branched structures such as light scattering techniques. The presence of sub-micronic gel structures may also be evidenced by AFM. Furthermore, one can imagine using this process to graft functional groups through nitroxide mediated polymerization (NMP) in order to control the grafting efficiency [1].

A current challenge with silicone is to achieve high expansion and at the same time to be able to hinder the post-relaxation and shrinkage in order to generate stable foams with very low foam bulk densities. Therefore, the post-crosslinking of the foam structure should

be investigated and may be solved with the addition of a promoter in future efforts. Additional works could also be conducted on the characterization of mechanical, insulation properties of the foam discussed in this dissertation. Besides, foam morphology might be improved by adding appropriate surfactants to reduce fluorosilicone nodule size and permeation rate at the bubble interface. Finally, in-situ visualization of the foaming step may give interesting results about the nucleation, cell growth and coalescence phenomenon which could also be valuable for foaming modeling.

A rheological property of major interest in foaming is the biaxial extensional viscoelasticity of the polymer + CO₂ system at large deformations (in the non-linear regime) at high pressures. However to my knowledge, at present, there is no instrumental technique to address this important rheological issue.

From this first trial of extrusion foaming, plenty of improvements may be brought. First, this study did not attempt to optimize the multivariable extrusion foaming conditions for maximum density reduction but focused on understanding of the effect of individual variables under a chosen condition. It is believed that multivariable optimization of these conditions is desirable to achieve further density reduction beyond what has been achieved here.

Here for understanding matters, the formulation used simplified formulations. It could be interesting to check the effect of additives especially plasticizers on the foaming behavior of TPV.

From a process point of view, the use of supercritical CO₂ with adequate tandem extrusion process would deliver foams with better morphologies and properties. The use of a cooling zone at the die exit will reduce the gas loss by diffusion and restrict the surface instabilities in speeding up LDPE crystallization. The modification of tooling, especially the die geometry is required to optimize the pressure drop rate in order to achieve higher expansion and refined cells. Finally, it would be outstanding to formulate and foam the TPV within the same process.

The TPV foaming might also be easier whether the dispersion of hollow fillers (expandable or not) is considered instead of gas foaming especially for soft grades.

[1] M.W. Bodley, J.S. Parent, A New Approach to Dynamic Vulcanization: Use of Functional Nitroxyls to Control Reaction Dynamics and Outcomes, *Industrial & Engineering Chemistry Research* **56** (43) (2017) 12247-12255.